Kv1.3 channels in mitochondria: A key coupling in cellular proliferation?

Faye Louise Styles

The University of Leeds, Faculty of Medicine and Health, Leeds Institute for Cardiovascular and Metabolic Medicine.

May 2019.

Submitted in accordance with the requirements for the degree of Doctor of Philosophy.

Declaration

The candidate confirms that the work submitted is her own and that appropriate credit has been given where reference has been made to the work of others. The right of Faye Louise Styles to be identified as Author of this work has been asserted by Faye Louise Styles in accordance with the Copyright, Designs and Patents Act 1988.

Acknowledgements

I would like to dedicate this work to Professor Chris Peers, without whom I would never have had this opportunity. Chris was, and always will be, a constant source of inspiration. I am very privileged to have been able to work with him.

Firstly, thank you to the British Heart Foundation for providing the funding for this project.

I would like to extend a huge thank you to my supervisors, Drs Lee Roberts, Piruthivi Sukumar, Jason Scragg and John Boyle for all your help and support during this project. A special thank you to you Lee for all of your extra effort, time and guidance throughout these last few months.

Thank you to Neil Turner for all of your pastoral support through some difficult times, and to Sally Boxall for your bio-imaging technical expertise.

Thank you to my Peers Group family, Jacobo, Emily J, Tania, Moza, Emily W, Jack, Hayley, Ming, Joe and Clare, for your advice, encouragement and friendship over the last four years. I wish you all the very best of luck in your future endeavours.
Thank you to all the other hardworking researchers and students at The University of Leeds, within both the Faculty of Medicine and Health and the Faculty of Biological Science, that helped me along this journey and made my time at the University enjoyable.

Thank you to my Mum and Dad, for always being so loving and supportive, and to all my family and friends for your encouragement along the way.

Finally, and most importantly, thank you Ben. I wouldn't have got through this without your love, support and advice. Thank you for always believing in me, and for not letting me crumble!

Abstract

The Kv1.3 channel increases cellular proliferation and migration in multiple cell types. Various mechanisms have been proposed to explain how the channel stimulates proliferation, but the topic remains controversial. Previously thought to be localised only to the plasma membrane, the channel has been found in the inner mitochondrial membrane. In cancer, mitochondrial Kv1.3 may regulate apoptosis, yet the role of mitochondrial Kv1.3 in non-pathophysiological states remains less well defined. Cellular proliferation has a high energy demand, requiring ATP for processes like signal transduction to DNA, RNA and protein synthesis. The distinct energy requirements of cellular proliferation coupled with the known mitochondrial localization of Kv1.3 may mean that the Kv1.3 channel links cellular energy metabolism to proliferation. This thesis investigates whether the mitochondrial Kv1.3 channel is an anti-proliferative target in HEK293/Kv1.3 cells. Overexpression of Kv1.3 in HEK293 cells increased glycolysis, mitochondrial membrane potential, oxidative phosphorylation, reactive oxygen species, non-mitochondrial respiration and proliferation. Inhibition of mitochondrial Kv1.3 channels with 100nM PAPTP reduced respiration and proliferation. Inhibition of ROS with 5µM MitoQ reduced proliferation. Kv1.3 pore mutants determined that the voltage sensor, as well as the tyrosine 447 residue on the C-terminal of the Kv1.3 channel, are needed to stimulate respiration in HEK293 cells. Mitochondrial Kv1.3 channels were also found in primary human saphenous vein smooth muscle cells. Upregulation of Kv1.3 drives pathological proliferation of vascular smooth muscle cells in conditions like atherosclerosis and hypertension, and these cells also have altered metabolism. This data shows that the mitochondrial Kv1.3 channel directly increases oxidative phosphorylation, non-mitochondrial respiration and proliferation in HEK293 cells, providing a novel link between mitochondrial Kv1.3 and cellular energy homeostasis. Although the exact mechanisms are unclear, these data suggest that mitochondrial Kv1.3, especially it's ion conduction independent properties, is a valid target for future research into Kv1.3 induced proliferation in VSMCs.

Table of Contents

List of Figures

List of Tables

List of Abbreviations

2DDG	2 Deoxy-D-glucose
ADP	Adenosine diphosphate
AMP	Adenosine monophosphate
AMPK	Adenosine monophosphate activated protein kinase
ANOVA	Analysis of variance
AS	Ascorbate
ATP	Adenosine triphosphate
BCA	Bicinchoninic acid
BSA	Bovine serum albumin
CCCP	Carbonyl cyanide m-chlorophenyl hydrazone
CoA	Coenzyme A
CREB protein	cAMP response element binding protein
CS	Citrate synthase
CVD	Cardiovascular disease
DAPI	4',6-diamidino-2-phenylindole
dd	Double distilled
DM2-OG	Dimethyl-2-oxoglutarate
DNA	Deoxyribonucleic acid
DPBS	Dulbecco's phosphate buffered saline
DTNB	5,5'-dithiobis-(2-nitrobenzoic acid)
EAG	Ether-à-go-go potassium channel
EB	Elution buffer
ECM	Extracellular matrix
EGTA	Ethylene glycol-bis (2-aminoethylether)-*N,N,N',N'*-tetraacetic acid
ER	Endoplasmic reticulum
ERK	Extracellular signal regulated protein kinase
ETS	Electron transport system
FAD	Flavin adenine dinucleotide
$FADH_2$	Reduced flavin adenine dinucleotide
FBS	Fetal bovine serum

FCCP	Carbonyl cyanide 4-(trifluoromethoxy)-phenylhydrazone
FLIM	Fluorescence lifetime imaging microscopy
GLUT	Glucose transporter
HEK293 cell	Human embryonic kidney cell 293
HEPES	4-(2-hydroxyethyl)-1-piperazineethanesulfonic acid
HRP	Horseradish peroxidase
HSVSMC	Human savenous vein smooth muscle cell
IV	Current voltage relationship
IMM	Inner mitochondrial membrane
IMS	Intermembrane space
KO	Knock-out
MAPK	Mitogen activated protein kinase
MCU	Mitochondrial calcium uniporter
MEK	Mitogen activated protein kinase kinase
MFI	Mean fluorescent intensity
MgTx	Margatoxin
MitoQ	10-(6'-ubiquinonyl) decyltriphenylphosphonium bromide
MMP	Mitochondrial membrane potential
MPTP	Mitochondrial permeability transition pore
NAD	Nicotinamide adenine dinucleotide
NADH	Reduced from of nicotinamide adenine dinucleotide
NFAT	Nuclear factor of activated T cells
NGS	Normal goat serum
OXPHOS	Oxidative phosphorylation
p	Statistical significance value
PAGE	Polyacrylamide gel electrophoresis
PAP-1	5-(4-Phenoxybutoxy) psoralen
PAPTP	3-(4-(4-((7-oxo-7H-furo[3,2-g] benzopyran-4-yl) oxy) butoxy) phenyl) propyl) triphenyl phosphonium iodide
PDZ	Post synaptic density protein
pH	Acid/base scale
PhS	Phenylsuccinic acid
P_i	Inorganic phosphate

PKA	Protein kinase A
PKB	Protein kinase B
PKG	Protein kinase G
PM	Plasma membrane
PVDF	Polyvinyl difluoride
Rhod-2 AM	Cell-permeant acetoxymethyl (AM) ester form of rhodamine-2
RNA	Ribonucleic acid
ROS	Reactive oxygen species
ROUT	Robust regression and outlier removal analysis
ROX	Residual oxygen consumption
RT	Room temperature
SDS	Sodium dodecyl sulphate
SEM	Standard error of the mean
ShK-Dap22	Stichodactyla helianthus (ShK) with a non-natural amino acid diaminopropionic acid (Dap) replacing Lysine at position 22.
SOD	Superoxide dismutase
SDS	Sodium dodecyl sulphate
SRC	Spare respiratory capacity
TBS	Tris buffered saline
TCA cycle	The citric acid cycle
TMPD	N, N, N', N'-Tetramethyl-p-phenylenediamine dihydrochloride
TMRM	Tetramethylrhodamine, methyl ester
TNB	Thio-bis-[2-nitrobenzoic acid]) cysteine
t-PMET	Trans-plasma membrane electron transport
TPP^+	Positively charged triphenyl phosphonium ion
Tris	Tris(hydroxymethyl) aminomethane
VDAC	Voltage dependent anion channel
Vm	Plasma membrane voltage
VSMCs	Vascular smooth muscle cells
WT	Wild-type

Chapter One

Introduction

1.1 Cardiovascular Disease

1.1.1 Overview

Cardiovascular disease (CVD) is an umbrella term for disorders of the heart and circulatory system. CVD diseases include coronary heart disease, cerebrovascular disease, rheumatic heart disease, heart failure and other disorders (Nabel, 2003). The two main causes of death from CVD are myocardial infarctions and strokes, accounting for over 85% of CVD deaths (World Health Organisation, 2018). Myocardial infarctions and strokes are acute events which block the passage of oxygenated blood to areas of the heart and brain, respectively. These events occur when there is rupture of an atherosclerotic plaque in the inner wall of blood vessels

1.1.2 Cost of CVD

In the UK the National Health Service spends £7 billion a year on CVD (British Heart Foundation, 2018) and the annual cost of CVD to the EU economy is €210 billion (Wilkins *et al.*, 2017). In 2008, a study calculated the one-year hospitalisation and medication costs for each patient with a history, or at risk of, atherothrombosis to be on average $7000 (Mahoney. *et al.*, 2008). In the United States, the direct medical costs of CVD were $273 billion in 2010, and this number is predicted to triple by 2030 (Heidenreich *et al.*, 2011). In addition, the real indirect costs of CVD, due to a lack of productivity, are expected to rise to $276 billion by 2030 in the United States alone (Heidenreich *et al.*, 2011). The prevalence of CVD is not only increasing in the United States (Khavjou, Phelps and Leib, 2016), but also elsewhere in the world (Wilkins *et al.*, 2017), especially in middle-low income countries (Gaziano *et al.*, 2010). CVD is the World's leading cause of death, with 17.9 million people dying as a result in 2016, an estimated 31% of deaths worldwide (World Health Organisation, 2018). In addition, worldwide, hypertension leads to 7.5 million deaths each year, which equates to 12.5%

of all deaths annually (World Health Organisation, 2013). In 2014, Public Health England revealed that hypertension was costing the NHS £2 billion per year (Public Health England, 2014).

1.1.3 Aetiology

VSMC proliferation is a prominent feature in the development, progression and treatment of CVD. Atherosclerosis is a progressive, chronic inflammatory disease of large arteries (Lusis, 2000). Atherosclerotic plaques develop from a build-up of lipids, immune cells, necrotic debris and VSMCs in the sub-endothelial layer of large blood vessel walls (Lusis, 2000). In addition, within the plaque exists inflammatory mediators, enzymes and extracellular matrix (ECM) secreted by VSMCs (Owens, Kumar and Wamhoff, 2004) (Figure 1.1 a, d and e). The accumulation of these cells and substances in the sub endothelial layer over time reduces the diameter of the vessel lumen, occluding blood flow (Rzucidlo, Martin and Powell, 2007). VSMCs can also migrate to the surface of the plaque to form a stabilising fibrotic cap (Lusis, 2000). However, activated macrophages within the plaque release inflammatory mediators and growth factors, stimulating VSMCs to proliferate more and to secrete matrix metalloproteases. Matrix metalloproteases are involved in plaque instability (Galis *et al.*, 1994) and neointimal hyperplasia (Porter *et al.*, 1999), two preceding events to plaque rupture.

Hypertension is a risk factor for multiple chronic diseases, including many cardiovascular disorders like heart failure, myocardial infarctions, stroke and vascular dementia (Touyz *et al.*, 2018). Hypertension arises from high vascular resistance and causes remodelling of the vessel wall, which eventually reduces the diameter of the lumen (Sonoyama *et al.*, 2007). The remodelling of the vessel wall is driven by VSMC proliferation (Owens, 1988; Mulvany, 1993) (Figure 1.1a, b and c), and control of this proliferation produces antihypertensive effects (Hadrava *et al.*, 1991). VSMC proliferation starts as an adaptive response to mechanical stress (the same advantageous response that would occur during vessel repair), but gradually becomes less controlled with an unchecked cell cycle leading to uncontrolled proliferation and de-differentiation of VSMCs (Owens, 1988). This results in media thickening, neointima hyperplasia and vessel stiffness (Nemenoff *et al.*, 2011).

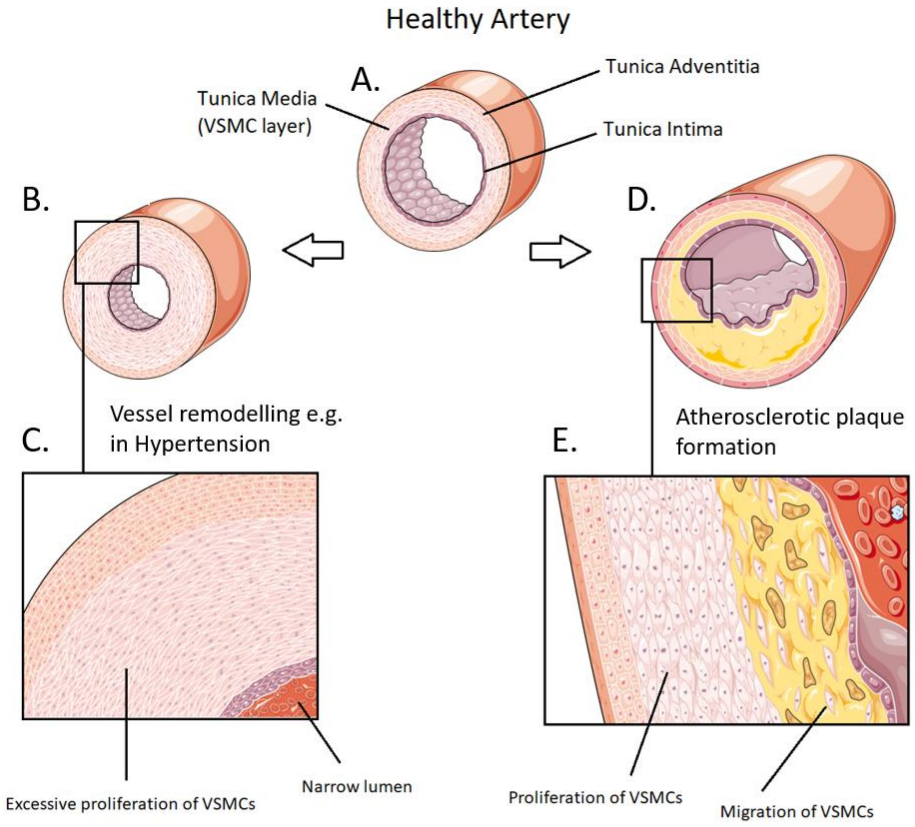

Figure 1.1 Vascular smooth muscle cell remodelling in arteries. A. Healthy artery consisting of three layers; Tunica Adventitia (outer), Tunica Media (middle, containing VSMCs) and Tunica Intima (inner). B and C. VSMC remodelling in hypertension, showing proliferation of VSMCs in the Tunica Media leading to hyperplasia of the vessel wall. D and E. VSMC remodelling in atherosclerotic plaque formation. Proliferation of VSMCs in the Tunica Media, and migration of VSMCs into the atherosclerotic plaque that builds between the Tunica Media and the Tunica Intima. Servier Medical Art was used to generate images (*Servier Medical Art*, no date)

1.1.4 Treatments

People at risk, and those who already have CVD, are advised to make lifestyle changes to reduce their risk of disease progression. Stopping smoking, eating a healthy balanced diet, reducing stress, maintaining a healthy weight, reducing alcohol consumption and exercising regularly are all commonly prescribed (National Health Service, 2018). Medication, such as statins, can be prescribed to reduce blood lipids, but these are associated with significant side effects such as gastrointestinal problems (Piepoli *et al.*, 2016). Other commonly prescribed drugs include bile acid sequestrants, fibrates and nicotinic acid, but they do not reduce the incidence of CVD events if

administered as a monotherapy, and again are associated with side effects (Piepoli *et al.,* 2016). Future lipid lowering pharmacological therapies may focus on monoclonal antibody therapies, after the success of phase III clinical trials with alirocumab (Robinson *et al.*, 2015) but further trials are needed. Anti-hypertensive treatments, glucose lowering drugs and anti-platelet therapy can also be used to reduce the risk of CVD events, but none are without side effects (Stewart, Manmathan and Wilkinson, 2017). For established CVD, surgical interventions like coronary artery bypass grafting, balloon angioplasty and stent implantation are common procedures (Lacolley *et al.*, 2012). However, alongside the risks of surgical procedures, the effectiveness of these treatments are all limited by pathological VSMC proliferation. Percutaneous coronary intervention (PCI) with stent implantation is the most widely used treatment for coronary artery disease (Serruys and Rutherford, 2016). Proliferation of VSMCs occurs in response to damage to the vessel wall during stenting (Rzucidlo, Martin and Powell, 2007).The vessel's response to the stenting procedure is the same as it would be to an injury; proliferation and migration of VSMCs at the stenting site, and secretion of ECM. This causes hyperplastic lesions to form over and around the stent which re-narrow the blood vessel lumen. In-stent restenosis commonly leads to myocardial infarctions and severe angina which requires hospitalisation (Chen *et al.*, 2006). However, while stents are becoming more advanced in their functional design, and drug eluting stents have reduced some problems associated with the devices (Liistro *et al.*, 2002), the issue of delayed restenosis is still profound, as reviewed in (Brancati *et al.*, 2017). Even heart transplantation can be affected by pathological proliferation of VSMCs, as cardiac allograft vasculopathy limits the long term success of the procedure (Maziar *et al.*, 2006). Having more efficient treatments of CVD and reducing the reoccurrence of surgical complications by inhibiting VSMC proliferation is therefore of pressing need.

1.2 Vascular Remodelling in CVD

1.2.1 VSMCs

VSMCs in mature mammals are specialised cells that line the walls of blood vessels and arrange themselves in a circumferential manner within the vessel Tunica Media (Figure 1.1). They control vascular tone, and so they have a direct role in regulating blood flow and distribution around the body (Matsumoto and Nagayama, 2012). Under normal conditions, these cells display a contractile phenotype, expressing vast numbers of ion channels, proteins and signalling molecules needed for contraction (Chamley-Campbell, Campbell and Ross, 1979) (Figure 1.2a). However, in certain circumstances this phenotype switches to a proliferative one, known as 'phenotypic modulation' or the 'phenotypic switch' (Owens, Kumar and Wamhoff, 2004) (Figure 1.2b). Hallmarks of this proliferative state include the production and secretion of extracellular matrix proteins and cytokines such as elastin, collagen and proteoglycans, that are necessary for the development of the blood vessel wall and mitosis and migration of the smooth muscle cells (Alexander and Owens, 2012). This irreversible proliferative phenotype is crucial in physiological processes such as vascular development and repair and has clearly developed as a protective mechanism in mammals over many years. Critically this phenomenon also occurs in response to environmental cues, including chemical, mechanical or inflammatory stimuli, causing neointimal hyperplasia of the blood vessel walls (Alexander and Owens, 2012). Inhibition of the VSMC switch to the proliferative, migratory and secretory phenotype may limit the progression of atherosclerosis, hypertension and CVD (Rzucidlo, Martin and Powell, 2007)

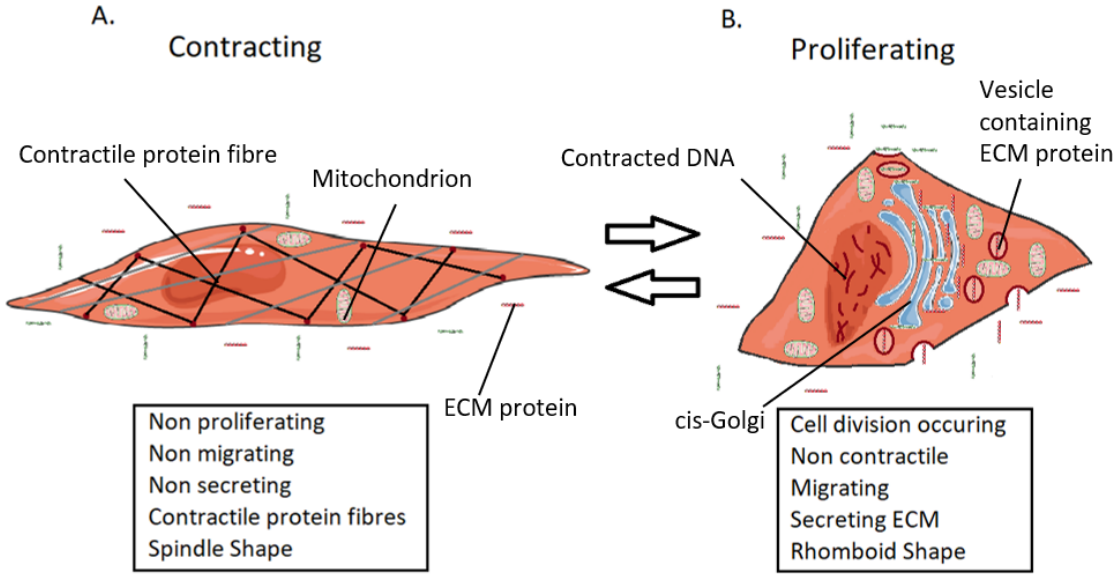

Figure 1.2 Vascular smooth muscle cell phenotypic switching. A. Contractile VSMC with an elongated spindle shape, contractile protein fibres and no secretion of ECM. B. Proliferating VSMC with a rhomboid shape and secretion of ECM. ECM = Extracellular Matrix. Servier Medical Art was used to generate images (*Servier Medical Art*, no date)

1.2.2 Mechanisms

Several mechanisms have been proposed for aberrant VSMC proliferation, but a better understanding of the mechanisms controlling VSMC phenotypic switching is needed. Proliferative and contractile states of VSMCs are likely to respond to local environmental cues that regulate genetic programmes and thus determine cell phenotype (Owens, Kumar and Wamhoff, 2004). These cues can be hormonal (Cutini and Massheimer, 2010; Wang and Sun, 2010; Ueda *et al.*, 2013), mechanical (Peter *et al.*, 1996; Qiu *et al.*, 2014) and traumatic (Marx, Totary-Jain and Marks, 2011), with damage to endothelial cells being a potent stimulator for VSMC proliferation (Hirschi, Rohovsky and D'Amore, 1998; Powell *et al.*, 1998). These triggers can lead to the release of inflammatory mediators (Selzman *et al.*, 1998) , growth factors (Lindner and Reidy, 1991) and gasotransmitters (Jeremy *et al.*, 1999; Su *et al.*, 2001) into the local environment that can act as mitogens by stimulating signalling pathways that lead to VSMC proliferation. In particular, platelet derived growth factor (PDGF) (Ross, 1981) and transforming growth factor beta1 (TGF-b) (Schulick *et al.*, 1998) are key mitogens which stimulate proliferation of VSMCs. The signal for VSMCs to proliferate is driven by

various cell signalling pathways, such as Protein Kinase C (PKC) (Liu *et al.*, 2007), Protein Kinase B (PKB) (Liu *et al.*, 2010), Mitogen Activated Protein Kinases (MAPK) (Suwanabol *et al.*, 2012; Cidad *et al.*, 2015) and Protein Kinase G (PKG) (Boerth *et al.*, 1997; Brophy *et al.*, 2002), which activate transcription pathways. Some transcription pathways leads to protein synthesis which supports proliferation of VSMCs, whilst other transcription pathways lead to the downregulation of contractile proteins (Rzucidlo, Martin and Powell, 2007; Bennett, Sinha and Owens, 2016). Contractile genes are regulated by serum response factor (SRF) which binds to a DNA sequence known as the CArG box (a conserved DNA sequence [CC(A/T) 6 GG]), and the SRF coactivator myocardin (Miano, 2003). In proliferating VSMCs, other transcription factors are more heavily involved, including c-fos and c-jun (Sylvester *et al.*, 1998; Zhao *et al.*, 2002) and nuclear factor of activated T cells (NFAT) (Hill-Eubanks *et al.*, 2003). Regulation of transcription by splicing factors like serine/arginine-rich splicing factor 1 (SRSF1) (Xie *et al.*, 2017), DNA binding proteins like the GATA family of zinc finger DNA-binding domain proteins e.g. GATA-6 (Xie *et al.*, 2015) and by epigenetics (Alexander and Owens, 2012) are additional mechanisms which regulate VSMC phenotype. The genes which are activated then regulate the expression and activity of a plethora of receptors, transporters and ion channels, which can support proliferation of VSMCs (Gomez and Owens, 2012). In particular interest for this work is the involvement of ion channels in VSMC proliferation, as they can be targeted pharmacologically to regulate their activity. Notable ion channels involved in VSMC proliferation include Ca^{2+} channels including T type (Duckles *et al.*, 2015), transient receptor potential canonical (TRPC) channels (Alonso-Carbajo *et al.*, 2017) and ORAI channels (Spinelli and Trebak, 2016), as well as K^+ channels (Cidad *et al.*, 2010; Lopez-Lopez, Cidad and Perez-Garcia, 2018). From here on in, this thesis will focus on the role of K^+ channels, in particular the Kv1.3 channel, in the phenotypic switching of VSMCs.

1.3 K^+ Channels

1.3.1 Overview

K^+ channels are proteins within cell membranes that allow K^+ ions to pass through the membrane, down their electrochemical gradient. K^+ channels are found in almost all species and play crucial roles in both excitable and non-excitable cells, regulating functions from cell volume, to hormone secretion and electrical impulse propagation (Hille, 2001). In mammals almost 80 genes encode K^+ channels, making them the most widely distributed ion channel (Maljevic and Lerche, 2013).

All K^+ channels have transmembrane domains that sit in the lipid bilayer, and it is predominantly the structure of these transmembrane domains that allows K^+ channels to be categorised. All K^+ channels consist of two distinct regions; a pore forming region to allow K^+ ions to pass through the channel and a regulatory region which allows for channel regulation. A selectivity filter in the pore ensures the channels are highly selective for K^+ over other ions (Doyle *et al.*, 1998). While the pore forming region is consistent in structure across all K^+ channels, the regulatory region can vary widely between K^+ channels and contributes to their classification (Kuang, Purhonen and Hebert, 2015). K^+ channels can be divided into four groups based on their structure and mode of activation;

- Inwardly rectifying potassium channels, Kir (2 transmembrane domains).
- Two pore potassium channels, K2P (4 transmembrane domains).
- Calcium activated potassium channels, KCa (6 or 7 transmembrane domains).
- Voltage gated potassium channels, Kv (6 transmembrane domains).

The structure of each of these types of K^+ channel is shown in Figure 1.3, along with their associated genes. The Kv channels make up the largest group of K^+ channels in mammals. With 40 genes encoding them in humans (Maljevic and Lerche, 2013), they are arguably the most structurally and functionally diverse members of all the voltage gated ion channels.

1.3.2 Voltage Gated K^+ Channels

The existence of these channels was first discovered over 60 years ago, through the pioneering work of Hodgkin and Huxley on the giant squid axon (Hodgkin and Huxley, 1952). Kv channels open in response to changes in the transmembrane potential, which allows for K^+ ions to flow through the channels to restore the resting membrane potential. Originally discovered in Drosophila, four groups of genes were found to code for Kv channels; shal, shaw, shab and shaker, and these have all been found to have human homologues. The Kv gene superfamily can be categorised into 12 families of channels, Kv1.x – Kv12.x (Gutman *et al.*, 2005). In Figure 1.3, Kv5.x, Kv6.x, Kv8.x and Kv9.x are omitted due to them being modifiers of other potassium channels (Gutman *et al.*, 2005).

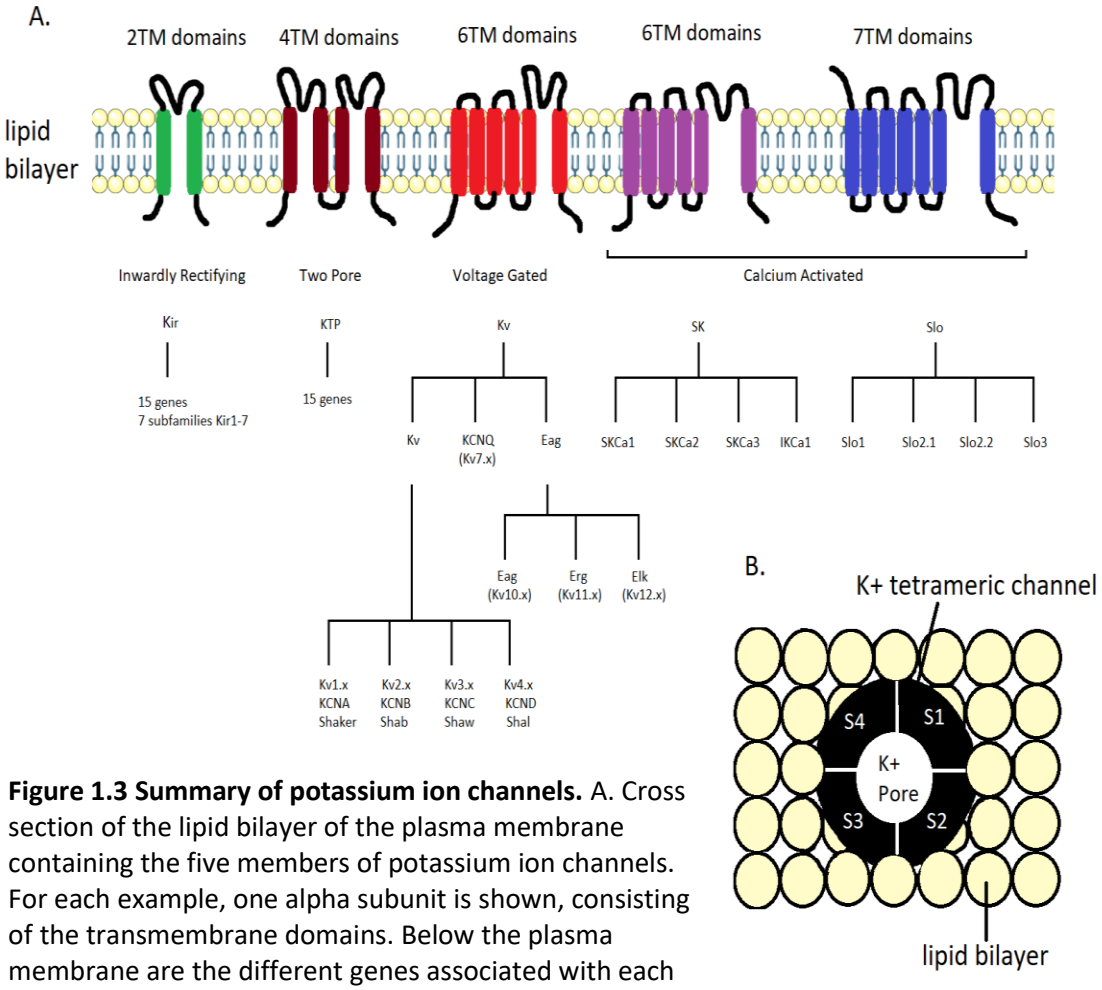

Figure 1.3 Summary of potassium ion channels. A. Cross section of the lipid bilayer of the plasma membrane containing the five members of potassium ion channels. For each example, one alpha subunit is shown, consisting of the transmembrane domains. Below the plasma membrane are the different genes associated with each example potassium channel. B. An above view of a potassium ion channel in the plasma membrane. Each potassium channel is made up of four alpha subunits, which create a tetramer around a central pore. Servier Medical Art was used to generate images (*Servier Medical Art*, no date).

1.3.2.1 Structure

In 1998, the KcsA channel was the first K^+ channel to have its structure characterised using x-ray crystallography (Doyle *et al.*, 1998). This work paved the way for the molecular characterisation of other K^+ channels, such as Kv1.2 in 2005 (Long, Campbell and MacKinnon, 2005). All mammalian Kv channels share a similar tetrameric structure (Figure 1.4), with each subunit consisting of two independently functioning domains; a voltage sensing domain and an ion conducting pore (Kuang, Purhonen and Hebert, 2015). Each of the four subunits contains six transmembrane hydrophobic alpha helixes, S1-S6, and a P loop which re-enters the membrane. The ion conduction pore is made up by the four S5-P-S6 helixes which are arranged in a circumferential manner, while the four S1-S4 helixes sit on the periphery of the pore and make up the voltage sensing domain which controls channel gating. It is the S4 helix that is involved most heavily in the voltage sensing ability of the channel, as each S4 helix contains positively charged arginine residues. These charged residues are known as gating arginines, and four are found at every third position on this transmembrane helix. The two independently functioning parts of each subunit (the voltage sensor and the ion pore) are attached between S4 and S5 by what is known as the S4-S5 linker.

Each gene encoding mammalian K_v channels codes for an individual subunit. As each functioning channel needs four subunits, the channels can exist as homotetramers or heterotetramers of different subunits within the same family (Gutman *et al.*, 2005). This is one way in which the diversity of Kv channels is increased. The channels can also undergo post-translational modifications that further increase their structural and functional diversity. Kv channels can undergo post-translational phosphorylation (Jerng, Pfaffinger and Covarrubias, 2004), ubiquitinylation (Henke *et al.*, 2004) and palmitoylation (Gubitosi-Klug, Mancuso and Gross, 2005).

Movement of the gating arginines across the transmembrane electric field contributes to a gating charge. Every time the channel opens, around 12-13 charges are transferred across the electric field. These arginines are present in all voltage gated K^+, Na^+ and Ca^{2+} channels and are imperative for their gating. This charge transfer precedes channel opening. Gating occurs when a change in membrane potential is sensed in the S4 region which leads to a pulling action on the S4-S5 linker, resulting in a conformational change of the channel which allows for K^+ to flow through the pore.

This mechanism is described as a ball and chain mode of action, with the chain (the linker) being able to pull the ball (the gate) out of the pore to allow for the passage of K^+ only. Inactivation/activation can also occur due to conformational changes to the channel (Nekouzadeh and Rudy, 2016).

The selectivity filter in these channels is positioned at the narrowest part of the pore. An amino acid sequence (Thr-Val-Gly-Tyr-Gly) or (Thr-Val-Gly-Phe-Gly) has been found to be essential for the potassium selectivity in Kv channels. As the K^+ ions flow through the channel pore they interact with the carbonyl groups of the aforementioned sequences. This removes the hydration shell from the K^+ ions and allows their diffusion through the channel. The size of the selectivity filter in the Kv channels allows for K^+ ions to interact with the channel proteins, while it is too large to have the same effect on smaller cations such as Na^+. The details of the Kv gating structure became clearer after the crystal structure of rat brain Kv1.2 (rat Kvα1.2/β2) was solved in 2005 (Long, Campbell, & MacKinnon, 2005). In addition to uncovering the mechanism of the gating, the structure of beta (β) subunits which associate with the alpha (α) subunits of the channel was also found (Figure 1.4b). For example, members of the Kv1.x family, bind with Kvβ1-3 proteins through their N-terminal tetramerisation sites. This produces a symetrical tetramer which exists on the intracellular side of the channel. These auxillary subunits are able to modulate the gating of the channel. The binding of different β subunits to the channel adds to the diversity of biophysical and pharmacological properties within the Kv channel family.

1.3.2.2 Location and Function

Along with this large amount of structural diversity, Kv channels are also expressed in a wide range of human tissues, including the central and peripheral nervous systems (Shah and Aizenman, 2014), in non-excitable cells of the immune system (Wulff *et al.*, 2003) and smooth muscle (Cidad *et al.*, 2010; Cheong *et al.*, 2011).

Kv channels allow propagation of electrical signals in the nervous system by determining the shape and size of action potentials, as the outward flow of K^+ from the cells repolarises the membrane after an electrical stimulation (Shah and Aizenman, 2014). Kv channels are subsequently key players in the role of neurotransmitter release. In addition, Kv channels regulate cell volume (Lang *et al.*, 2007; Perez-Garcia,

Cidad and Lopez-Lopez, 2018), cellular proliferation and migration (Lopez-Lopez, Cidad and Perez-Garcia, 2018), and are also involved in metabolism and insulin signalling (Xu *et al.*, 2003, 2004; Tucker *et al.*, 2013).Kv channels are also highly expressed in immune cells and can activate T lymphocytes (Wulff *et al.*, 2003). In all cells, the channels regulate the resting plasma membrane potential (Ouadid-Ahidouch and Ahidouch, 2013). Therefore, Kv channels have been proposed as therapeutic targets for diseases ranging from cancer and autoimmune diseases to neurological, metabolic and cardiovascular disorders.

1.4 Kv1.3

1.4.1 Overview

Kv1.3 is a voltage-gated, shaker-related potassium channel of the delayed rectifier family that is encoded for by the KCNA3 gene. This channel was originally discovered in 1984, when a study linked it to the proliferation of human T lymphocytes (DeCoursey *et al.*, 1984). It was originally classified as an 'n-type' channel, for its prevalence in 'normal' human T lymphocytes. This channel was found it to be a delayed rectifier Kv channel (Cahalan *et al.*, 1985) and shares 60-70% identity with the channel encoded by the shaker gene in Drosophila (Kamb, Tseng-Crank and Tanouye, 1988). In 1991 this 'n type' channel was renamed mammalian shaker-related voltage gated K+ channel, Kv1.3, encoded by the KCNA3 gene (Chandy, 1991). The structure of Kv1.3 is shown in Figure 1.4. Readers are directed to (Chen *et al.*, 2010) to see x-ray crystallography of the closely related Kv1.2 channel.

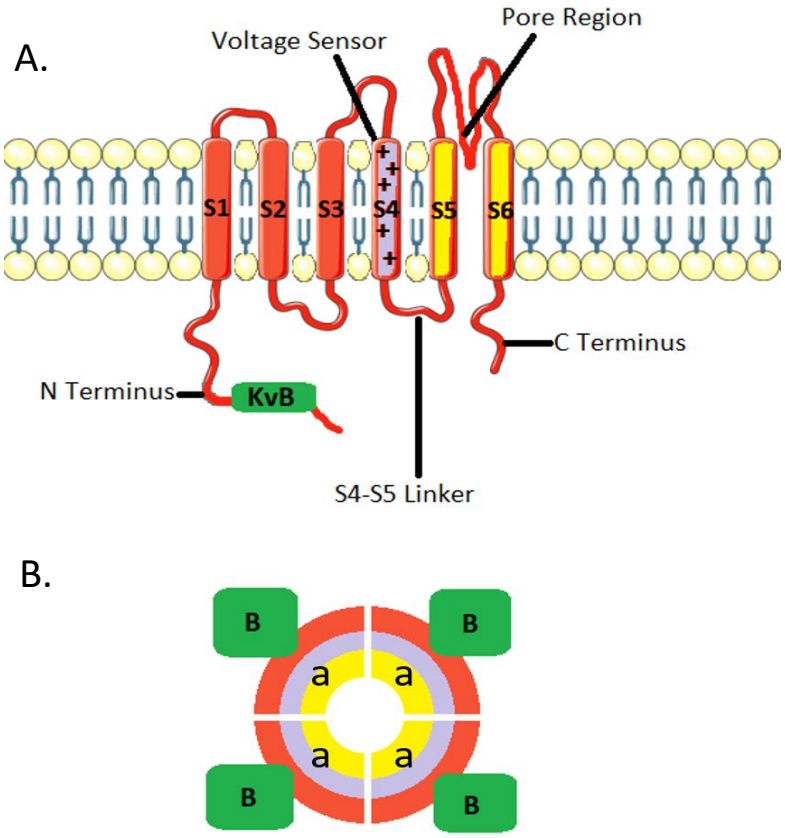

Figure 1.4 Structural components of the Kv1.3 potassium channel. A. The 6 transmembrane domains of the alpha subunit of the Kv1.3 channel situated in the lipid bilayer. The voltage sensor is on S4, the fourth transmembrane domain. The pore region is situated between S5 and S6. The S4-S5 linker is associated with the channel gating. The KvB on the N Terminus is the beta subunit binding domain. B. Schematic of the Kv1.3 channel as it would be seen from above. The four beta subunits are shown (green squares), with one attached to each of the four alpha subunits. Servier Medical Art was used to generate images (*Servier Medical Art*, no date).

1.4.2 Location and function

Kv1.3 channels have been found in brain tissue (Swanson *et al.*, 1990; Veh *et al.*, 1995; Bednarczyk *et al.*, 2010; Bielanska *et al.*, 2010) the olfactory bulb (Stuhmer *et al.*, 1989), epithelial cells (Grunnet *et al.*, 2003), adipose tissue (Xu *et al.*, 2004), macrophages (Kan *et al.*, 2016), lymphocytes (Cahalan *et al.*, 1985), and both skeletal (Hamilton *et al.*, 2014) and smooth muscle cells (Villalonga *et al.*, 2007; Cidad *et al.*, 2010; Bielanska *et al.*, 2012). Originally thought to only be expressed in the plasma membrane of cells, they have now been located at other intracellular sites, such as the nucleus (Jang *et al.*, 2015), the cis-Golgi (Zhu, Yan and Thornhill, 2014) and the inner mitochondrial membrane (Szabo *et al.*, 2005).

Kv1.3 channels have been found to contribute to cellular proliferation (Cidad *et al.*, 2010; Cheong *et al.*, 2011), cell cycle progression (Deutsch and Lee, 1988), cell volume regulation (Deutsch and Lee, 1988), apoptosis (Leanza *et al.*, 2012) and the control of the membrane potential (Blackiston, McLaughlin and Levin, 2009). Plasma membrane and intracellular Kv1.3 channels may have distinct roles. Mitochondrial Kv1.3 channels have been found to regulate apoptosis in cancer cells (Szabo *et al.*, 2005). Kv1.3 channels at the nucleus may regulate cellular proliferation via regulation of transcription factors like c-fos and CREB (Jang *et al.*, 2015).

1.4.3 Biophysical phenotype

At voltages between -70 and -90mV Kv1.3 channels are typically closed, but open in response to a depolarisation of the membrane potential. Activation of Kv1.3 channel occurs between -60 and -50mV, where the channel displays a steep open probability with a midpoint of -40mV (Mahnke *et al.*, 2013). The activation of these channels occurs quickly, over a few milliseconds, whereas the inactivation occurs over a much longer time course, and takes about 200ms (at +50mV) to occur (Panyi, 2005). The inactivation midpoint of Kv1.3 channels is also very steep, occurring at around -45mV (McCormack *et al.*, 1999) and displaying a c type pattern of inactivation (Rasmusson *et al.*, 1998). This shows that Kv1.3 channels have a very small window current.

1.4.4 Regulation

Other membrane proteins have been found to regulate Kv channels. KCNE peptides modulate the Kv1.3 channel in a way similar to β subunits, for example KCNE4 can supress Kv1.3 currents by altering channel trafficking to the membrane, surface expression at the membrane and channel gating (Sole *et al.*, 2009). Cortactin can also regulate Kv1.3 trafficking to the membrane (Hajdu *et al.*, 2015), as can post synaptic density (PDZ) proteins which additionally regulate clustering at the membrane and channel activity (Marks and Fadool, 2007; Szilagyi *et al.*, 2013). Kv1.3 channels exhibit caveolin binding sites. Upon binding to the channel, caveolin inhibits channel activity (Perez-Verdaguer *et al.*, 2016). Integrin receptors also interact and control Kv1.3 channels (Levite *et al.*, 2000). Post-translational modification of Kv1.3 can occur by glycosylation (Zhu, Yan and Thornhill, 2012), palmitoylation (Velez *et al.*, 2016) and phosphorylation (Jimenez-Perez *et al.*, 2016) which can regulate the channel's interactions with other proteins. Phosphorylation of Kv1.3 is the most common post-translational modification, with the channel being a substrate for many protein kinases (Chung and Schlichter, 1997b, 1997a). Of note, the Kv1.3 channel can also be modulated by ROS (Cayabyab *et al.*, 2000). ROS can regulate cysteine, methionine, tyrosine, or histidine residues on ion channels (Cayabyab *et al.*, 2000). Finally, Kv1.3 may also be regulated by substrates and products of metabolism, such as glucose (Tucker *et al.*, 2013) and ATP (Chung and Schlichter, 1997b).

1.4.5 Pharmacology

Inhibitors of Kv1.3 have been developed that either block the channel pore or prevent the channel from activating (Perez-Garcia, Cidad and Lopez-Lopez, 2018). Toxins derived from organisms such as scorpions (Bartok *et al.*, 2014; Rashid *et al.*, 2014), snakes (Yang *et al.*, 2014) and sea anemones (Rashid *et al.*, 2013; Chang *et al.*, 2015) inhibit Kv1.3 by blocking the channel pore, whereas plant derived psoralens like PAP-1 (Kundu-Raychaudhuri *et al.*, 2014) and Psora-4 (Leanza *et al.*, 2013) keep the channel in its inactive state. The ShK peptides derived from sea anemones are some of the most specific and potent Kv1.3 inhibitors, originating from toxins derived from sea anemones (Rashid *et al.*, 2013). Most inhibitors, especially the toxin type, target only plasma membrane Kv1.3 channels, as they are impermeable to the lipid membrane. Recent advances in Kv1.3 pharmacology have chemically altered Kv1.3 inhibitors so

that they are able to target Kv1.3 channels at specific intracellular sites. Leanza and colleagues attached a delocalized cation, triphenyl phosphonium (TPP) moiety, onto a (5-(4-Phenoxybutoxy)psoralen) (PAP-1) derivative, targeting the Kv1.3 inhibitor to the negatively charged mitochondria, thus specifically inhibiting mitochondrial Kv1.3 channels (Leanza *et al.*, 2017; Mattarei *et al.*, 2018). Intracellular and organelle targeting of compounds is key to specificity of a drug. It is important to note that not all compounds are specific for Kv1.3, e.g. Margatoxin (Bartok *et al.*, 2014), as it also inhibits Kv1.2 with a similar affinity to Kv1.3 channels (Kd = 6.4pM) and has low affinity for Kv1.1 (Kd =4.2nM) (Bartok *et al.*, 2014).

1.5 Pharmacological targeting of Kv1.3 in disease

1.5.1 Oncology

Inhibition of Kv1.3 by pharmacological or genetic means inhibits the growth of cancer tumours, thus Kv1.3 inhibitors are fast becoming a promising therapeutic avenue within oncology (Comes *et al.*, 2013; Teisseyre, Gasiorowska and Michalak, 2015). Recent work has focused on the inhibition of mitochondrial Kv1.3 channels, using TPP bound psoralen inhibitors, to promote ROS-dependent apoptosis of tumour cells (Mattarei *et al.*, 2018).

1.5.2 Immunology

The majority of the research into Kv1.3 channel characterisation and function has been carried out in T lymphocytes (T cells). T cells differentiate into effector memory T cells (TEM) upon repeated contact with a particular antigen. This process is characterised by increased expression and activity of Kv1.3 channels in TEM cells (Chandy *et al.*, 2004). In autoimmune diseases, where there is increased differentiation and proliferation of TEM cells lead to attack of endogenous tissue, Kv1.3 inhibitors are promising therapeutic agents. Kv1.3 inhibitors are being researched to treat Multiple Sclerosis (Yuan *et al.*, 2018), Sjogren's Syndrome (Legany *et al.*, 2016), Rheumatoid Arthritis (Tanner *et al.*, 2017), Chronic Inflammatory Diseases such as Chronic Kidney Disease (Kazama *et al.*, 2012), Inflammatory Bowel Disease (Kazama, 2015) and Ulcerative Colitis (Koch Hansen *et al.*, 2014), as well as inflammatory conditions off the airways

such as asthma (Koshy *et al.*, 2014) and COPD (Kazama and Tamada, 2016). Dalazatide, an analogue of ShK peptide has been successful in treating plaque psoriasis in a Phase 1b clinical trial, and is currently ready for Phase 2 trials (Tarcha *et al.*, 2017). In addition, Kv1.3 activity may be harnessed and modulated in B lymphocytes (Wulff *et al.*, 2004), natural killer cells (Koshy *et al.*, 2013) and macrophages (Vicente *et al.*, 2003; Kan *et al.*, 2016) to prevent their activation, differentiation and proliferation for therapeutic benefit in inflammatory conditions.

1.5.3 Neurology

Astrocytes, oligodendrocytes and microglial cells are all glial cells of the central nervous system (CNS). Previously only thought to be the 'housekeepers' of the CNS, it is now widely accepted that glial cells can regulate the excitability of neurons by secreting chemical signalling molecules and displaying high levels of proliferation and migration (Stebbing, Cottee and Rana, 2015). These neuroinflammatory properties are thought to be a hallmark of many neurodegenerative diseases and this change in glial cell behaviour is partly regulated by Kv1.3 channels. In oligodendrites, Kv1.3 regulates the progression of the cell cycle of proliferating oligodendrite progenitor cells (Chittajallu *et al.*, 2002), through a platelet derived growth factor driven mechanism (Vautier *et al.*, 2004). Kv1.3 channel upregulation also occurs in microglial cell activation (Rangaraju *et al.*, 2015). In healthy tissue in the CNS, astrocyte proliferation exists at a very low level. Upon injury, proliferation increases along with an upregulation of Kv1.3-like delayed rectifier potassium currents (MacFarlane and Sontheimer, 1997), however the exact identity of these delayed rectifier currents has not been elucidated to. Glial cell inflammation and secretion of factors involved in the pathogenesis of neurodegenerative disorders such as Alzheimer's Disease (Lowinus *et al.*, 2016) and Parkinson's Disease (Zhang *et al.*, 2018). Kv1.3 inhibitors have shown promising results at reducing the severity of brain injuries from stroke by reducing microglial neuroinflammation (Chen *et al.*, 2018).

1.5.4 Vascular Biology

In a gene expression analysis of 87 ion channels, only two genes were upregulated in proliferating VSMCs; the genes coding for the Kv1.3 channel and its associated β subunit, Kvβ2.1 (Cidad *et al.*, 2010). Cultured proliferating VSMCs have increased

expression of Kv1.3 channels, and their sensitivity to the inhibitor PAP-1 increases 6-fold compared to contractile VSMCs (Cidad *et al*., 2010). Kv1.3 inhibitors reduce VSMC proliferation and migration in *in vitro* and *in vivo* models (Cidad *et al.*, 2010; Cheong *et al.*, 2011). While the involvement of Kv1.3 in VSMC phenotypic switching is universally agreed, the mechanism that underlies it is controversial; three main themes have emerged.

1.6 Mechanisms of Kv1.3 induced proliferation

1.6.1 Membrane potential

It has been proposed that Kv1.3 regulates phenotypic switching of VSMC via alterations in the plasma membrane potential. Activation of Kv1.3 channels causes efflux of K^+ from the cytosol and hyperpolarisation of the plasma membrane potential (Vm). Activation of Kv1.3 is proposed to regulate the oscillations in Vm that occur throughout the cell cycle (Blackiston, McLaughlin and Levin, 2009). Hyperpolarisation of the Vm will lead to a more negatively charged cytosol compared to the extracellular milieu. This will increase the driving force for cation entry, which will cause water to follow and cell volume to increase. Cell volume will oscillate throughout the cell cycle in line with Vm, and there is an optimum volume for proliferation (Herrmann *et al.*, 2012). Alteration of the Vm and/or the cell volume by activation of Kv1.3 can alter other ion fluxes in the cell. An increase in intracellular Ca^{2+} can activate cell signalling pathways which drive proliferation. Some researchers propose that it is the downstream effects of Kv1.3 activation on Ca^{2+} fluxes which drive proliferation (Cheong *et al.*, 2011). This mechanism may be more prevalent in the immune system, where cells, such as T lymphocytes are heavily reliant on Ca^{2+} signalling (Chandy *et al.*, 2004). Kv1.3 mediated hyperpolarisation of Vm has been proposed to be essential for proliferation of VSMCs (Neylon *et al.*, 1999; Neylon, 2002). Cheong *et al*., also suggest that Kv1.3 induced changes to Vm are essential to drive Ca^{2+} induced proliferation (Cheong *et al.*, 2011). However, in VSMCs, both Kv1.3 and Kv1.5 channels have similar effects on membrane potential but very different effects on proliferation (Cidad *et al.*, 2010, 2012). In addition, in femoral VSMCs, depolarisation induced by inhibition of other K^+ channels or by a high extracellular K^+ concentration did not affect

proliferation, suggesting the Vm is not the main determinant of proliferation in these cells (Cidad *et al*., 2010). Therefore, even though K^+ flux through the Kv1.3 channel can contribute to proliferation, the final outcome of Kv1.3 proliferation must be triggered by an ion conduction-independent signalling pathway.

1.6.2 Voltage Sensing

Another proposed mechanism suggests that Kv1.3 channels have non-conducting roles which drive proliferation. Non-conducting Kv1.3 channels which have an intact voltage sensor are able to increase proliferation of HEK293 cells to the same extent as WT Kv1.3 channels (Cidad *et al*., 2012; Jimenez Perez *et al*., 2016). Kv1.3 may sense Vm and control progression of the cell cycle via a polyamine synthesis pathway (Pegg, 2016). Another explanation is that key signalling residues on the Kv1.3 channel participate in translating the pro-proliferative signal. The Kv1.3 channel has been found to contain 17 tyrosine residues, of which several are accessible to tyrosine phosphorylation (Fadool and Levitan, 1998; Fadool *et al.*, 2000; Marks and Fadool, 2007). Kv1.3/Kv1.5 chimeric channels indicate that there are putative docking sites on a YS segment of the C-terminus of the Kv1.3 channel. Upon sensing a change in Vm, there is a conformational change in the Kv1.3 channel from closed to open which exposes this YS segment to phosphorylation. Phosphorylation of the Kv1.3 channel then initiates MAPK signalling via extracellular signal-regulated kinase (ERK), which drives progression of the cell cycle (Jimenez-Perez *et al.*, 2016). Non-conducting roles of other ion channels have been described (Urrego *et al.*, 2014), such as the EAG channel (Hegle, Marble and Wilson, 2006) and the KCa channel (Millership *et al.*, 2011). Both the EAG and KCa channels require conformational changes which allow MAPKs, including ERK, c-jun N-terminal kinases (JNK) and p38 kinases to interact with the channels and stimulate proliferation via activating signalling pathways (Hegle, Marble and Wilson, 2006; Millership *et al.*, 2011). Thus, Kv1.3 may be a kinase substrate and part of a voltage-initiated intracellular signalling network.

1.6.3 Association with other proteins

Kv1.3 channels interact with other proteins that can modulate channel activity and/or contribute to stabilising and to scaffolding the channel within the membrane. In knock-out (KO) Kv1.3 mice, expression of channel-associated proteins, such as tyrosine

kinases, PDZ-containing proteins and adaptors is re-organised (Fadool *et al.*, 1997). Re-organisation of plasma membrane proteins may also occur if Kv1.3 is upregulated in the membrane, with alterations to proteins like integrins and PDZ proteins leading to altered regulation of Kv1.3 and potentially increased proliferation (Levite *et al.*, 2000; Marks and Fadool, 2007). In addition, there is increasing evidence for the Kv1.3/Kv1.5 ratio to be the determining factor driving cellular proliferation in oligodendrite progenitor cells (Attali *et al.*, 1997), microglial cells (Kotecha and Schlichter, 1999) and VSMCs (Cidad *et al*., 2010). Cidad et al., proposed that it was the ratio of Kv1.5/Kv1.3 which determined VSMC phenotype, with a high ratio (increased Kv1.5) reducing proliferation and a low ratio (increased Kv1.3) that increased proliferation (Cidad *et al.*, 2010). Increased Kv1.3 to decreased Kv1.5 channel expression would alter the balance of K^+ in cells, as the channels have different voltage dependencies (Perez-Garcia, Cidad and Lopez-Lopez, 2018). In addition, if both of these channels have non-conducting functions (Cidad *et al.*, 2012; Jimenez-Perez *et al.*, 2016), they may alter cell signalling pathways which regulate the cell cycle and proliferation. Interestingly, intracellular organelles also have specific transmembrane potentials, and it may be that Kv1.3/Kv.1.5 ratio contributes to the potential in these organelles too. Mitochondrial Kv1.3 in the inner mitochondrial membrane regulates cell growth and apoptosis of cancer cells via its effect on the mitochondrial membrane potential (MMP) (Szabo *et al.*, 2005; Teisseyre, Gasiorowska and Michalak, 2015; Leanza *et al.*, 2017). A decrease in mitochondrial Kv1.5 has been found to promote proliferation in human cancer cell lines (lung, glioblastoma and breast cancer), whilst its reinstatement reduces proliferation and promotes apoptosis (Bonnet *et al.*, 2007). The contribution of each of these channels to proliferation, apoptosis and cellular energy status in VSMCs and other non-cancerous cell types remains poorly defined. Therefore, in this thesis, we explored the role of mitochondrial Kv1.3 on the proliferation, bioenergetic status and the functional link between the two, in HEK293 cells.

1.7 Mitochondria

1.7.1 Structure

Mitochondria are organelles present in almost all eukaryotic cells. They are thought to have arisen from a proteobacterium being engulfed by a host archaebacterium and have evolved to become part of the eukaryotic cell. The general structure of a mitochondrion is shown in Figure 1.5. Mitochondria have two membranes; the outer mitochondrial membrane (OMM), which separates the mitochondrial contents from the cytosol, and an inner mitochondrial membrane (IMM), which encompasses the matrix. The matrix is the site of key metabolic processes including fatty acid β-oxidation and the conversion of Acetyl-CoA to reducing equivalents needed for oxidative phosphorylation (OXPHOS) in the Krebs/TCA (the citric acid) cycle, essential for cellular energy status. The IMM has a large surface area due to multiple folds/invaginations termed cristae. Embedded in these cristae are the multiple protein complexes which participate in OXPHOS. There are 5 multi-subunit enzymatic complexes in the IMM, complexes I, II, III, IV and V, with the fifth being the adenosine triphosphate (ATP) synthase that resynthesises ATP from adenosine diphosphate (ADP) and inorganic phosphate (Pi). Respectively, complexes I-IV are called NADH: ubiquinone oxidoreductase, succinate dehydrogenase, cytochrome bc1 complex and cytochrome c oxidase. The two membranes are separated by the intermembrane space (IMS). Across the IMM exists an electrochemical gradient comprised of both a chemical component and an electrical component (Nicholls and Ferguson, 2013). The electrical component is the voltage difference between the IMS and the matrix, normally around 160-200mV (Szabo and Zoratti, 2014), while the chemical component is the pH of the matrix, determined by the concentration of H^+ protons (Nicholls and Ferguson, 2013).

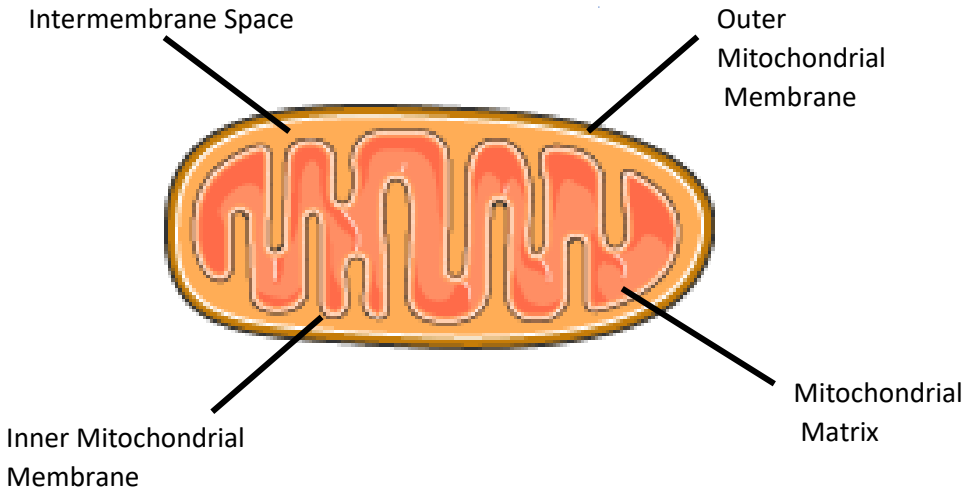

Figure 1.5 Simple structure of a mitochondrion. The outer mitochondrial membrane encases the organelle. The intermembrane space separates the outer mitochondrial membrane and the inner mitochondrial membrane. The inner mitochondrial membrane is folded into invaginations and encases the matrix. Servier Medical Art was used to generate images (*Servier Medical Art*, no date)

1.7.2 Primary Function – Oxidative Phosphorylation

OXPHOS in the IMM involves the generation of ATP from chemical energy released when reducing equivalents donate electrons to the electron transport system (ETS), where they are transferred across the mitochondrial complexes to be accepted by the terminal electron acceptor, oxygen (O_2), at complex IV (Figure 1.6). The reducing equivalents of nicotinamide adenine dinucleotide (NADH) and flavin adenine dinucleotide ($FADH_2$) are donated to the complexes at the beginning of the ETS. NADH reduces complex I (complex I gains two electrons from one NADH molecule) and $FADH_2$ reduces complex II (complex II gains two electrons from one $FADH_2$ molecule), before electrons are transferred along the ETS via a series of redox reactions. The electron transporter ubiquinone/co-enzyme Q10 transports electrons from complexes I and II to complex III, whilst cytochrome c carrier transports electrons from complex III to complex IV. At complex IV O_2 is reduced to water (H_2O). These redox reactions release energy which is used to actively pump H^+ ions across the IMM at complexes I, III and IV from the matrix to the IMS. For each pair of electrons donated, 4 protons are pumped at complexes I and III, while only 2 are pumped at complex IV. This process results in an electrochemical gradient generated across the IMM. This gradient drives

the flow of protons down their electrochemical gradient through the ATP synthase, by chemiosmotic coupling (Mitchell, 1961), and generates ATP. NADH can be used as an indirect measure of the amount of ATP generated in the cell (Blacker and Duchen, 2016). ATP is exported out of the matrix via the adenine nucleotide transporters (ANTs). As O_2 is the terminal electron acceptor, its consumption reflects ATP resynthesis via OXPHOS and so O_2 consumption can be measured to estimate the ATP production within cells. Often, electron transfer between complexes is not 100% efficient, and electrons 'leak' from the complexes. These free electrons are mopped up by O_2 molecules, generating reactive oxygen species (ROS).

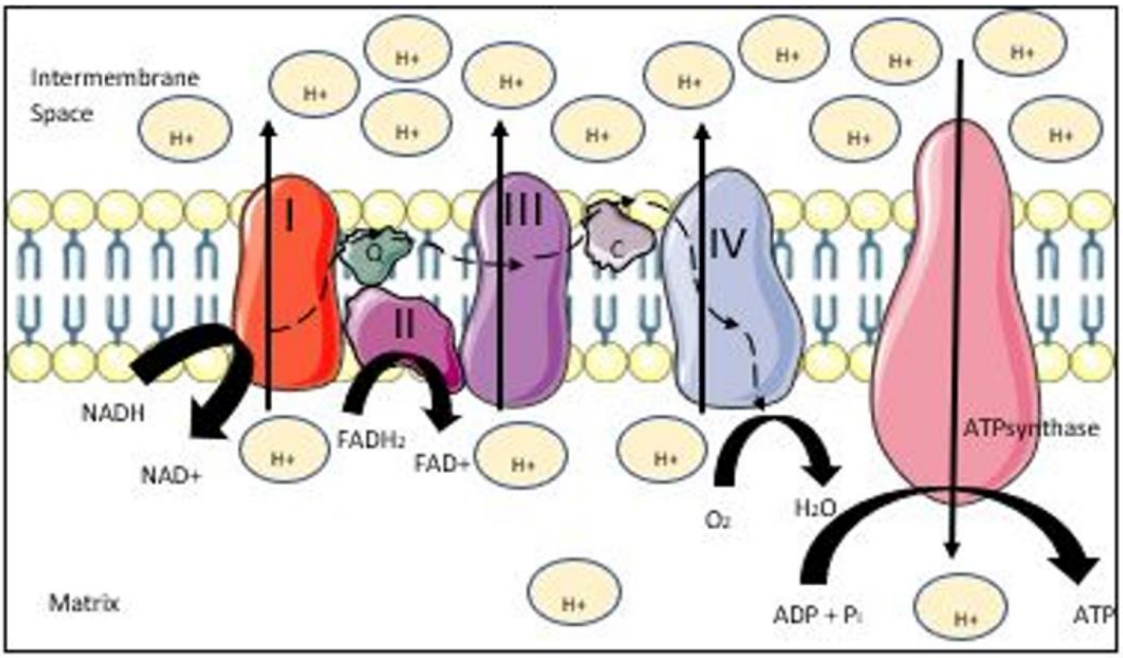

Figure 1.6 Proteins of the electron transport chain in the inner mitochondrial membrane. Complexes 1-4 (I, II, III, IV) of the electron transport chain, along with ATP synthase. Diagram shows how the electrochemical gradient is set up via proton pumping into the intermembrane space of the mitochondria. H^+ = hydrogen protons, Q = ubiquinone/co-enzyme Q10, C = cytochrome c, $NADH/NAD^+$ = reduced/oxidised nicotinamide adenine dinucleotide (respectively), $FADH_2/FAD^+$ = reduced/oxidised flavin adenine dinucleotide (respectively), O_2 = oxygen, H_2O = water, ATP = adenosine triphosphate, ADP = adenosine diphosphate, P_i = inorganic phosphate. Dashed line shows the passage of electrons between the protein complexes. Black vertical arrows show direction of H^+ pumping. Black curved arrows show chemical reactions occurring. Servier Medical Art was used to generate images (*Servier Medical Art*, no date).

1.8 Associated Bioenergetic Pathways

1.8.1 NAD^+

NAD^+ is a coenzyme found in all living cells (Verdin, 2015). It is made up of vitamin B3, or niacin, and ATP. The role of NAD^+ was first elucidated to by Otto Warburg, who isolated NAD^+ and discovered it to be vital for hydrogen transfer in biochemical pathways (Warburg, Posener and Negelein, 1924; Warburg, 1925). The niacin accepts and carries one hydrogen atom and two electrons. Once NAD^+ has accepted the hydrogen and electrons, it becomes known as NADH, the reduced form of the coenzyme, thus NADH is often referred to as a 'reducing equivalent'. NADH becomes a hydrogen and electron donor, capable of oxidising other NAD^+ molecules and Complex I of the ETS. NADH diffuses through the OMM but needs IMM transporters, such as the malate/aspartate and glycerol 3 phosphate shuttles, to enter the matrix. Although the main function of NAD^+/NADH is to participate in the redox reactions of metabolism, an emerging role for NAD^+/NADH has been found in cell signalling (Canto, Menzies and Auwerx, 2015). NAD^+/NADH can tightly regulate signalling molecules like sirtuins and poly ADP ribose polymerases (PARPs). In low O_2 situations NAD^+/NADH can contribute to the production of lactic acid. NAD^+ and NADH can also be phosphorylated, and NADP/NADPH molecules are important for cellular antioxidant defences and have a role in biosynthesis of lipids such as cholesterol (Yang *et al*., 2008; Blacker and Duchen, 2016). NAD^+ and $NAD(P)^+$ both participate in redox reactions in the cell and their pools are of similar size (Ronchi *et al.*, 2013).

1.8.2 Glycolysis

Glucose is a major source of energy for the production of new cell mass, and it is metabolised to pyruvate during glycolysis. Glycolysis is an anaerobic process which occurs in the cytosol once glucose has entered the cell. As glucose is a large polar molecule, transporters are needed to facilitate its entry into the cytosol. There are two main types of glucose transporter in the plasma membrane of cells, sodium-glucose linked transporters (SGLTs) which are localised to the intestinal mucosa and the proximal tubule of the nephron, and facilitated diffusion glucose transporters (GLUTs) (Navale and Paranjape, 2016). In VSMCs, GLUT1 and GLUT4 are involved in glucose uptake, with GLUT1 being the main facilitator of glucose entry and GLUT4 facilitating glucose uptake when stimulated by insulin (Park *et al.*, 2005; Lin *et al.*, 2013). Glycolysis involves a series of enzymatic reactions, summarised in Figure 1.7. Glycolysis oxidises glucose to release energy to generate ATP and reduces two molecules of NAD^+ to NADH. For every molecule of glucose that is oxidised to pyruvate, 2 molecules of ADP and 2 molecules of P_i are re-synthesised to two molecules of ATP. If O_2 is limited, fermentation of pyruvate occurs, and it is anaerobically metabolised to lactic acid. It has been suggested that glycolysis, especially pyruvate fermentation, synthesises the macromolecular building blocks needed to support cell proliferation (Vander Heiden, Cantley and Thompson, 2009; Sullivan *et al.*, 2015). If O_2 is not limited, pyruvate can undergo a series of reactions, specifically the link reaction and the Krebs cycle, which lead to large amounts of ATP being generated via OXPHOS. Glycolysis is regulated by three enzymes; hexokinase, phosphofructokinase and pyruvate kinase (Figure 1.7). Each of these enzymes are regulated by different molecules; hexokinase is inhibited by glucose 6 phosphate, phosphofructokinase is inhibited by high ATP, citrate and pH but is stimulated by adenine monophosphate (AMP) and fructose-2,6-biphosphate, and finally pyruvate kinase is allosterically regulated by fructose-1, 6-biphosphate (Naish, Syndercombe Court and Revest, 2009).

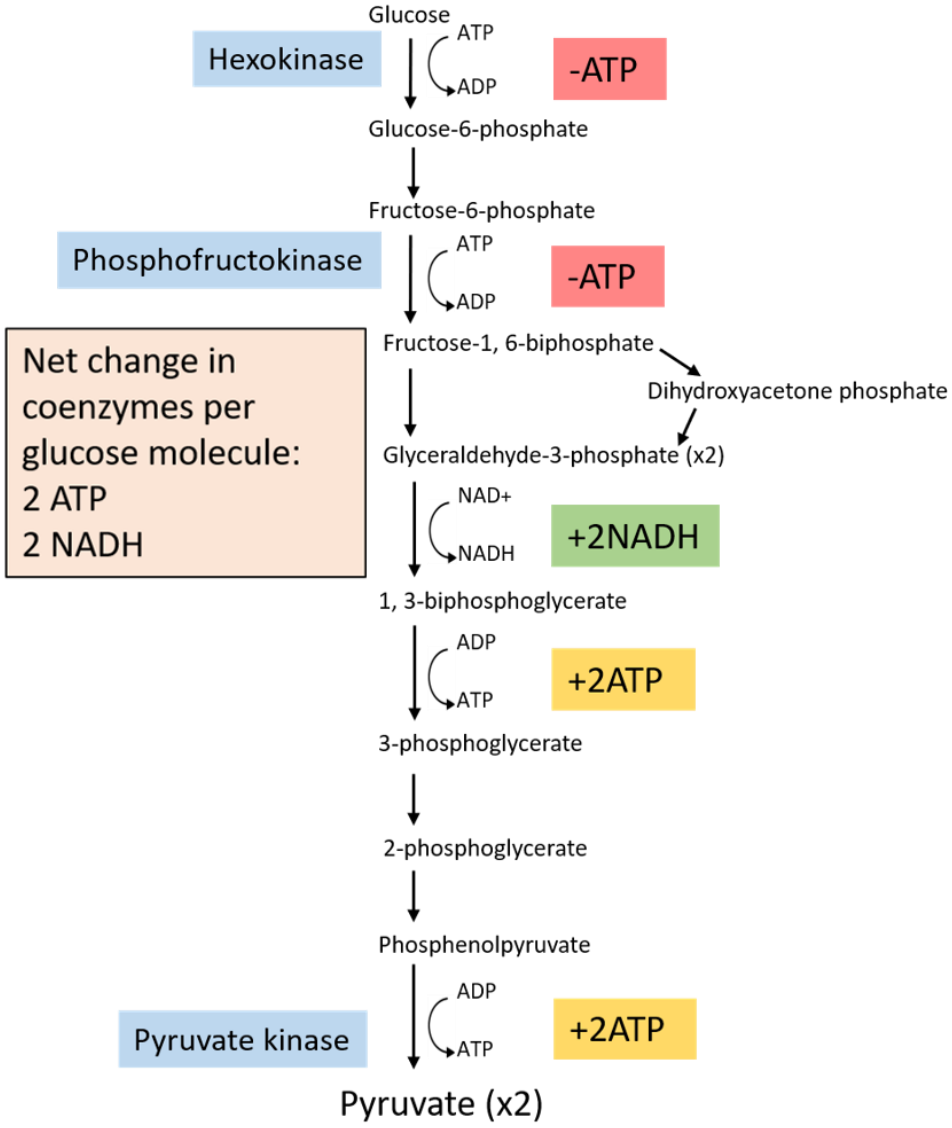

Figure 1.7 Glycolysis pathway. Schematic shows the metabolism of glucose to pyruvate. The process is regulated by three enzymes, hexokinase, phosphofructokinase and pyruvate kinase (blue boxes). The first stage of glycolysis is ATP consuming (red boxes). The second stage of glycolysis produces NADH (green box) and ATP (yellow boxes). Image adapted from Medical Science by Naish, Syndercombe Court and Revest, 2009.

1.8.3 Link Reaction

Pyruvate is transferred into the mitochondrial matrix by mitochondrial pyruvate carriers (McCommis and Finck, 2015). In the matrix, pyruvate is oxidatively decarboxylated, and then combined with Co-enzyme A to form Acetyl-CoA. The link reaction is catalysed by pyruvate dehydrogenase (Figure 1.8), and the link reaction acts as the bridge between glycolysis and the Krebs Cycle. As one molecule of glucose is metabolised to two molecules of pyruvate during glycolysis, the link reaction occurs twice for every glucose molecule. Thus, for every molecule of glucose, 2 Acetyl-CoA molecules, 2 NADH molecules, 2 CO_2 molecules and 2 H^+ are produced. The Acetyl-CoA molecules can then enter the Krebs Cycle. The Link Reaction is regulated by pyruvate dehydrogenase and many factors can affect the activity of this enzyme. Whilst Ca^{2+} and insulin can stimulate pyruvate dehydrogenase activity, high Acetyl-CoA and high NADH can inhibit the activity of it (Naish, Syndercombe Court and Revest, 2009).

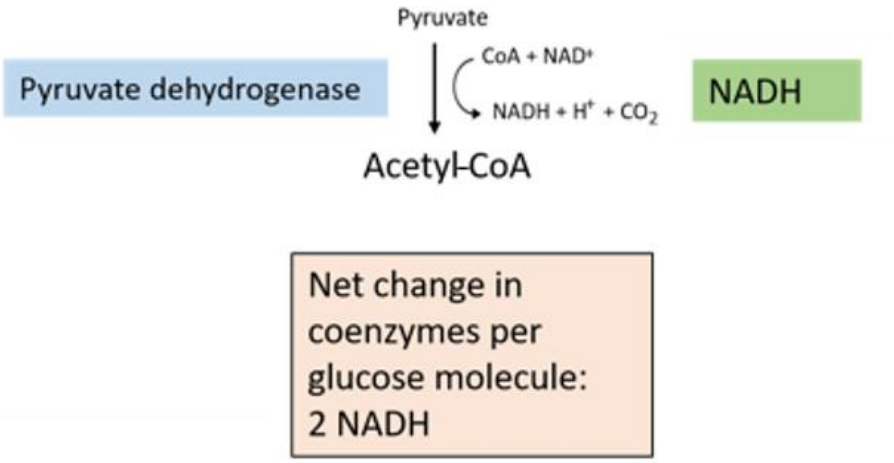

Figure 1.8 Link Reaction pathway. Pyruvate is broken down into Acetyl-CoA. The process is regulated by one enzyme; pyruvate dehydrogenase (blue box). NADH is produced (green box). Image adapted from Medical Science by Naish, Syndercombe Court and Revest, 2009.

1.8.4 The Citric Acid Cycle (TCA cycle) / Krebs Cycle

The TCA cycle is series of enzymatic reactions that occur in the mitochondrial matrix which break down Acetyl-CoA into CO_2 and H_2O and generate the reducing equivalents NADH and $FADH_2$ (Figure 1.9). Citrate synthase first catalyses the reaction of Acetyl-CoA and oxaloacetate, producing citrate. Citrate is then isomerised to isocitrate, which then undergoes dehydrogenation to oxalosuccinate. Oxalosuccinate is decarboxylated to alpha-ketoglutarate, which is oxidatively decarboxylated to Succinyl-CoA by alpha-ketoglutarate dehydrogenase. Succinyl-CoA is converted to succinate, which generates ATP, before succinate dehydrogenase converts succinate to fumarate. Fumarase converts fumarase to malate before oxaloacetate is regenerated by malate dehydrogenase. During these enzymatic reactions, electrons and hydrogen are released to NAD^+ and FAD^+. For every molecule of Acetyl-CoA which enters the Krebs cycle, 2 CO_2, 1 GTP, 3 NADH and 1 $FADH_2$ molecules are formed. Thus, per glucose molecule, 4 CO_2, 2 GTP, 6 NADH and 2 $FADH_2$ are produced. The NADH and $FADH_2$ then enter the ETS, whilst the GTP is converted to ATP. The Krebs Cycle is regulated by the enzymes citrate synthase, isocitrate dehydrogenase and dehydrogenase. Citrate synthase is sensitive to the availability of its substrates, oxaloacetate and Acetyl-CoA, but is also inhibited by ATP and activated by ADP, whilst isocitrate dehydrogenase and dehydrogenase are both sensitive to NAD^+ levels (Naish, Syndercombe Court and Revest, 2009).

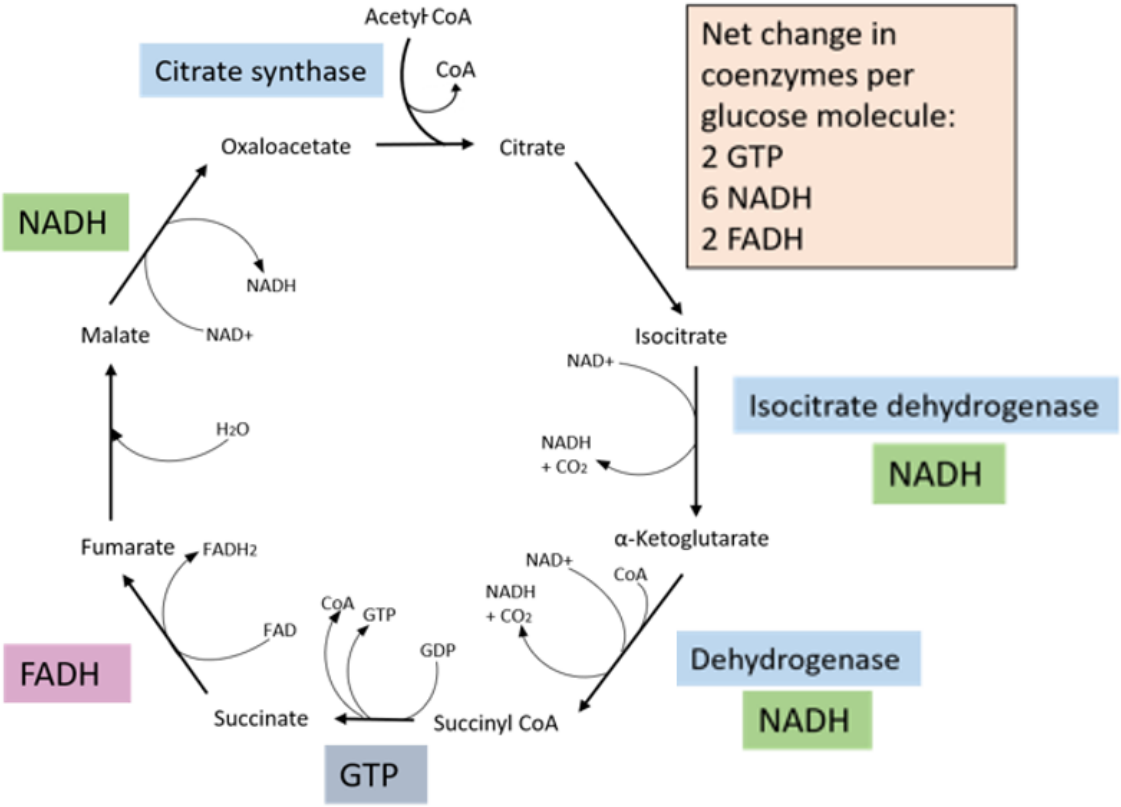

Figure 1.9 The TCA Cycle. Acetyl-CoA is fed into the TCA cycle. The process is regulated by three enzymes; citrate synthase, isocitrate dehydrogenase, and dehydrogenase (blue boxes). NADH (green boxes), GTP (grey box) and FADH (purple box) are produced. Image adapted from Medical Science by Naish, Syndercombe Court and Revest, 2009.

1.8.5 Fatty acid β-oxidation

Fatty acids are highly efficient energy storage molecules and per gram, contain almost twice the amount of energy as carbohydrates. β-oxidation of fatty acids is an oxidative process that occurs in the mitochondrial matrix. It involves the metabolism of fatty acids into Acetyl-CoA (Figure 1.10). Before fatty acids enter the mitochondria, they are conjugated with CoA to form a long-chain fatty-acyl-CoA. This is then modified to acylcarnitine which can pass across the mitochondrial membrane. Before beta oxidation can occur in the matrix, this acylcarnitine is converted back to a long chain Acyl-CoA. Acyl-CoA is then oxidised in a 4-step process (Abcam, no date), as displayed in Figure 1.10. Briefly, this process involved dehydrogenation of Acyl-CoA to Trans-2-Enoyl-CoA, hydration of this molecule to 3-Hydroxyacyl-CoA, dehydrogenation to Beta-Ketoacyl-CoA before finally thiolytic cleavage of this molecule to produce an Acetyl CoA and an Acyl-CoA molecule that is two carbons shorter than the previous one. This Acyl-CoA can re-enter the beta oxidation pathway, and the Acetyl-CoA can then enter the Krebs cycle to provide energy from fats. During the process of β-oxidation, NADH and $FADH_2$ are generated, which then can enter the ETS. The process is regulated by the activity of 4 enzymes; Acyl-CoA dehydrogenase, Enoyl-CoA hydratase, 3-Hydroxyacyl-CoA dehydrogenase and Beta-Ketoacyl-CoA thiolase (Naish, Syndercombe Court and Revest, 2009).

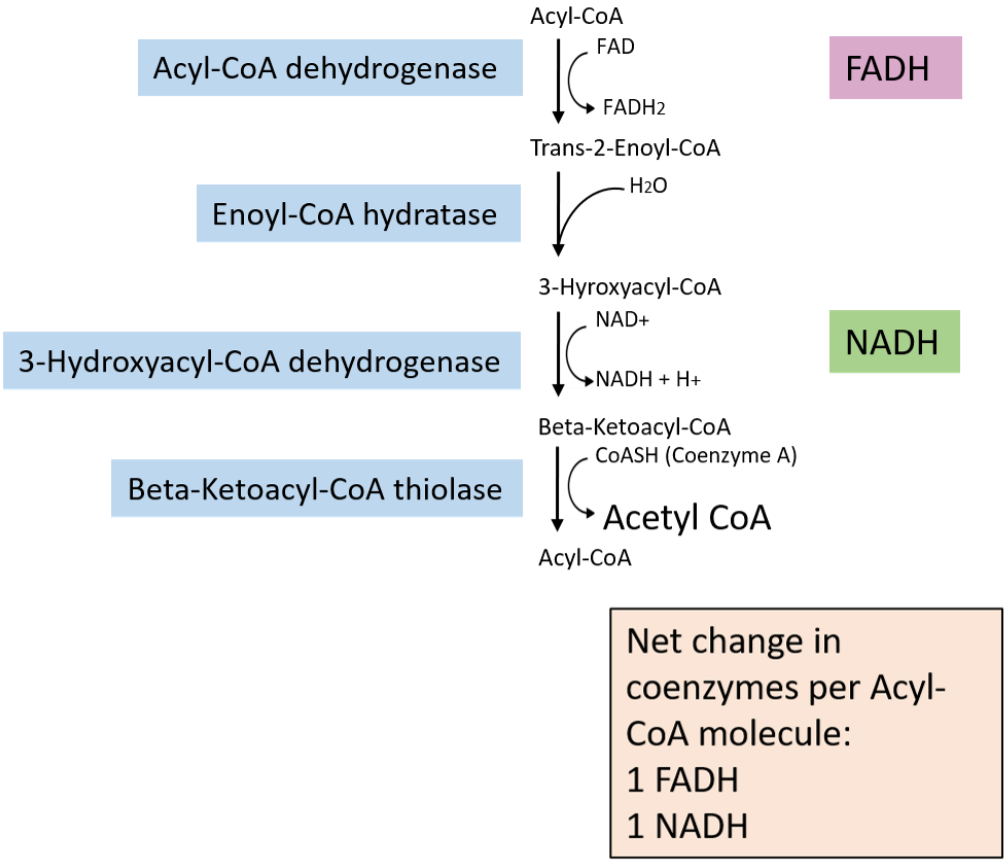

Figure 1.10 The beta oxidation pathway. Acyl-CoA is recycled by beta oxidation. The process is regulated by four enzymes; Acyl-CoA dehydrogenase, Enoyl-CoA hydratase, 3-Hydroxyacyl-CoA dehydrogenase, Beta-Ketoacyl-CoA thiolase (blue boxes). FADH (purple box) and NADH (green box) is produced. Acetyl-CoA is produced at the final stage of beta oxidation. Image adapted from Medical Science by Naish, Syndercombe Court and Revest, 2009.

1.8.6 Amino Acid Metabolism

Under certain conditions, like fasting, amino acids can be used to provide energy. The first step is to remove the amine group from the amino acid, by a process called transamination. In transamination, the amine group is transferred to another amino acid, most commonly alpha ketoglutarate, which forms glutamate. Glutamate can either be used for protein synthesis or in other transamination reactions. Glutamate can also be converted to glutamine, which is transported to the liver to enable removal of ammonium. Ammonium is incorporated into urea in the liver, released into the blood and excreted via the kidneys. After the removal of the amine group from an amino acid the carbon backbone can be converted into different metabolic intermediates, depending on the type of amino acid. There are two main types of

amino acid; glucogenic and ketogenic. Glucogenic amino acids are the more abundant type and are converted to pyruvate or intermediates of the Krebs Cycle, where they serve as precursors to glucogenesis. Ketogenic amino acids are broken down into Acetyl CoA or Acetoacetyl CoA, both which give rise to ketone bodies or fatty acids. Therefore, it is these ketogenic amino acids that can be directly oxidised to release energy. In summary, amino acid catabolism can give rise to pyruvate, Acetyl-CoA or Acetoacetyl CoA and a number of TCA cycle intermediates, thus, amino acids are able to be integrated into energy metabolism (Figure 1.11).

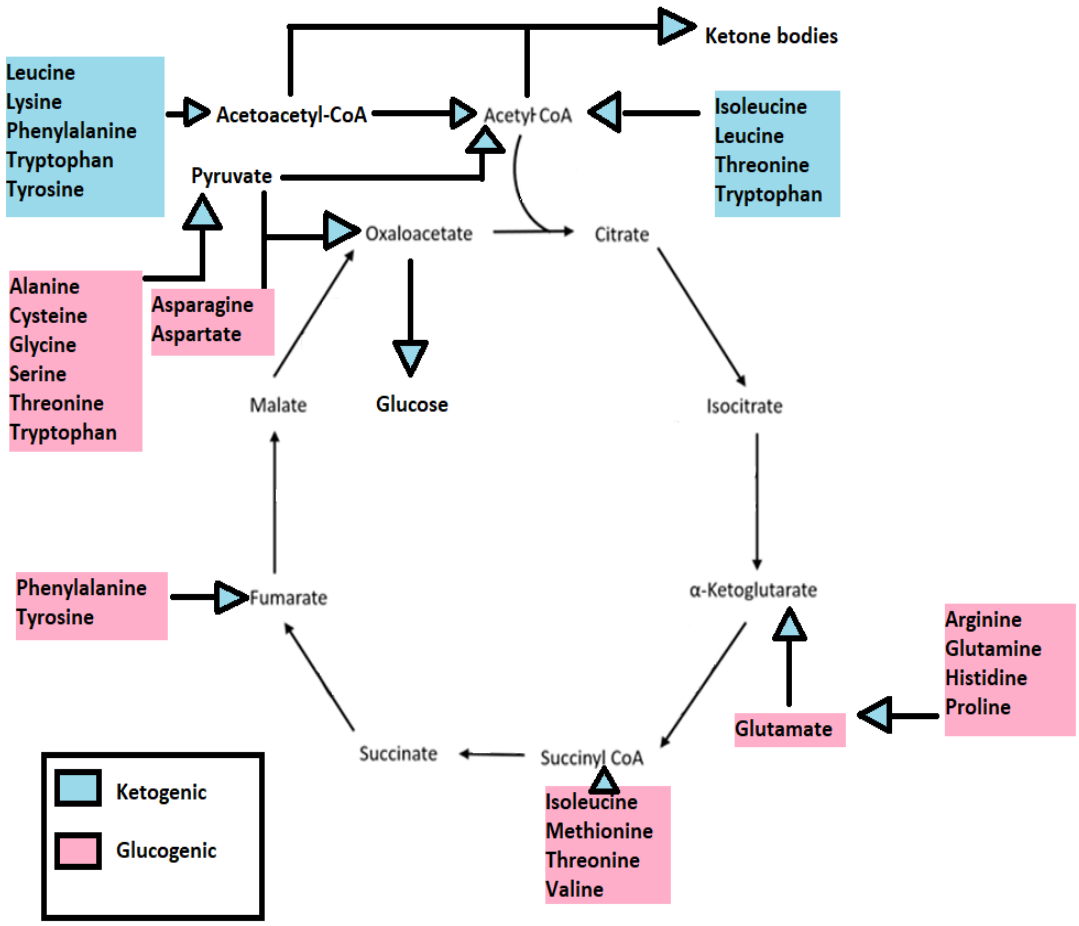

Figure 1.11 Integration of Amino Acids into Energy Metabolism. Diagram shows how both ketogenic (blue boxes) and glucogenic (pink boxes) amino acids are integrated into multiple different stages of energy metabolism.

1.8.7 Integration of Bioenergetic Pathways.

The integration of bioenergetic pathways is summarised in Figure 1.12. Amino acids, glucose and fatty acids are transported across the plasma membrane and into the cytoplasm. Glucose and amino acids can both undergo metabolism to pyruvate, which can enter the Link Reaction and be converted to Acetyl-CoA, which can then enter the TCA cycle. Acetyl Co-A is also generated by amino acids, like leucine, being converted into Acetyl-CoA and also by β-oxidation of Acyl CoA. Some amino acids, like glutamine, can be converted directly into TCA cycle intermediates such as alpha-ketoglutaric acid. Acetyl-CoA and/or the amino acid TCA cycle intermediates then generate reducing equivalents for the ETS, the common ending for all of these metabolic pathways.

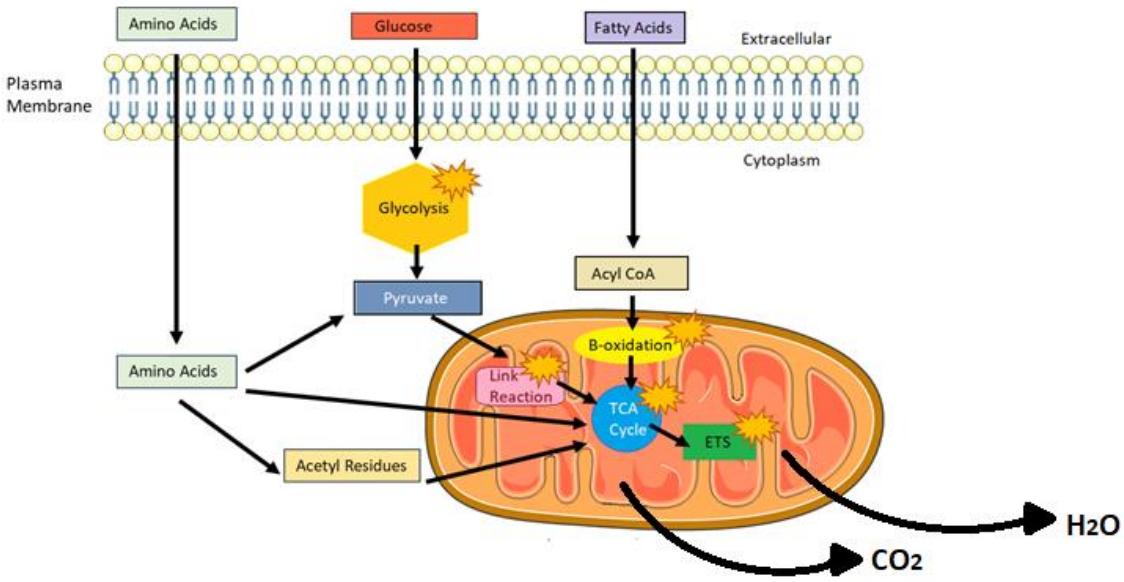

Figure 1.12 Integration of Metabolic Pathways. Diagram showing the metabolism of amino acids, glucose and fatty acids. Amino acids, glucose and fatty acids cross the lipid bilayer and are metabolised, before they enter the mitochondria where they eventually converge in the TCA Cycle and enter the electron transport system. TCA Cycle = the citric acid cycle. ETS = electron transport system. Carbon dioxide (CO_2) and water (H_2O) are the metabolic waste products.

1.9 Additional Mitochondrial Functions

Our canonical understanding of the function of mitochondria is that they are the 'powerhouses of the cell' i.e. their main function is to resynthesise ATP using OXPHOS. However, within the last decade, a new role for mitochondria as key co-ordinators of intracellular signalling has emerged (Antico Arciuch *et al.*, 2009; Chandel, 2015). Mitochondria can regulate biosynthetic, cell signalling, apoptosis, redox and anti-oxidant defence pathways (Herst *et al.*, 2017). These organelles have also been found to contain cell signalling kinases, such as the MAPK ERK, which may maintain the MMP in times of cellular stress in neurons (Lee *et al.*, 2004; Poderoso *et al.*, 2008; Galli *et al.*, 2009), and may also maintain lung tumour cell phenotypes in a ROS dependent manner (Galli *et al.*, 2008). Mitochondrial ERK activation causes nuclear translocation, where information about mitochondrial bioenergetics and redox status is passed to nuclear pathways that control proliferation and differentiation (Antico Arciuch *et al.*, 2009). Thus, these organelles are key metabolic sensors which mediate both cell survival and apoptosis (Chiong *et al.*, 2014).

1.10 Mitochondrial Ion Channels

1.10.1 Overview

Many ion channels are located in the mitochondrial membranes (Szabo and Zoratti, 2014) (Figure 1.13). In the OMM there are channels that regulate apoptosis, such as Bcl-2 family proteins and ANT channels which allow adenine nucleotides to enter and exit the mitochondria. In addition, there are OMM channels that allow proteins to enter and exit the organelle, such as TOM40, and voltage dependent anion channels (VDACs) that allow passage of anions into and out of the mitochondria. These OMM channels all allow for optimal functioning of the mitochondria (Szabo and Zoratti, 2014). In the IMM there are numerous channels selecting for K^+ ions, like the TASK-3, Kv1.3 and calcium activated potassium channels BK_{Ca}, IK_{Ca} and SK_{Ca}, the roles of which will be discussed in more detail in the next section. There are also channels that select for Ca^{2+}, such as the mitochondrial calcium uniporter (MCU) and the ryanodine receptor (RyR), which are thought to be involved in regulating calcium signalling, which has roles in proliferation to apoptosis (Rizzuto *et al.*, 2012). Magnesium (Mg^{2+}) is an

essential component of cells, and the mitochondria facilitate its storage in the matrix via Mg^{2+} selective channels (Mrs2) (Kolisek *et al.*, 2003). In the IMM there are also non-selective anion and cation channels, like the inner membrane anion channel (IMAC) and TIM22 and TIM23, respectively, and the nonselective mitochondrial permeability pore (MPTP), which control cell survival and apoptosis (Szabo and Zoratti, 2014) .There are other mitochondrial proteins which act as ion channels, such as acetylcholine receptors of the OMM, and uncoupling proteins (UCP) and the n-methyl-d-aspartate (NMDA) glutamate receptors of the IMM, which their functions remain a subject of debate (Szabo and Zoratti, 2014). These channels are tightly regulated to avoid disruption to the balance of ions in the mitochondria, and in addition to ion channels there exists a plethora of exchangers and transporters which maintain ionic balance of the mitochondria (Bernardi, 1999).

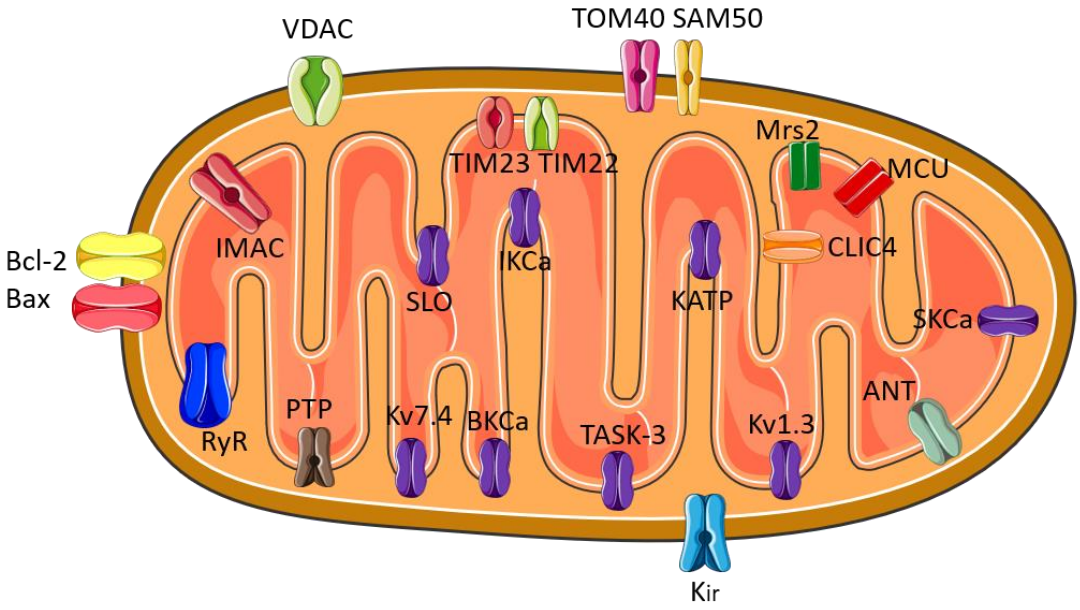

Figure 1.13 Ion channels of the mitochondrial membranes. Outer membrane channels; voltage dependent anion channels (VDAC), inwardly rectifying potassium channels (Kir), protein import pores (TOM40 and SAM50) and Bcl-2 family members (Bcl-2 and Bax). Inner membrane channels; potassium channels (twin pore potassium channel, TASK-3, big, intermediate and small conductance calcium activated potassium channels, BKCa including SLO2, IKCa and SKCa (respectively), voltage gated potassium channels, Kv1.3 and Kv7.4, and ATP regulated potassium channel, KATP), magnesium channels (magnesium permeable channel, Mrs2), calcium channels (ryanodine receptor, RyR, and mitochondrial calcium uniporter, MCU), non-selective cation channels (TIM23 and TIM22), anion selective channels (inner membrane anion channel, IMAC, inner membrane chloride channel, CLIC4), non-selective channels (permeability transition pore, PTP) and inner membrane carriers which act as ion channels (adenine nucleotide translocator, ANT). Image adapted from Szabo and Zoratti (2014).

1.10.2 Limitations to mitochondrial ion channel research

It is important to note that mitochondrial ion channel research is limited by the current techniques on offer to accurately identify mitochondrial ion channels. Western blotting of the mitochondrial membranes for channel proteins is a common technique used to identify ion channels that reside here. However, this approach is often blighted by contamination of the blot by membranes from other organelles. A multifaceted approach also consisting of immunocytochemistry and electrophysiology would be advised for all mitochondrial ion channel research (Szabo and Zoratti, 2014). To confirm ion channels exist in the mitochondrial membranes, molecular identification is needed. Despite modern proteomic technologies, molecular identification is still a challenge as most mitochondrial ion channels are thought to be encoded by the nucleus and do not have an independent organelle specific identity. Proteomics is also hindered by the fact that most ion channels exist in low abundance in most cells making molecular identification even more challenging (Szabo and Zoratti, 2014).

1.11 Mitochondrial K^+ Cycle

1.11.1 Overview

Ion channels tightly regulate mitochondrial H_2O and ion balance to control mitochondrial volume. A high matrix volume would risk rupturing the IMM and OMM, leading to cell death. Increased matrix volume can also alter biochemical pathways of the cell, for example, increase fatty acid oxidation in the matrix (Garlid and Paucek, 2003). In the cytoplasm, the concentration of K^+ is around 120mM. A concentration gradient for K^+ ions exist across the inner mitochondrial membrane, whereby the concentration of K^+ in the mitochondrial matrix is approximately 30% the concentration in the cytoplasm, around 80mM (Nicholls and Ferguson, 2013). This gradient exists due to the mitochondria having a pH gradient of -0.5 because 3x the amount of H^+ is pumped out of the matrix than what comes in (Garlid, 1996). K^+ flow down its concentration gradient into the matrix can increase mitochondrial volume as water would follow the ions, causing the matrix to swell and possibly rupture (Costa *et al.*, 2006). A system must therefore be in place to counterbalance this swelling upon opening of mitochondrial K^+ channels (Garlid, 1996; Garlid and Paucek, 2003). The main exchanger responsible for K^+ removal from the matrix is the H^+/K^+ exchanger, an

electroneutral exchanger which extrudes 1 K^+ ion in exchange for 1 H^+ ion. Activation of the H^+/K^+ exchanger is crucial to maintaining the ionic balance of the matrix. However, the activity of the exchangers, transporters and channels of the IMM are interlinked, and a change in the activity of one is likely to affect the activity of others. Increased activity of the H^+/K^+ exchanger, may increase the H^+ concentration in the matrix stimulating H^+ extrusion mechanisms, for example the leucine zipper- EF hand-containing transmembrane 1 protein, LETM1 (Jiang, Zhao and Clapham, 2009). Influx of K^+ into the matrix may lead to alkalinisation that results from increased proton pumping to compensate for increased K^+ entry through mitochondrial K^+ channels (Costa *et al.*, 2006).

1.11.2 Mitochondrial K^+ channels

K^+ channels exist in both the IMM and OMM and can be active under both physiological and pathophysiological conditions (Bednarczyk *et al.*, 2013). Eight mitochondrial K^+ channels have so far been described, however their functions remain poorly understood. The mitochondrial K^+ channels are the ATP-regulated channel (Smith, Nehrke and Brookes, 2017), calcium-regulated channels of large, intermediate and small conductance (Krabbendam *et al.*, 2018), voltage-regulated Kv1.3 (Szabo and Zoratti, 2014) and Kv7.4 channels (Testai *et al.*, 2015), two-pore-domain TASK-3 channel (Szabo and Zoratti, 2014) and the SLO2 channel (Wojtovich *et al.*, 2011). It is thought the primary role of these ion channels is to maintain the MMP (Garlid and Paucek, 2003). However, there are suggestions that these channels regulate respiration, mitochondrial volume and ROS production (Laskowski *et al.*, 2016) and may even act as biological sensors of gasotransmitters (Walewska, Szewczyk and Koprowski, 2018).

1.11.2.2 Mitochondrial Kv1.3

The role of mitochondrial Kv1.3 channels in physiological conditions has not been explored in detail, despite plasma membrane (PM) Kv1.3 channels being implicated in energy homeostasis and body weight regulation (Xu *et al.*, 2003; Tucker, Overton and Fadool, 2008). Under physiological conditions, the channel is expected to allow inward flux of K^+ into the matrix, as long as a gradient exists for its entry (Bernardi, 1999). Along with other K^+ channels, it is thought that mitochondrial Kv1.3 could regulate

MMP, matrix volume and ROS production (Laskowski *et al.*, 2016). However, the channel has been implicated in the apoptosis of lymphocytes and cancer cell lines (Szabo *et al.*, 2005; Szabó *et al.*, 2008; Leanza *et al.*, 2017; Venturini *et al.*, 2017; Mattarei *et al.*, 2018). Mitochondrial Kv1.3 channels can interact with the apoptotic protein Bax to induce apoptosis (Szabó *et al.*, 2008). Bax independent mechanisms of apoptosis can also occur, whereby inhibiton of mitochondrial Kv1.3 channels causes MMP hyperpolarisation, and an increase in ROS, which activates the MPTP causing depolarisation and a fatal release of cytochrome c (Szabo and Zoratti, 2014). Therefore, the channel may be cytoprotective in tumour cells where mitochondrial Kv1.3 controls apoptosis, via a reactive oxygen species mediated pathway (Gulbins *et al.*, 2010; Malinska, Mirandola and Kunz, 2010; Leanza *et al.*, 2012; L Leanza *et al.*, 2013).When mitochondrial Kv1.3 inhibitors were used at lower concentrations, apoptosis did not occur in pancreatic ductal adenocarcinoma cells (PDACs), and proliferation was slightly stimulated (Peruzzo *et al.*, 2017). However, the opposite effect was seen in a colon cancer cell line, COLO357 cells, where proliferation was reduced (Peruzzo *et al.*, 2017). This suggests a cell specific effect of mitochondrial Kv1.3 on proliferation. As inhibition of K^+ flow through mitochondrial Kv1.3 can result in apoptosis and in some circumstances reduced proliferation, mitochondrial K^+ flow likely plays an important role in cellular homeostasis and survival. Studies investigating the role of Kv1.3 in OXPHOS are limited. In 2014, no role was found for Kv1.3 in spontaneous cellular respiration of mouse skeletal muscle cells, as inhibition of these cells with PAP-1, Psora-4 and MgTx did not change the O_2 uptake of these cells (Hamilton et al., 2014). However, MgTx would not inhibit mitochondrial Kv1.3 channels, as only PAP-1 and Psora 4 are membrane permeable, albeit not mitochondrially targeted. This study also did not interrogate the contributions of glycolysis and OXPHOS to spontaneous cellular respiration. Therefore, we cannot exclude a role for mitochondrial Kv1.3 channels in respiration.

1.11.3 Mitochondrial K^+ Flow and Respiration

K^+ influx through other mitochondrial K^+ channels can affect respiration. K^+ influx into the mitochondria stimulates respiration without uncoupling the ETS from OXPHOS (Bajgar *et al.*, 2001; Kowaltowski *et al.*, 2001; Garlid *et al.*, 2003). The mitoK_{ATP} channel increases K^+ influx into the mitochondria causing a depolarisation of the MMP, which is

counterbalanced by an increased respiration rate, and more H^+ pumping into the IMS (Manon *et al.*, 1995). This did not lead to matrix alkalinisation because Pi/H^+ and H^+/ K^+ exchangers brought more H^+ into the matrix. In this study Manon *et al*. found that although matrix pH did not change, the rate of the H^+ proton cycle did. There are other reports of K^+ influx into the mitochondria stimulating respiration. Mitochondrial K_{ATP} channel openers have been found to increase respiration (Malinska, Mirandola and Kunz, 2010). Diazoxide and pinacidil, K_{ATP} openers, also increase the rate of O_2 consumption in a K^+ flow dependent manner (Kopustinskiene, Pollesello and Saris, 2004; Kopustinskiene *et al.*, 2010). K^+ influx into the matrix through other K^+ channels can also stimulate respiration. Heinen et al. observed that activation of BK_{Ca} channels changed mitochondrial bioenergetics, increased respiration and stimulated superoxide production due to K^+ influx into the matrix (Heinen *et al.*, 2007). However, the MMP was maintained due to activation of the K^+/H^+ exchanger. High concentrations of channel openers caused MMP depolarisation via K^+ flow into the matrix through BK_{Ca} channels (Heinen *et al.*, 2007). In additon, energetic performance is improved by specific activation of K^+ fluxes through K_{Ca} channels in heart mitochondria (Aon *et al.*, 2010). The control of respiration may result from a structural and functional coupling of BK_{Ca} channels to respiratory complexes of the ETS (Bednarczyk *et al.*, 2013).

1.11.4 Mitochondrial K^+ Flow and Cytoprotection

In addition to the cytoprotective roles of mitochondrial Kv1.3 channels previously mentioned (1.11.2.2), mitochondrial K^+ influx through other channels, like K_{ATP} and $BK_{Ca,}$ may also be cytoprotective, supporting a physiological role for K^+ entry into the mitochondrial matrix (Kang *et al.*, 2007; Sakamoto *et al.*, 2008; Malinska, Mirandola and Kunz, 2010). K^+ influx into the matrix causes partial depolarisation of the IMM which reduces the driving force for Ca^{2+} influx and therefore prevents triggering of the MPTP (Kang *et al.*, 2007; Sakamoto *et al.*, 2008). Activation of the BK_{Ca} channels has also been found to reduce ROS, regulate mitochondrial volume and improve mitochondrial respiratory control (Kang *et al.*, 2007). In addition, K^+ influx into the matrix through SK_{Ca} prevents mitochondrial dysfunction (Dolga *et al.*, 2013). However, the cytoprotective roles of K^+ influx into the matrix are not definitive. Sassi et al., found that mitochondrial IK_{Ca} had no effect on cell proliferation or cell death (Sassi *et al.*, 2010). There are contrasting reports of whether K^+ influx into the matrix alters the

MMP (Manon *et al.*, 1995; Heinen *et al.*, 2007; Kang *et al.*, 2007). The effect on MMP is likely to depend on the expression of mitochondrial K^+ channels and thus the size of the resulting influx of K^+ into the matrix (Heinen *et al*., 2007).

1.12 Metabolism and Proliferation

1.12.1 Role of Kv1.3 in Metabolism

The metabolic role for *mitochondrial* Kv1.3 channels in physiological situations remains poorly defined. However, Kv1.3 channels *in general*, have been linked to metabolic homeostasis, but these effects cannot be attributed to Kv1.3 channels at any particular location in the cell. For example, Kv1.3 channels have been implicated in regulating body weight and energy homeostasis in mice, as Kv1.3 KO animals had a higher metabolic rate, as measured by indirect calorimetry, and lower body weight to their WT counterparts (Xu *et al.*, 2003). Genetic abolition of Kv1.3 channels in mice also sensitised adipose tissue and skeletal muscle to insulin, and increased expression of GLUT4 at the plasma membrane (Xu *et al.*, 2004). Pharmacological inhibition of PM Kv1.3 channel with ShK-186 counteracted the negative effects of an obesity promoting diet in mice by reducing weight gain, adiposity, fatty liver, blood levels of cholesterol, glucose, insulin and leptin and enhanced peripheral insulin sensitivity, leading the researchers to conclude Kv1.3 blockade could be a potential therapy for insulin resistance and obesity (Upadhyay *et al.*, 2013). In addition, genetic identification of Kv1.3 channels in human samples found a variant in the promoter region of the Kv1.3 gene that was associated with impaired glucose tolerance and insulin sensitivity (Tschritter *et al.*, 2006). KO Kv1.3 in melanocortin null receptor 4 mice reduced weight and adiposity due to increased locomotor activity and energy expenditure (Tucker, Overton and Fadool, 2008). In 2013, Tucker *et al*. went on to declare Kv1.3 channels were ‘metabolic sensors’ in mitral cells, after finding that they were a substrate for phosphorylation by insulin (Tucker *et al.*, 2013). In the same study the authors showed that the Kv1.3 channels themselves were sensitive to metabolically active D-glucose which increased Kv1.3 current amplitude in HEK293 cells (Tucker *et al.*, 2013). These results indicate that Kv1.3 may sense energy status to activate sensory neurons governing smell or sight. It also indicates that Kv1.3 channels in other areas of the body may also sense energy status. Co-localisation of Kv1.3 channels and GLUT4 has been

found in the PM OF mouse olfactory bulbs (Kovach *et al.*, 2016), suggesting this association, or association of Kv1.3 and other GLUT transporters, may occur in other cell types.

However, in other studies no observation was made of Kv1.3 affecting weight gain and adiposity as long term treatments of rats with the plasma membrane Kv1.3 inhibitor Vm24 had no effect on body weight, adiposity and serum glucose levels, but did reduce serum insulin concentration and increase GLUT4 mobilisation to the PM (Jaimes-Hoy *et al.*, 2017). In addition, in another study Kv1.3 channels in human and mouse tissues were found to be insensitive to insulin (Straub *et al.*, 2011). In addition, there are contradictory studies describing inhibition as opposed to activation of mitral cell Kv1.3 channels due to insulin dependent tyrosine phosphorylation (Fadool *et al.*, 1997, 2000; Fadool and Levitan, 1998; Marks and Fadool, 2007). Therefore, the effects of Kv1.3 on metabolism are likely to be tissue specific, and no study to date has explored the specific role of mitochondrial Kv1.3 channels in metabolism.

Kv1.3 channels have also been linked to mitochondrial structure and expression. Kv1.3 channels were found to increase mitochondrial biogenesis in T lymphocytes (DeCoursey *et al.*, 1984). Deletion of Kv1.3 channels was found to alter mitochondrial morphology, resulting in smaller mitochondria, in mice olfactory bulbs (Kovach *et al.*, 2016). In addition, blockade of Kv1.3 channels with a targeted mitochondrial inhibitor caused mitochondrial swelling in cancer cells (Mattarei *et al.*, 2018).

1.12.2 Proliferation linked to metabolism

Cellular proliferation has a high energy demand as ATP is required for processes like signal transduction, as well as DNA, RNA and protein synthesis (Lodish H, Berk A, Zipursky SL, Matsudaira P, Baltimore D, 2000; Vander Heiden, Cantley and Thompson, 2009; Oronsky *et al.*, 2014; Pontes, Sevostyanova and Groisman, 2015). Cancer cells are characterised by a highly proliferative and migratory phenotype and upregulate certain bioenergetic metabolic pathways. Increased glucose uptake , glycolysis and lactate production in the presence of adequate cellular O_2 levels, is well described in cancer biology and is known as aerobic glycolysis, or the Warburg Effect (Warburg, 1925; Kroemer and Poussegur, 2008). There are suggestions that the increase in glycolysis is to maximise the synthesis of macromolecules needed for growth and

proliferation (Vander Heiden, Cantley and Thompson, 2009). However, highly proliferating cells may also retain, and in some circumstances also upregulate, their capacity for OXPHOS (Jose, Bellance and Rossignol, 2011; Ho *et al.*, 2012; Robinson *et al.*, 2012; Gentric, Mieulet and Mechta-Grigoriou, 2017; Liberti and Locasale, 2016)) .The metabolic flexibility demonstrated by highly proliferating cells may help them adapt to a changing nutrient environment (Ho *et al.*, 2012; Robinson *et al.*, 2012; Lu *et al.*, 2015). This may explain why inhibition of glycolysis is unable to slow the proliferation of cancer cells, as they can switch to OXPHOS to meet energy demand (Robinson *et al.*, 2012).

High ROS production is also a characteristic of rapidly proliferating cells (Trachootham *et al.*, 2008) and could be a consequence of electron leak from increased OXPHOS (Griffiths and Rutter, 2009; Vinnakota, Dash and Beard, 2011; Doonan *et al.*, 2014). An increased MMP is also common amongst cells with high energy demands (Summerhayes *et al.*, 1982; Fantin *et al.*, 2002; Heerdt, Houston and Augenlicht, 2005; Houston, Augenlicht and Heerdt, 2011; Forrest, 2015; Martinez-Reyes *et al.*, 2016). The increased electrical gradient increases the driving force for proton re-entry into the matrix, via the ATPsynthase. In addition, the larger the MMP the more resistant cells are to apoptosis (Zamzami *et al.*, 1996). However, a hyperpolarised IMM may not always translate to increased OXPHOS, as in pulmonary artery hypertension where SMCs switch to a proliferative state, the SMCs exhibit IMM hyperpolarisation, but have reduced respiration and increased glycolysis (Dromparis and Michelakis, 2013). The factors leading to the differences in MMP between highly proliferating pathophysiological cancer cells and their physiological counterparts remains unclear (Kalyanaraman *et al.*, 2017). One theory is that in cancer cells, aerobic glycolysis causes IMM hyperpolarisation, due to reverse proton pumping of the ATP synthase (Forrest, 2015). In addition, MMP is linked to the availability of substrates that enter the mitochondria for oxidation, thus an increase in glycolysis can increase MMP (Poulsen *et al.*, 2008; Olsen *et al.*, 2009). In addition, ATP from glycolysis can also maintain MMP and prevent apoptotic cell death in activated macrophages (Garedew, Henderson and Moncada, 2010).

1.12.3 Proliferation and metabolism of VSMCs

Mitochondria are highly expressed in VSMCs, providing energy for contraction (Kuznetsov *et al.*, 2009). Mitochondrial metabolism in VSMCs is now recognised as having a key role in cell growth and proliferation (Salabei and Hill, 2013). There is evidence to suggest that control of mitochondrial metabolism may regulate pathological proliferation of VSMCs, as mitochondrial dysfunction is a key determining VSMC phenotype (Chiong *et al.*, 2014). Healthy VSMCs display high rates of glucose metabolism and lactate production under normal and well oxygenated conditions (Butler and Siegman, 1985), resulting in around 90% of the flux through glycolysis resulting in lactate production. It is thought in healthy VSMCs, only 30% of ATP produced is from mitochondrial processes (Paul, 1983). Despite this, damage to VSMC mitochondrial DNA and VSMC mitochondrial dysfunction is thought to occur in atherosclerosis (Yu and Bennett, 2014). In a similar way to the Warburg effect in cancer cells, VSMCs may rewire their metabolic pathways; reducing mitochondrial metabolism, but increasing fatty acid oxidation and glycolysis, to provide biosynthetic molecules to support proliferation, such as NADPH, nucleotides, phospholipids, sugars and amino acids (Vander Heiden, Cantley and Thompson, 2009; Moncada, Higgs and Colombo, 2012; Salabei and Hill, 2013). However, there is also evidence that VSMCs can increase mitochondrial activity when proliferating (Moncada, Higgs and Colombo, 2012). When ATP is in high demand, mitochondrial pyruvate dehydrogenase activity is increased, which increases the delivery of glycolytic substrates to the mitochondria (Sharma *et al.*, 2005). In support of increased mitochondrial activity in proliferating VSMCs, in response to growth stimulation by PDGF, VSMCs have increased glycolysis and OXPHOS (Perez *et al.*, 2010).

There is a link between mitochondrial morphology and respiratory states, with high O_2 consumption and mitochondrial respiration occurring in elongated mitochondria that have undergone fusion (Parra *et al.*, 2008, 2011; Kuzmicic *et al.*, 2011), whilst oxidative capacity is reduced in fragmented mitochondria (Chen *et al.*, 2003). Fusion and fission may indeed regulate proliferation and differentiation (Mitra, 2013). When VSMC are proliferating, their mitochondria are dynamic and fragmented (Bonnet *et al.*, 2006; Marsboom *et al.*, 2012; Susan *et al.*, 2012; Salabei and Hill, 2013), suggesting that glycolytic metabolism may be dominant over mitochondrial respiration (Marsboom *et*

al., 2012). However, Salabei and Hill, found that glycolytic metabolism decreased when VSMCs underwent phenotypic switching (Salabei and Hill, 2013). Although this seems contradictory, if glycolysis was still a dominant bioenergetic pathway, the mitochondria may still exhibit fragmentation. Fatty acid oxidation may increase in proliferating VSMCs to increase production of ATP as oxidation of one lipid molecule generates more ATP than oxidation of one carbohydrate molecule, thus providing more energy for proliferation (Salabei and Hill, 2013).

Although the contribution of OXPHOS to proliferating VSMCs is not conclusive across all studies, an increased level of ROS among proliferating VSMCs suggests it is an active bioenergetic process in these cells (Mercer *et al.*, 2012). Alterations in ROS are commonly seen in atherosclerosis, which further damage the vascular environment (Mercer *et al.*, 2012). ROS can lead to lipid peroxidation, and damage to mitochondrial DNA which could lead to mitochondrial dysfunction which may lead to further deterioration of metabolic pathways (Ballinger, 2005; Nissanka and Moraes, 2018).

1.13 Aims and Objectives

1.13.1 Aims

VSMCs exhibit Kv1.3 upregulation and activation during the phenotypic switch that results in pathological proliferation, migration and de-differentiation in many vasculopathies associated with CVD. Multiple mechanisms which govern Kv1.3-induced VSMC proliferation have been proposed but the mechanisms remain unclear. Finding the mechanism that drives Kv1.3-induced proliferation of VSMCs is of clinical importance as new therapies are needed to improve outcomes for those with CVD. This thesis will explore whether mitochondrial Kv1.3 regulates cellular energy production, and thus links Kv1.3 to the proliferative state of the cell through adaptation of mitochondrial OXPHOS. By targeting therapies, such as Kv1.3 inhibitors, to cellular organelles where the channels may have a key role, such as the mitochondria, pharmacological treatments may become more effective and specific with fewer side effects.

1.13.2 Objectives

- Determine the bioenergetic and structural effects on the mitochondria of overexpressing Kv1.3 channels in HEK293 cells and identify intracellular localisation of Kv1.3 channels (Chapter Three).

- Determine the role of mitochondrial Kv1.3 in the respiratory phenotype regulated by Kv1.3 in HEK293 cells (Chapter Four).

- Define the mechanism/s through which mitochondrial Kv1.3 regulate and link cellular oxidative metabolism and proliferation (Chapter Five).

- Determine ion-conduction independent effects of Kv1.3 channel on oxidative metabolism using Kv1.3 mutant channels (Chapter Six).

Chapter Two

Methods and Materials

2.1 Cell Culture

Sterile plasticware was purchased from Corning (Corning Ltd, Flintshire, UK) or Star Labs (Star Labs, Surrey, UK). All reagents were obtained from Gibco (Life Technologies, Paisley, UK) or Sigma (Sigma Aldrich, Dorset, UK) unless otherwise stated.

2.1.1 WT HEK293 cells

Wild-type (WT) HEK293 cells were obtained from ECACC, Public Health England, Porton Down, UK. Culture medium contained: DMEM, 10% (v/v) fetal bovine serum (BioSera, East Sussex, UK), 1% (v/v) Antibiotic/ Antimycotic, 1% (v/v) Non-Essential Amino Acids, 0.1% (v/v) Gentamicin (50mg/ml). All cells were grown in 75cm^2 flasks and sub-cultured each week once 70-90% confluence was reached. Culture medium was removed from the flask, and the cells washed with 10ml of Dulbecco's phosphate buffered saline (DPBS). Cells were then incubated with 2ml of 0.05% TrypleE Express for 2-3 minutes (37^{o}C; 95% air, 5% CO_2). The side of the flasks were then gently tapped to ensure full cell detachment. 10ml of complete growth media was added to neutralise the trypsin, and the resulting cell suspension was placed in a 50ml falcon tube. This was then centrifuged for 6 minutes at 600g (rcf) in an Eppendorf Centrifuge 5424 (Eppendorf UK Ltd, Stevenage, UK). The supernatant was removed, and the cells were resuspended in 1ml of culture media. Live cells were then counted using 0.4% Trypan Blue to stain for dead/dying cells and a Bio-Rad automated TC10 cell counter (Bio-Rad Laboratories, California, USA). Various dilutions of cells were used, normally 1:10, 1:20, 1:40 and 1:80 (cells: medium), with 20ml being the final flask volume (75cm^3 flasks). The flasks were then placed into a humidified incubator to grow (37^{o}C; 95% air, 5% CO_2). If a low dilution of cells had been plated, and confluency was to be expected the following week, then after 4 days a media change would occur.

2.1.2 HEK293/Kv1.3 cells

HEK293 cells engineered to overexpress the mouse Kv1.3 channel were a gift from José Ramón López López and colleagues, University of Valladolid, Spain. Stable transfection was carried out by Dr Jason Scragg, University of Leeds, UK. Culture medium was the same as WT HEK293 cells but with the addition of 0.4mg/ml Geneticin Sulphate G418 (Santa Cruz Biotechnology) dissolved in 200µl 1M NaOH. Cells were used between passages 3 and 18 and sub-cultured using the same method as WT HEK293 cells.

2.1.3 HEK293/Kv1.3-P118 cells

These are HEK293 cells engineered to express human Kv1.3 channels tagged with mCherry fluorescent protein (P118). The DNA encoding this protein was again a gift from José Ramón López López, as above. Culture medium and culturing method were the same as HEK293/Kv1.3 cells.

2.1.4 HEK293/Kv1.3 mutant cells (P89, P93 and P121)

HEK293 cells were engineered to express mutated human Kv1.3 channels tagged with either mCherry (P121) or GFP (P89, P93). The DNA encoding these proteins were gifts from José Ramón López López, as above. Culture medium and culturing method were the same as HEK293/Kv1.3 cells.

2.1.5 HEK293/Kv1.5 cells

HEK293 cells were engineered to overexpress the human Kv1.5 (KCNA5) channel. Human Kv1.5 cDNA was amplified from a human foetal brain cDNA library (Clontech, Wooburn Green, Buckinghamshire, UK) using PCR, and transfected into HEK293 cells, as previously described (Al-Owais *et al.*, 2017). Stable transfection was carried out by Dr M. Al-Owais, University of Leeds, UK. Culture medium was the same as WT HEK293 cells but with the addition of 4.5µg/ml blasticidin. Cells were used between passages 3 and 18 and cultured using the same method as WT HEK293 cells.

2.1.6 Human Saphenous Vein Smooth Muscle Cells (HSVSMCs)

These cells were obtained from saphenous vein (SV) of patients undergoing coronary artery bypass graft surgery at Leeds General Infirmary, with consent and ethical approval. Patient demographics are shown in Table 2.1. Culture medium contained:

DMEM, 10% (v/v) fetal bovine serum (BioSera, East Sussex, UK), 1% (v/v) glutamine (200mM,), 1% (v/v) penicillin/streptomycin ((5,000 U/mL)). Cells were used between passages 3 and 6. Cells were isolated using the well-established protocol of Dr Karen Porter, University of Leeds, UK (Porter *et al.*, 2002). Briefly, segments of SV were taken from patients and chopped into small fragments ($1mm^3$). These explants were placed in 2ml of Roswell Park Memorial Institute medium supplemented with 10% FCS, in a $25cm^3$ culture flask. The cells were left for 4-5 weeks in a humidified incubator (37^oC; 95% air, 5% CO_2) so that the cells could migrate out of the explants and become confluent. Passage of the cells into normal $T75cm^3$ culture flasks then ensued. Cells were cultured in the same way as HEK293 cells. However, due to their slower rate of growth, the flasks were seeded with higher concentrations of cells i.e. ratios of 1:10 and 1:20 (cells: medium), with 20ml being the final flask volume. Media was changed twice weekly.

Patient ID	Gender	Age at surgery (yrs)	Diabetes (Y/N)
1318	M	47	N
1321	M	44	N
1322	F	67	N
1330	M	47	N
1335	M	56	N
1336	M	66	N
1337	M	74	N
1339	M	61	N
1340	M	64	N
1341	M	72	N
1344	M	67	N
1349	M	69	N
1353	M	74	Y
1354	M	72	Y
1356	Unknown	Unknown	Unknown
1358	M	61	N
1359	M	61	Y

Table 2.1 Patient demographics for human SV cells. Data for gender, age at surgery and diabetic status is shown for all patients apart from SV1356. M = male, F = female, yrs = years, Y = yes, N = no.

2.2 Generation of the HEK293/Kv1.3 mutant clones

All reagents were obtained from Sigma (Sigma Aldrich, Dorset, UK) unless otherwise stated.

2.2.1 Generation of Luria-Bertani (LB) agar plates

LB agar was prepared by adding kanamycin (30 µg/ml final concentration) into autoclaved 3.5% LB agar. 20ml of agar solution was poured into each 60 x 15mm petri dish and then left to set for 40 minutes. They were then turned over for a further 40 minutes to allow excess moisture to drip off the agar. Each plate then had its edge sealed with paraffin paper and was stacked into columns whilst remaining upside down. These columns were then covered with foil and left in the fridge overnight. The following morning the foil and parafilm were removed and the plates placed in a pre-warmed oven at 37 ºC for 1 hour.

2.2.2 DNA retrieval

Filter paper carrying 2µg bacteria containing the DNA constructs for mutated Kv1.3 channels were placed in 200µl distilled water to retrieve around 10ng/µl DNA. This was stored at -20ºC. The DNA encoded four types of K^+ channel:

Kv1.3-P118: Wild type human Kv1.3 channels with mCherry fluorescent tag. mCherry excitation (nm)/ emission (nm) wavelengths were 587/610.

Kv1.3-P121: Human Kv1.3 channels with intact pore regions, and intact voltage sensors, but with defective phosphorylation due to a point mutation from tyrosine to alanine at position 447 on the C-terminus of the channel. These channels were also tagged with fluorescent mCherry.

Kv1.3-P89: Mouse Kv1.3 channels, with mutated pores, intact voltage sensors and intact C-terminals, tagged with EGFP (enhanced green fluorescent protein). EGFP excitation (nm)/ emission (nm) wavelengths were 488/507.

Kv1.3-P93: Mouse Kv1.3 channels with mutated pores and mutated voltage sensors, tagged with EGFP.

2.2.3 Generation of Kv1.3 mutant plasmids

Generation of Kv1.3 mutant plasmids was carried out by José Ramón López López et al., University of Valladolid, Spain. Data in sections 2.2.3.1 and 2.2.3.2, Tables 2.2 and 2.3, and Figures 2.1 and 2.2, was sourced from the López López group.

2.2.3.1 Plasmid generation

Information on the plasmids used for each of the mutant channels is summarised in Table 2.2, and the plasmid maps are shown in Figure 2.1. KCNA3 cDNA was cloned into the MCS region of both pEGFP-N3 and pmCherry-N1 (Figures 2.1A and 2.1B, respectively). The primer pairs used are shown in the final column of Table 2.2. This generated C-terminal EGFP (Kv1.3-P89 and Kv1.3-P93) and mCherry (Kv1.3-P121 and Kv1.3-p118) fusion proteins (Figures 2.1C and 2.1D, respectively), which were sequence verified.

Mutant Kv1.3 Channel	Original Plasmid	Type of Kv1.3 (KCNA3) cDNA	Fusion Protein Plasmid	Primer Sequence (5' to 3') (forward and reverse)
Kv1.3-P89 and Kv1.3-P93	pEGFP-N3	mKv1.3	pEGFP-N3-mKv1.3	5'-ATC**GAATTC**AGACATGACCGTGGTG-3' 5'-CA**GAATTC**TGGACATCAGTGAATATCTTCTTGA-3'
Kv1.3-P121 and Kv1.3-P118 (WT)	pmCherry-N1	hKv1.3	pmCherry-N1-hKv1.3	5'-AAT**GAATTC**CCGACATGACCGTGGTGCC-3' 5'- ATT**GGATCC**ACATCGGTGAATATCTTTTTGATG -3'

Table 2.2 Plasmids for mutant Kv1.3 channels. Table showing the plasmids used for each mutant Kv1.3 cell type, the type of Kv1.3 channel (mKv1.3 = mouse Kv1.3 (Source Bioscience), hKv1.3 = human Kv1.3 (MagNA Pure Systems, Roche)), the fusion plasmid generated, and the primer sequence used for their generation. All plasmids were sourced from Clontech.

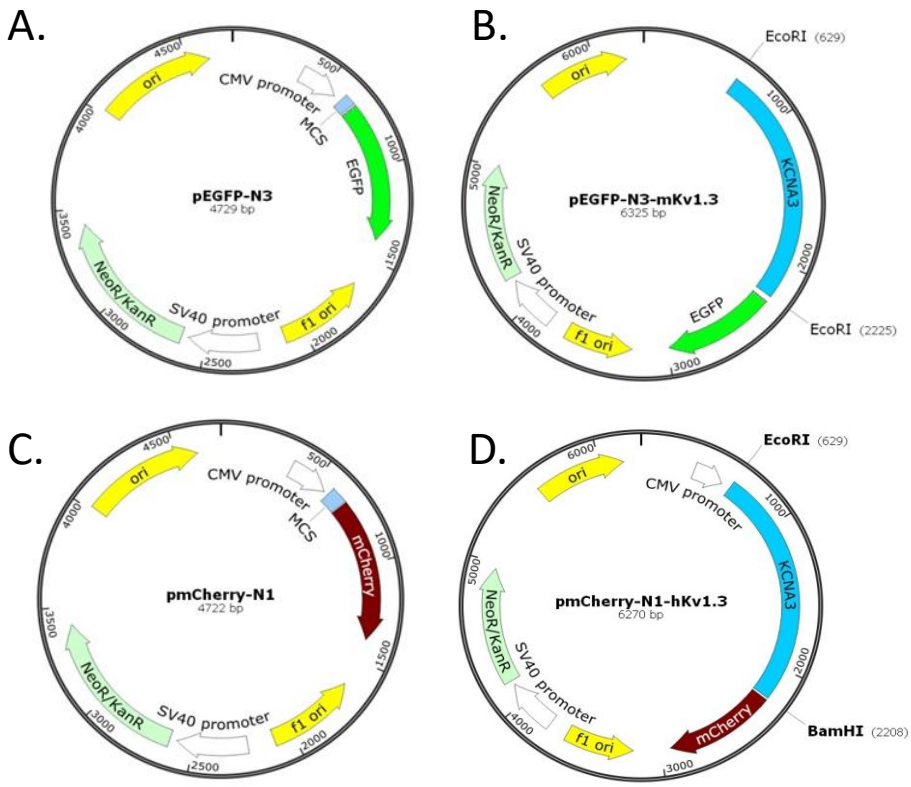

Figure 2.1 Plasmid maps for mutant Kv1.3 channels. A. Original pEGP-N3 plasmid, note the MCS region between the CMV promoter and the EGFP. B. pEGP-N3 plasmid with the insertion of mKv1.3 (KCNA3) at the MCS region (pEGP-N3-mKv1.3). C. Original pmCherry-N1 plasmid, note the MCS region between the CMV promoter and the mCherry. D. pmCherry-N1 plasmid with the insertion of hKv1.3 (KCNA3) at the MCS region (pmCherry-N1-hKv1.3).

2.2.3.2 Kv1.3 channel mutations

QuikChange II Site Directed Mutagenesis Kits (Stratagene) were used for mutagenesis of the Kv1.3 channel. Mutagenesis was carried out according to manufacturer's instructions. The mutant primer pairs which were used are shown in Table 2.3. All DNA constructs were sequence-verified to confirm the integrity of the mutation.

2.2.3.2.1 Kv1.3-P89 channels

The mKv1.3-EGFP fusion protein was mutated to produce a non-conducting Kv1.3 point-mutant with intact gating properties and voltage sensitivity, generated by a single point mutation from tryptophan (W) at position 389 to phenylalanine (F) in the S5-S6 linker (Figure 2.2A). These channels were identical to the Kv1.3WF (W389F) population described by Cidad et al., (2012).

2.2.3.2.2 Kv1.3-P93 channels

The mKv1.3-EGFP fusion protein was mutated to produce a non-conducting, voltage-insensitive Kv1.3 mutant generated by the same W389F point mutant as above, but with an additional triple mutation in the S4 region. These three additional point mutations were; arginine (R) at position 320 to asparagine (N), leucine (L) at position 321 to alanine (A) and arginine (R) at position 326 to isoleucine (I) (Figure 2.2B). These channels were identical to the Kv1.3WF3X (R320N/L321A/R326I) population described by Cidad et al., (2012). This triple mutation shifts the channel activation to potentials below -170 mV. This means that the channel stays inactive at physiological voltages and functions as an inward rectifier (Miller & Aldrich, 1996).

2.2.3.2.3 Kv1.3-P121 channels

The hKv1.3-mCherry fusion protein was mutated to produce a phosphorylation defective Kv1.3 mutant with intact voltage sensing and gating properties, generated by a single point mutant from tyrosine (Y) at position 447 to alanine (A) (Figure 2.2C). These channels were identical to the Kv1.3-Y447A population described in Jimenez Perez et al., 2016.

Mutant Kv1.3 Channel	Mutation	Primer Sequence (5' to 3') (forward and reverse)
Kv1.3-P89	W389F	5'-TTTAACAGTATCCCGGATGCCTTC**TTC**TGGGCAGTAGTAA-3' 5'-TTACTACTGCCCA**GAA**GAAGGCATCCGGGATACTGTTAAA-3'
Kv1.3-P93	W389F	5'-TTTAACAGTATCCCGGATGCCTTC**TTC**TGGGCAGTAGTAA-3' 5'-TTACTACTGCCCA**GAA**GAAGGCATCCGGGATACTGTTAAA-3
	R320N	5'-TGGCCATTCTGAGAGTCATC**AAC**GCAGTAAGGGTTTTCCGCATCTT-3' 5'-AAGATGCGGAAAACCCTTACTGC**GTT**GATGACTCTCAGGATGGCCAG-3'
	L321A	5'-CCTGAGAGTCATCCGC**GCA**GTAAGGGTTTTCCGC -3' 5'-GCGGAAAACCCTTAC**TGC**GCGGATGACTCTCAGG -3'
	R326I	5'-CGCCTAGTAAGGGTTTTC**ATC**ATCTTCAAGCTCTCCCG-3' 5'-CGGGAGAGCTTGAAGAT**GAT**GAAAACCCTTACTAGGCG -3’
Kv1.3-P121	Y447A	5’-AAT**GAATTC**CCGACATGACCGTGGTGCC-3’ 5'- ATT**GGATCC**ACATCGGTGAATATCTTTTTGATG -3'

Table 2.3 Primer pairs that were used for site directed mutagenesis of the Kv1.3 channel. Table shows the mutant channel, the name of the mutation, and the primer sequence used for its generation.The base pairs from the mutated residues are highlighted in bold.

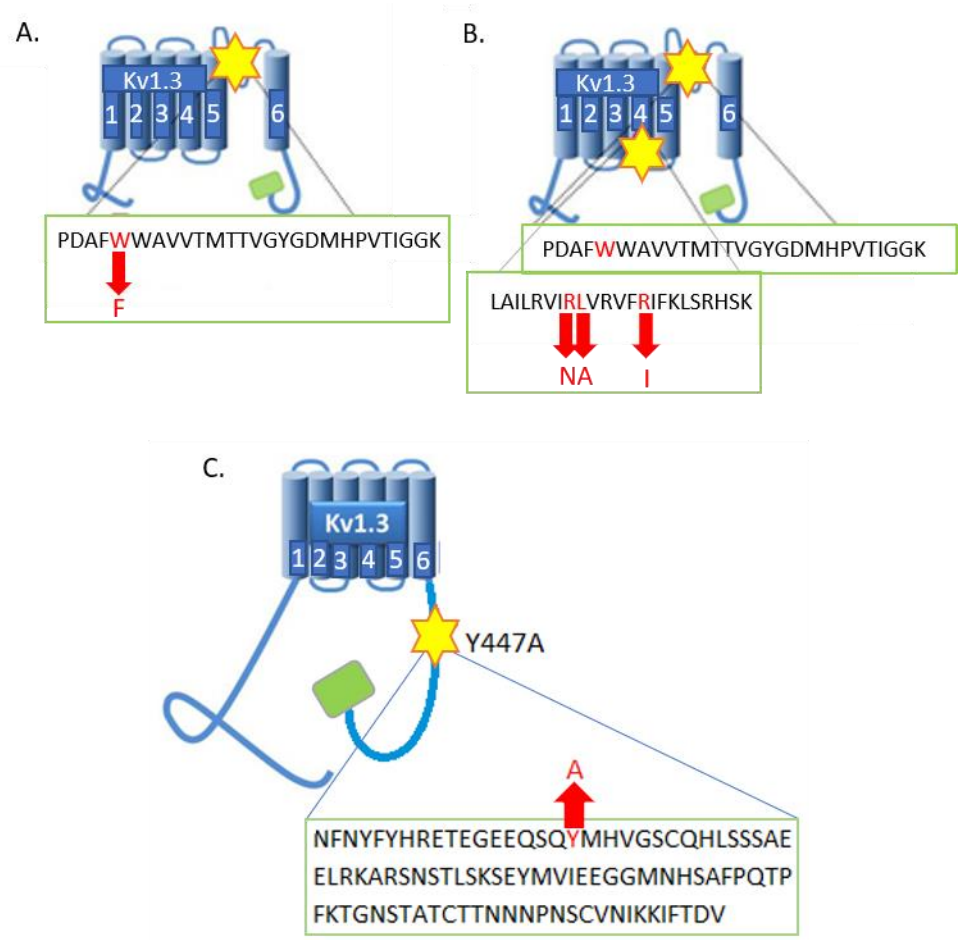

Figure 2.2 Schematic showing the location of the mutations in the Kv1.3 channels. A. Single point mutation (W389F) in S5-S6 linker of the Kv1.3-P89 channel. B. Single point mutation (W389F) in S5-S6 linker plus three additional point mutations (R320N, L321A and R326I) in the S4 voltage sensor region of the Kv1.3-P93 channel. C. Single point mutation (Y447A) in the C-terminus of the Kv1.3-P121 channel.

2.2.4 DNA amplification

DNA constructs were thawed at room temperature and 50µl aliquots of competent E. coli cells (Invitrogen) were thawed on ice for a few minutes. 4µl of each DNA construct was added to an aliquot of E. coli cells, flicked gently to mix contents and then placed on ice for 30 minutes. Heat shock was given by placing the mix in a 42°C water bath for 30 seconds before being returned to the ice for 5 minutes. 950µl of SOC media (Invitrogen) was added and the aliquots were placed in a shaker at 37ºC and 250rpm for 1 hour. Three cell solutions were made up from each stock, with dilutions being made with SOC media. The final solutions were a 100% cell stock, a 1:4 and a 1:20 dilution. A cell spreader was sterilised with 100% ethanol and flamed with a Bunsen burner, before being used to spread 200µl of each cell solution onto the pre-warmed agar plates. The lids were then placed on the plates and they were put in the oven overnight. Next morning the plates were covered with parafilm and placed in the fridge until use.

Two single colonies from each construct were selected from agar plates. Each colony was dropped into LB broth containing 30µg/ml kanamycin. These universals were placed in the shaker overnight at 37ºC and 300rpm. Next morning a cloudy LB broth signified successful amplification of the bacterial colony. Glycerol stocks were made by combining 650µl of 80% glycerol with 650µl each culture broth in small tubes. The tubes were inverted 4-6 times to mix the contents and then stored in the -80ºC freezer.

2.2.5 Harvesting of DNA – Mini Prep

For this procedure, a QIAprep Spin Miniprep Kit (Qiagen, Hilden, Germany) was used and the manufacturer's protocol was followed. The LB broth from each culture was split into two microtubes, each containing 1.5ml. The two microtubes were labelled A and B for each clone (1 and 2) of each cell Kv1.3 channel type (P118, P121, P89 and P93). The tubes were spun down at 7,000g for 3 minutes and the resulting supernatant was poured off. 250µl of P1 buffer was added to every microtube A. The pellet was resuspended by vigorous pipetting before the 250µl cell suspension was used to resuspend the pellet in microtube B. For every Kv1.3 channel type, there was now only two microtubes containing E. coli bacterial pellets for clone 1 and clone 2. 250µl of P2 buffer was added to each of the 8 microtubes. Each microtube was inverted 4-6 times

and left for no longer than 5 minutes before the addition of 350µl neutralisation buffer. Microtubes were again inverted 4-6 times to mix and then centrifuged for 10 minutes and 18,000g (Eppendorf Centrifuge 5424). The supernatant was then poured into spin columns and centrifuged for another 1 minute at 18,000g. The liquid in the collection tubes was discarded, each column was reassembled and 500µl PB buffer was added. This was centrifuged for another minute at 18,000g, the flow through was discarded and the columns were reassembled. 750µl PE buffer was added to the columns which were centrifuged at the same settings for another minute and then the flow through discarded. The columns were then placed in clean microtubes. 50µl elution buffer (EB) was applied directly to the membranes in the columns and left to stand for 1 minute before being centrifuged for a final minute at 18,000g. The resulting elution solutions contained the desired plasmid DNA which were then stored at -20°C.

2.2.6 Restriction analysis of DNA sequences

Restriction enzymes were used to check that the sequence of interest has been incorporated into the harvested bacterial plasmids. The restriction enzyme EcoR1 cuts the 5-prime end of the sequence and the restriction enzyme BamH1 cuts at the 3-prime end. The sequence is around 1500bp (base pairs) with the whole plasmid consisting of around 6200bp (6.2Kbp) (Figure 2.1).

For each sample, a restriction control was performed, which consisted of 15µl de-ionised water added to 5µl DNA. For the restriction digestion, a reaction mix was made up with 20µl of 10x Reaction Buffer 3, 20µl of 10x BSA and 100µl de-ionised water. 5µl of each sample of DNA was mixed with 14µl reaction mix and 1µl BamH1. Tubes were flicked gently and collected by pulse centrifugation. All tubes were then placed into a dry bath for 2 hours at 37°C. Then the samples were flicked gently and pulsed for another few seconds. They were placed on ice for 5 minutes before being stored back in the freezer at -20°C.

2.2.7 Gel electrophoresis

Gels were prepared by adding 3µl ethidium bromide into 100 mL TAE (Tris-acetate-EDTA) buffer containing 0.4% agarose (ThermoFisher Scientific). The DNA samples were prepared by adding 1µl of 0.25% bromophenol blue loading dye into 5µl of either the cut DNA (treated with restriction enzymes) or uncut DNA (control). 1kb DNA ladder

(New England Biosciences, UK) was used. 5µl of sample was loaded onto each well of the gel and the gel electrophoresis was performed at 80V for 90 minutes. Gel was imaged on a Bio-Rad gel image cabinet (Bio-Rad Laboratories, Hertfordshire, UK). From this, the clones which had the largest bands were selected for the maxi prep as they contained the most DNA.

2.2.8 Harvesting of DNA – Maxi Prep

For this procedure, a QIAGEN Plasmid Maxi Kit (Qiagen, Hilden, Germany) was used. Four 250ml conical flasks were prepared the day before the maxi prep. 2g LB broth was added to each of the flasks and mixed with 100ml de-ionised water. This was swirled vigorously to dissolve any lumps, lidded and taped before being sent for autoclaving.

On the day of the experiment, 5ml LB broth was placed in four 25ml universals and 3µl kanamycin (50µg/ml) was added to each. The shaker was turned on to 37°C and 300rpm. A Bunsen burner was set up and used to sterilise an ethanol-soaked heat loop 3 times. The glycerol stocks of the selected clone from each Kv1.3 channel type were retrieved from the -80°C freezer. The heat loop was sterilised again and used to scoop the first sample of glycerol into the LB broth, before this was repeated for the remaining samples. This procedure was carried out quickly to minimise the glycerol from thawing. The LB broth/DNA mixture was then put in the shaker for 8 hours until it was sufficiently cloudy.

60µl kanamycin (50µg/ml) was added to the 100ml LB broth in the pre-prepared conical flasks. After 8 hours in the shaker, the universals containing the LB broth/DNA mixture were each tipped into one of the flasks. The flasks were covered with foil and placed back in the shaker overnight.

Early the next morning, the P3 maxi prep buffer was placed in the fridge to chill. The centrifuge (Eppendorf Centrifuge 5424 R) was turned on, set to 4°C and left to cool down for 20 minutes.

The conical flasks were removed from the shaker. Each flask was divided into two 50ml falcon tubes, which were centrifuged for 25 minutes at 4000rpm. The supernatants were then discarded, and the pellets placed on ice. 10ml P1 buffer was used to resuspend the pellets (NB this was 10ml P1 in total per Kv1.3 channel clone – one

pellet was resuspended first, then this suspension was transferred to the other pellet to resuspend). After the manual resuspension, the four remaining falcon tubes were given a short pulse on a vortex mixer (Stuart, Cole-Palmer, Staffordshire, UK) to break up any remaining clumps of cloned bacteria. 2ml of P2 buffer was added to each tube and left for 5 minutes maximum at room temperature. Filter caps were put onto four filter cartridges, which were then placed into clean falcon tubes. Before the 5-minute P2 incubation was over, 10ml P3 was added to each bacterial mix, and the tubes were inverted 6 times. The bacterial lysates were then added to the barrels of the filter cartridges and left for 10 minutes at room temperature. The caps were removed, and a plunger was inserted into the cartridge. This was pushed down, and the filtered lysate was collected at the bottom of the falcon tube. The lysate was spun in the 4°C centrifuge (Eppendorf Centrifuge 5424 R) at 4,000rpm for 90 minutes. During the last 15 minutes of the spin, a Qiagen-tip 500 column (Qiagen, Fisher Scientific) was equilibrated with 10ml QBT buffer (Qiagen, Fisher Scientific) and allowed to drain. The supernatant from the centrifuged lysate was poured into the column and allowed to flow through. The column was washed twice with 30ml QC buffer (Qiagen, Fisher Scientific). The DNA was then eluted with 5ml elution buffer per Kv1.3 channel clone. The eluate was caught in a fresh plastic centrifuge tube, to which 7ml RT isopropanol (Sigma Aldrich) was added. This was spun at 4°C for 30 minutes at 4,000rpm (Eppendorf Centrifuge 5424 R). The supernatant was poured off and 5ml of 70% ethanol (Sigma Aldrich) was added. This was spun again at 4°C and 4,000rpm for 45 minutes (Eppendorf Centrifuge 5424 R). The supernatant was removed and then pellet was left to air dry for 5 minutes. Any remaining liquid was removed using tissue and cotton buds. 1ml TE (Tris EDTA) buffer (pH 8, Sigma Aldrich) was then added to dissolve the DNA. To assess the purity of the DNA, a NanoDrop spectrophotometer (NanoDrop 2000 UV-Vis Spectrophotometer, ThermoFisher Scientific) was used (range 2-15,000 ng/µl). DNA samples were then stored at -20°C. All constructs were verified by DNA sequence analysis before transfection by Sanger sequencing (Genewiz, Bishop's Stortford, Hertfordshire, UK).

2.2.9. Cell transfection

Transfection reagents (Cell Line Nucleofector Kit V) and equipment (Nucleofector™) are obtained Lonza (Lonza, Castleford, UK). Transfection mixture was made by combining 328µl of Nucleofector Solution with 72µl supplement. Pelleted WT HEK293 cells (10^6 cells per sample) were resuspended in 100µl of transfection mixture. 2.5µg (as calculated using the NanoDrop Microvolume Spectrophotometer, ThermoFisher Scientific, Loughborough, UK) of each DNA sample was added to the cell solutions. The cell/DNA solutions were then transferred into transfection cuvettes, which were then placed in turn into a Nucleofector™ Device (Lonza, Castleford, UK). Programme Q-01 was applied to each cuvette. 500µl media was then added to each cuvette, and the transfected cell solutions were transferred to 75cm^2 flasks. These cells were left for two days to recover, before the selection antibiotic was added (G418, 1mg/ml). The cells were left to grow to confluency, when they were lifted and used to seed flasks at very low dilutions (1:80, 1:160, 1:320). These flasks were left for 2 weeks for the colonies of surviving cells to grow to appropriate size. Media was replaced regularly to maintain cell viability. Colonies were identified by holding the flask up to light, and then highlighted by tracing their perimeter with a marker pen on the bottom of the flask. When colonies had grown to an appropriate size, media was removed from the T75cm^2 flasks and the cells washed with DPBS. The roof of the flask was broken into and peeled away to enable access to the cell colonies. Sterile cloning cylinders were coated with high vacuum seal grease and then pressed down firmly for 10 seconds around each of the selected colonies. Five colonies from each Kv1.3 channel clone were selected and 200µl 0.05% TrypleE Express was added to the inside of the cloning cylinders. This was left for 2 minutes before 200µl complete media was added to neutralise the TrypleE. This solution was mixed thoroughly before each suspension from the cylinders were removed and placed into separate T25cm^2 flasks. 5ml media containing 1mg/ml G418 media was added to each flask. These were then left to reach confluency, when they could undergo experimental testing for Kv1.3 channel expression and phenotype.

2.3 Proliferation Assays

All reagents were obtained from Gibco (Life Technologies, Paisley, UK) unless otherwise stated.

Cells were grown in 75cm^2 flasks and selected at 70-90% confluence. The cell pellets that were obtained by detachment and centrifugation as described above were resuspended in complete media. An aliquot of that was used to obtain the live cell numbers using trypan blue. Cells were seeded in a 24 well plate at a density of 2x10^4 cells (HEK293 cells) or 1x10^4 cells (HSVMSCs) per well. Cells were plated in complete media and left to adhere to the wells for a minimum of 6 hours (HEK293 cells) or overnight (HSVSMCs). Then the complete media was replaced by no serum media. Cells were incubated in serum free media overnight (HEK293 cells) or for 2.5 days (HSVSMCs). This allowed the cells to become dormant, and thus created a synchronised growth state when complete media was re-added, in addition to the required drug being investigated (Table 2.4), on Day 0 of the assay. Drugs were added on Day 0 and left for the entire length of the proliferation assay. Day 0 was when the initial cell counts for the assay were carried out. Depending on the assay, additional counting occurred on days 0, 1, 2 and 3, or just day 3 (HEK293 cells), or on days 0, 2, 4 and 7, or just day 4 (HSVSMCs). For HSVSMCs, proliferation assays were originally 7 days in length to determine optimum assay length (which was then found to be 4 days of proliferation). Counts were carried out as explained using Bio-Rad TC10 automated cell counter (Bio-Rad Laboratories, California, USA) (HEK293 cells) or using a manual haemocytometer (HSVSMCs). For each condition, cells were counted in triplicate and the mean (±SEM) was generated. Please note, detachment of HSVSMCs using TrypleE express needed a longer incubation time that HEK293 cells, with 4-5 minutes used to detach cells from T75cm^2 flasks and 5-6 minutes in the 24-well plate wells. Proliferation assays for HEK293/Kv1.5 cells were carried out by Dr M. Al-Owais, University of Leeds.

Drug	Source	Mode of Action	Concentration
PAP-1	Product P6124, Sigma Aldrich	Inhibits all cellular Kv1.3 channels	0.1nM-30nM
ShK-Dap22	Product 3220, Tocris Bioscience	Inhibits plasma membrane Kv1.3 channels	1pM-200pM
PAPTP	Gifted by Dr Robin Bon, Leeds University	Inhibits mitochondrial Kv1.3 channels	3nM-100nM
MitoQ	Gifted by Professor Mike Murphy, University of Cambridge	Scavenges mitochondrial ROS	5µM

Table 2.4 Drugs added on Day 0 of proliferation assays. From left to right, columns show the name of the drug, it's source, its mode of action and the working concentration used. ROS = reactive oxygen species.

2.4 High Resolution Respirometry

2.4.1 O2k Oxygraph and DatLab software

All equipment sourced from Oroboros Instruments, Innsbruck, Austria unless otherwise stated. Before each experiment, a standard air calibration was carried out in the respirometer (Gnaiger, 2016).

The O2k Oxygraph contains two chambers in which cell suspensions are placed and their oxygen (O_2) consumption measured. Each chamber is maintained in a copper block that maintains the temperature at 37°C. The chamber itself is a 16mm Duran glass cylinder which holds a volume of 2ml. Each chamber is attached to a Clark type polarographic O_2 sensor. The electrode measures the partial pressure of dissolved O_2 in an aqueous solution. It consists of a gold cathode, a silver anode and a potassium chloride electrolyte reservoir separated from the chamber sample by a 25µm FEP film membrane. The chambers are sealed with a stopper that contains a central capillary which enables chemicals to be titrated into the chambers. A 15x6mm electromagnetic stirrer bar sits in the bottom of the chamber to ensure maximum mixing of the aqueous sample suspension and to ensure a stable signal of the polarographic O_2

sensor (constant stir speed of 750rpm). The decline in chamber O_2 concentration every 2s is recorded by DatLab software (DatLab Software. Oroboros Instruments, Innsbruck, Austria) that translates the respirometer data to a computer. At the O_2 sensor, a polarisation voltage of 0.8V allows an amperometric signal to be converted to a voltage signal, which is recorded and used for data acquisition and analysis. All measurements are expressed as O_2 consumption, pmol per million cells per second (pmol *s*Mill). To remove the aqueous samples from the chambers, an ISS integrated suction pump (120V) was used. ISS plastic tubing connected the waste solution to a 2-litre waste bottle containing Virkon disinfectant (LanXess, Newbury, UK).

2.4.2 Chemicals and medium

All mitochondrial ETS inhibitors were purchased from Sigma (Sigma Aldrich, Missouri, USA), unless otherwise stated. Inhibitors were added to the chambers via the capillary in each chamber stopper. Hamilton micro syringes (either 10mm^3 or 25mm^3, Oroboros Instruments, Innsbruck, Austria) were used to treat cell samples with the compounds listed in Table 2.5. All of the compounds were made up in advance using well established protocols (Gnaiger, 2014) and stored at -20°C. All compounds were kept on ice during experiments.

Respirometry medium was HEK293 cell culture medium without the addition of FBS. Media as follows: DMEM (31885), 1% (v/v) Antibiotic/ Antimycotic ((100x) 15240- 062), 1% (v/v) Non-Essential Amino Acids ((100x) 11140-035), 0.1% (v/v) Gentamicin ((50 mg/mL)15750060).

2.4.3 Cell preparation

T75cm^2 flasks, at 70-80% confluence, were selected and cells counted (as in Section 2.1.2). Cell pellet was resuspended in 0% FBS media in a 50ml falcon tube. Enough media was added to ensure cell suspension had a concentration of 1 x 10^6 cells/cm^3. The cell suspension was then added to the respirometer chambers (or pre-treated with PAPTP, see Table 2.5).

2.4.4 Whole-cell respirometry protocol

To analyse whole cell respiration, the techniques used were based on the protocols created by Professor E. Gnaiger (Oroboros Instruments, Innsbruck, Austria). Cells were

placed into each chamber (37^{o}C) of the OROBOROS Oxygraph-O2k respirometer. After closure of the chambers and once routine respiration stabilised mitochondrial activity was assessed using four drugs; oligomycin, FCCP, rotenone and antimycin A. Addition of 1µl oligomycin was added into each chamber to block the ATP synthase and destroy the link between the ETS and ATP production. This reduced the mitochondrial O_2 flow, as far less protons could cross the IMM through the ATP synthase, and subsequently less were able to combine with O_2 to form H_2O. The only protons which were able to cross the IMM are those which leak across. This reduced O_2 flow and allowed any changes in O_2 flow as result of drugs to be localised to the function of the ETS. Next, FCCP was titrated in steps of 1µl until maximal uncoupling of the ETS was observed. As a protonophore, FCCP disrupts the H^+ proton gradient which is created by the ETS, by permeabilising the IMM. This leads to H^+ protons flooding into the mitochondrial matrix. At complex IV, O_2 is combined with 4 protons, but due to oligomycin inhibiting the ATP synthase there is feedback inhibition of OXPHOS. As the concentration of FCCP increases, this feedback inhibition is relieved and O_2 consumption increases until it reaches a maximum level i.e. the ETS is maximally uncoupled. 5µl of rotenone and then 5µl antimycin A were added after maximum uncoupling by FCCP had been achieved. This was to disable the ETS and block all OXPHOS, enabling non-mitochondrial O_2 to be calculated.

Drug	Product details	Function	Concentration
Oligomycin	75351, Sigma-Aldrich	ATP synthase inhibitor	2µg/ml
FCCP	C2920, Sigma-Aldrich	Protonophore (permeabilises the IMM) Uncouples respiration	Titrations of 0.5µM
Rotenone	R8875, Sigma-Aldrich	Complex I inhibitor	2.5µM
Antimycin A	A8674, Sigma-Aldrich	Complex III inhibitor	0.5µM
TMPD	A4034, Sigma-Aldrich	Artificial substrate for reducing cytochrome C	2mM
Ascorbate	T3134, Sigma-Aldrich	Maintains TMPD in its reduced state	0.5mM
Sodium Azide	S2002, Sigma-Aldrich	Inhibits all mitochondrial respiration	20mM
PAP-1	P6124, Sigma-Aldrich	Inhibits all cellular Kv1.3 channels	100-300nM
ShK-Dap22	3220, Tocris Bioscience	Inhibits plasma membrane Kv1.3 channels	500nM
PAPTP	Gifted by Dr Robin Bon, Leeds University	Inhibits mitochondrial Kv1.3 channels	100nM (30 minute pre-treatment)

Table 2.5 Compounds and inhibitors used in respiratory experiments. Data shown, from left column to right; name of drug, product code, mode of action and working concentration.

2.4.5 Assessing Kv1.3 effect on respiration

After closure of the O2k chambers, and establishment of a stable level of routine respiration, the Kv1.3 inhibitors PAP-1 and ShK-Dap22 could be added directly to the chambers prior to oligomycin treatment (see Table 2.5 for details). ShK-Dap22 respirometry was carried out by Dr J. Boyle, University of Leeds. For targeted inhibition of mitochondrial Kv1.3 channels, cells were pre-treated with the mitochondrial Kv1.3 inhibitor PAPTP (see Table 2.5 and Section 2.11 for details). This inhibitor was added to the cell suspension prior to it being added to the O2k chambers. Pre-treatment was for 30 minutes in a humidified incubator (37^{o}C; 95% air, 5% CO_2).

2.4.6 Assessing activity of the malate/aspartate shuttle

DM-2OG stimulates the malate/aspartate shuttle (Scaduto, 1994) whilst PhS inhibits it (Stamenkovic *et al.*, 2015). The malate/aspartate shuttle is a protein complex in the IMM that transports NADH into the matrix (Naish, Syndercombe Court and Revest, 2009). WT HEK293 cells were treated with 2mM DM-2OG to see if respiration increased compared to untreated WT HEK293 cells. HEK293/Kv1.3 cells were treated with 5mM PhS to see if respiration decreased compared to untreated HEK293/Kv1.3 cells. WT HEK293 and HEK293/Kv1.3 cells were cultured as in Section 2.1. 24 hours prior to the experiment, media was replaced for 20ml fresh media containing either 2mM DM-2OG (WT HEK293 cells) or 5mM PhS (HEK293/Kv1.3 cells). Cells were returned to a humidified incubator (37°C; 95% air; 5% CO_2) for 24 hours. Normal respiratory protocol was then followed (Section 2.4.4).

2.4.7 Assessing contribution of glycolysis to respiration

2-Deoxy-D-Glucose inhibits glycolysis by competitively inhibiting the production of glucose 6 phosphate from glucose by hexokinase (Zhong *et al.*, 2009). HEK293/Kv1.3 and WT HEK293 cells were treated with 5mM 2DDG prior to respirometry to confirm that the increased OXPHOS in HEK293/Kv1.3 cells was not largely due to increased glycolysis. Cells were cultured according to methods section 2.1. 24 hours prior to the respirometry experiment, culture media was removed and replaced with 20ml fresh

media with the addition of 5mM 2DDG. Cells were returned to a humidified incubator (37°C; 95% air; 5% CO_2) for 24 hours. Normal respiratory protocol was then followed (Section 2.4.4).

2.4.8 Complex IV activity

At the end of the whole-cell respirometry protocol, detailed in 2.4.4, after addition of rotenone and antimycin A, the activity of complex IV could be investigated. Ascorbate (ascorbate sodium salt) and TMPD (N, N, N', N'-Tetramethyl-p-phenylenediamine dihydrochloride) were added to the chambers of the O2k Oxygraph (details in Table 2.5). TMPD acts as an artificial substrate for reducing complex IV, by donating electrons, and it is kept in the appropriate reduced state by ascorbate. 20mM sodium azide (details in Table 2.5) was then added to inhibit all mitochondrial respiration and act as control to correct for background O_2 consumption that can occur due to oxidation of TMPD (Kuznetsov and Gnaiger, 2018). This assay can be used as a surrogate measure for mitochondrial content in the cells (Larsen *et al.*, 2012).

2.4.9 Data analysis

Data was analysed using DatLab 6 software (Oroboros Instruments, Innsbruck, Austria), whereby the magnitude of O_2 consumption was measured from the respirometer trace at different time points across the experiment. Figure 2.3 shows an example respirometry trace and how it was analysed. Measurements were taken routinely at four points; when O_2 consumption initially plateaued after closure of the chambers (routine respiration), after the application of oligomycin (leak respiration), at the peak uncoupled state from FCCP titration (ETS respiration) and finally once OXPHOS had been inhibited with rotenone and antimycin A (residual O_2 consumption, ROX). For complex IV activity experiments, measurements were also taken at the peak O_2 consumption after addition of ascorbate and TMPD.

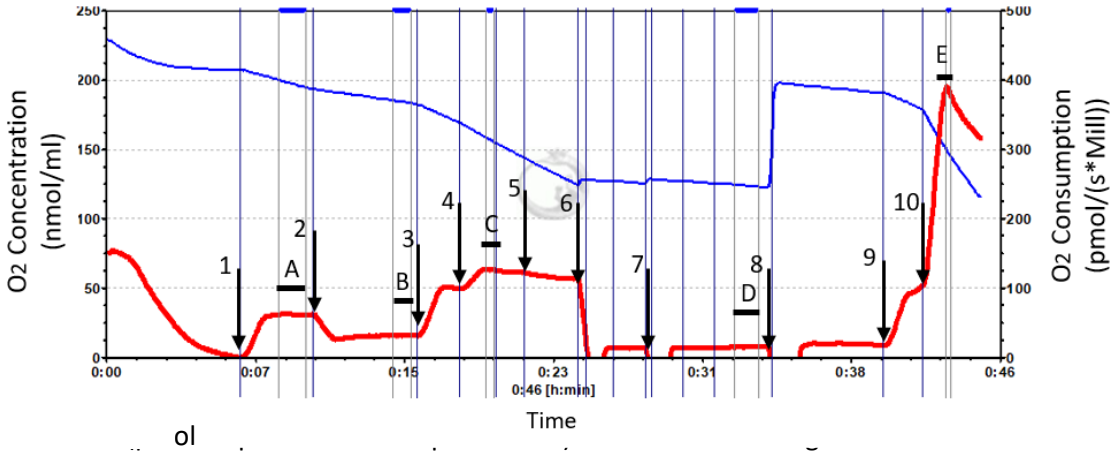

ol

O_2 concentration in the chamber (nmol/ml), measured on the left Y axis. Black arrows show the different stages of the protocol. Briefly, chamber is closed (1), oligomycin added (2), FCCP titrated (3,4 and 5), rotenone added (6), antimycin A added (7), chamber was re-oxygenated (8), ascorbate added (9) and TMPD added (10). Black horizontal lines show where measurements were taken during post-experiment trace analysis, where A is routine respiration, B is leak respiration, C is maximum ETS capacity, D is ROX and E is maximum complex IV capacity.

2.5 Immunocytochemistry

All reagents were obtained from Gibco (Life Technologies, Paisley, UK) or Sigma (Sigma Aldrich, Dorset, UK) unless otherwise stated.

2.5.1 Cell preparation

Sterile coverslips were placed into each well of a 6-well plate, washed with 1ml poly-L-lysine, and left to dry. T75cm^2 flasks were selected at 70-90% cell confluence. The cells were lifted, plated at appropriate dilutions with 10% FBS media, and left to grow to 30-40% confluence.

2.5.2 Detection of Kv1.3 channels

2.5.2.1 Mutant Kv1.3 cells and HEK293/Kv1.3-P118 cells

Kv1.3 channels in mutant Kv1.3 cells (HEK293/Kv1.3-P89, P93 and P121), and in HEK293/Kv1.3-P118 cells were detected by their fluorescent tags (Section 2.2.2) using a Zeiss LSM800 Upright confocal microscope. Images were processed using Zen Lite

(Zeiss, Cambridge, UK) and Image J software (Java-based image processing program developed at the National Institutes of Health by Wayne Rasband, NIH, UK).

2.5.2.2 WT HEK293 and HEK293/Kv1.3 cells

Once the cells had reached the optimum confluence they were fixed with 4% paraformaldehyde containing DPBS at RT for 20 minutes. The cells were washed 3 times with 1ml DPBS and incubated for 20 minutes at RT in DPBS containing 0.05% Triton X100 and 10% NGS. The cells were washed again with DPBS (with 1% NGS), before the coverslips were inverted onto a parafilm covered glass plate containing the primary antibody (diluted in 1% NGS, see Table 2.6 for a list of antibodies). This was then placed into a humidified box and left overnight in the fridge (4°C). Next morning the coverslip washed with 1ml DPBS (1% NGS) for 3x5 minutes. An appropriate dilution of the secondary antibody was made up in DPBS (1% NGS, see Table 2.7 for a list of antibodies), and applied to cells for 1hr (RT, in the dark). Cells were then washed with DPBS (1% NGS) for 3x5 minutes. The coverslips were mounted with 5-10µl of VECTASHIELD HardSet Antifade Mounting Medium with DAPI (VECTOR Laboratories Ltd, Peterborough, UK) on a glass microscope slide and left to dry (RT, in the dark). Images were then taken on either a Zeiss LSM510, LSM700 inverted or an LSM880 Upright confocal microscope and images processed and analysed as above (2.5.2.1).

2.5.2.3 HSVSMCs

Method was the same as above in 2.5.2.2 but imaged only on a Zeiss LSM510 inverted confocal microscope and processed and analysed as above (2.5.2.1)

2.5.3 Detection of the mitochondrial network

All cells were prepared on coverslips as mentioned in the above protocol (Section 2.5.1). 3D analysis of the mitochondrial network in WT HEK293 and HEK293/Kv1.3 cells was carried out on an LSM800 Upright Confocal Microscope using z-stack composites of twenty 1µm slices through the cell.

2.5.3.1 MitoTracker

Before fixation occurred, cells were incubated for 30 minutes (37^{o}C; 95% air, 5% CO_2) with MitoTracker reagents (see Table 2.6 for concentrations used and detection wavelengths). After treatment with MitoTracker, normal immunocytochemistry protocol resumed (as in section 2.5.2.1).

2.5.3.2 Anti-Cox IV labelling

The protocol outlined in section 2.5.2.1 was followed. The primary antibody used was targeted to mitochondrial complex IV protein and the secondary antibody was Alexa Fluor 488 or Alexa 555 (see Table 2.6 for details). Alexa Fluor 488 used with mCherry tagged Kv1.3 cells (HEK293/Kv1.3-P118 and HEK293/Kv1.3-P121) and Alexa Fluor 555 used with GFP tagged Kv1.3 cells (HEK293/Kv1.3-P89 and HEK293/Kv1.3-P93).

Determination of Kv1.3 channel co-localised within the mitochondrial network was carried out using a co-localisation analysis application in Image J.

2.5.4 Detection of cellular ROS

All cells were prepared on coverslips as mentioned previously (Section 2.5.2.1). Before fixation, cells were treated with 5µM CellROX Deep Red (ThermoFisher Scientific, Loughborough, UK) with or without 100µM menadione pre-treatment. Menadione (ThermoFisher) is an oxidative stress inducer and was used as a positive control (Tongul and Tarhan, 2014). To treat cells with menadione, it was added directly to culture wells and incubated for 1 hour (37^{o}C; 95% air, 5% CO_2). To treat cells with CellROX, the reagent was added directly to the culture well and the cells incubated for 30 minutes (37^{o}C; 95% air, 5% CO_2). Normal immunocytochemistry protocols then resumed as the cells were prepared for imaging (Section 2.5.2.1)

For each cell type i.e. WT HEK293 or HEK293/Kv1.3, three images were analysed during each experimental repeat (n=3 for the total experimental repeats). For each image, the mean fluorescent intensity (MFI) of 10 regions of cells was recorded using the line scan function in Image J.

Primary Antibodies	Dilution	Secondary Antibodies	Excitation nm/Emission nm	Dilution
Anti-Kv1.3 Clone L23/27, mouse monoclonal. (NeuroMab, Antibodies Incorporated, Davis, UK)	1:500	Invitrogen Alexa Fluor 488 Donkey anti-Mouse IgG (H+L) (ThermoFisher)	490/525	1:2000
Anti-COX IV Mouse monoclonal. (Abcam, Cambridge, UK)	1:500	Alexa Fluor 488 (as above) or Alexa Fluor 555 Donkey anti-mouse IgG (H+L). (ThermoFisher)	490/525 553/568	1:2000 1:2000
		Other Fluorescent Reagents		
		Diamidino-2-phenylindole (DAPI) VECTASHIELD HardSet Antifade Mounting Medium with DAPI. (VECTOR Laboratories)	360/460	1.5µg/ml
		MitoTracker Red CMXRos (ThermoFisher)	579/599	100nM (HEK293 cells) 250nM (HSVSMCs)

Table 2.6 Reagents used in immunocytochemistry experiments. Dilutions of primary antibodies (anti-Kv1.3 and anti-COX IV) and their associated secondary antibodies (Alexa Fluor 488 and 555) are listed, as well as their appropriate excitation and emission wavelengths (nm). Concentrations and excitation/emission wavelengths (nm) are given for the nuclear dye DAPI, the mitochondrial network dye MitoTracker, and the cell ROS dye Cell ROX Deep Red.

2.6 Electrophysiology

All reagents were obtained from Gibco (Life Technologies, Paisley, UK) or Sigma (Sigma Aldrich, Dorset, UK) unless otherwise stated.

2.6.1 Solutions

Extracellular Solution: 141mM $NaCl_2$, 10mM HEPES (4-(2-hydroxyethyl)-1-piperazineethanesulfonic acid), 4.7mM KCl_2, 1.2mM $MgCl_2$, 1.8mM $CaCl_2$ (Fluka Analytical, Romania), 10mM glucose (D+ glucose ACS reagent anhydrous (Acros Organics, ThermoFisher Scientific). pH 7.4 with NaOH.

Intracellular Solution: 10mM EGTA (ethylene glycol-bis (2-aminoethylether)-N, N, N', N'-tetraacetic acid), 10mM HEPES, 125mM KCl, $MgCl_2$ 4mM, MgATP 5mM. pH 7.2 with KOH.

2.6.2 Cell preparation

For electrophysiology, cells were plated onto sterile glass coverslips (22x22mm) and placed in a 6 well plate. 1-2ml media was added to each well and the cells were plated at a low enough dilution to ensure single cells would be present 3 days later. The cells were left overnight to attach to the coverslips, before the complete media was replaced for media free of any antibiotics the next morning. The cells were left for a further 1-2 days in antibiotic free media, to improve the integrity of the cell membranes (incubated at 37°C; 95% air, 5% CO_2). On the day of the experiment, coverslips were transferred into 35mm petri dishes containing 1ml antibiotic free media. The coverslips were cut into fragments using a diamond cutter so one fragment at a time could be transferred into the recording chamber.

2.6.3 Electrophysiology rig set-up

On the day of the experiment, extracellular and intracellular solutions were pre-warmed to RT before using. A recording chamber was mounted over a CK40 light microscope (Olympus, London, UK). The recording chamber was continuously perfused with extracellular medium. This solution was placed into one of four reservoirs

connected to a 4-way Hamilton tap (Hamilton GB Ltd) by plastic Tygon tubing (0.83mm internal diameter, Merck, UK). To ensure continuous flow of solution, a suction tube connected to a vacuum pump (JUN-AIR, Redditch, UK) removed extracellular solution from the recording chamber. Borosilicate glass capillary tubes (0.86mm internal diameter, Harvard Apparatus, Cambridge, UK) were pulled on a micropipette puller (PP-83; Narishige, London, UK) to produce pipettes with a resistance of 3-7 MΩs when placed in the recording chamber. The pipettes were filled with intracellular solution ensuring no air bubbles formed. The pipette was then attached securely onto the electrode holder, ensuring that the silver/silver chloride recording electrode was both connected to the head stage and in contact with the intracellular solution. A silver/silver chloride ground electrode was placed in the recording chamber. The position of the head stage was controlled by a micromanipulator (Patch Star (PS-700BC), Scientifica, East Sussex, UK) which allowed for very precise movements of the pipette. The electrode holder had an air outlet that was attached to more Tygon tubing. This allowed manual suction to be delivered to the membrane, causing it to rupture and therefore create the whole-cell configuration. To minimise electrical noise, all apparatuses were contained inside a Faraday cage. A common earth point was used for grounding individual electrical items. Patch clamp experiments were recorded on an Axopatch 200B amplifier (ALA Scientific Instruments, NY, USA), before being stored and digitized using a Digidata 1322A (Axon, Molecular Devices, CA, USA) and pClamp 10 (Molecular Devices), respectively.

2.6.4 Protocols

IV relationships were measured by stepping from a holding potential of −80 mV to voltages between −60 and +60 mV in 10 mV increments for 300ms. Kv1.3 current screening was measured using a single pulse protocol stepping from −80 to +40 mV for 200ms.

2.6.4.1 Inhibition of Kv1.3 channels

Electrophysiology solutions and equipment were set up as described in Section 2.6. In addition, additional extracellular solutions were made up containing different concentrations of the Kv1.3 inhibitors PAP-1 (200nM and 1µM) and ShK-Dap22 (20pM and 80pM). Once whole cell recordings had stabilised, extracellular solution was

changed for one containing either PAP-1 or ShK-Dap22. Whole cell currents were recorded over a time course of 12 minutes. For time course experiments, cells were held at -80mV and then repeatedly depolarised to +60mV (100ms, 0.2 Hz). Currents recorded and analysed as previously described (Section 2.6). Experiments were carried out by Dr M. Al-Owais, University of Leeds.

2.7 Western Blotting

All reagents and materials purchased from Bio-Rad (Bio-Rad Laboratories, Inc, CA USA) unless otherwise stated. Western Blotting was carried out by Dr T. Hettiarachchi, University of Leeds.

2.7.1 Buffers

Cell sample buffer (stored at RT): 125mM tris(hydroxymethyl) aminomethane (Tris) HCl, pH 6.8, 2% (w/v) sodium dodecyl sulphate (SDS) , 20% (w/v) glycerol, 20µg/µl bromophenol blue and 10% β-mercaptoethanol.

Running Buffer (made up fresh on day of experiment): 10x Tris/Glycine/SDS running buffer (1610772). 25mM Tris, 192mM glycine, 0.1% SDS, pH 8.3 following dilution to 1x with water.

Transfer Buffer (made up fresh on day of experiment): 10x Tris/Glycine transfer buffer (1610734). 25mM Tris, 192mM glycine, pH 8.3 following dilution to 1x with water.

2.7.2 Cell culture, lysis and protein extraction

Cells grown to 90% confluence were washed with ice cold DPBS. The flask was placed on ice and cells were lysed by addition of 800µl M-per TM mammalian protein extraction reagent (Perbio Science, Tattenhall, Cheshire, UK) containing Complete Mini protease inhibitors (Roche Diagnostics UK Ltd, Lewes, East Sussex, UK). A cell scraper was used to aid removal of cells from the bottom of the flask. The protein lysate was collected and centrifuged at 15,000g for 3 minutes and the supernatant was used immediately (stored on ice) or stored in the freezer (-80°C) until use.

2.7.3 BCA protein assay

Protein levels of the cell lysates were then determined using a bicinchoninic acid (BCA) assay kit according to manufacturer's instructions (Pierce, Illinois, USA). Total protein content is displayed as a colour change from green to purple in the protein samples. The purple coloured complex strongly absorbs light at 562nm. Protein standards were

defrosted (from storage at -20 degrees) at RT, and if samples were frozen, they were defrosted on ice. 10µl of each protein standard, and 2.5µl of each cell lysate sample, was pipetted into a well of a sterile 96 well plate. A working reagent solution was made up using a 1:40 ratio of Reagent B to Reagent A. 200µl of working reagent was then added to each well containing standard or sample. The plate was placed into a humidified incubator for 30 minutes at 37°C. The plate was then analysed using a pre-configured BCA assay setting, which detected purple fluorescence using a green light filter (excitation/emission 525nm/580–640nm). The data was analysed with GraphPad Prism. The protein content of samples was determined using the linear fitting of standards. 25-50 µg of samples were used for SDS-polyacrylamide gel electrophoresis (PAGE). Samples were mixed with loading buffer to make the total loading volume to 40µl.

2.7.4 SDS-PAGE

Gels were 12.5%, 0.75mm thick polyacrylamide-SDS gels (Bio-Rad) and were run on vertical mini gel (11cm x 11cm) apparatus (Mini Protean III electrophoresis cell, Bio-Rad, Hemel Hempstead, UK). The gel cassette sandwich was inserted into the electrode assembly and then running buffer was poured over the gel. The gel comb was removed and either the cell samples or molecular weight marker was pipetted slowly into each of the wells to avoid overflow. For the molecular weight marker, 7µl of Precision Protein Plus Dual Colour Standard was added to either side of the samples. Gels were separated at 36mA for around 1 hour, or until the markers of interest had reached the right position.

2.7.5 Electrophoretic transfer

The proteins were transferred onto 0.45µm polyvinyl difluoride membranes (PVDF) (Millipore Corporation, Massachusetts, USA). Before the transfer could take place, the membrane, 2x sponges and 2x mini trans blot filter paper (Bio-Rad, Hemel Hempstead, UK) were soaked in methanol (Fisher Scientific, Rockford, USA) and then in transfer buffer. Blotting cassettes were assembled as follows: anode, sponge, filter paper, membrane, gel, filter paper, sponge, cathode. Blotting cassettes were then inserted into a Mini Trans-Blot electrophoretic transfer cell (Bio-Rad, Hemel Hempstead, UK).

An ice block was placed on the back of the transfer cell, before transfer buffer was poured over the cassette to cover it. The transfer was then run at 30V overnight.

2.7.6 Immunodetection

Then the cassettes were disassembled, and the membranes were blocked with 5% fat free milk powder in PBS-Tween (0.05%) for 1 hour. Membranes were immunostained with antibodies raised against the Kv1.3 channel, complex IV mitochondrial protein, the beta subunit of ATP synthase and β-actin (Table 2.7). All antibodies were diluted in 5% fat free milk in Tris buffered saline (TBS) tween and incubated at RT for 3 hours. Blots were then washed for 30 minutes in TBS tween and incubated with a HRP secondary antibody (Table 2.7) diluted in 5% fat free milk (TBS tween) for one hour. Membranes were washed again for 30 minutes in TBS tween, before they were left to dry slightly. This was to enable annotation with a LI-COR WesternSure pen (LI-COR Biosciences, Nebraska, USA). The pen was used primarily to highlight the standard ladder bands. A 1:1 mixture of LI-COR Western Sure ECL luminol enhancer solution with LI-COR Western Sure ECL stable peroxide was made up and used to wash the membranes for 5 minutes. The membranes were imaged immediately on a C-Digit Blot Scanner (LI-COR Biosciences) for 12 minutes, at a high resolution. Densitometry was carried out using Image J analysis software.

Primary Antibodies	Dilution	Secondary Antibody	Dilution
Anti-Kv1.3 clone L23/27 mouse monoclonal primary antibody (NeuroMab, NIH)	1:500	HRP goat anti mouse IgG H+L secondary antibody (LI-COR Biosciences UK Ltd, Cambridge, UK)	1:20,000
Anti COX IV [Abcam33985] mouse monoclonal primary antibody (Abcam, Cambridge)	1:500		
Anti β-Actin Clone AC-15 mouse monoclonal primary antibody (Sigma Aldrich)	1:600		
Anti ATPB [Abcam65378] rabbit polyclonal antibody (Abcam, Cambridge)	1:500	HRP goat anti rabbit IgG H+L secondary antibody (LI-COR Biosciences UK Ltd, Cambridge, UK)	

Table 2.7 Antibodies used in western blot experiments. From left to right columns; name of the primary antibody, primary antibody dilution ratio, the corresponding secondary antibody and finally the secondary antibody dilution ratio.

2.8 Cairn Photometry

All reagents were obtained from Gibco (Life Technologies, Paisley, UK) or Sigma (Sigma Aldrich, Dorset, UK) unless otherwise stated.

2.8.1 Perfusion medias

Perfusion media was made up in advance and pre-warmed to RT before experiment. Perfusate was the same extracellular solution as that used for electrophysiology (Section 2.6.1) and made up in 1L double distilled (dd) H_2O.

Perfusion solution with mitochondrial inhibitors: extracellular solution with the addition of 20µM FCCP (carbonyl cyanide - p - (trifluoromethoxy)phenylhydrazone) and 2.5µM oligomycin.

Wash solution: ddH_2O

2.8.2 Cell culture

Cells needed for cairn photometry were plated onto sterile glass coverslips (22x22mm) within a 6 well plate. The coverslips had been pre-coated with sterile filtered poly-l-lysine to improve their adherence to the coverslip during perfusion. 2ml media was added to each well and the cells were plated at appropriate number to ensure 90% confluency on the day of experiment.

2.8.3 TMRM treatment

On the day of experiment, cells were washed with DPBS and then treated with 20nM Tetramethylrhodamine, methyl ester (TMRM) in media for 30 minutes (at 37°C; 95% air, 5% CO_2). After incubation, TMRM media was removed, cells were washed with DPBS and then left in HBSS (Hank's balanced salt solution with calcium and magnesium) whilst wrapped in foil until needed for the experiment. The coverslips were cut into fragments using a diamond cutter so one fragment at a time could be transferred into the recording chamber.

2.8.4 Cairn photometry rig set up

The recording chamber sat above an inverted epi-fluorescence microscope and was continuously perfused with solution. The perfusion system relied on gravity to pull the solutions down from the holding tubes into the perfusion bath. The holding tubes were

three 50ml disposable syringes that were connected by Tygon tubing (2.5mm outside diameter, 0.83mm inside diameter; Merck, UK) to a 6-way tap (Hamilton GB Ltd., UK). From this tap, more tubing delivered the perfusate to the cells in the perfusion bath via a metal inflow tube. Perfusate was removed from the bath via a metal suction tube, connected to tubing that was connected to a peristaltic pump (Gilson, Minipulse 3, Anachem, UK) that disposed of the waste. Recordings were taken using a Cairn Research ME-SE Photometry system (Cairn Research, Cambridge, UK). The TMRM was excited by a Xeon Arc lamp with a monochromator to select the excitation wavelength of 548nm. Upon excitation of TMRM, light was emitted at 574nm. This was then converted from photon energy into electrical energy via a photomultiplier before the Cairn Optoscan analysed the data. The data acquisition engine 1.6.1 Software was used to visualise the traces.

2.8.5 TMRM detection

A fragment of coverslip containing TMRM treated cells was placed into the recording chamber. Cells were brought into focus until TMRM staining could be seen by eye down the eyepiece of the microscope. In the three holding tubes there was one containing normal perfusion media, one with perfusion media plus mitochondrial inhibitors (section 2.8.1), and finally one with just ddH_2O. The cells were primarily perfused with the original perfusate (containing no mitochondrial inhibitors). When the recordings were started, the trace was run for about 200 seconds to record a baseline measurement. The normal perfusion media was then switched to the one containing 20µM FCCP and 2.5µM oligomycin. The FCCP depolarised cells and caused a reduction in the TMRM fluorescence, whilst the oligomycin prevented the ETS running backwards and counteracting the effects of the FCCP. The recording was left until the signal had reached a plateau. The recording trace was stopped, and the perfusion media was then replaced for H_2O to wash the system out. Three traces were taken from each coverslip of cells, and three coverslips over different days and cell passages were used to compile mean values for the TMRM signal in WT HEK293 and HEK239/Kv1.3 cells. The trace was analysed using Graphing (an in-house plug-in application) and GraphPad Prism. The initial TMRM signal was recorded, as was the fall in the TMRM fluorescence with application of FCCP and Oligomycin.

2.9 Citrate Synthase Assay

Products were purchased from Sigma Aldrich (Sigma Aldrich, Missouri, USA), unless otherwise stated.

2.9.1 Stocks prepared monthly

Acetyl-CoA (10mM): 12.14mg Acetyl-CoA + 1.5ml ddH_2O. Aliquoted out into 300µl vials and stored at -20°C. Kept on ice during experiment.

Tris HCl buffer (1M, pH 8.1): 2.422g Tris + 20ml ddH_2O. Corrected pH with HCl acid. Stored in fridge at 4°C for one month.

Tris HCl buffer (0.1M, pH 7.0): 2ml 1M Tris HCl buffer + 15ml ddH_2O. Corrected pH to 7 with HCl. Added 3ml ddH_2O. Stored in fridge at 4°C for one month.

2.9.2 Stocks prepared on day of experiment

1mM DTNB: 2mg 5,5'-Dithiobis (2-nitrobenzoic acid) (DNTB) + 5ml 1M Tris HCL buffer 8.1.

10mM oxaloacetate: 6.6 mg diethyl oxaloacetate sodium salt (OAA) + 4.5ml ddH_20 + 0.5ml 1M Tris HCL buffer Ph 8.1.

Citrate synthase (CS) standard: 2µl undiluted CS (8.9mg/ml, 370 units/mg) + 998µl (1:500) 0.1M Tris HCL pH 7 buffer, to give 6.586 U/ml. Kept on ice.

Buffer Solution: 900µl PBS, 25µl Acetyl CoA and 100µl DTNB (0.25mM Acetyl CoA and 0.1mM DTNB). This amount of solution was enough to fill five wells of a 96 well plate. For more wells, the amount of components needed to be multiplied accordingly.

2.9.3 Cell lysis and protein extraction

Cells were grown in T75cm^2 flasks and selected when 70-90% confluent. The cells were lifted and pelleted as previously described (Section 2.1). The pellet was washed once using DPBS and 125µl of Cell LyticM (Mammalian Cell Lysis Reagent C2978, Sigma Aldrich, Dorset, UK) was used to resuspend the cells. The cell solution was placed into a 1.5ml microtube and slotted into a MACSmix Tube Rotator (Miltenyi Biotec, Surrey, UK) for 15 minutes. After this, the cell solution was placed into an Eppendorf Centrifuge 5424 (Eppendorf UK Ltd, Stevenage, UK) at 15,000g for 15 minutes. 100µl of

the supernatant was removed and this became the cell lysate sample. This sample was then used for both the BCA assay and the proceeding CS assay.

2.9.4 BCA assay

BCA assay was carried out according to the manufacturer's instructions (Pierce, Illinois, USA) and as previously described (Section 2.7.3).

2.9.5 CS assay principle

CS is the primary enzyme in the Krebs cycle and is used as an exclusive marker for the mitochondrial matrix (Eigentler *et al.*, 2015). Therefore, CS can be used to measure the size of the mitochondrial network in cells. The enzyme catalyses the reaction of Acetyl-CoA with oxaloacetate to produce citrate. During citrate synthesis, DTNB is converted to Thio-bis-[2-nitrobenzoic acid]) cysteine (TNB) which can be detected at 412nm. The amount of TNB correlates to the amount of citrate produced and thus how much CS enzyme was present in the mitochondrial matrix. The equation below summarises this reaction:

oxaloacetate + Acetyl-CoA + H_2O → citrate + CoA-SH + H+ CoA-SH + DTNB → TNB + CoA-S-S-TNB

(↑ Absorbance at 412nm)

2.9.6 CS assay

2.9.6.1 Equipment set up

CS activity was measured spectrophotometrically at 412nm with a Varioskan Flash microplate reader (Thermo Fisher Scientific Varioskan® Flash, Waltham, MA) using an established method (Eigentler et al., 2015).The Varioskan Flash reader first underwent a pre-programmed wash protocol using ddH_2O. Then the system was loaded and primed with oxaloacetate 5ml stock in a 7ml bijoux tube.

2.9.6.2 Protocol

Cell samples were measured in triplicate in a sterile 96 well, clear plastic plate (3599, Costar, Corning Inc., Corning, NY). 200µl buffer solution and 1µl of cell sample was added to each experimental well. Two negative controls (200µl buffer) and two positive controls (200µl buffer + 1µl CS standard) were added to each plate.

The 96 well plate was then inserted into the machine, and the experiment was started. The recording period lasted for 10 minutes and measurements of the CS fluorescence were taken every 30 seconds. Once recording stopped, the raw data files were exported into a Microsoft Excel file (Microsoft Corporation, Redmond, Washington, USA). The protein content (µg/ml) that was assessed by the BCA assay at the beginning of the experiment, was used in the above step to normalise the values. Data given as a measure of international units (IU) per mg protein (IU/mg).

2.10 Flow Cytometry

All reagents were obtained from Gibco (Life Technologies, Paisley, UK) or Sigma (Sigma Aldrich, Dorset, UK) unless otherwise stated.

Before the experiments, CCCP (carbonyl cyanide *m*-chlorophenyl hydrazine) was left to equilibrate to room temperature (protected from light), whilst cell culture media, 0.05% TrypleE Express, DPBS and Hank's balanced salt solution (HBSS) were warmed to 37°C.

2.10.1 Cell preparation

Cells in T75cm^2 flasks were selected when they had reached 70-90% confluence. Cells were detached and pelleted as before (Section 2.1.1). The supernatant was disposed of, and the cell pellet resuspended in 1ml HBSS. A sample was taken and counted as before (Section 2.1.1) using an automated TC10 cell counter (Bio-Rad Laboratories, Hertfordshire, UK). Enough HBSS was then added to the cell suspension to give a concentration of approximately 1x10^6 cells/ml. The cell suspension was then divided, with 1ml placed into 1.5ml microtubes, ready to be treated with fluorescent reagents (Table 2.8). Before staining the cells with fluorescent reagents (reagents and detection wavelengths described in Table 2.8), cells could be pre-treated with 100nM PAPTP for 30 minutes in a humidified incubator (37°C; 95% air; 5% CO_2). In all protocols, one microtube was left unstained to serve as a negative control.

2.10.2 Protocols

2.10.2.1 Mitochondrial membrane potential

Three microtubes containing 1x10^6 cells in suspension were treated with 20nM TMRM. One microtube was additionally treated with 50µM CCCP (Sigma Aldrich). Another microtube was additionally treated with 0.5µM rotenone (Sigma Aldrich) and 2.5µM

antimycin A (Sigma Aldrich). All three microtubes were then incubated for 30 minutes in a humidified incubator (37°C; 95% air; 5% CO_2).

2.10.2.2 Mitochondrial Ca^{2+}

Three microtubes were treated with 1µM Rhod-2 AM (0.02% pluronic acid) for 30 minutes at (37°C; 95% air, 5% CO_2). The cells were then left to de-esterify for 30 minutes before imaging (RT, in the dark). During the de-esterification period, one microtube was treated with 50µM CCCP, and one was treated with 0.5µM rotenone and 2.5µM antimycin A.

2.10.2.3 NADH autofluorescence

A large proportion of NADH autofluorescence is due to mitochondrial NADH because NAD is non-fluorescent and the level of cytosolic NADH is normally low (Buckler and Turner, 2013). Mitochondrial NADH can be oxidised to NAD by uncoupling mitochondrial respiration, while NAD can be reduced to NADH by inhibiting the electron transport system (Buckler and Turner, 2013). Uncouplers like CCCP and electron transport inhibitors like rotenone and antimycin A can be used to define a range for the mitochondrial NADH signal between conditions of maximal oxidation and reduction. Three microtubes containing $1x10^6$ cells/ml were prepared as above. Before imaging, one microtube of cell suspension was treated with 50µM CCCP, and one microtube treated with a combination of 0.5µM rotenone and 2.5µM antimycin A (30 minutes in a humidified incubator (37°C; 95% air; 5% CO_2)).

2.10.3 Data recording and analysis

The samples were pelleted by centrifugation for 3 minutes at 600g in an Eppendorf Centrifuge 5424 (Eppendorf UK Ltd). The supernatants were then removed, and the cell pellet was washed twice with HBSS. The cells were resuspended in a final volume of 500µl HBSS. The samples were then analysed on a flow cytometer, with the appropriate excitation wavelength and emission filters (Table 2.8). Gates were applied using the unstained control, and the debris and duplicate cells were excluded. Standard compensation was applied using the CCCP-treated sample. The flow cytometer used was a BD LSRFortessa™ cell analyser (BD Biosciences, Franklin Lakes, NJ, USA) and the software used for data collection and analysis was the associated BD FACSDiva software (BD Biosciences, Franklin Lakes, NJ, USA).

Fluorescent Reagent	Function	Concentration	Detection Wavelength
RHOD-2AM	Cellular Ca^{2+} detection	20nM	548/574 nm
TMRM	MMP detection	1µM	552/581 nm
NADH Autofluorescence*	NADH detection	N/A	350-360/470 nm

Table 2.8. Fluorescent reagents used in flow cytometry experiments. From left to right columns, data shown is the name of the reagent, the function, the working concentration and its detection wavelength. * NADH autofluorescence is a property of the cell not a reagent.

2.11 Kv1.3 inhibitors

2.11.1 PAP-1: 5-(4-Phenoxybutoxy) psoralen. Product P6124, Sigma Aldrich (Sigma Aldrich, Dorset, UK). Soluble in DMSO. Stored at -20°C in the dark to prevent photo-oxidation.

2.11.2 ShK-Dap22: Cat. No. 3220. Tocris Bioscience (Bio-Techne, Abingdon, UK). Soluble in H_2O up to 1mg/ml. Stored at -20°C in the dark to prevent photo-oxidation.

2.11.3 PAPTP: Kindly gifted by Dr Robin Bon, LICAMM, Leeds University. A positively charged TPP moiety was attached to a PAP-1 derivative, as described by (Leanza *et al.*, 2017). Soluble in DMSO. Stored at -20°C in the dark to prevent photo-oxidation.

2.11.3.1 Synthesis of PAPTP

The mitochondriotropic compound PAPTP was synthetized as shown in Figure 2.4. For full details, see STAR Methods in Leanza et al., 2017.

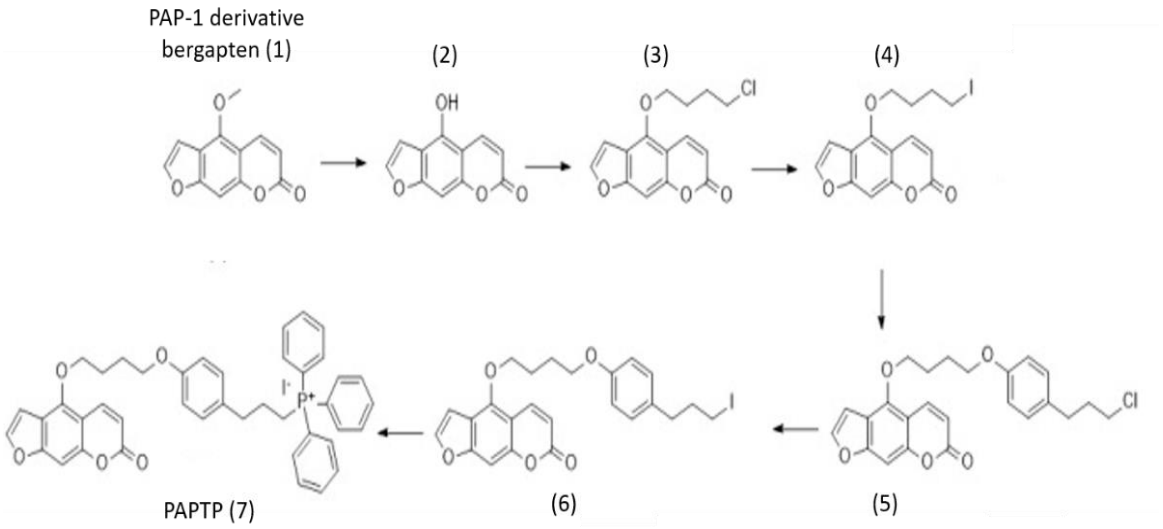

Figure 2.4 Synthesis of PAPTP. Image adapted from Leanza et al., 2017. **(1)** Bergapten. **(2)** 4-Hydroxy-7H-furo[3,2-g] benzopiran-7-one. **(3)** 4-(4-clorobutoxy)-7H-furo [3, 2, g] benzopyran-7-one. **(4)** 4-(4-iodobutoxy)-7H-furo[3,2-g] benzopyran-7-one. **(5)** 4-(4-(4-(3-chloropropyl) phenoxy) butoxy)-7H-furo[3,2-g] benzopyran-7-one. **(6)** 4-(4-(4-(3-iodopropyl) phenoxy) butoxy)-7H-furo[3,2-g] benzopyran-7-one. **(7)** (3-(4-(4((7-oxo-7H-furo[3,2-g] benzopyran-4-yl) oxy) butoxy) phenyl) propyl) triphenyl phosphonium iodide (PAPTP).

2.12 Data Analysis and Statistics

Data was input into GraphPad Prism (Version 6.03, GraphPad Software Inc, La Jolla, CA, USA), where unpaired Student's T-Tests and/or one-way ANOVA Tests (followed by Dunnet's or Tukey's post hoc test, as appropriate) were used to analyse the data. Statistical significance was determined when $p<0.05$. ROUT analysis was used to remove outliers.

Chapter Three

Kv1.3 expressing HEK293 cells have an increased rate of proliferation and respiration.

3.1 Introduction

The Kv1.3 channel increases cellular proliferation through a number of mechanisms, including ion conducting effects on plasma membrane potential (Blackiston, McLaughlin and Levin, 2009), Ca^{2+} influx (Cheong *et al.*, 2011) and cell volume regulation (Herrmann *et al.*, 2012). Non-conducting properties of the channel (Cidad *et al.*, 2012) and potential effects on cell signalling pathways (Lee *et al.*, 2014) have also been implicated in proliferation. These mechanisms may not be mutually exclusive in driving cell proliferation.

The Kv1.3 channel is localized to the inner mitochondrial membrane (IMM) of T lymphocytes (Szabo *et al.*, 2005), hippocampal neurons (Bednarczyk *et al.*, 2010), astrocytes (Cheng, Debska-Vielhaber and Siemen, 2010) and in cells isolated from a number of cancers (Mattarei *et al.*, 2018). In cancer, mitochondrial Kv1.3 may regulate apoptosis. Inhibiting Kv1.3 activates a reactive oxygen species (ROS)-mediated signalling cascade resulting in Bax/Bak independent cell death (Leanza *et al.*, 2012). However, the role of mitochondrial Kv1.3 in non-pathophysiological states is less well defined.

Kv1.3 overexpressing HEK293 cells are a robust model for investigating the effects of Kv1.3 on cellular physiology (Peers *et al.*, 2005; Scragg *et al.*, 2008; Cidad *et al.*, 2010, 2012; Duckles *et al.*, 2015; Jimenez-Perez *et al.*, 2016). Cellular proliferation has a high energy demand, requiring ATP for processes ranging from signal transduction to DNA, RNA and protein synthesis (Vander Heiden, Cantley and Thompson, 2009; Oronsky *et al.*, 2014; Pontes, Sevostyanova and Groisman, 2015). The distinct energy requirements of cellular proliferation (Lodish et al., 2000) coupled with the known mitochondrial localization of Kv1.3 (Szabo *et al.*, 2005) may mean that this ion channel

links cellular energy metabolism to proliferation. Preliminary data generated in our laboratory indicates that Kv1.3 overexpressing HEK293 cells have increased O_2 consumption and respiratory capacity compared with wild type (WT) HEK293 cells.

VSMC proliferation occurs in vasculopathies like atherogenesis and restenosis (Cheong *et al.*, 2011). The vessel remodelling by proliferation of VSMCs is modulated by Kv1.3 (Cidad *et al.*, 2012). Proliferating VSMCs have altered metabolism compared to quiescent cells (Perez *et al.*, 2010) yet the mechanisms which control this are unclear. It is also unknown whether Kv1.3 channels exist in VSMC mitochondria.

3.2 Aims and Objectives

The aim of this Chapter was to investigate the effect of Kv1.3 on cellular proliferation, energetics and respiration. A key set of objectives were designed to interrogate this aim:

1) To determine the robustness of the HEK293 Kv1.3 overexpressing cell line as a model of functional Kv1.3 channels.

2) To study the effects of Kv1.3 overexpression in HEK293 cells on proliferation.

3) To assess the effects of Kv1.3 on cellular respiration and energetics, identify the specificity of these effects compared to the related Kv1.5 channel, and to investigate whether Kv1.3 localises to the mitochondrial network in HEK293 cells.

4) To investigate the potential relevance to human physiology by identifying cellular location of Kv1.3 in human saphenous vein smooth muscle cells (HSVSMCs).

3.3 Results

3.3.1 Confirmation of the HEK293/Kv1.3 cell line as a stably transfected overexpression system of functional Kv1.3 channels.

Immunocytochemistry and immunoblotting were used to confirm that the HEK293/Kv1.3 cells were overexpressing the Kv1.3 channel (Figure 3.1). Using an anti-Kv1.3 antibody, and a fluorescent secondary antibody, increased Kv1.3 was detected in the HEK293/Kv1.3 cells compared with WT HEK293 cells (Figure 3.1A and 3.1B). The channels are dispersed throughout the HEK293/Kv1.3 cells, indicating Kv1.3 channels are expressed within intracellular locations. As a secondary confirmation western blotting identified a low level of Kv1.3 protein expression in WT HEK293 cells, which was significantly higher in the HEK293/Kv1.3 cells (Figure 3.1C and 3.1D). Kv1.3 protein corresponds to a band of approximately 68-75 kDa. Non-specific staining by Alexa Fluor 488 in WT HEK293 and HEK293/Kv1.3 cells was assessed in cells without anti-Kv1.3 primary antibody incubation (Figure 3.2). The image in Figure 3.1A is not representative of the amount of Kv1.3 protein, as detected by wester blot, in WT HEK293 cells (Figure 3.1C and D).

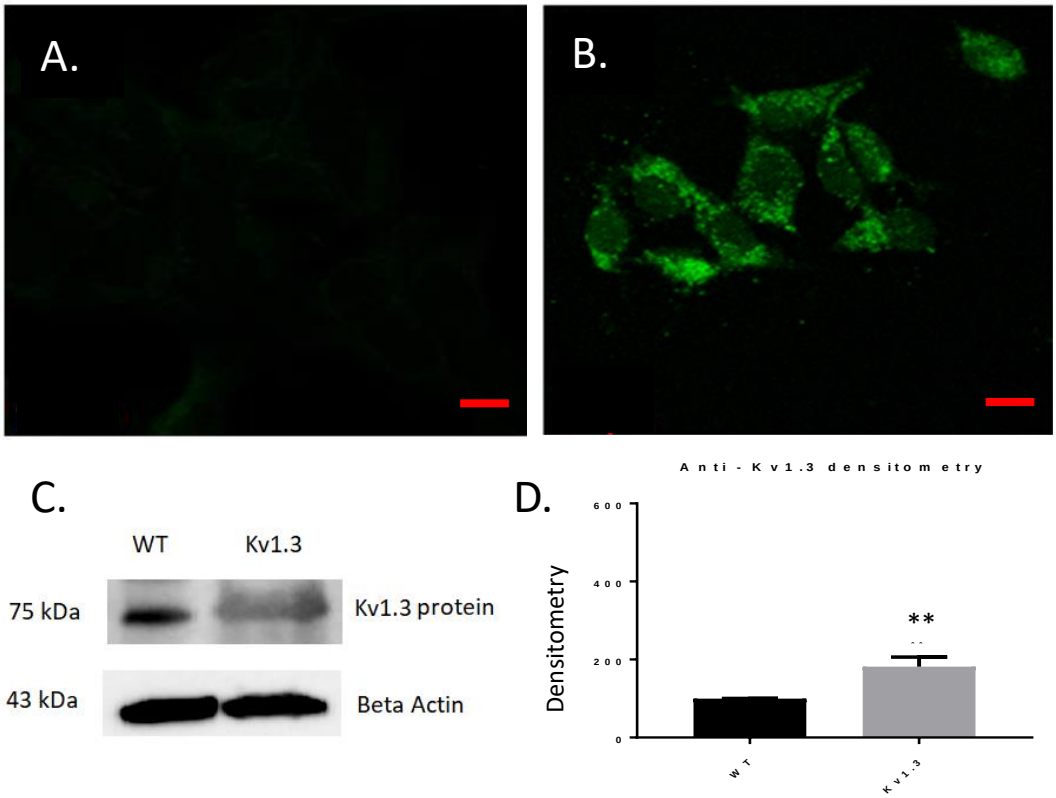

Figure 3.1 Increased Kv1.3 channel and protein expression in HEK293/Kv1.3 cell line. A and B. Representative images of WT HEK293 (A) and HEK293/mKv1.3 cells (B) treated with Anti-Kv1.3 Clone L23/27, mouse monoclonal primary antibody and Alexa Fluor 488 Donkey anti-Mouse IgG (H+L) secondary antibody. Scale bars represent 10 µM. C. Representative western blots for 67-75kDa Kv1.3 protein, Kv1.3 (top panel), β-Actin control (bottom panel). D. Western blot densitometry data quantifying Kv1.3 protein in WT HEK293 and HEK293/Kv1.3 cells. Data analysed using a Student's t-test. ** $p<0.01$. WT HEK293 Kv1.3 protein expressed as 100 percent. Data expressed as mean ± SEM (n=5). WT = WT HEK293 cells, Kv1.3 = HEK293/Kv1.3 cells. Data in C and D was generated by Dr T. Hettiarachchi, University of Leeds.

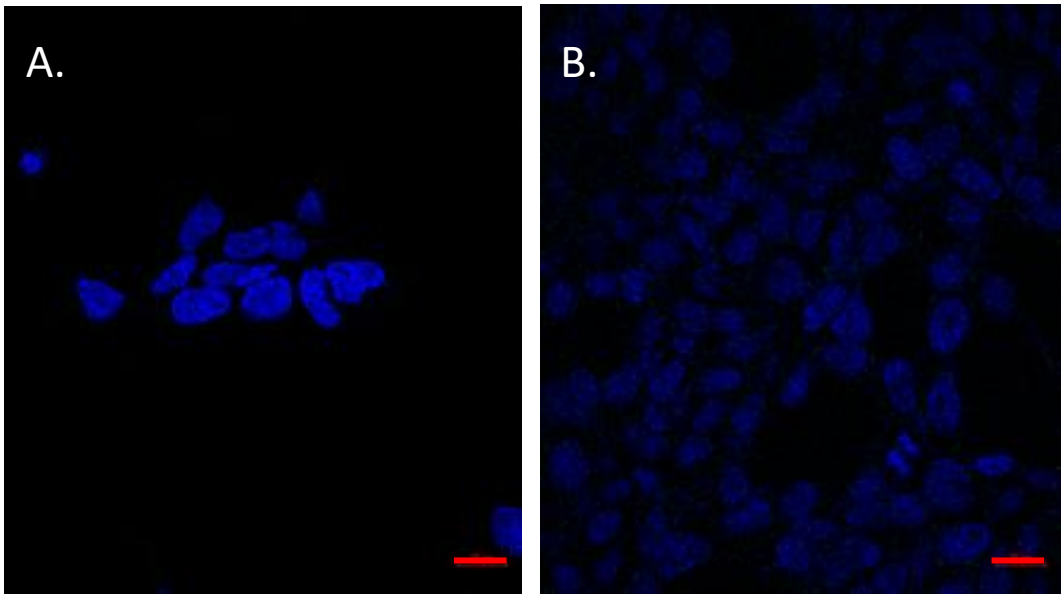

Figure 3.2 Alexa Fluor 488 provides a specific secondary antibody in HEK293/Kv1.3 and WT HEK293 cells. WT HEK293 (A) and HEK293/Kv1.3 (B) cells stained with Alexa Fluor 488 Donkey anti-Mouse IgG (H+L) secondary antibody (green). Cell nuclei stained with diamidino-2-phenylindole (DAPI) (blue). Scale bars (red lines) represent 20µM.

The functional properties of Kv1.3 channels were investigated using whole cell patch clamp electrophysiology (Figure 3.3). Cells were held at a holding potential of -80mV and periodically depolarised in 10mV steps from -60mV to +60mV to record the K^+ current leaving the cells. This current was significantly greater in HEK293/Kv1.3 cells (Figure 3.3A) compared with WT HEK293 cells (Figure 3.3B). The IV relationship is shown in Figure 3.3C. At any voltage on the X axis, HEK293/Kv1.3 cells have a much higher K^+ ion current than WT HEK293 cells. In Figure 3.3D, the K^+ ion currents at +40mV in WT HEK293 cells and HEK2933/Kv1.3 cells are shown. In Figure 3.3D, the Kv1.3 channels in the HEK293/Kv1.3 cells were tagged with fluorescent mCherry marker protein and denoted HEK293/Kv1.3-P118 in the figure. These cells also elicited a much greater K^+ current than WT HEK293 cells when depolarized from -80mV to +40mV (Figure 3.3D). The mCherry marker protein does not affect Kv1.3 channel biophysics (Jimenez-Perez *et al.*, 2016).

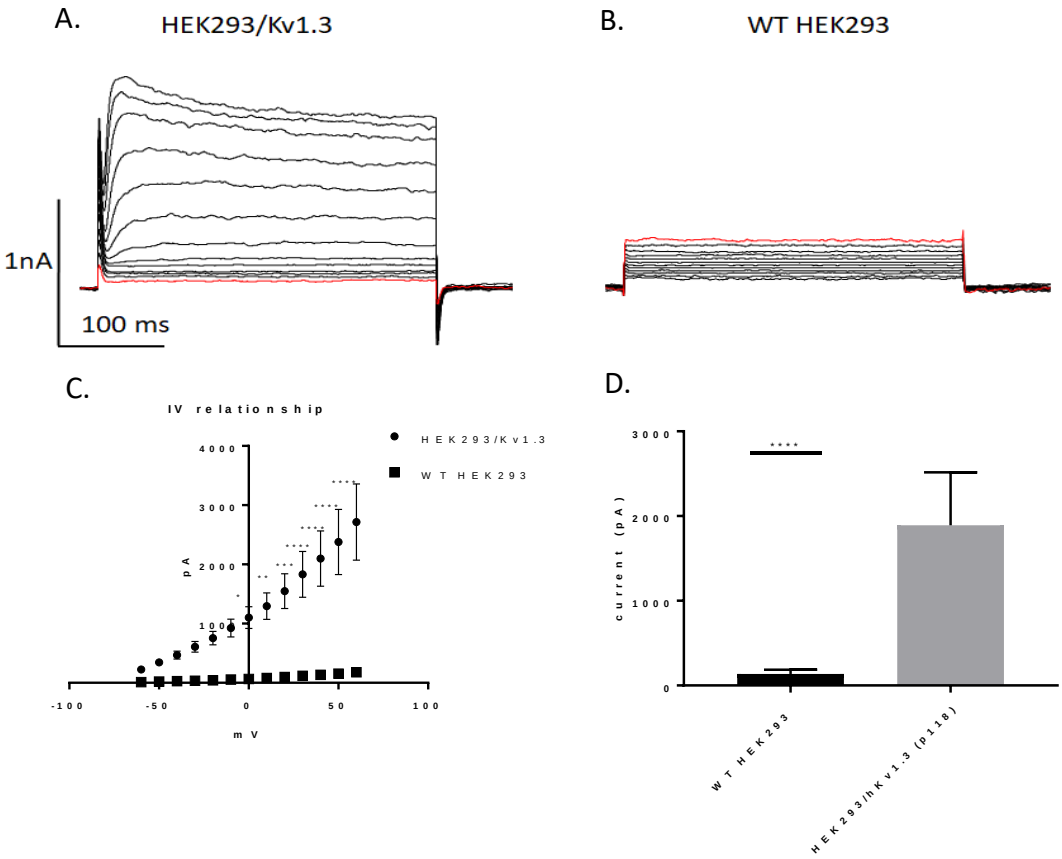

Figure 3.3 HEK293/Kv1.3 cells have a larger potassium ion current than WT HEK293 cells. A and B. Example potassium ion currents in HEK293/Kv1.3 (A) and WT HEK293 cells (B), as determined by whole cell patch clamp electrophysiology. C. IV current traces of both HEK293/Kv1.3 cells (black dots) and WT HEK293 cells (black squares). Currents evoked by step-depolarisations from -60 to +60mV. Data expressed as mean ± SEM (n=7 for HEK293/Kv1.3, n=6 for WT HEK293 cells). Data analysed using two way ANOVA * $p<0.05$, ** $p<0.01$, *** $p<0.001$, **** $p<0.0001$. D. Size of potassium currents (pA) in HEK293/Kv1.3-P118 (grey bar) and WT HEK293 cells (black bar) evoked by a single step depolarization from −80 to +40 mV. Data analysed using Student's t-test **** $p<0.0001$. Data expressed as mean ± SEM (n=6 for each cell type). Data in A, B and C was generated by Dr M. Al-Owais, University of Leeds.

3.3.2 HEK293/Kv1.3 cells have increased proliferation and respiration compared to WT HEK293 cells.

The rate of cell proliferation was interrogated in HEK293/Kv1.3 and WT HEK293 cells. HEK293/Kv1.3 cells exhibited an increased rate of proliferation compared to WT HEK293 cells (Figure 3.4A and B). Figure 3.4B shows HEK293/Kv1.3 cell proliferation normalised to the Day 0 cell count to account for variability between average Day 0 counts in the two cell lines.

A.

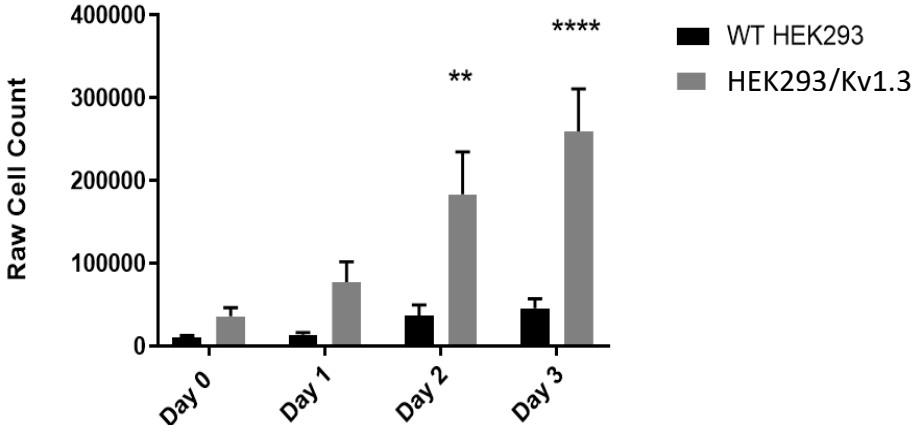

B.

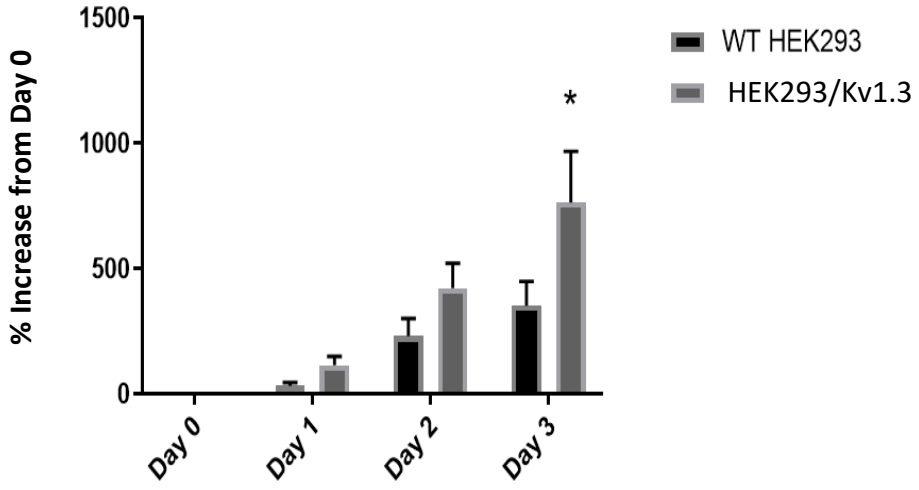

Figure 3.4 HEK293/Kv1.3 cells have an increased proliferation rate compared to WT HEK293 cells. A. HEK293/Kv1.3 cells (grey bars) proliferate more quickly than WT HEK293 cells (black bars). B. Data from graph (A) was normalised to Day 0 and expressed as percent increase from Day 0. Again, WT HEK293 data was shown in black bars and the HEK293/Kv1.3 data was in the grey bars. WT HEK293 data shown by black bars, HEK293/Kv1.3 data shown by grey bars. Data expressed as the mean ± SEM (n=3). For each day, data was analysed using Student's t-test * $p<0.05$.

High Resolution Respirometry was used to assess the effect of Kv1.3 overexpression on mitochondrial function in HEK293 cells. A whole cell coupling control protocol was used, using a previously described method (Gnaiger, 2014). Coupling control protocols in whole cells use membrane-permeable inhibitors of OXPHOS, like oligomycin and antimycin A, and uncouplers like FCCP to interrogate cellular respiration (Gnaiger, 2014).

In Figure 3.5, there are representative respirometry traces for HEK293/Kv1.3 (Figure 3.5A) and WT HEK293 cells (Figure 3.5B). The points at which measurements of O_2 consumption were taken are highlighted; R, L, ETS and ROX. R represents 'Routine Respiration' which is the basal level of respiration reached once the chamber is closed. L represents 'Leak Respiration' and represents the depressed O_2 flow that exists after inhibition of ATP-synthase by oligomycin. Leak refers to the movement of H^+ protons down the electrochemical proton gradient from the IMS across the IMM and into the matrix. ETS represents the O_2 flow at 'maximum capacity of electron transport system' which is measured after maximum uncoupling by a protonophore like FCCP. ROX is Residual Oxygen Consumption and represents 'non-mitochondrial O_2 consumption' after complete inhibition of mitochondrial respiration. The black arrows show the time points at which the uncoupler FCCP was added. Note that in WT HEK293 cells it took more titrations of FCCP to reach maximal ETS uncoupling than in HEK293/Kv1.3 cells.

In Figure 3.5A and B, the higher the red trace line on the Y axis, the greater the O_2 consumption by the cells per second. The lower the blue trace line on the Y axis, the lower the concentration of O_2 in the chambers. In A, after closure of the chamber, the O_2 consumption by the cells (red line) is higher on the Y axis at R, L, ETS and ROX than in B, suggesting that HEK293/Kv1.3 cells have increased respiration than WT HEK293 cells. The mean results from all coupling control protocols in WT HEK293 and HEK293/Kv1.3 cells are shown in Figure 3.5C. HEK293/Kv1.3 cells had significantly higher respiration than WT HEK293 cells. The routine level of O_2 consumption was higher in HEK293/Kv1.3 cells, indicating higher basal respiration. HEK293/Kv1.3 cells had higher leak respiration, indicating more H^+ proton movement into the matrix when ATP-synthase was inhibited. The maximum capacity of the ETS was also larger in HEK293/Kv1.3 cells.

Due to the nature of the coupling control protocol (Gnaiger, 2014), interrogation of the maximum capacity of the ETS requires repeated titrations of FCCP until no further increase in O_2 consumption is recorded in response to the protonophore. Interestingly, WT HEK293 cells required more titrations of FCCP before they were maximally uncoupled (Figure 5A and 5B). This meant that ultimately WT HEK293 cells were treated with higher concentrations of FCCP. The reasons for this remain unclear but a greater response to FCCP in HEK23/Kv1.3 cells suggests that there is a greater electrochemical gradient for H^+ across the inner mitochondrial membrane than in WT HEK293 cells. This suggests that the treatment with FCCP caused rapid diffusion of H^+ into the matrix leading to more H^+ being able to bind to O_2 at complex IV. This would lead to a much greater O_2 consumption in HEK293/Kv1.3 cells. To get the same amount of H^+ binding to O_2 in WT HEK293 cells, much more protonophore is required.

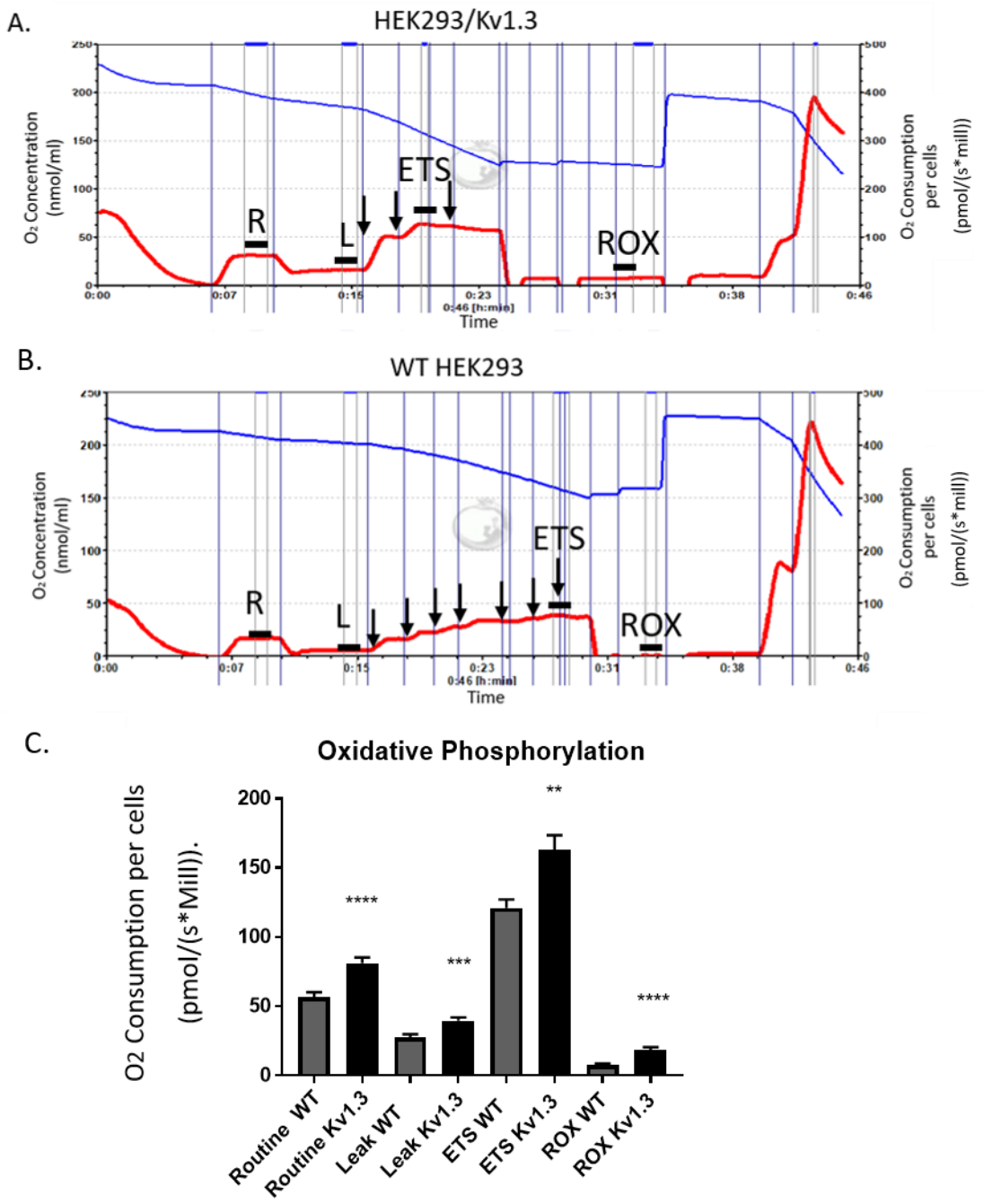

Figure 3.5 HEK293/Kv1.3 cells have increased OXPHOS compared to WT HEK293 cells. Example respirometry traces from HEK293/Kv1.3 cells (A) and WT HEK293 cells (B). Each trace is generated from a single enclosed chamber containing 2 million cells. Red line represents O_2 consumption throughout the respiratory protocol (pmol/(s*mill)). Blue line represents O_2 concentration in the chamber (nmol/ml). Black horizontal lines show the points at which O_2 consumption was measured (R = Routine Respiration, L = Leak Respiration, ETS = Electron Transport System Maximum Respiration, ROX = Residual Oxygen Consumption. L was measured after addition of 2µg/ml oligomycin, ETS after titrations of 0.5µM FCCP and ROX after addition of 2.5µM rotenone and 0.5µM antimycin A. Black arrows show the points at which FCCP was added to the chamber. C. Results from respirometry experiments in HEK293/Kv1.3 (black bars) and WT HEK293 cells (grey bars). For each cell type, O_2 consumption has been measured at points denoted by R, L, ETS and ROX in (A) and (B). Data expressed as the mean ± SEM (n = 38, HEK293/Kv1.3 cells and n=27, WT HEK293 cells). At each point in the experiment (R, L, ETS and ROX), data from each cell type was analysed using a Student's t-test ** p<0.01, *** p<0.001 and **** p<0.0001.

In Figure 3.5 it is important to note that non-mitochondrial O_2 consumption, as identified by ROX, was higher in HEK293/Kv1.3 cells. Therefore, baseline data was corrected for ROX (Figure 3.6). Figure 3.6A shows the Routine (basal) Respiration of WT HEK293 cells and HEK293/Kv1.3, where HEK293/Kv1.3 cells have a significantly higher Routine O_2 consumption than WT HEK293 cells. There are no differences in Leak Respiration between the two cell types (Figure 3.6B). The measurement of Routine and Leak Respiration can be used to assess the ATP turnover in cells (Figure 3.6C) by finding the difference between the two figures. HEK293/Kv1.3 cells have a higher ATP turnover than WT HEK293 cells and O_2 consumption is also significantly higher in HEK293/Kv1.3 cells at the FCCP-induced, maximum uncoupled state (Figure 3.6D). By finding the difference between this maximum respiration measurement and the Routine Respiration, the spare respiratory capacity (SRC) can be calculated. HEK293/Kv1.3 cells have a larger SRC than WT HEK293 cells (Figure 3.6E). As mentioned previously, as well as these increases in mitochondrial OXPHOS, the non-mitochondrial O_2 consumption (the ROX) is significantly much larger in HEK293/Kv1.3 cells (Figure 3.6F).

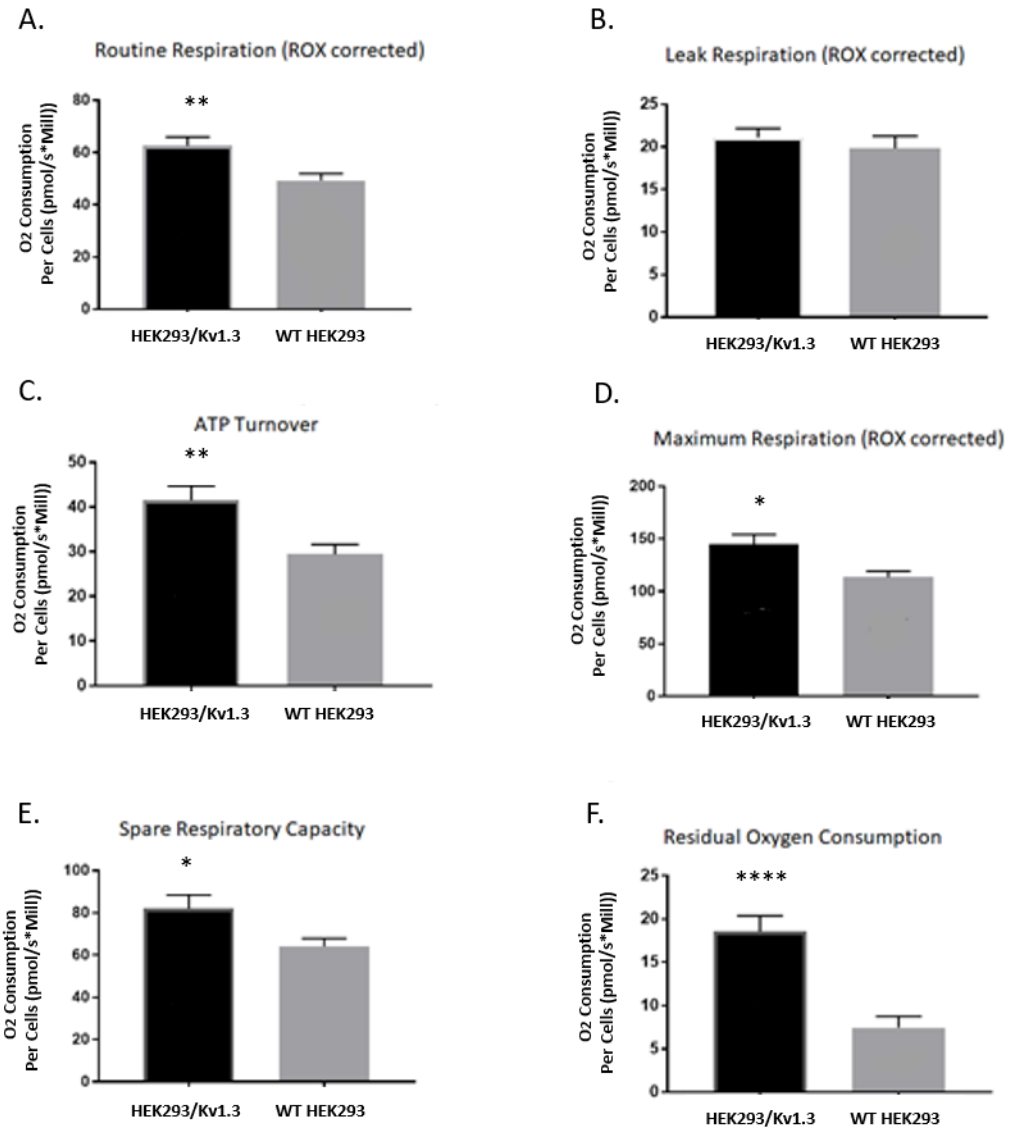

Figure 3.6. Residual oxygen consumption-corrected respiration in WT HEK293 and HEK293/Kv1.3 cells. In all graphs (A-F) HEK293/Kv1.3 (Kv1.3) cell data is shown in the black bars, WT HEK293 (WTHEK) cell data is shown in the grey bars. A. Routine (basal) Respiration rate of HEK293/Kv1.3 cells and WT HEK293 cells B. Leak Respiration of HEK293/Kv1.3 cells and WT HEK293 cells. C. ATP turnover in HEK293/Kv1.3 cells and WT HEK293 cells. ATP turnover calculated by finding the difference between routine respiration (A) and leak respiration (B). D. Maximum Uncoupled Respiration in HEK293/Kv1.3 cells and WT HEK293 cells. E. Spare respiratory capacity (SRC) in HEK293/Kv1.3 and WT HEK293 cells. SRC is calculated by finding the difference between Maximum Uncoupled Respiration (D) and Routine (basal) Respiration (A). F. Residual Oxygen Consumption (ROX) in HEK293/Kv1.3 and WT HEK293 cells. Data was analysed using a Student's t-test * $p<0.05$ **$p<0.01$ **** $p<0.0001$. Data expressed as the mean ± SEM (n = 27 for WT HEK293 cells and n=38 for HEK293/Kv1.3 cells)

3.3.3 Overexpression of Kv1.5 in HEK293 cells decreases mitochondrial respiration.

In contrast to Kv1.3, overexpression of Kv1.5 in WT HEK293 cells reduces cellular proliferation (Cidad *et al.*, 2015). This was confirmed in our lab by Dr M. Al-Owais, who carried out proliferation assays with HEK293/Kv1.5 cells. HEK293/Kv1.5 cells proliferated significantly less than HEK293/Kv1.3 and WT HEK293 cells over 3 days (Figure 3.7). To investigate whether a K^+ channel which reduces proliferation in HEK293 cells also reduces respiration, HEK293/Kv1.5 cells were examined using High Resolution Respirometry (Figure 3.8) as described previously. HEK293/Kv1.5 cells had lower Routine (basal) and Leak Respiration then either WT HEK293 or HEK293/Kv1.3 cells, independent of correction for ROX (Figure 3.8A and B). However, there was no significant difference in the maximum respiration rate between HEK293/Kv1.5 and WT HEK293 cells. There is also no difference in ROX between HEK293/Kv1.5 and WT HEK293. There are however significant differences between maximum and residual O_2 consumption in HEK293/Kv1.3 and HEK293/Kv1.5. These data suggest that the opposing effects on proliferation by Kv1.3 and Kv1.5 channel overexpression is mirrored by effects on mitochondrial respiration.

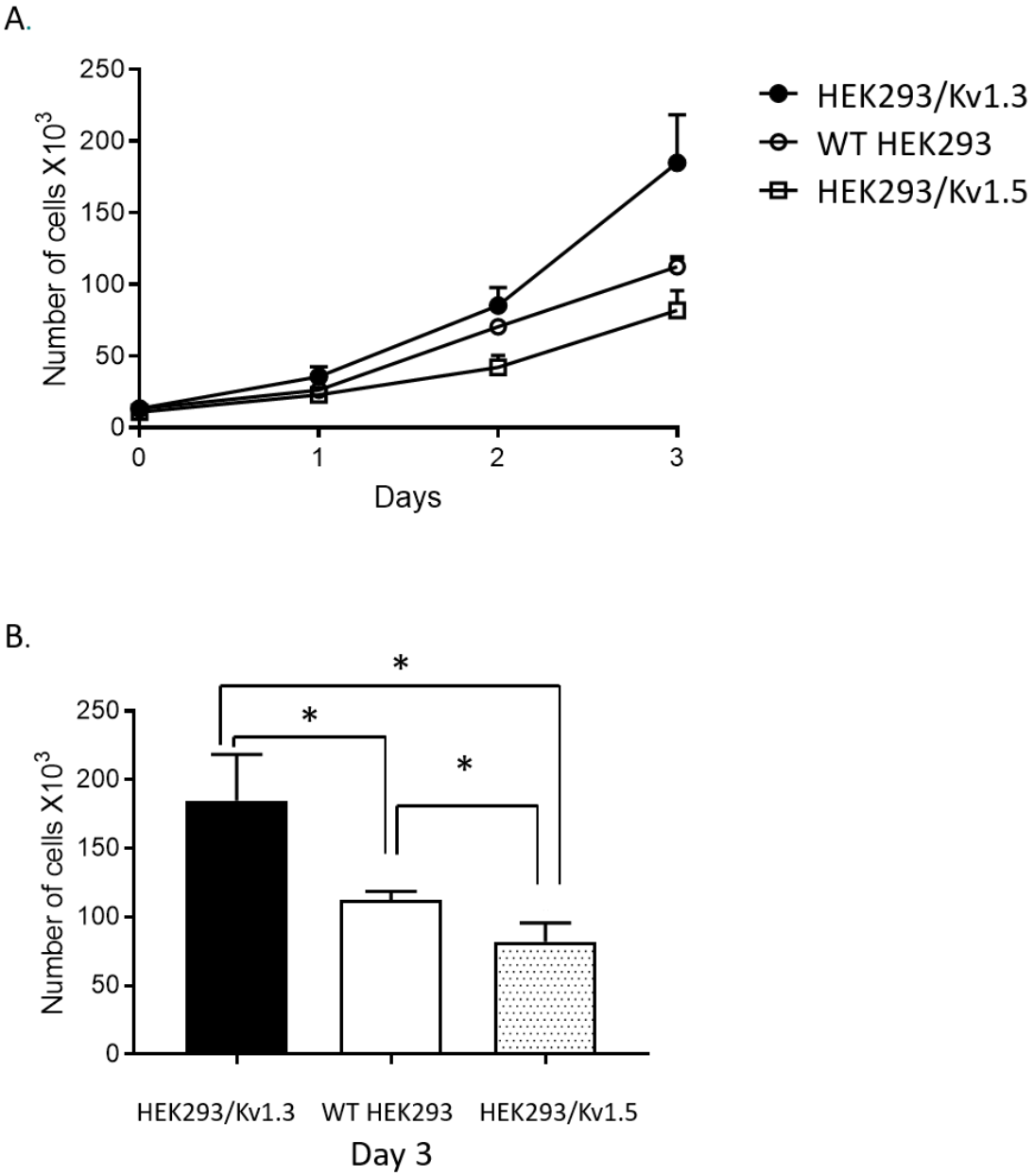

Figure 3.7 HEK293/Kv1.5 cells have decreased proliferation compared to WT HEK293 cells. A. HEK293/Kv1.3 (n=12, black circles), WT HEK293 (n=15, white circles) and HEK293/Kv1.5 (n=12, white squares) cell counts at days 0, 1, 2 and 3. Data expressed as the mean ± SEM. B. Mean cell counts (± SEM) at day 3 for HEK293/Kv1.3 cells (n =12, black bars), WT HEK293 cells (n = 15, white bar) and HEK293/Kv1.5 cells (n=12, dotted bar). Student's t-test confirmed HEK293/Kv1.3 cell proliferation was significantly increased, and HEK293/Kv1.5 cell proliferation was significantly decreased compared to WT HEK293 cells. * $p<0.05$. Experiments and statistical analysis carried out by Dr M. Al-Owais, Leeds University.

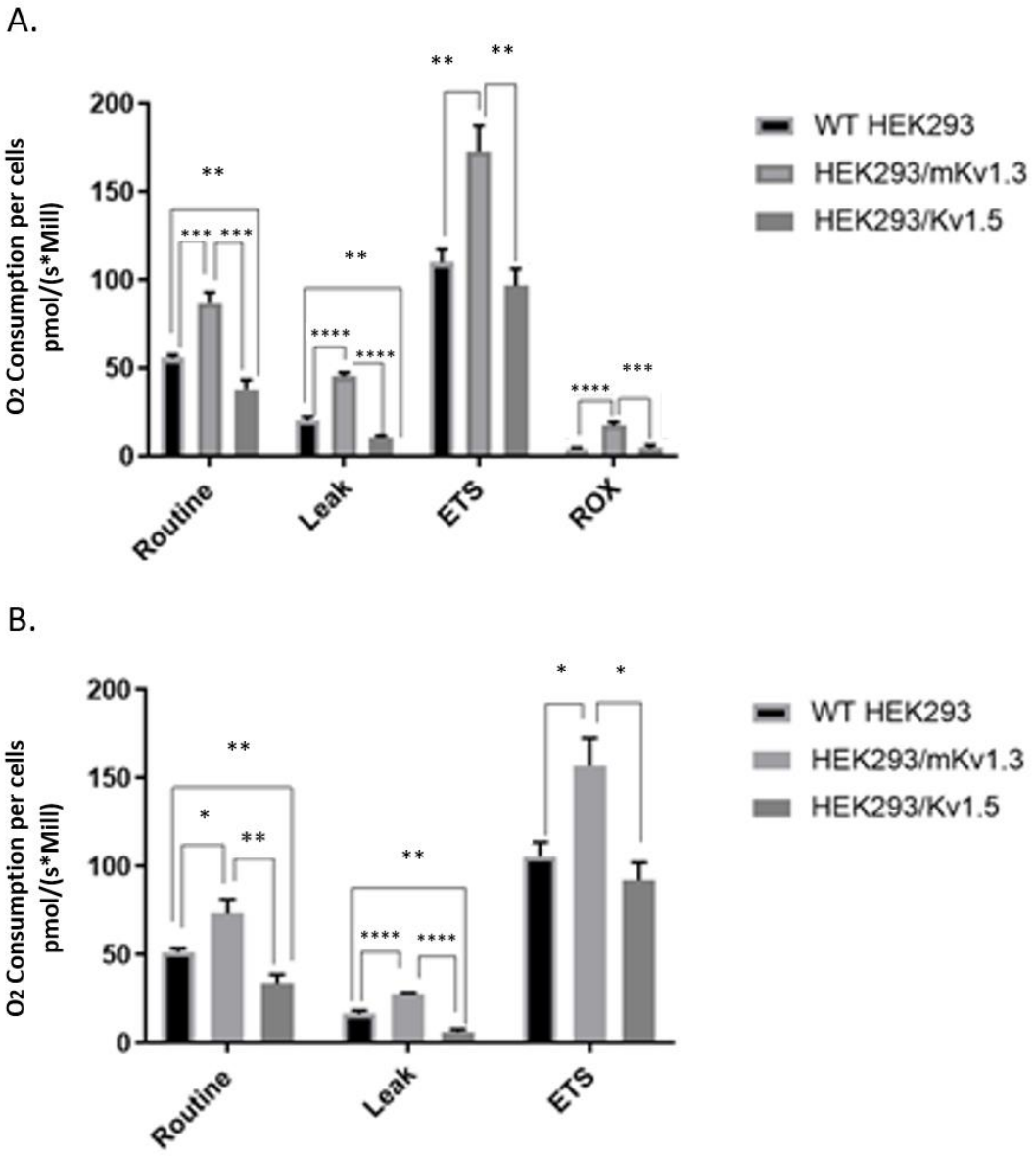

Figure 3.8 HEK293/Kv1.5 cells have reduced OXPHOS compared to WT HEK293 and HEK293/Kv1.3 cells. A. Comparison of respiration in WT HEK293 (black bars), HEK293/Kv1.3 (light grey bars) and HEK293/Kv1.5 (dark grey bars) cells. Oxygen consumption (O_2 consumption per million cells per second (pmol(s*Mill))) was measured at four points; routine=Routine/Basal Respiration, leak=Leak Respiration, ETS=maximum uncoupled respiration and ROX=non-mitochondrial oxygen consumption. B. Data from (A) corrected for ROX. In A and B, data expressed as mean ± SEM (WT HEK293, n=8, HEK293/Kv1.3, n=10, HEK293/Kv1.5, n=5). Data was analysed using one-way ANOVA * $p<0.05$, ** $p<0.01$, *** $p<0.001$ and **** $p<0.0001$.

3.3.4 Kv1.3 channels co-localise with the mitochondrial network in HEK293/Kv1.3 cells.

Immunocytochemistry was employed to investigate the cellular localization of Kv1.3 channels in WT HEK293 and HEK293/Kv1.3 cells. Cells were stained to identify Kv1.3 channels (anti-Kv1.3 antibody with a green fluorescence secondary reporter), and mitochondria (MitoTracker CMXRos, red fluorescence) and imaged using confocal microscopy (Figure 3.9). HEK293 cells do not exhibit autofluorescence within the Mitotracker detection wavelengths (Figure 3.10). Co-localisation of the channel with mitochondria was determined by the extent of yellow/orange fluorescence resulting from the overlap from Kv1.3 and mitochondrial staining. As expected HEK293/Kv1.3 cells were observed to have greater staining for the Kv1.3 channel (Figure 3.9A vs D). Surprisingly, HEK293/Kv1.3 cells exhibited greater staining for mitochondria (Figure 3.9B vs E). In both WT HEK293 and HEK293/Kv1.3 cells, the Kv1.3 channels were observed to co-localize with mitochondria (Figure 3.9C and F).

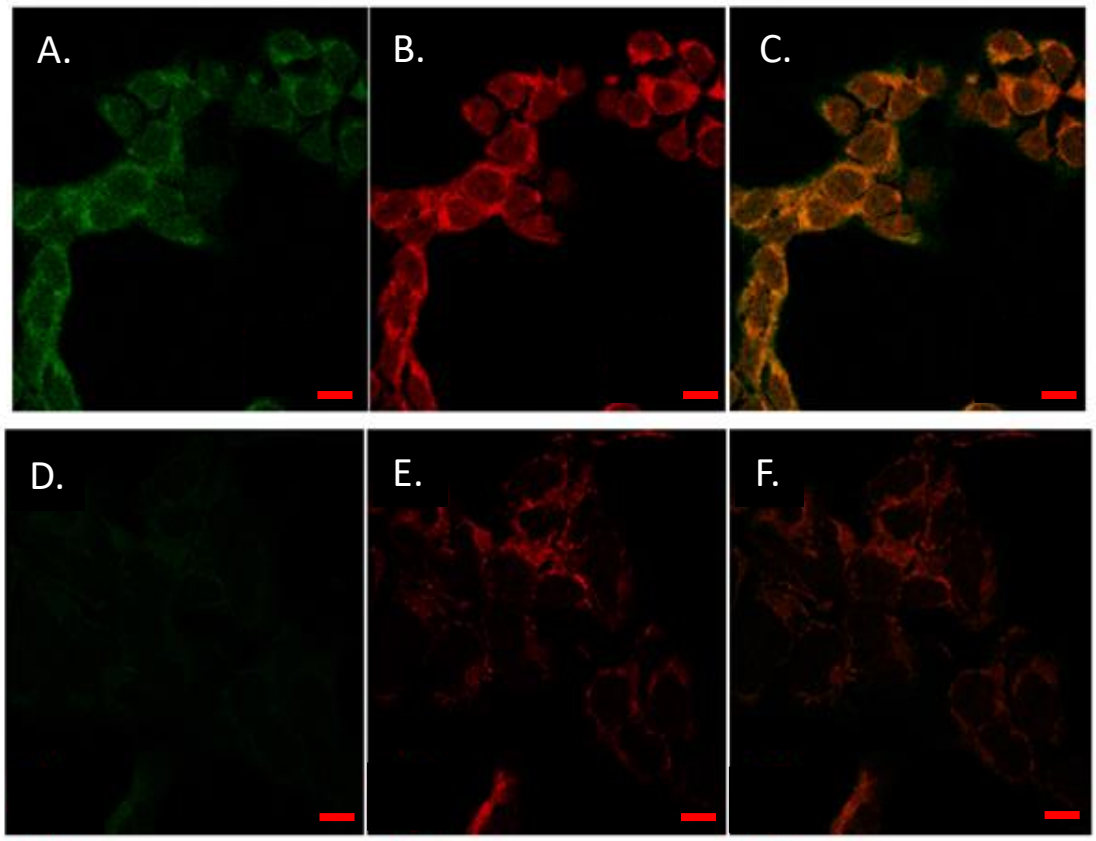

Figure 3.9 Mitochondrial and Kv1.3 co-localisation in HEK293/Kv1.3 cells. A, B and C = HEK293/Kv1.3 cells. Left panel (A) shows Kv1.3 channels stained with Anti-Kv1.3 monoclonal primary antibody Alexa Fluor 488 secondary antibody (green fluorescence). Centre panel (B) shows mitochondria stained with MitoTracker Red CMXRos (red). Right panel (C) is composite image of previous two images, indicating Kv1.3 localisation to the mitochondria (yellow/orange). Scale bars are 10µM. D, E and F = WT HEK293 cells. Left panel (D) shows cells stained with Anti-Kv1.3 monoclonal primary antibody Alexa Fluor 488 secondary antibody. Centre panel (E) shows mitochondria stained with MitoTracker Red CMXRos (red). Right panel (F) is composite image of previous two images. Scale bars are 10µM.

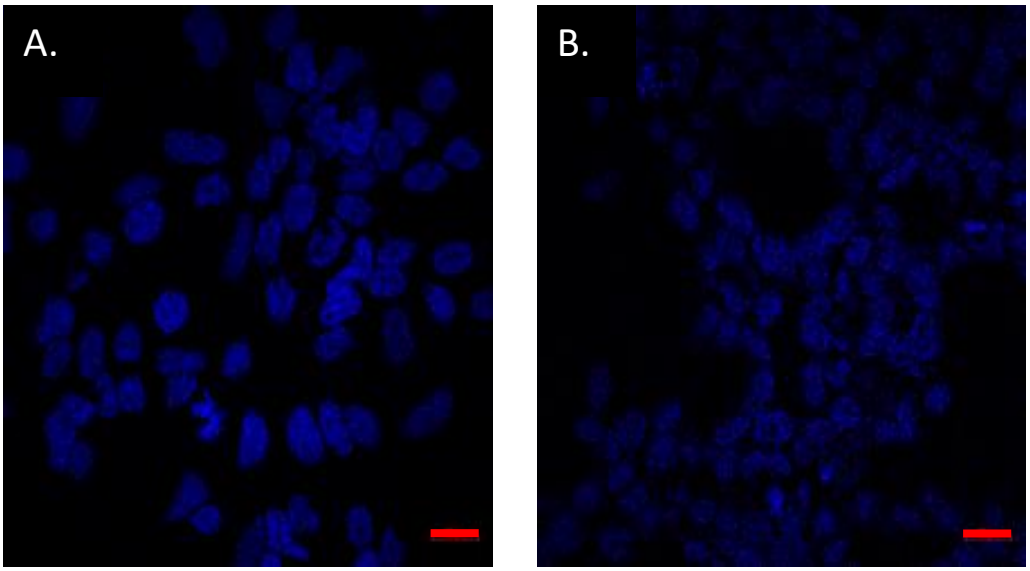

Figure 3.10 MitoTracker controls in WT HEK293 and HEK293/Kv1.3 cells. MitoTracker controls in WT HEK293 (A) and HEK293/Kv1.3 cells (B). Cells were stained with diamidino-2-phenylindole (DAPI) (blue) for nuclei detection. Excitation/emission wavelengths were 360nm/460nm. Cells also excited at the MitoTracker detection wavelengths of 579nm/599nm (excitation/emission) to test for any red autofluorescence in these cells. Scale bars represent 20 µm.

A second immunocytochemistry method was used to investigate Kv1.3 and mitochondrial co-localisation in HEK293/Kv1.3 cells (Figure 3.11). In Figure 3.11 the HEK293/Kv1.3 cells expressed mCherry-tagged Kv1.3 channels and were referred to as HEK293/Kv1.3-P118 cells. WT HEK293 cells did not contain the marker protein and so were used as a control for background fluorescence at mCherry detection wavelengths. No antibodies against the Kv1.3 channel were used in Figure 3.11, only the mCherry fluorescence (red) was used to detect Kv1.3 channels in HEK293/Kv1.3-P118 cells. The mitochondrial network was stained using an anti-COX IV antibody against cytochrome c oxidase (complex IV) of the mitochondrial respiratory chain. An Alexa 488 secondary antibody was used to highlight COX IV staining (green fluorescence). Co-localisation was determined by the crossover between the red (mCherry) and green (COX IV) fluorescence producing yellow/orange fluorescence if co-localisation existed. Images A-H show immunostained HEK293/Kv1.3-P118 cells and images I-P show WT HEK293 cells. The presence of yellow/orange fluorescence in (D) backed up the findings in Figure 3.9C, that Kv1.3 channels can co-localise with

mitochondria in HEK293 cells. HEK293/Kv1.3 cells do not exhibit autofluorescence within the COX IV detection wavelengths (Figure 3.11F). WT HEK293 cells do not display autofluorescence within both mCherry detection wavelengths (Figure 3.11K and O) or within COX IV detection wavelengths.

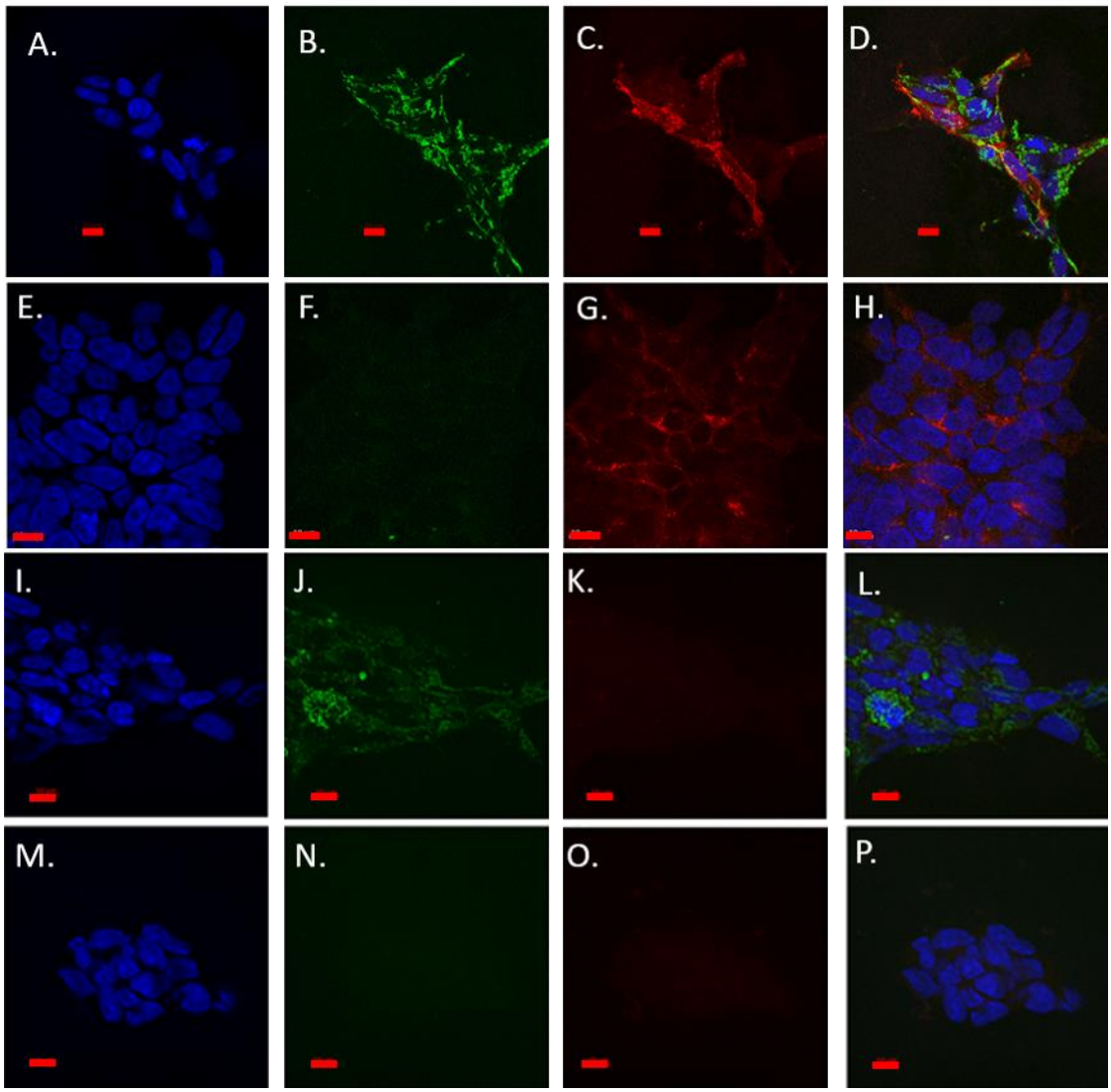

Figure 3.11 Mitochondrial and Kv1.3 co-localisation in HEK293/Kv1.3-P118 cells. A – H) Kv1.3 channel and mitochondrial co-localisation in HEK293/Kv1.3-P118 cells. A. DAPI staining of cell nuclei (blue). B. Immunostaining of cytochrome C oxidase to visualise the mitochondria (green). C. Red fluorescence of mCherry tagged Kv1.3 channels. D. Composite image of DAPI nuclear stain (blue), cytochrome C oxidase immunostain (green) and mCherry-tagged Kv1.3 cells (red). E. DAPI staining of cell nuclei (blue). F. Control for non-specific binding by the Alexa Fluor secondary antibody. Staining was performed as in (B) but without anti-COXIV antibody. G. Red fluorescence of mCherry tagged Kv1.3 channels. H. Composite image of E, F and G. **I - P)** Immunostaining of WT HEK293 cells for Kv1.3 channel and mitochondrial co-localisation. I. DAPI staining of cell nuclei (blue). J. Immunostaining of cytochrome C oxidase to visualise the mitochondria (green). K. Control for background red fluorescence. L. Composite image of DAPI nuclear stain (blue), cytochrome C oxidase immunostain (green) and background fluorescence (red). M. DAPI staining of cell nuclei (blue). N. Control for non-specific binding by the Alexa Fluor secondary antibody. Staining was performed as in (J) but without anti-COXIV antibody. O. Control for background red fluorescence. P. Composite image of M, N and O. All scale bars are 10µm.

3.3.5 Kv1.3 channels co-localise with the mitochondrial network in Primary Human Saphenous Vein Smooth Muscle Cells.

To examine whether the Kv1.3 channel mitochondrial localisation identified in HEK293 cells translate to primary human cells, the cellular localization of Kv1.3 channels was investigated in primary human saphenous vein smooth muscle cells (HSVSMCs). HSVSMCs were isolated from patients undergoing surgery at Leeds General Infirmary. Kv1.3 channels visualised using an anti-Kv1.3 antibody and Alex Flour secondary detection antibody (green fluorescence) and mitochondria were stained using Mitotracker Red CMXRos (red fluorescence) (Figure 3.12A and B, respectively). Co-localisation of Kv1.3 with the mitochondrial network is identified by yellow/orange fluorescence in the composite image (Figure 3.12C). Kv1.3 and mitochondrial staining was performed on HSVSMCs isolated from three other independent patients (Figure 3.12D, E and F). Kv1.3 channels were identified as present in the mitochondria of the HSVSMCs.

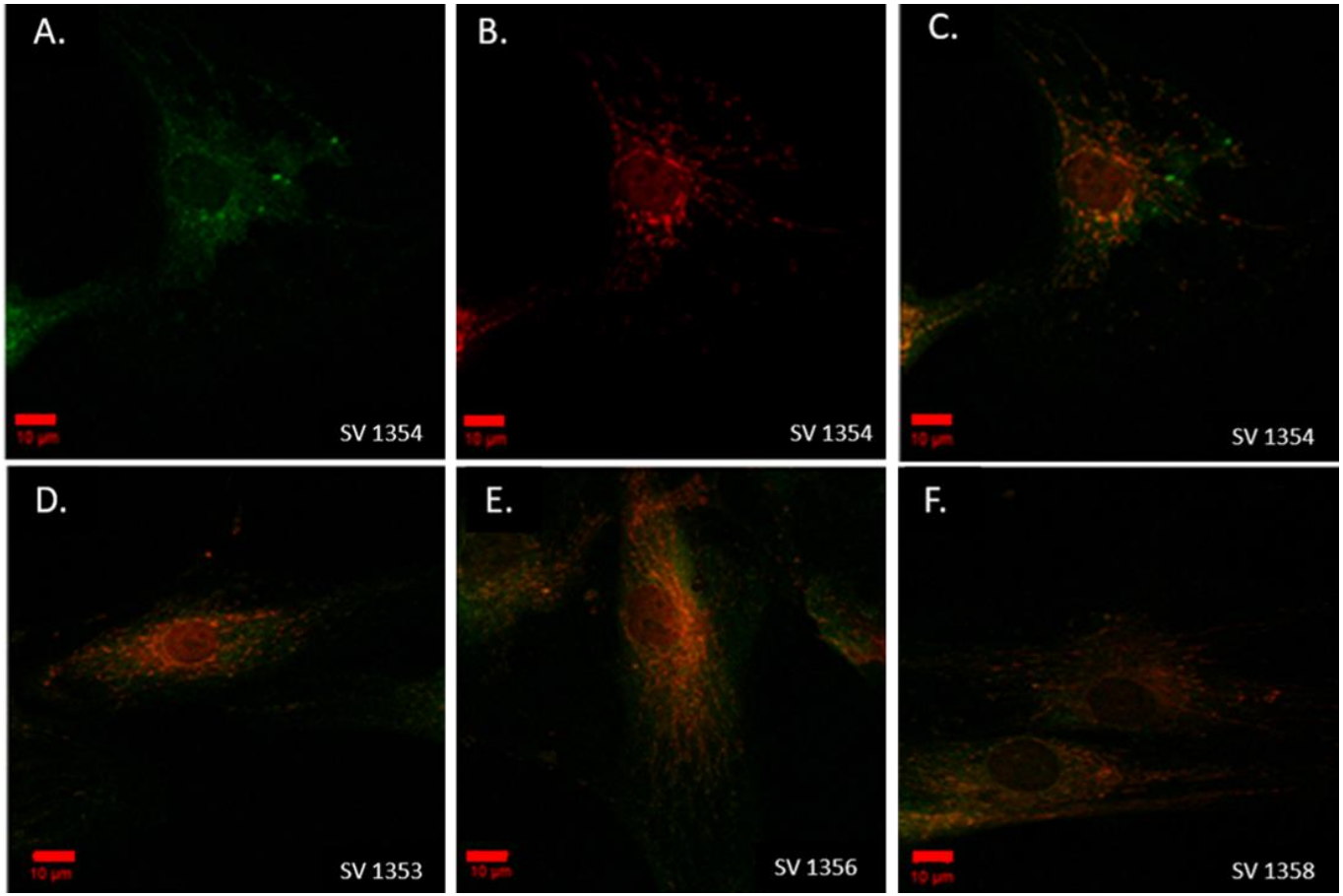

Figure 3.12 Kv1.3 channels co-localise with mitochondria in primary human vascular smooth muscle cells. Data shows cells isolated from four independent patients. Top row shows immunostained cells from one patient. Bottom row shows cells from three patients. A. Kv1.3 channels detected by anti-Kv1.3 clone L23/27 NEUROMAB mouse monoclonal primary antibody with Alexa Fluor 488 secondary antibody (green). B. Mitochondrial network stained with MitoTracker Red CMXRos. C. Composite images of A and B, with yellow/orange fluorescence indicating Kv1.3 channel co-localisation with the mitochondria. D, E and F show composite images, as in (C), generated by staining cells with the anti-Kv1.3 antibody in (A) and MitoTracker Red CMXRos in (B). Yellow/orange fluorescence indicates Kv1.3 channel co-localisation with the mitochondria. Scale bars represent 10µm.

3.3.6 HEK293 and HEK293/Kv1.3 cells have comparable amounts of mitochondria.

To determine whether Kv1.3 expression alters mitochondrial content, a citrate synthase (CS) activity assay was performed in WT HEK293 and HEK293/Kv1.3 cells. CS is an enzyme present in the mitochondrial matrix which catalyses the condensation of Acetyl-CoA and oxaloacetate to produce citric acid. The hydrolysis of Acetyl-CoA in this reaction, produces a CoA molecule attached to a thiol group. This thiol group reacts with DTNB to produce TNB, which fluoresces and can be measured spectrophotometrically. Thus, the amount of CS directly relates to the amount of TNB fluorescence measured during this assay. The CS activity assay is a proxy measure for mitochondrial content (Eigentler *et al.*, 2015), but it is better than other measures, such as measuring mitochondrial DNA. Mitochondrial DNA is not a good biomarker for mitochondrial content in skeletal muscle cells (Larsen *et al.*, 2012) and suffers from multiple mitochondrial genome copy errors which lead to false results (Malik and Czajka, 2013). There was no difference in the activity of CS in WT HEK293 and HEK293/Kv1.3 cells (Figure 3.15A), indicating no significant difference in the mitochondrial content of these cells.

A second assessment of mitochondrial content in WT HEK293 and HEK293/Kv1.3 cells was performed. High resolution respirometry was utilised to assess complex IV activity, another common biomarker for mitochondrial content (Larsen *et al.*, 2012). Cells were acutely treated with ascorbate and TMPD and cellular respiration measured. TMPD artificially reduces complex IV by acting as an electron donor, whilst ascorbate maintains TMPD in its reducing state. There was no significant difference in the complex IV respiration in WT HEK293 and HEK293/Kv1.3 cell (Figure 3.14B). As with the citrate synthase assay these data indicate that mitochondrial content in these cells is not altered by Kv1.3 expression.

Next, the protein expression of key mitochondrial respiratory chain components was examined in HEK293/Kv1.3 cells (Figure 3.13C, D and E). The protein expression of mitochondrial ATP synthase, as determined by the expression of the ATP beta subunit, was not different in HEK293/Kv1.3 cells compared to WT HEK293 cells (Figure 3.13C). Complex IV protein expression was also examined. Interestingly, a significant increase in complex IV in HEK293/Kv1.3 cells was identified (Figure 3.13D). However, on closer examination the band corresponding to complex IV on the blot for HEK293/Kv1.3 cells

suggests that there may be more of the protein complex in the transgenic cells (Figure 3.13E). This phenomenon is not seen in the bands for the β-actin control or ATP synthase. As complex IV represents a multiprotein complex this finding may suggest that assembly of the complex is altered in the presence of increased mitochondrial Kv1.3.

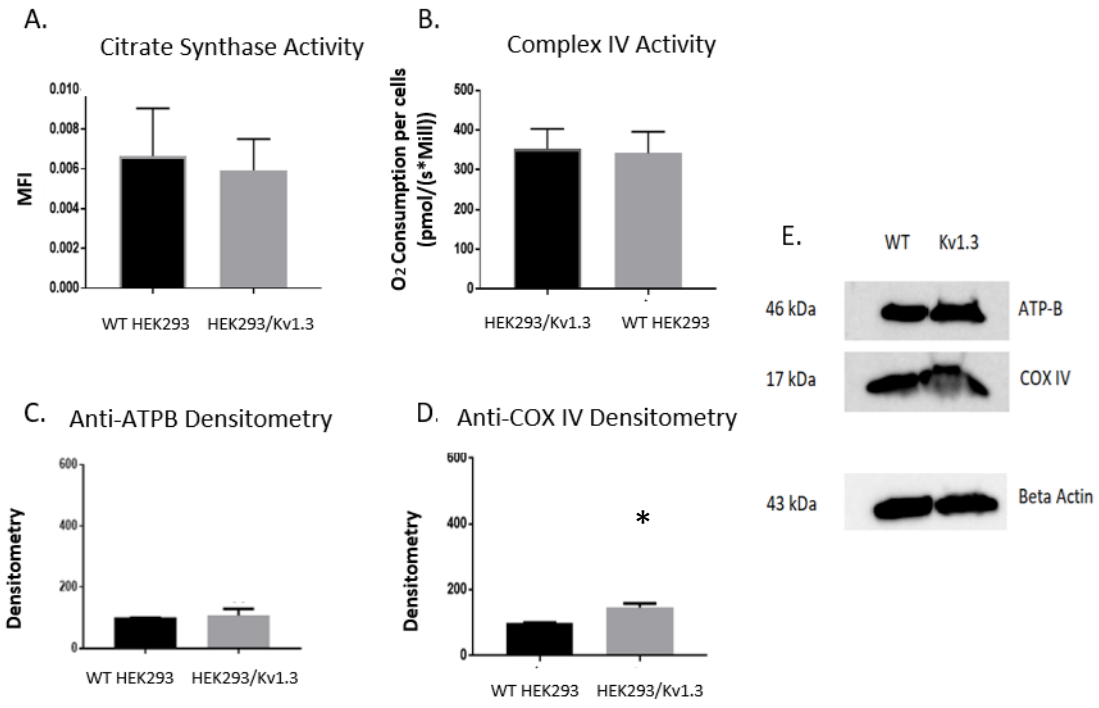

Figure 3.13 Kv1.3 expression does not alter mitochondrial content in HEK293 cells. A. Citrate synthase activity assay in WT HEK293 (black) and HEK293/Kv1.3 (grey) cells. Data expressed as the mean fluorescent intensity of TNB ± SEM (n=3). B. Results from complex IV respiratory assay in HEK293/Kv1.3 (black) and WT HEK293 (grey) cells. Data expressed as the mean oxygen consumption (pmol/(s*Mill)) ± SEM (n=5). C. Mean densitometry from mitochondrial ATP synthase protein western blotting in WT HEK293 (black) and HEK293/Kv1.3 (grey) cells. Data expressed as percent of WT HEK293 protein ± SEM (n=3). D. Mean densitometry from complex IV western blotting in WT HEK23 (black) and HEK293/Kv1.3 (grey) cells. Data is expressed as a percentage of WT HEK293 protein ± SEM (n=5). E. Example blots showing ATP synthase beta subunit protein (top row), COX IV protein (middle row), and beta actin protein loading control (bottom row), in WT HEK293 (left column) and HEK293/Kv1.3 (right column) cells. For A-D, data was analysed by Student's t-tests, * $p<0.05$. Data in C, D and E was generated by Dr T. Hettiarachchi, University of Leeds.

A 3-dimensional (3D) imaging immunocytochemistry approach was used to investigate the mitochondrial content of HEK293/Kv1.3 cells (Figure 3.14). Cells were stained with Mitotracker (red) and imaged using 3D confocal microscopy. Images provide a complex interpretation of the mitochondrial cellular network. The degree of mitochondrial staining was similar in both WT HEK293 and HEK293/Kv1.3 cells. 3D imaging was also used to examine HEK293/Kv1.3 cells immunostained for mitochondrial complex IV (Figure 3.15 A-D). The gross structure of the mitochondrial network was unchanged by Kv1.3 expression (Figure 3.15D vs H).

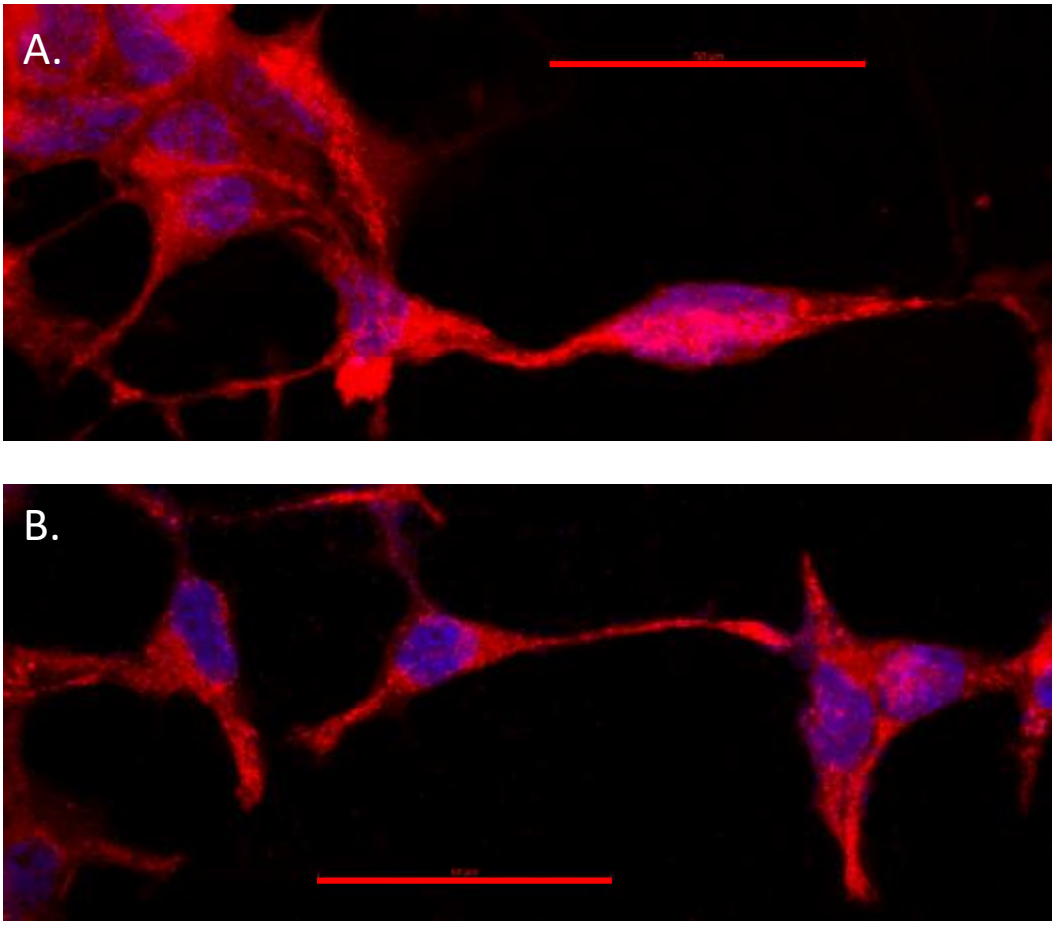

Figure 3.14 Kv1.3 expression does not alter mitochondrial networks in HEK293 cells. Mitochondrial networks in WT HEK293 and HEK293/Kv1.3 cells. 3D images of WT HEK293 cells (A) and HEK293/Kv1.3 cells (B) pre-treated with 100nM MitoTracker Red CMXRos. Cell nuclei are stained with diamidino-2-phenylindole (DAPI) (blue). Images are z-stack composites of twenty 1µm slices through the cell. These are representative images of three biological replicates. Scale bars represent 50µm.

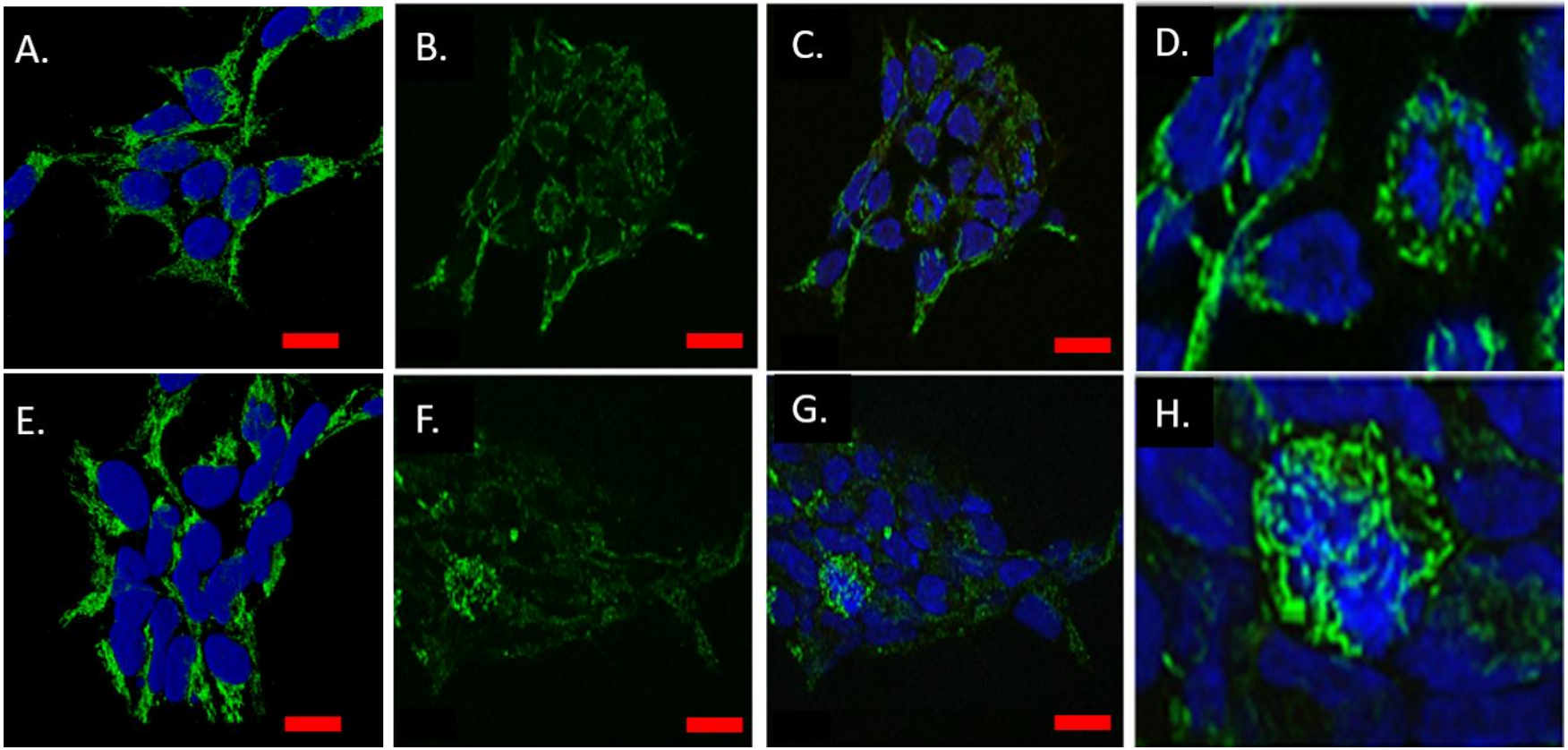

Figure 3.15 Kv1.3 expression does not alter mitochondrial complex IV protein content or affect the structure of the mitochondrial network in HEK293 cells. Comparison of mitochondrial networks in HEK293/Kv1.3 cells (top row) and WT HEK293 (bottom row). A and E. Three-dimensional image of cell mitochondrial network stained for complex IV (green). Cell nuclei are stained with diamidino-2-phenylindole (blue). B and F. Cell mitochondrial network stained for complex IV (green). C and G. Mitochondrial network staining for complex IV (green) with cell nuclei staining by diamidino-2-phenylindole (DAPI) (blue). D and H. Magnified images of complex IV and nuclear co-stained images highlighting the mitochondrial network. All scale bars represent 20µm.

3.4 Discussion

This chapter characterised the HEK293/Kv1.3 cell line and identified a distinct proliferative and mitochondrial respiration phenotype resulting from Kv1.3 expression in HEK293 cells.

The stable expression of ion channels in HEK293 cells as an experimental model is well established (Elies, Dallas, *et al.*, 2014; Elies, Scragg, *et al.*, 2014; Al-Owais *et al.*, 2015; Duckles *et al.*, 2015). The HEK293 cell line is commonly used due to their high proliferation rate, and their propensity for transfection (discussed in Stepanenko and Dmitrenko, 2015). The HEK293/Kv1.3 model has been used successfully to investigate the mechanisms of Kv1.3 induced proliferation, where overexpression of WT Kv1.3 and mutant Kv1.3 channels have led to the discovery of ion-conduction independent roles for Kv1.3 in proliferation (Cidad *et al.*, 2012; Jimenez-Perez *et al.*, 2016).

HEK293/Kv1.3 cells were found to express functional Kv1.3 channels. WT HEK293 cells were also found to express low levels of Kv1.3 protein. Kv1.3 channels have previously been observed in HEK293 cells (Jiang *et al.*, 2002). However, expression was to a sufficiently low level in comparison with HEK293/Kv1.3 cells that they were considered a suitable control. In addition, electrophysiology experiments confirmed that there were significantly increased potassium currents in HEK293/Kv1.3 cells and that the contribution of the endogenous Kv1.3 channels to the observed currents in HEK293 cells is negligible. This view is widely held, and researchers generally view the endogenous ion channel currents as insignificant when compared to the currents generated with channel overexpression in HEK293 cells (Varghese *et al.*, 2006). Therefore the HEK293 cells were considered a reliable stable transfection and overexpression system for Kv1.3 (Thomas and Smart, 2005).

HEK293/Kv1.3 cells displayed significantly higher levels of proliferation than WT HEK293 cells (Figure 3.4). This finding supports data from Cidad et al., who also saw this effect in HEK293 cells overexpressing the Kv1.3 channel (Cidad *et al.*, 2012; Jimenez-Perez *et al.*, 2016). The Kv1.3 channel has been a focus of research into proliferative disorders of vascular cells since 2010 (Cidad *et al.*, 2010, 2012; Cheong *et al.*, 2011; Jimenez-Perez *et al.*, 2016). A study investigating the expression profile of 87

ion channels in various vascular beds found that Kv1.3 was upregulated during the phenotypic switch of VSMCs from a contractile state to a proliferative one (Cidad *et al.*, 2010). This study found that sensitivity to 5μM correolide, a non-selective potassium channel blocker, indicated that a larger proportion of the overall K^+ current in proliferative VSMCs was attributable to Kv1 channels. Kv1.3 upregulation was confirmed by a 6-fold increase in sensitivity to the selective Kv1.3 blockers PAP-1 and Margatoxin, (MgTx) and increased Kv1.3 immunoreactivity in both an *in vitro* preparation and *in vivo* injured VSMCs. In addition, inhibition of Kv1.3 by pharmacological blockade with PAP-1 and molecular mutation reduced VSMC proliferation and migration.

In this chapter HEK293/Kv1.3 cells were analysed in a high-resolution respirometer. Kv1.3 overexpressing cells displayed significantly higher O_2 consumption and ATP turnover rates than WT HEK293 cells. To the best of the authors' knowledge, no link has previously been described between Kv1.3 channels and oxidative phosphorylation. However, in 2014 Hamilton et al., found that there was no role for Kv1.3 in oxidative phosphorylation in mouse skeletal muscle cells (Hamilton *et al.*, 2014). Interestingly, in rat olfactory bulbs, which contain high levels of Kv1.3 channels in the neurons, there is a respiratory control ratio which indicated mitochondrial activity was twice as high as neighbouring cells of the hypothalamus (Benani *et al.*, 2009).

In contrast, there have been several studies linking Kv1.3 to metabolic disorders. Kv1.3 has been implicated in the regulation of both body weight and energy homeostasis (Xu *et al.*, 2003). Xu et al., found that knockout Kv1.3 mice had a higher metabolic rate and displayed significantly lower body weight than those with the Kv1.3 gene. In 2004, the same group identified a role for Kv1.3 in modulation of peripheral insulin sensitivity, as both pharmacological inhibition and gene knockout of Kv1.3 upregulated GLUT4 at the plasma membrane (Xu *et al.*, 2004). Tucker and colleagues found that the genetic ablation of Kv1.3 in melanocortin 4 receptor-null mice led to reduced body mass and adiposity in these animals compared to WT animals, partly due to increased energy expenditure and metabolism (Tucker, Overton and Fadool, 2008). Kv1.3 pharmacological blockade suggests utility as a potential therapeutic for obesity and insulin resistance (Upadhyay *et al.*, 2013).

These findings appear to run contrary to the observations of this chapter describing which increased O_2 consumption in cells overexpressing the Kv1.3 channel, suggesting an increased metabolic rate. Despite this contradiction, it is plausible that the low body weight of the knockout/Kv1.3 inhibited animals could have been due in part to a lower level of cell growth and proliferation in these animals, a possibility that was not addressed in these studies. It could also suggest that Kv1.3 has specific effects on adipocyte hyperplasia in obesity. Finally, if Kv1.3 plays a physiological role in mitochondrial metabolism, channel KO or inhibition may lead to upregulation of other metabolic pathways to compensate (Obermeyer *et al.*, 2013; Hardie *et al.*, 2017).

In addition, more recent studies have also identified opposing metabolic effects of Kv1.3 to those put forward by both Xu et al. and Tucker et al., (referenced above), including no observation of a role for Kv1.3 in weight gain and adiposity in rats (Jaimes-Hoy *et al.*, 2017) and no effect on insulin sensitivity of mice or in insulin insensitive human tissues (Straub *et al.*, 2011).

The results highlighted in this chapter pose additional key questions, including whether the incidence of an increased respiratory rate is directly related to the Kv1.3 channel, and drives the increased proliferative rate, or vice versa in which the increased proliferative rate is the initiator of increased energy metabolism. The possibility remains that the two process are carefully co-ordinated to facilitate effective cell growth. It is interesting to note that when Kv1.5 channels were transfected into the HEK293 cells, there was reduction in cellular respiration and proliferation in direct contrast to HEK293/Kv1.3 cells. Although not a well-established mitochondrial ion channel, there is some evidence which suggests that Kv1.5 channels are found in the inner mitochondrial membrane (Leanza *et al.*, 2014). It may be that the ratio of Kv1.3 to Kv1.5 channels determines the phenotypic state of vascular smooth muscle cells (Cidad *et al.*, 2010; Jimenez-Perez *et al.*, 2016).

Kv1.3 channels have been found on the inner mitochondrial membrane of various cell types (Szabo *et al.*, 2005; Bednarczyk *et al.*, 2010; Cheng, Debska-Vielhaber and Siemen, 2010; Mattarei *et al.*, 2018). This chapter used immunocytochemistry to identify localisation of Kv1.3 channels to the mitochondrial network of HEK293 cells and HSVSMCs.

Voltage gated potassium channels have been previously linked to mitogenesis in T lymphocytes (DeCoursey *et al.*, 1984). However, the increased rate of cellular respiration in Kv1.3 overexpressing cells appeared to be dependent on increased rates of substrate oxidation as opposed to increased mitochondrial content. Kv1.3 channel overexpression in HEK293 cells did not affect the size or structure of the mitochondrial network as determined by CS activity assay, complex IV respiratory activity, assessment of mitochondrial protein concentrations and mitochondrial network imaging. However, the protein band corresponding to mitochondrial complex IV in western blotting displayed retarded progress on the gel which may correspond to an increased mass of the protein complex. This may represent an effect of Kv1.3 overexpression on the formation or synthesis of the multiprotein complex. Nevertheless, the activity of complex IV was unaffected by Kv1.3 overexpression and therefore the potential protein modification does not appear to have a direct functional effect on the respiratory role of complex IV under the tested experimental conditions. In Figure 3.9 E it appears that WT HEK293 cells have decreased mitochondrial networks in comparison to Figure 3.9 B. However, this seems to be an anomaly, as in Figure 3.14 there is no obvious difference in the mitochondrial networks in WT HEK293 and HEK293/Kv1.3 cells. The difference in the level of immunostaining in Figure 3.9 could arise from either impaired staining of the mitochondria by MitoTracker CMXRos, or impaired imaging on the microscope. For example, it appears that in HEK293/Kv1.3 cells there is flooding of Mitotracker into the cell nuclei (Figure 3.9 B). This suggests an incorrect concentration of the fluorescent agent in this sample of HEK293/Kv1.3cells. Co-localisation analysis of mitochondria and Kv1.3 channels can be found in Chapter 6, Figure 6.3.

Genetic deletion of Kv1.3 channels in mice gives rise to animals with altered mitochondrial morphology (Kovach *et al.*, 2016). These animals had smaller mitochondria with a more circular shape than wild type mice. Although no quantitative measure of cristae was carried out, the researchers observed that these structures were more longitudinally arranged in wild type animals. In addition, a recent study testing mitochondrially targeted Kv1.3 inhibitors on cancer cells found that these compounds caused mitochondrial swelling (Mattarei *et al.*, 2018). It is well established that mitochondrial potassium cycling is tightly regulated in order to protect the

mitochondria from damaging changes in cell volume that can affect bioenergetics (Garlid, 1996; Garlid and Paucek, 2003). An integral part of mitochondrial matrix volume homeostasis is the K^+/H^+ antiporter (Garlid and Paucek, 2003). In this study, no differences were observed in the structure of mitochondria in cells overexpressing Kv1.3. However, more advanced methods, such as electron microscopy of the mitochondrial ultrastructure, should be considered for further analyses. A more advanced imaging method may also be able to determine whether Kv1.3 overexpression effects complex IV expression or protein size. For example, the cristae may become more folded, as high metabolic rates have been found to cause structural changes of the IMM and matrix (Lehninger, 1982), generating a greater surface area to express higher amounts of complex IV. However, no change in complex IV activity was observed in the HEK293/Kv1.3 cells investigated as part of this study. However, it may be that no difference in mitochondrial structure was due to tight regulation of mitochondrial volume homeostasis, which causes swift extrusion of the excess influx of K^+ into the matrix through Kv1.3 channels (Garlid and Paucek, 2003).

In summary, this chapter set out to characterise and investigate the proliferative and cellular energy phenotype of Kv1.3 overexpression in HEK293 cells. Increased rates of proliferation and respiration could not be attributed to differences in mitochondrial number or general structure. In addition, Kv1.3 was found to reside in the mitochondria of both HEK293/Kv1.3 cells and HSVSMCs.

Chapter Four

Mitochondrial Kv1.3 channels regulate proliferation and respiration in HEK293 cells.

4.1 Introduction

The ion channel Kv1.3 has previously been shown to have a regulatory role in cellular proliferation in multiple cell types including HEK293 and vascular smooth muscle cells (Cidad *et al.*, 2010, 2012; Cheong *et al.*, 2011; Jimenez-Perez *et al.*, 2016). Kv1.3 channels can be found on the plasma membrane of cells, but have also been identified in intracellular locations, including the IMM (Szabo *et al.*, 2005; Bednarczyk *et al.*, 2010; Cheng, Debska-Vielhaber and Siemen, 2010; Mattarei *et al.*, 2018). Szabo and colleagues proposed that that mitochondrial and plasma membrane Kv1.3 channels may have distinct effects on cell function, in that plasma membrane channels regulate the membrane potential, proliferation and maturation of T lymphocytes, whilst IMM channels regulate apoptosis (Szabo *et al.*, 2005; Szabó *et al.*, 2008). Using the unique properties of several pharmacological Kv1.3 channel inhibitors, the distinct function of Kv1.3 channels localised to either intracellular or extracellular-facing plasma membrane locations can be probed (Leanza *et al.*, 2012). The sea anemone toxin ShK and its analogues are highly potent and specific inhibitors of plasma membrane Kv1.3 (Kalman *et al.*, 1998; Norton, Pennington and Wulff, 2004; Rashid *et al.*, 2013; Upadhyay *et al.*, 2013). These toxins cannot enter the cell but bind to the outer vestibule of the Kv1.3 channel in the plasma membrane, blocking the external entrance to the channel's pore. In contrast, 5-(4-phenoxybutoxy) psoralen (PAP-1), a member of the psoralen family of plant derived Kv1.3 inhibitors, can diffuse across the plasma membrane. PAP-1 can, therefore, inhibit intracellular Kv1.3 channels, and functions by binding to residues that become accessible when the Kv1.3 channel is in

its c-type inactivated state (Schmitz *et al.*, 2005). Once bound, PAP-1 causes a conformational change in the protein structure which prevents the channel from returning to its active state, inhibiting K^+ flow through the channel. PAP-1 non-specifically inhibits intracellular Kv1.3 channels, including those located at the cis-Golgi, nucleus and the mitochondria (Rasmusson *et al.*, 1998) (Hoshi and Armstrong, 2013). However, PAP-1 derivates can be bound to triphenyl phosphonium (TPP) lipophilic cation to-target the inhibitor to the mitochondria forming PAPTP (Leanza *et al.*, 2017). The PAPTP conjugate is positively charged and is attracted to the negatively charged mitochondrial membrane (Leanza *et al.*, 2012, 2017; Mattarei *et al.*, 2018).

The role of Kv1.3 in physiological mitochondrial function has thus far received little attention (Khanna *et al.*, 2001). In Chapter Three, Kv1.3 overexpressing HEK293 cells were shown to have increased rates of both cellular proliferation and mitochondrial respiration. In addition, Kv1.3 was confirmed to localise to the mitochondrial network in both HEK293 and HSVSMCs. The development of pharmacological tools, such as Shk, PAP-1 and PAP-1-TPP (PAPTP) facilitate the investigation of the extracellular, intracellular and mitochondrial-specific roles of Kv1.3 channels, respectively.

4.2 Aims and Objectives

This chapter aimed to investigate and characterise the distinct role of plasma membrane and mitochondrial Kv1.3 channels in cellular proliferation and mitochondrial respiration. To achieve this aim a key set of objectives were designed:

1) To investigate the effect of intracellular Kv1.3 inhibition using PAP-1 on the cellular proliferation of HEK293 and HSVSMCs.

2) To determine the effect of plasma membrane Kv1.3 channel inhibition using Shk on cellular proliferation.

3) To use Shk, PAP-1 and PAPTP to characterise the effect of plasma membrane, intracellular and mitochondrial-specific Kv1.3 channel inhibition, respectively, on cellular respiration in HEK293 cells.

4.3 Results

4.3.1 Inhibition of intracellular Kv1.3 channels with PAP-1 reduces proliferation of HEK293/Kv1.3 cells at low concentrations.

PAP-1 is a plasma membrane-permeable and highly specific inhibitor of the Kv1.3 channel (Schmitz *et al.*, 2005). In Chapter Three HEK293/Kv1.3 cells were observed to have an increased rate of proliferation compared to WT HEK293 cells. Therefore, the effect of PAP-1 Kv1.3 channel inhibition on the proliferation of WT HEK293 cells (Figure 4.1) and HEK293/Kv1.3 (Figure 4.2). PAP-1, in the concentration range 0.1nM to 30nM, had no effect on the proliferation of WT HEK293 cells (Figure 4.1A). In HEK293/Kv1.3 cells there was a trend for a reduction in proliferation with concentrations of PAP-1 between 0.3nM and 3nM (Figure 4.2A). Day 3 count for cells treated with 1nM PAP-1 was 54% of the mean count for untreated control cells. However, this reduction was not significant by ANOVA, likely due to a high degree of variation in the controls. The WT HEK293 and HEK293/Kv1.3 cells were counted using an automated cell counter, and Trypan Blue was used to assess cell viability. PAP-1 had no effect on WT HEK293 or HEK293/Kv1.3 cell viability assessed using a cell count of detached cells in the proliferation assay media (Figures 4.1B and 4.2B, respectively) or Trypan Blue staining of HEK293/Kv1.3 cells (Figure 4.2C). This confirms the trend for decreased proliferation with lower PAP-1 concentrations was not due to cell death.

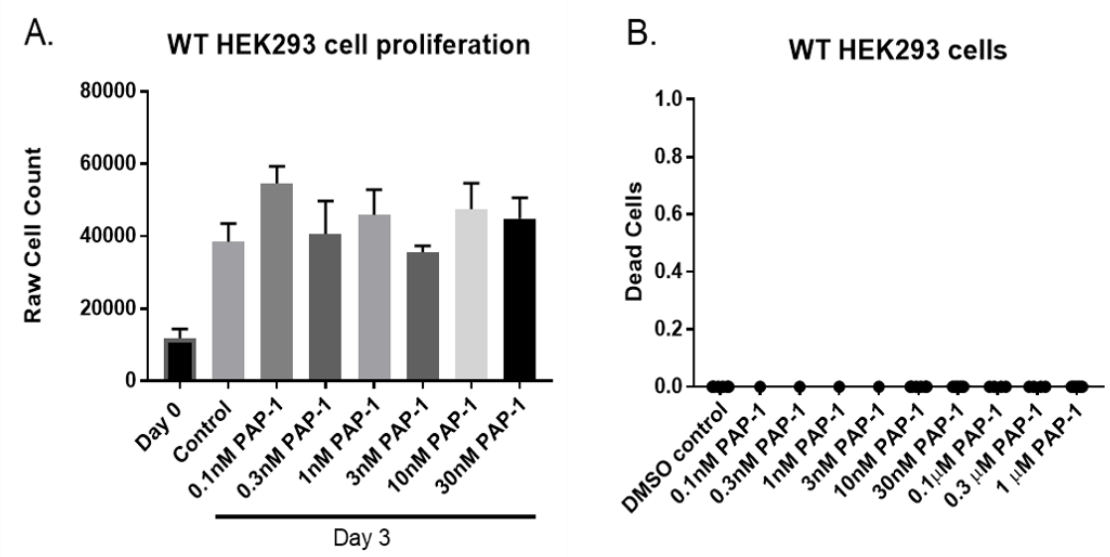

Figure 4.1 Proliferation of WT HEK293 cells is unaffected by PAP-1. A. Dose response curve of the effect of PAP-1 (0.1nM – 30nM) on WT HEK293 cell proliferation after 3 days of growth. Data is expressed as the raw cell counts. Wells were counted in triplicate, and the averages from each repeat collected and displayed on the graphs with the SEM. One-way ANOVA was carried out and the results were not significant $p>0.05$. Day 0, Day 3 Control, 10nM and 30nM counts (n=5), 0.1nM-3nM (n=3). B. Dead cell counts for WT HEK293 cells treated with PAP-1 (0.1nM-1μM). ROUT analysis performed, and an outlier removed. Control, 10nM and 30nM counts (n=5), 0.1nM-3nM (n=1) and 0.1μM-1 μM (n=4).

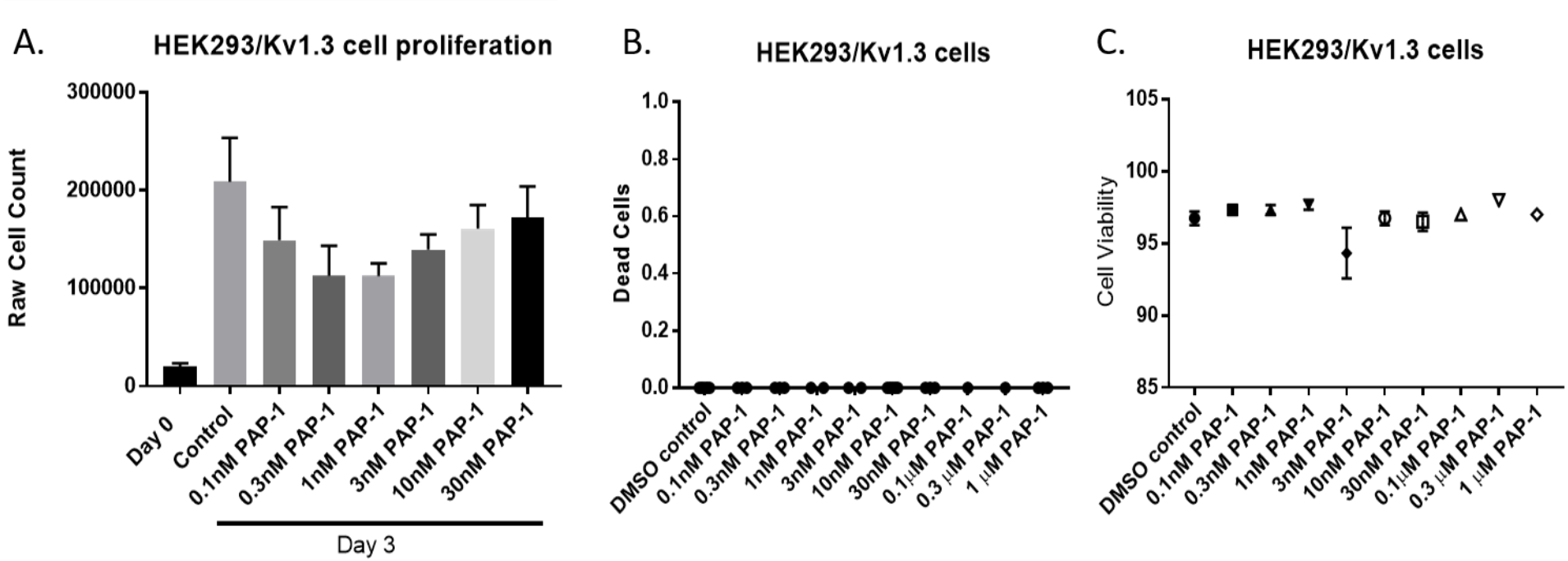

Figure 4.2 Proliferation of HEK293/Kv1.3 cells trends towards a reduction at low nanomolar concentrations of PAP-1. A. Dose response curve showing the effect of PAP-1 (0.1nM-30nM) on HEK293/Kv1.3 cell proliferation after 3 days of growth. Day 0, Day 3 Control, 10nM and 30nM counts (n=5), 0.1nM-3nM (n=3). Data is expressed as the raw cell counts. Wells were counted in triplicate, and the averages from each repeat collected and displayed on the graphs with the SEM. One-way ANOVA was carried out and the results were not significant $p>0.05$. B. Dead cell counts for HEK293/Kv1.3 cells treated with PAP-1 (0.1nM-1μM). ROUT analysis performed, and an outlier removed. Control and 10nM (n=5), 0.1nM, 0.3nM, 30nM and 1μM (n=3), 1nM and 3nM (n=2) and 0.1μM and 0.3μM (n=1). C. Viability of HEK293/Kv1.3 cells treated with PAP-1 (0.1nM-1μM). Viability expressed as a percentage of alive cells. Control, 10nM and 30nM (n=4), 0.1nM-3nM (n=3), 0.1μM-1 μM (n=1). Data expressed as mean ± SEM and was analysed (0.1nM-30nM PAP-1) using one-way ANOVA. Results were not significant $p>0.05$.

To ensure that PAP-1 inhibited Kv1.3 channels, whole cell patch clamp electrophysiology was carried out on HEK293/Kv1.3 cells (Figure 4.3). PAP-1 reduced the K^+ ion current in HEK293/Kv1.3 cells (Figure 4.3), however, a high concentration of the drug (1µM) was required to inhibit the whole cell K^+ current. This concentration is in excess of the low nanomolar concentrations observed to inhibit proliferation. This is a surprising result and is not what is echoed in the literature, whereby the plasma membrane K^+ ion currents are strongly inhibited by 0.1µM PAP-1 (Perez-Garcia, Cidad and Lopez-Lopez, 2018).

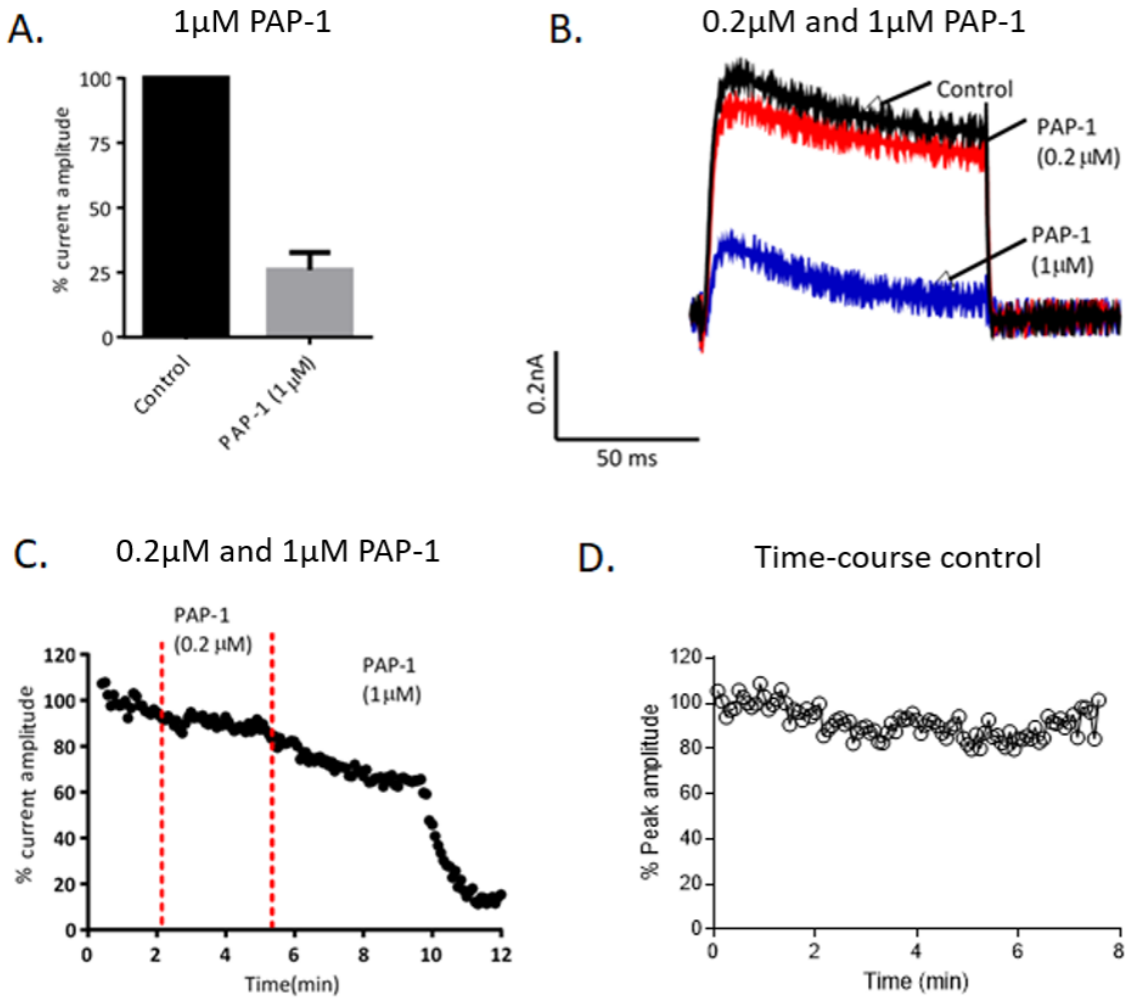

Figure 4.3 PAP-1 inhibits the potassium ion current in HEK293/Kv1.3 cells. A. Percentage decrease in Kv1.3 current amplitude with 1µM PAP-1 (n=5). B. Whole cell voltage clamp trace showing inhibition of Kv1.3 current by PAP-1 (0.2µM-1 µM). C. Time course experiment of a single HEK293/Kv1.3 cell, with percentage decrease in Kv1.3 current amplitude with PAP-1 (0.2µM-1µM) plotted against time and peak current amplitude normalized to cell size. D. Example time-course control of a HEK293/Kv1.3 cell being held at -80mV for 8 minutes. Experiments were carried out by Dr M. Al-Owais, University of Leeds.

4.3.2 PAP-1 can reduce proliferation of HSVSMCs.

In Chapter Three (Figures 3.9, 3.11 and 3.12), Kv1.3 channels were observed intracellularly and within the mitochondrial network of HEK293 and HSVSMCs. To assess whether the presence of these channels could affect proliferation in a clinically and physiologically relevant model, PAP-1 was applied to HSVSMCs during a proliferation assay (Figure 4.4). HSVSMCs proliferate at a slower rate than HEK293 cells with a high degree of inter-patient variability (Figure 4.4A and B). Therefore, a 7 day proliferation assay was adopted. Cell counts were made on days 0, 2, 4 and 7. The results of this assay on HSVSMCs isolated from three patients is shown in Figure 4.4B. Based on this data day 4 was assessed as a suitable time point to use for subsequent proliferation assays in HSVSMCs (Figure 4.4C). Low nanomolar concentrations of PAP-1 trended towards inhibiting the proliferation of the HSVSMCs, assessed at day 4 of proliferation (Figure 4.4C). One-way ANOVA did not find that PAP-1 significantly decreased proliferation compared to Day 4 control, possibly due to the high variability in control counts. However, Day 3 counts of cells treated with 3-30nM PAP-1 were significantly lower than those treated with 1µM PAP-1. Cells were counted manually using Trypan Blue staining for cell death. PAP-1 did not increase Trypan Blue staining (Figure 4.4C), therefore effects on proliferation are unlikely to be due to cytotoxic effects on HSVSMCs.

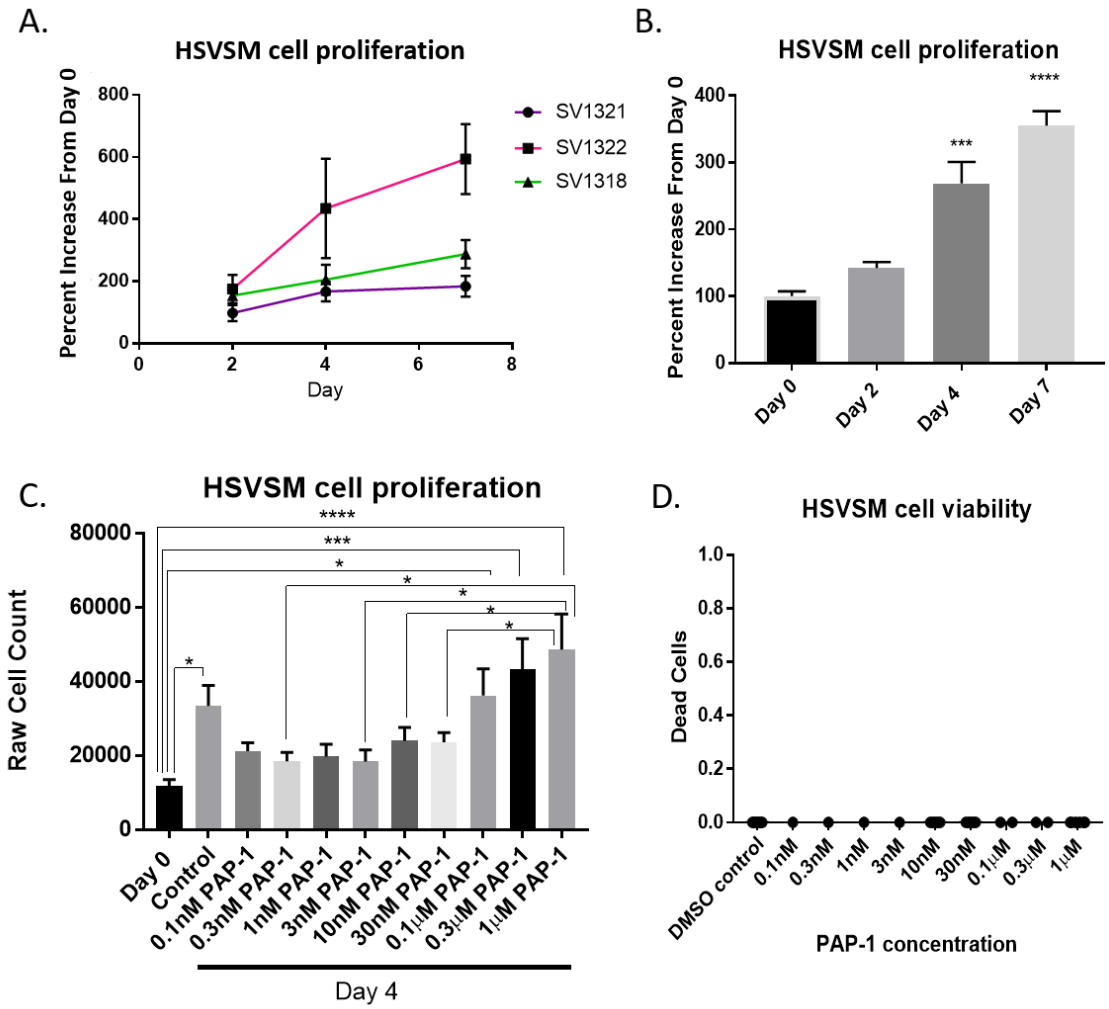

Figure 4.4 PAP-1 inhibits HSVSM cell proliferation. A. The proliferation of HSVSM cells from three patients; SV1321, SV1322 and SV1318. Wells were counted in triplicate on days 0, 2, 4 and 7. Data expressed as the mean percent increase from day 0 ± SEM. B. Mean proliferation data from (A). One-way ANOVA was used for statistical analysis, *** p<0.001, **** p<0.0001. C. The effect of PAP-1 (0.1nM-1μM) on HSVSM cell proliferation after 4 days. Wells were counted in triplicate for each experimental repeat. Day 0, Day 4 control, 10nM and 30nM (n=13; SV1330, SV1335, SV1336, SV1337, SV1339, SV1340, SV1341, SV1344, SV1349, SV1354, SV1356, SV1358 and SV1359), 0.1nM-3nM (n=5; SV1349, SV1354, SV1356, SV1358 and SV1359) and 0.1μM-1μM (n=8; SV1330, SV1335, SV1336, SV1337, SV1339, SV1340, SV1341 and SV1344). Data expressed as mean raw cell count (± SEM). Data analysed using ROUT analysis to remove outliers and one-way ANOVA with Tukey's post hoc test, * p<0.05, *** p<0.001, **** p<0.0001. D. Dead cell counts for HSVSM cells with PAP-1 treatment (0.1nM-1μM) after 4 days. Control (n=7), 0.1nM-3nM (n=1), 10nM and 30nM (n=5), 0.1μM and 0.3μM (n=2) and 1μM (n=6).

4.3.3 PAP-1 decreases mitochondrial respiration in HEK293 cells.

The Routine Respiration of HEK293/Kv1.3 cells was analysed using the O2k Oxygraph. This respiration rate is designated Routine 1. PAP-1 was added to the respirometry chambers and the respiration rate measured. This respiration rate is designated Routine 2. PAP-1 decreased the O_2 consumption of HEK293/Kv1.3 cells (Figure 4.5). The addition of the OXPHOS and electron transport chain inhibitors oligomycin (ATP synthase inhibitor) and FCCP (OXPHOS uncoupler) had very little effect on the respiratory function of the cells after treatment with PAP-1. Addition of rotenone (complex I inhibitor) and antimycin A (complex III inhibitor) caused an initial, rapid decrease in O_2 consumption, which led O_2 consumption to fall well below zero, as indicated by the dotted downward line on the trace in Figure 4.5. However, the cells recovered very quickly and their O_2 consumption always stabilised above zero. The resultant residual O_2 consumption (ROX) was due to non-mitochondrial sources. The decrease in O_2 consumption below zero with rotenone and antimycin A occurred in all HEK293 cells tested in the respirometer, and ROX was always measured once O_2 stabilised above zero. The decrease in O_2 consumption below zero may have been due to the larger volume of rotenone and antimycin being added to chambers (5µl) compared to oligomycin and FCCP (1µl), which momentarily disrupted the O_2 consumption measurements.

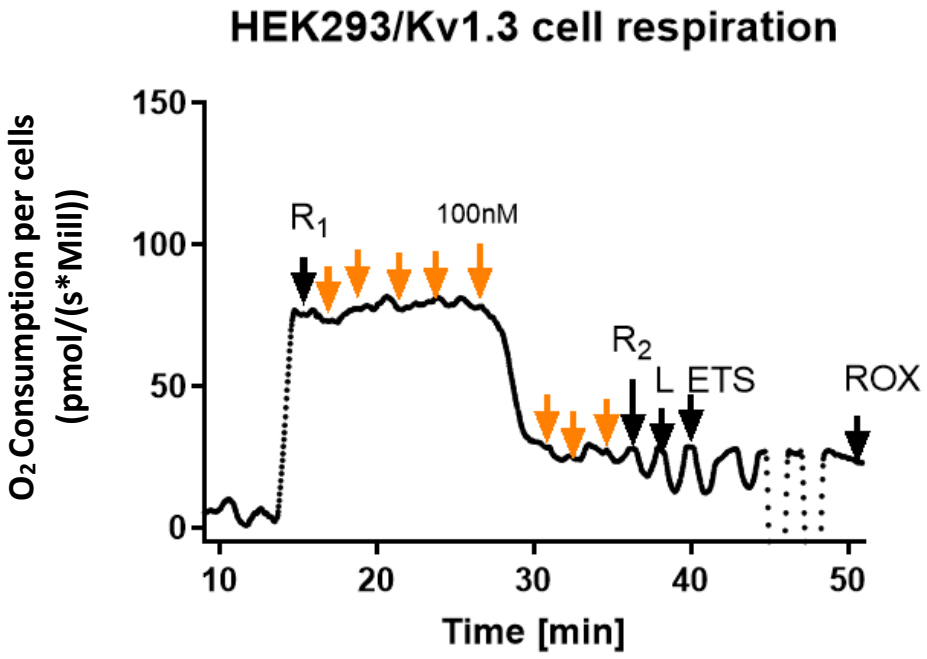

Figure 4.5 PAP-1 can reduce oxygen consumption of HEK293/Kv1.3 cells. An example trace showing the O_2 consumption (pmol per million cells per second, pmol/(s*Mill)) in HEK293/Kv1.3 cells treated with PAP-1 (final concentration 200nM). Orange arrows represent the points at which PAP-1 was added to the chamber. Black arrows represent the points at which measurements were taken; R_1=Routine Respiration, R_2=Routine Respiration after PAP-1 treatment, L=Leak Respiration, E=ETS (electron transport system) uncoupling and ROX=residual O_2 consumption.

Strikingly, the severe increase in cellular O_2 consumption with FCCP (Figure 4.6A) was inhibited in PAP-1 treated cells (Figure 4.6B and C) suggesting the inhibitory effect of PAP-1 is due to inhibition of the ETS. PAP-1 decreases routine respiration by 60% in HEK293/Kv1.3 cells when respiration is uncorrected for ROX (Figure 4.6B), and by 90% when respiration is corrected for ROX (Figure 4.6C). Moreover PAP-1 significantly decreased ATP turnover (Figure 4.7) and spare respiratory capacity in HEK293/Kv1.3 cells (Figure 4.8).

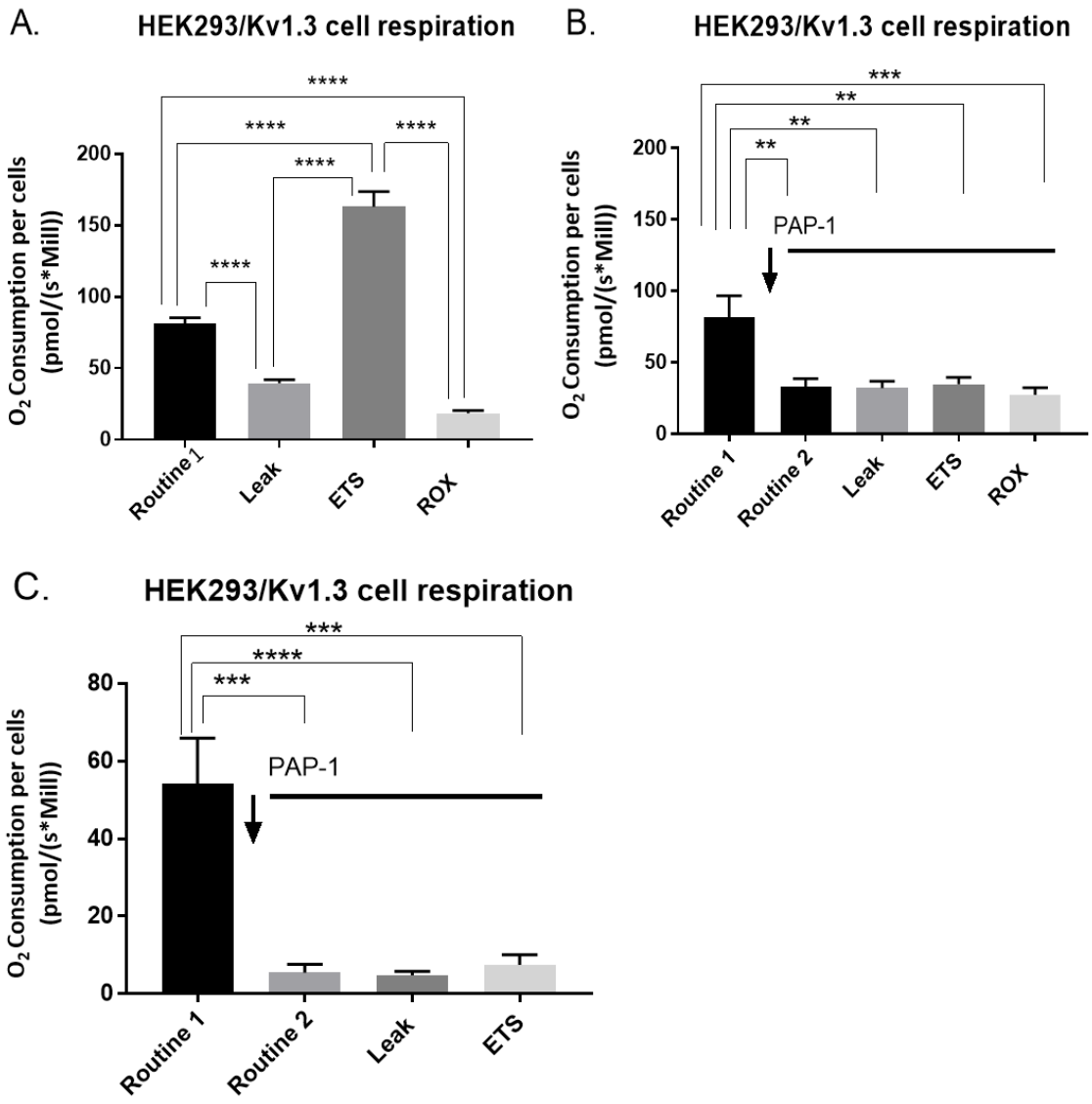

Figure 4.6 PAP-1 reduces oxidative phosphorylation in HEK293/Kv1.3 cells. A. Oxygen (O_2) consumption (pmol per second per million cells, pmol/(s*Mill)) in total HEK293/Kv1.3 cells (n=38). O_2 consumption was measured at four points; Routine 1=Routine Respiration, Leak=Leak Respiration, ETS=electron transport system uncoupling and ROX=residual O_2 consumption. Data expressed as the mean O_2 consumption ± SEM. Data analysed using one-way ANOVA with Tukeys multiple comparison test, **** $p<0.0001$. B. O_2 consumption (pmol per second per million cells, pmol/(s*Mill)) in total HEK293/Kv1.3 cells treated with 100-300nM PAP-1 (n=6). Black arrow represents PAP-1 addition to the chamber. O_2 consumption measured at five points; Routine 1=Routine Respiration before PAP-1 addition, Routine 2=Routine Respiration after PAP-1 addition, Leak, ETS and ROX as in (A). Data expressed as the mean O_2 consumption ± SEM. Data analysed using one-way ANOVA with Tukeys multiple comparison test, ** $p<0.01$, *** $p<0.001$. There were no significant differences between Routine 2, Leak, ETS and ROX. C. Data in (B) corrected for residual O_2 consumption (ROX). Data analysed using one-way ANOVA with Tukey's multiple comparison test, *** $p<0.001$, **** $p<0.0001$.

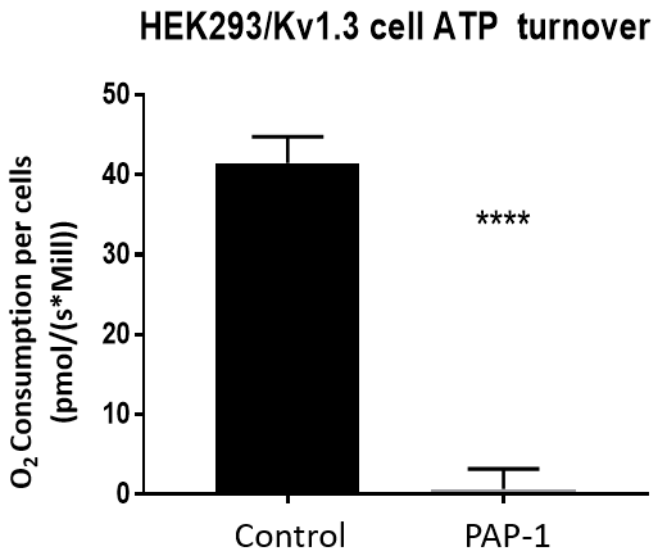

Figure 4.7 Effect of PAP-1 on ATP Turnover Rate of HEK293/Kv1.3 cells. ATP turnover rate in total HEK293/Kv1.3 cells (n=38) and in HEK293/Kv1.3 cells (n=6) treated with PAP-1 (100-300nM). ATP turnover is the difference between Routine and Leak Respiration. Data expressed as mean O_2 consumption (pmol/(s*Mill)) ± SEM. Data analysed using Student's t-test, **** $p<0.0001$.

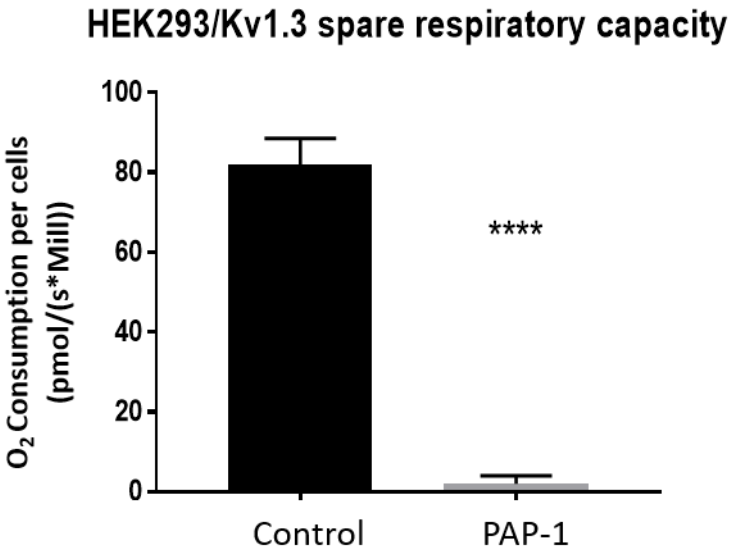

Figure 4.8 Effect of PAP-1 on Spare Respiratory Capacity of HEK293/Kv1.3 cells. Spare Respiratory Capacity (SRC) in total HEK293/Kv1.3 cells (n=38) and in HEK293/Kv1.3 cells treated with PAP-1 (n=6) (100nM-300nM). SRC is the difference between Routine Respiration and maximum uncoupling of the electron transport system. Data expressed as mean O_2 consumption (pmol/(s*Mill)) ± SEM. Data analysed using Student's t-test, **** $p<0.0001$.

4.3.4 WT HEK293 respiration was decreased by PAP-1

WT HEK293 cell respiration was also affected by acute administration of PAP-1 (100-200nM). An example experiment trace is shown in Figure 4.9. 100nM PAP-1 caused an initial rapid reduction in WT HEK293 O_2 consumption, which then plateaued, and then reduces again following addition of another 100nM PAP-1. As was the case in HEK293/Kv1.3 cells, addition of oligomycin (before Leak Respiration (L) was measured) and FCCP (before ETS Respiration (ETS) was measured) had little effect on the respiration of WT HEK293 cells which had been treated with PAP-1. Again, addition of rotenone and antimycin A (before ROX was measured) caused a severe reduction in O_2 consumption below zero, as shown by the downward dotted trace line (between ETS and ROX measurements), which rapidly recovered and stabilised above zero.

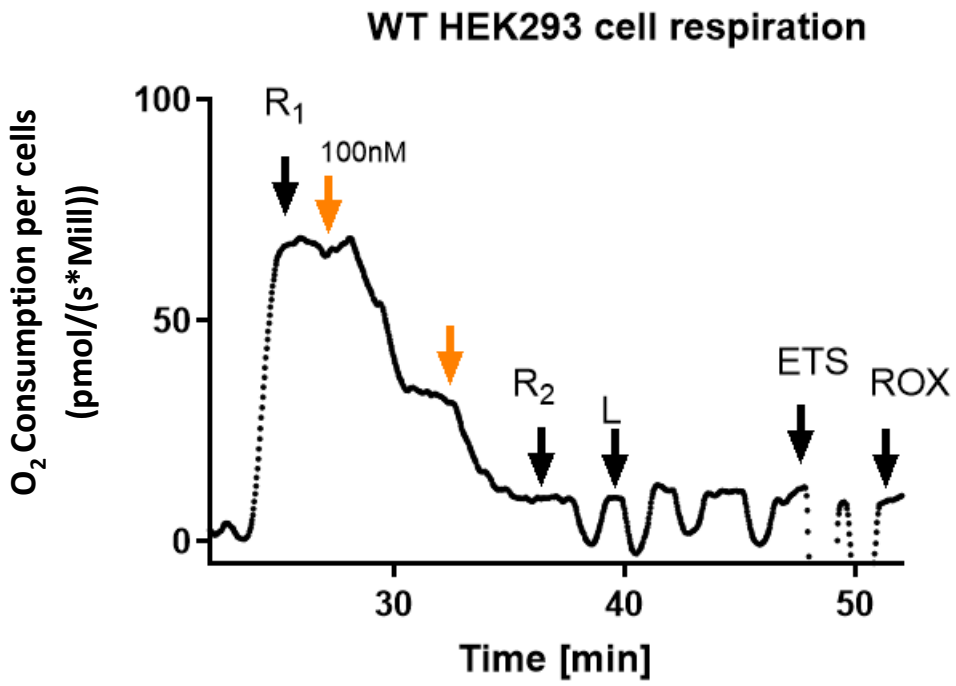

Figure 4.9 PAP-1 can reduce oxygen consumption of WT HEK293 cells. An example trace showing the O2 consumption (pmol per million cells per second, pmol/(s*Mill)) in WT HEK293 cells treated with PAP-1 (final concentration 200nM). Orange arrows represent the points at which PAP-1 was added to the chamber. Black arrows represent the points at which measurements were taken; R_1=Routine Respiration, R_2=Routine Respiration after PAP-1 treatment, L=Leak Respiration, E=ETS (electron transport system) uncoupling and ROX=residual O2 consumption.

Figure 4.10 shows all the respirometry data for PAP-1 treated WT HEK293 cells. The concentrations of PAP-1 used on WT HEK293 cells were between 100-200nM. Once again, the severe increase in cellular O_2 consumption with FCCP (Figure 4.10A) was inhibited in PAP-1 treated cells (Figure 4.10B and C), supporting the idea that the inhibitory effect of PAP-1 is due to inhibition of the ETS. PAP-1 decreases Routine Respiration by 78% in WT HEK293 cells when respiration is uncorrected for ROX (Figure 4.10B), and by 85% when respiration is corrected for ROX (Figure 4.10C). Due to the variation in PAP-1 concentrations on WT HEK293 cells (100-200nM), and the variation between the concentrations used on HEK293/Kv1.3 cells(100nM-300nM), no direct comparisons can be made between the effect of PAP-1 on the two cells types. All that can be concluded is that inhibition of Kv1.3 channels with PAP-1 is able to reduce respiration in HEK293 cells. In addition, PAP-1 was able to reduce ATP turnover (Figure 4.11) and SRC (Figure 4.12) in WT HEK293 cells. However, due to the severity of the response to PAP-1 in HEK293 cell respiration, and the lack of a HEK293/Kv1.3 cell-specific effect, these results raise the possibility that PAP-1 has off target effects on respiration, rather than due to targeted inhibition of mitochondrial Kv1.3 channels.

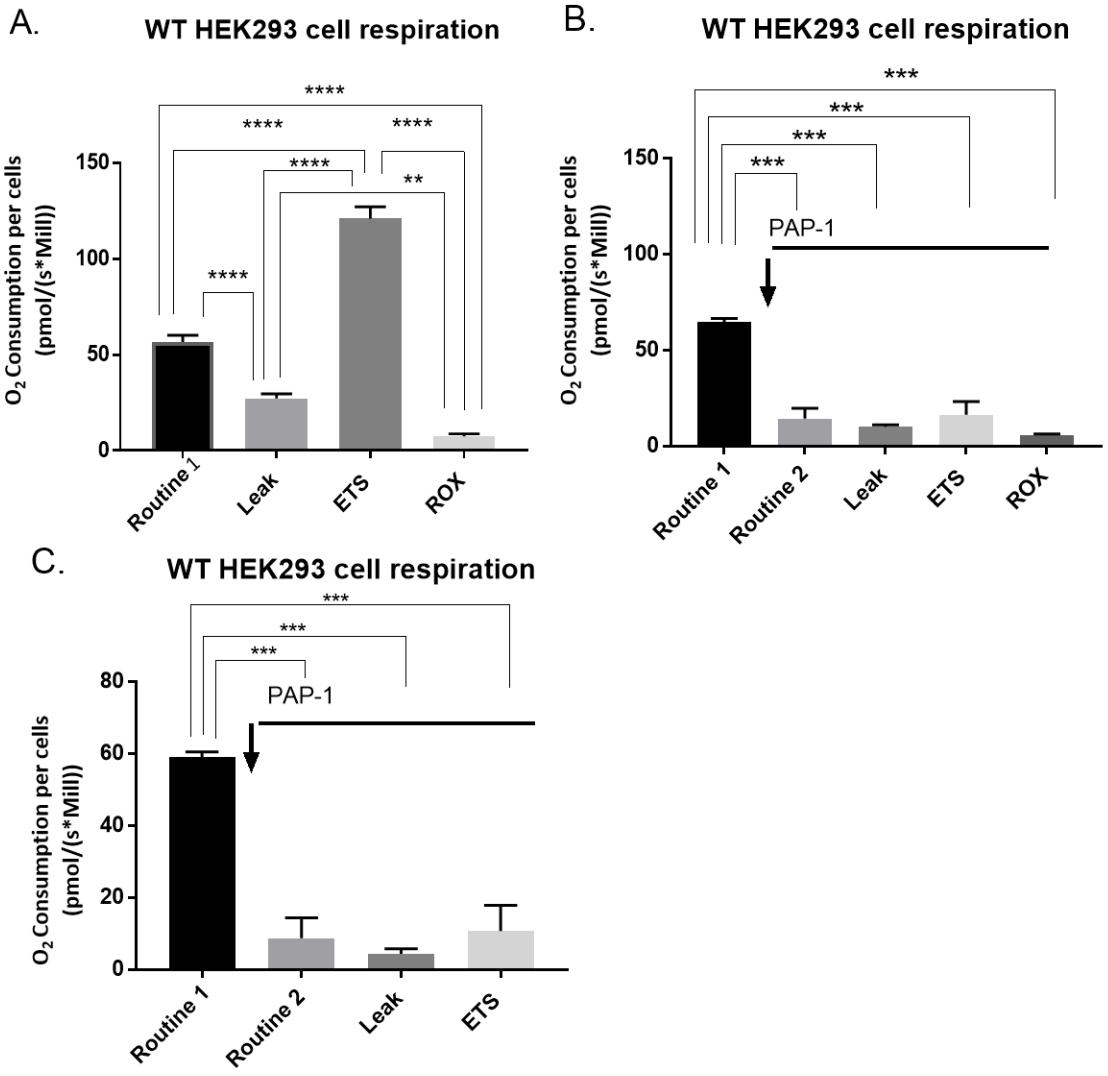

Figure 4.10 PAP-1 can reduce Routine Respiration in WT HEK293 cells. A. Oxygen (O_2) consumption (pmol per million cells per second, pmol/(s*Mill)) in total WT HEK293 cells (n=27). O_2 consumption was measured at four points; Routine1=Routine Respiration, Leak=Leak Respiration, ETS=electron transport system uncoupling and ROX=residual O_2 consumption. Data expressed as the mean O_2 consumption ± SEM. Data analysed using one-way ANOVA with Tukeys multiple comparison test, ** $p<0.01$, **** $p<0.0001$. B. O_2 consumption (pmol/(s*Mill) in total WT HEK293 cells treated with 100-200nM PAP-1 (n=3). Black arrow represents PAP-1 addition to the chamber. O_2 flow measured at five points; Routine1=Routine Respiration before PAP-1 addition, Routine2=Routine Respiration after PAP-1 addition, Leak, ETS and ROX as in (A). Data expressed as the mean O_2 consumption ± SEM. Data analysed using one-way ANOVA with Tukeys multiple comparison test, *** $p<0.001$. There were no significant differences between Routine 2, Leak, ETS and ROX. C. Data for (B) corrected for ROX. Data analysed using one-way ANOVA with Tukeys multiple comparison test, *** $p<0.001$.

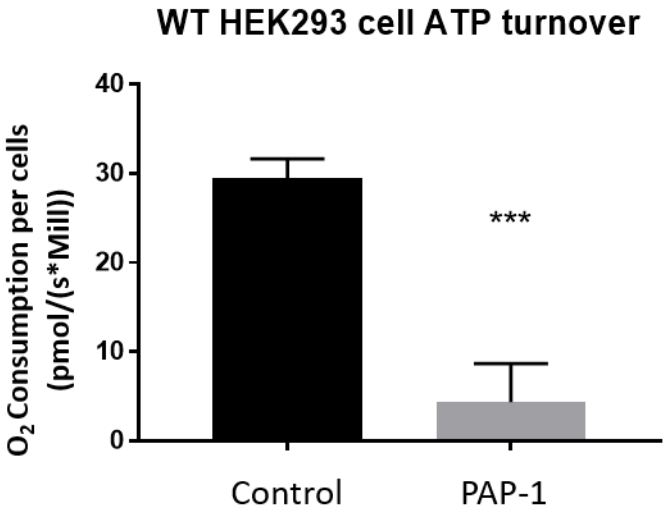

Figure 4.11 PAP-1 reduces ATP turnover of WT HEK293 cells. ATP turnover in control WT HEK293 cells (left column, n=27) and in PAP-1 treated WT HEK293 cells (right column, n=3). ATP turnover is the difference between Routine Respiration and Leak Respiration. Data analysed by Student's t-test and was significant, *** p>0.001.

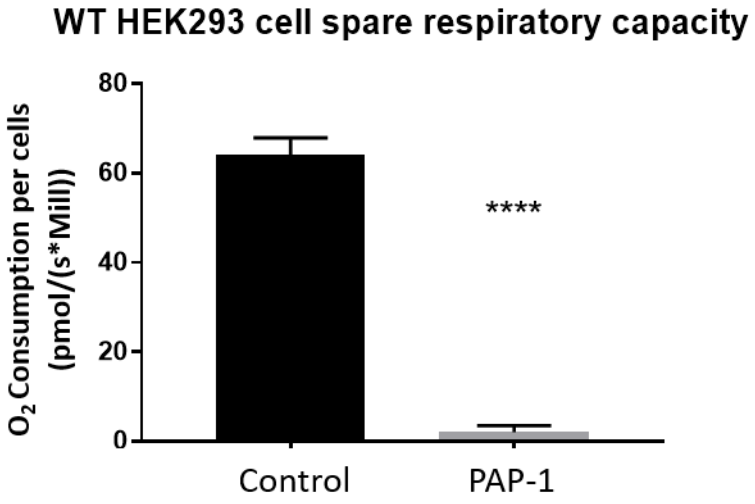

Figure 4.12 PAP-1 reduces spare respiratory capacity of WT HEK293 cells. Spare Respiratory Capacity (SRC) in control WT HEK293 cells (left column, n=27) and PAP-1 treated WT HEK293 cells (right column, n=3). SRC is the difference between maximum ETS capacity and Routine Respiration. Data was analysed using Student's t-tests, *** p<0.001.

4.3.5 ShK-Dap22 inhibits plasma membrane potassium currents but does not decrease proliferation in HEK293/Kv1.3 cells.

ShK-Dap22 is an analogue of the potent inhibitor of Kv1.3 channels, ShK, derived from the sea anemone Stichodactyla Helianthus (Rashid *et al.*, 2013). It cannot permeate the cell's plasma membrane, and therefore cannot bind to intracellular Kv1.3 channels. The EC_{50} of ShK-Dap22 is 23pM for inhibition of Kv1.3 currents. A dose-response assay was used to assess the effect of ShK-Dap22 (1-200pM) on the proliferation of WT HEK293 (Figure 4.13A) and HEK293/Kv1.3 cells (Figure 4.14A). ShK-Dap22 did not affect the proliferation of WT HEK293 (Figure 4.13A) or HEK293/Kv1.3 cells (Figure 4.14A). ShK-Dap22 did not induce cell death in WT HEK293 cells, as assessed by counting detached cells in the culture media of the wells in the proliferation assay (Figure 4.13B) and by Trypan Blue viability of cells (Figure 4.13C). ShK-Dap22 did have a cytotoxic effect on HEK293/Kv1.3 cells, as on one occasion there was an increase in the floating cells in the media of the well of the proliferation assay with 50pM ShK-Dap22 (Figure 4.14B). As this was not sustained and/or increased with further increases in ShK-Dap22 concentration, it is likely that the effect on cell death was not associated with the concentration of the toxin. In addition, Trypan Blue staining of HEK293/Kv1.3 cells did not detect any cytotoxic effects of ShK-Dap22 (Figure 4.14C). This is supported by the fact that across all five repeats of the ShK-Dap22 dose response assay, there was no consistent and significant decrease in the cell counts with 50pM ShK-Dap22 (Figure 4.14A).

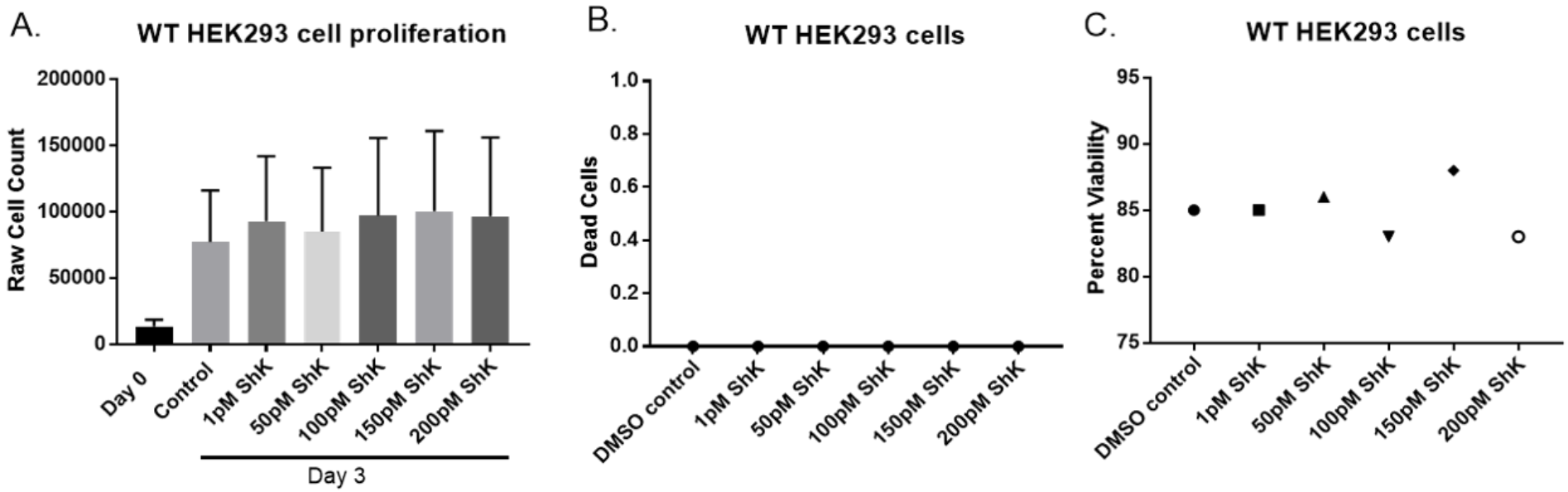

Figure 4.13 ShK-Dap22 does not affect the proliferation of WT HEK293 cells. A. Dose response curve of WT HEK293 cells treated with ShK-Dap22 (1pM-200pM) (n=3). Black bar = Day 0 counts, grey bars = Day 3 counts. Data is expressed as the mean raw cell counts ± SEM, wells were counted in triplicate. B. Viability counts for WT HEK293 cells treated with ShK-Dap22 (n=1). Detached cells in the media were stained with Trypan Blue and counted using a manual haemocytometer. C. Percentage of viable WT HEK293 cells during counting, calculated on the automated cell counter by trypan blue staining (n=1).

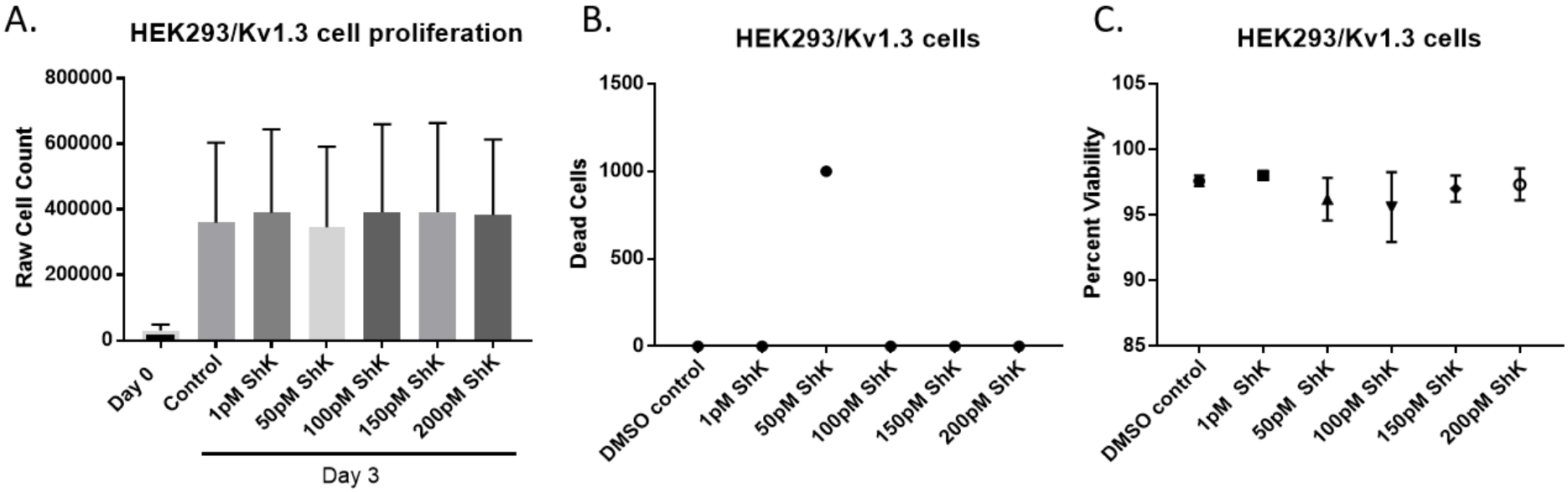

Figure 4.14 ShK-Dap22 does not affect the proliferation of HEK293/Kv1.3 cells. A. Dose response curve of HEK293/Kv1.3 cells treated with ShK-Dap22 (1pM-200pM) (n=5). Black bar = Day 0 counts, grey bars = Day 3 counts. Data is expressed as the mean raw cell counts ± SEM, wells were counted in triplicate. B. Viability counts for HEK293/Kv1.3 cells treated with ShK-Dap22, as assessed by counting dead cells floating in the media of the wells (n=1). C. Percentage of viable HEK293/Kv1.3 cells during counting, calculated on the automated cell counter by Trypan Blue staining (n=5 for control, 50pM and 100pM, n=3 for 1pM, 150pM and 200pM. Data expressed as the mean percentage viability ± SEM. Data was analysed using a one-way ANOVA Test ($p>0.05$).

Electrophysiology was used to confirm that ShK-Dap22 inhibited the plasma membrane Kv1.3 channels in HEK293/Kv1.3 cells (Figure 4.15). ShK-Dap22 (80pM) reduced the potassium currents in HEK293/Kv1.3 cells (Figure 4.15).

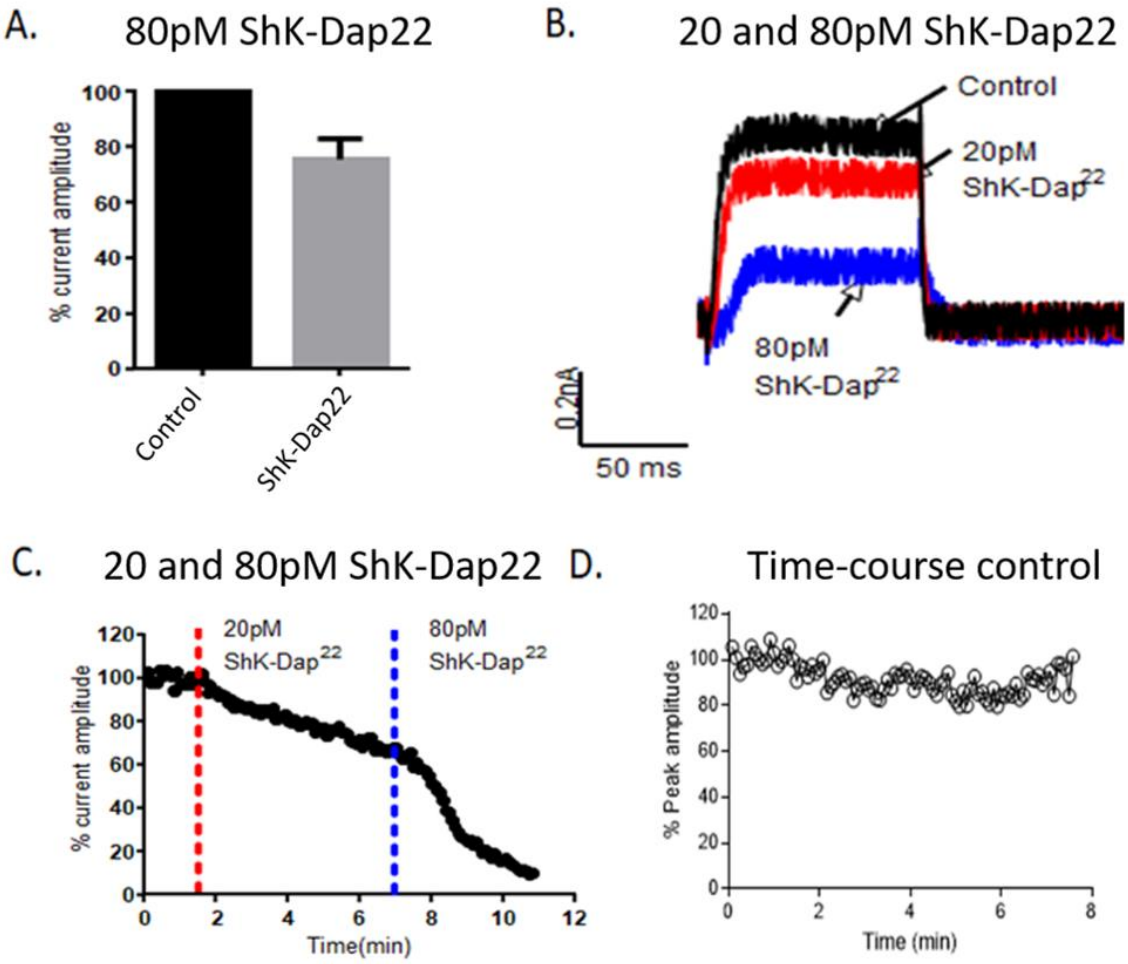

Figure 4.15 ShK-Dap22 inhibits the potassium ion current in HEK293/Kv1.3 cells. A. Percentage decrease in Kv1.3 mean current amplitude with 80pM ShK-Dap22 (n=5 ± SEM). B. Whole cell voltage clamp trace showing inhibition of Kv1.3 current by ShK-Dap22 (20pM-80pM). C. Time course experiment of a single HEK293/Kv1.3 cell, with percentage decrease in Kv1.3 current amplitude with ShK-Dap22 (20pM and 80pM) plotted against time and peak current normalised to cell size. D. Example time-course control of a HEK293/Kv1.3 cell being held at -80mV for 8 minutes. Experiments were carried out by Dr M. Al-Owais, University of Leeds

4.3.6 ShK-Dap22 has no effect on the respiration of HEK293/Kv1.3 cells.

HEK293/Kv1.3 cells were treated with 500pM ShK-Dap22 in an OROBOROS Oxygraph-2K High Resolution Respirometer (Figure 4.16). 500pM was the final concentration tested as ShK-Dap22 was titrated periodically throughout the experiment in steps of 50pM. The concentration was increased to determine a concentration-dependent response in the respiration rate. No response to 500pM ShK-Dap22 was observed in HEK293/Kv1.3 cells across Routine, Leak, ETS or ROX Respiration stages (routine, leak, ETS or ROX).

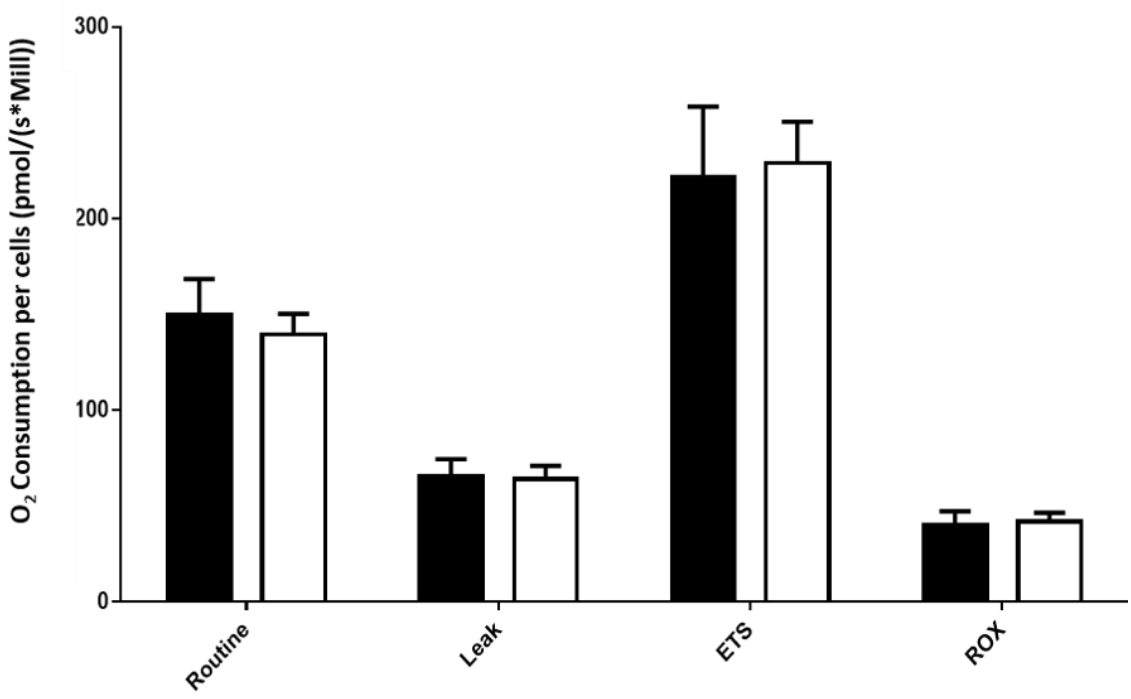

Figure 4.16 ShK-Dap22 has no effect on the respiration of HEK293/Kv1.3 cells. Respiration (O_2 consumption, pmol per million cells per second (pmol/s*Mill)) of HEK293/Kv1.3 cells treated with 500pM ShK-Dap22 (white bars). Black bars = untreated control data. Data is expressed as the mean O_2 consumption at Routine, Leak, ETS and ROX Respiration ± SEM (n=3). Data was analysed using Student's t-tests for Routine, Leak, ETS and ROX. No significant difference was observed between drug treated and control cells ($p>0.05$). Experiments were carried out by Dr J. Boyle.

4.3.7 A mitochondrially targeted Kv1.3 channel inhibitor decreases HEK293/Kv1.3 cell proliferation.

Next, the role of mitochondrial Kv1.3 channels as regulators of cellular proliferation was investigated. A mitochondrially targeted, PAP-1 derivative, PAPTP was synthesised by Dr Robin Bon at Leeds University, following the protocol provided by Leanza et al., (2017) (see Methods Section 4.11)

A dose-response assay was set up to assess the effect of PAPTP (3nM-100nM) on HEK293/Kv1.3 cell proliferation (Figure 4.17). PAPTP did not affect proliferation in WT HEK293 cells (Figure 4.17A) and had no significant effects on cell viability as determined by Trypan Blue staining (Figure 4.17B). 100nM PAPTP had a tendency to reduce HEK293/Kv1.3 cell proliferation (Figure 4.17C) although this was not significant by ANOVA. The decrease in proliferation was not due to cytotoxic effects of 100nM PAPTP on HEK293/Kv1.3 cells (Figure 4.17D), again determined by a Trypan Blue viability assay. The total reduction in proliferation by 100nM PAPTP was calculated as 28.98% of control proliferation (Figure 4.18A), and this was significant when analysed with Student's t-test. In addition, the effect of 100nM PAPTP on HEK293/Kv1.3 cells may have been underestimated, as the potency of PAPTP reduced with experimental repeat (Figure 4.18B).

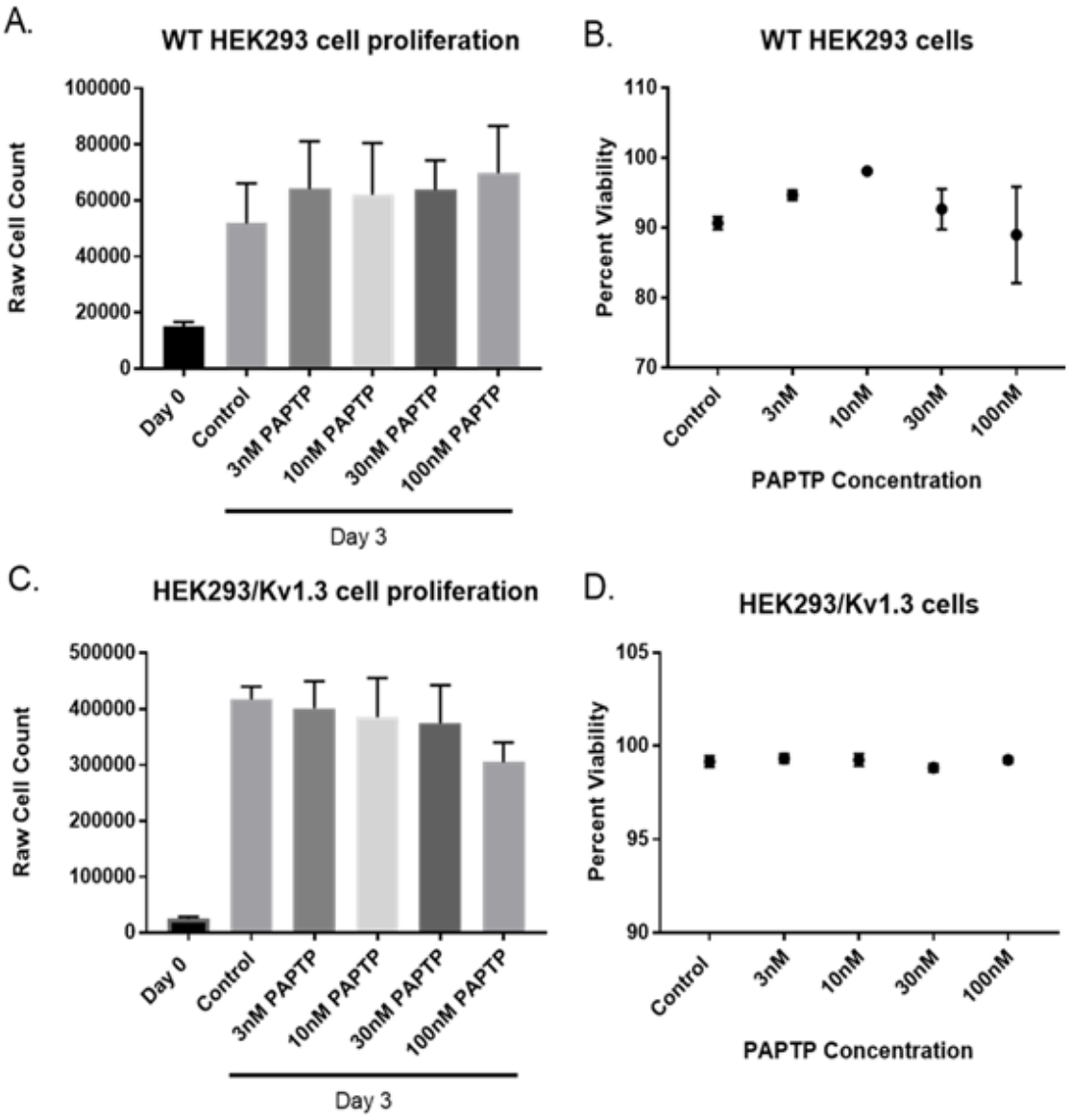

Figure 4.17 PAPTP tends to reduce proliferation in HEK293/Kv1.3 cells at 100nM. A. Dose response proliferation assay of WT HEK293 cells treated with PAPTP (3nM-100nM). Black bar = Day 0 counts, grey bars = Day 3 counts, (n = 3). Statistical analysis was carried out using a one-way ANOVA ($p>0.05$). Wells were counted in triplicate. Raw cell counts expressed on graph as mean ± SEM. B. Percentage viability of WT HEK293 cells, as assessed by trypan blue staining in the automated TC10 cell counter (n=3). Data expressed as the mean percentage viability ± SEM. Statistical analysis was carried out using one-way ANOVA ($p>0.05$). C. Dose response proliferation assay of HEK293/Kv1.3 cells treated with PAPTP (3nM-100nM). Black bar = Day 0 counts, grey bars = Day 3 counts, (n = 4). Statistical analysis was carried out using a one-way ANOVA ($p>0.05$). Wells were counted in triplicate. Cell counts expressed on graph as mean ± SEM. D. Percentage viability of HEK293/Kv1.3 cells, as assessed by trypan blue staining in the automated TC10 cell counter (n=4). Data expressed as the mean percentage viability ± SEM. Statistical analysis was carried out using one-way ANOVA ($p>0.05$).

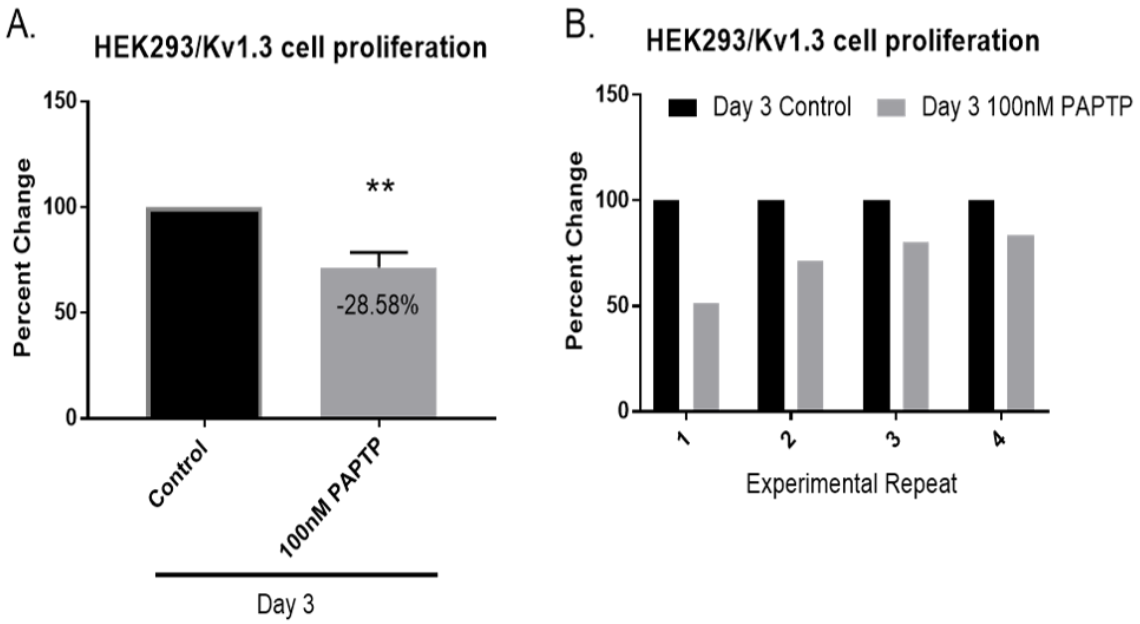

Figure 4.18 100nM PAPTP can reduce HEK293/Kv1.3 proliferation despite losing potency. A. 100nM PAPTP decreased the proliferation of HEK293/Kv1.3 cells (n=4). Data is from Figure 4.17c displayed as mean percentage change from Day 3 control proliferation ± SEM. Student's t-tests were used for analysis (** $p<0.01$). B. PAPTP lost its potency across the experimental repeats (1-4). Black bars = HEK293/Kv1.3 control day 3 counts. Grey bars = HEK293/Kv1.3 PAPTP treated (100nM) day 3 counts.

4.3.8 100nM PAPTP can reduce respiration in HEK293/Kv1.3 cells.

The effect of mitochondrially targeted Kv1.3 channel inhibition on respiration rate using 100nM PAPTP was examined in WT HEK293 and HEK293/Kv1.3 cells (Figure 4.19). In HEK293/Kv1.3 cells 100nM PAPTP reduced Routine Respiration, increased Leak Respiration and reduced ETS Respiration (Figure 4.19A). In WT HEK293 cells, 100nM PAPTP did not affect Routine or ETS Respiration rates but did increase the rate of Leak Respiration (Figure 4.19B).

In these experiments, cells were incubated for 30 minutes (37°C; 95% air, 5% CO_2) in serum free cell suspension prior to respirometry, to facilitate PAPTP intracellular accumulation and mitochondrial targeting to Kv1.3 channels. This pre-treatment phase may have reduced the respiration rate of the cells (compared to Figure 3.5, Chapter Three). This reduction in respiration is apparent for example in Figure 4.19, where there is little difference between the Routine Respiration O_2 consumption in HEK293/Kv1.3 and WT HEK293 cells. The reduction in O_2 consumption during this pre-treatment phase was disproportionate between HEK293/Kv1.3 and WT HEK293 cells and may have reduced the response to 100nM PAPTP in HEK293/Kv1.3. cells.

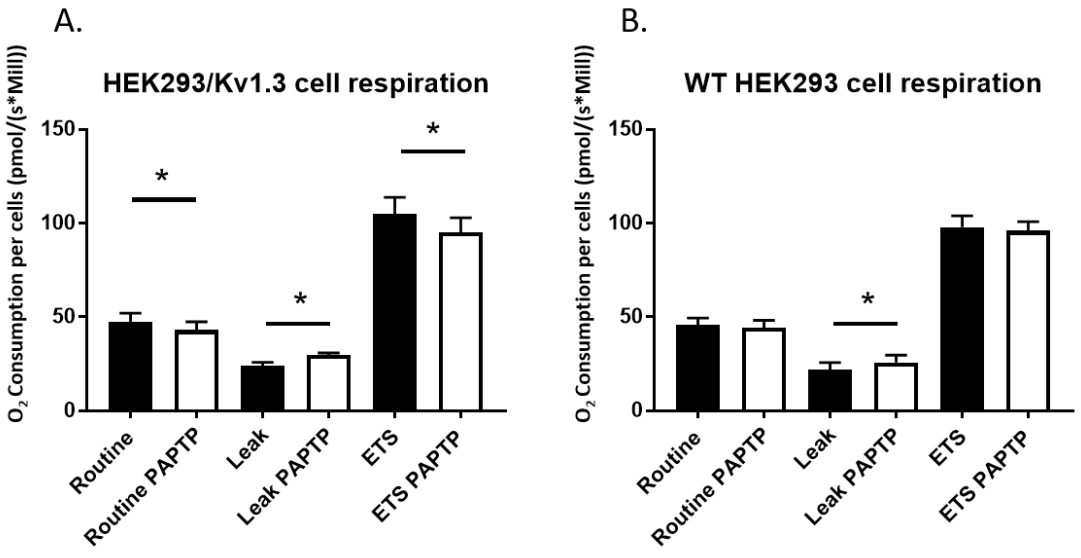

Figure 4.19 The effect of 100nM PAPTP on HEK293/Kv1.3 respiration. A. The effect of 100nM PAPTP on Routine, Leak and ETS Respiration in HEK293/Kv1.3 cells (n=5). Data is corrected for residual O_2 consumption (ROX). B. The effect of 100nM PAPTP on Routine, Leak and ETS Respiration in WT HEK293 cells (n=4). Data is corrected for ROX and displayed as the mean ± SEM. Data was analysed using Student's t-tests on routine, leak and ETS respiration, * $p<0.05$.

PAPTP (100nM) reduced ATP turnover rate in HEK293/Kv1.3 cells by 45.6%, compared to a 22.1% in WT HEK293 cells (Figure 4.20). Therefore, PAPTP was twice as efficient at reducing ATP turnover in HEK293/Kv1.3 cells. This was likely to do with the fact that 100nM PAPTP significantly reduced Routine Respiration in HEK293/Kv1.3 cells but not in WT HEK293 cells (Figure 4.19). In addition, 100nM PAPTP reduced SRC in HEK293/Kv1.3 cells (Figure 4.21A), likely due to the reductions seen in Routine Respiration and ETS Respiration (Figure 4.19), but not in WT HEK293 cells (Figure 4.21B).

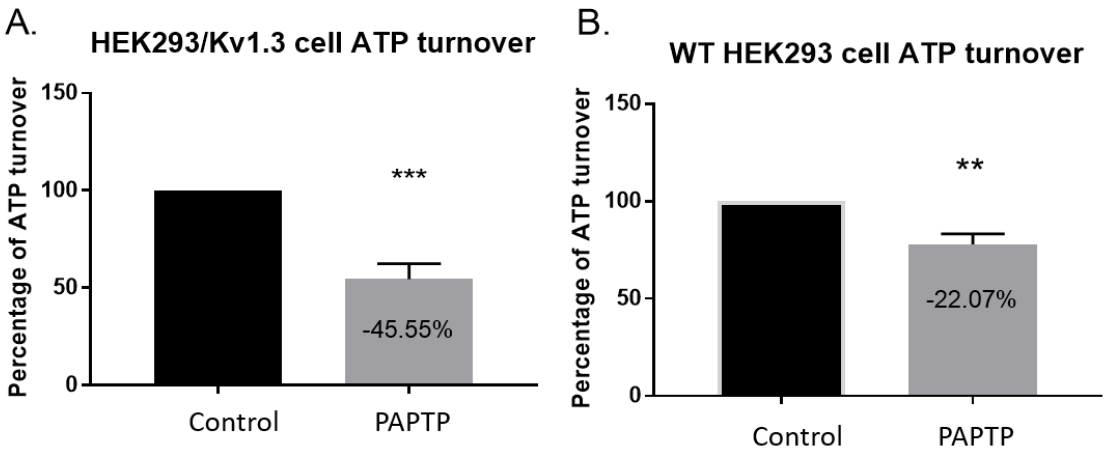

Figure 4.20 100nM PAPTP reduced ATP turnover in both HEK293/Kv1.3 cells and WT HEK293 cells. ATP turnover was calculated by finding the difference between Routine Respiration and Leak Respiration (Figure 4.19). A. PAPTP reduced HEK293/Kv1.3 cell ATP turnover by 45.55% (n=6). B. PAPTP reduced WT HEK293 cell ATP turnover by 22.07% (n=4). Data corrected for residual O_2 consumption and expressed as a percentage of control ± SEM. Data analysis carried out by Student's t-tests (** $p<0.01$, *** $p<0.001$).

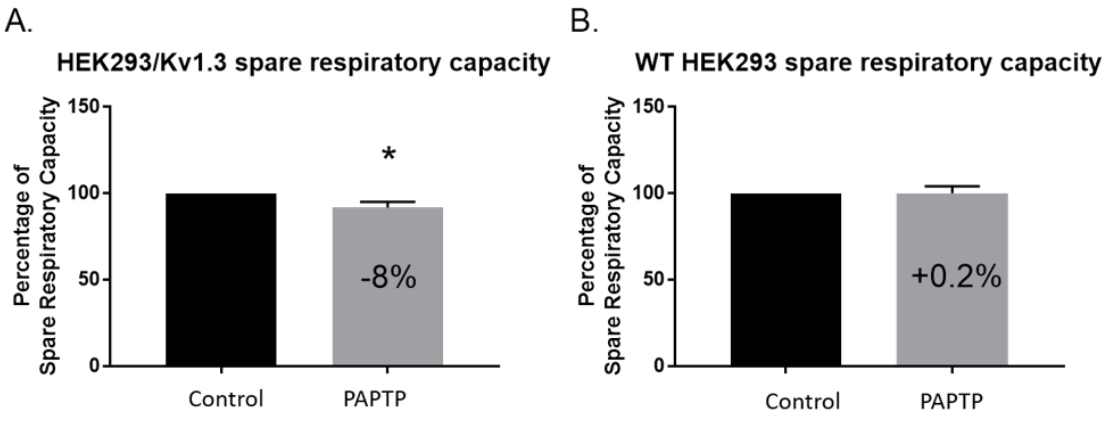

Figure 4.21 100nM PAPTP reduced spare respiratory capacity in HEK293/Kv1.3 cells. Spare Respiratory Capacity (SRC) was calculated by finding the difference between ETS Respiration and Routine Respiration (Figure 4.19). A. PAPTP reduced HEK293/Kv1.3 cell SRC by 8% (n=6). B. PAPTP had no significant effect on WT HEK293 cell SRC (n=4). Data corrected for residual O_2 consumption and expressed as a percentage of control ± SEM. Data analysis carried out by Student's t-tests (* $p<0.05$).

4.4 Discussion

This chapter confirms that the Kv1.3 inhibitor PAP-1 reduces cellular proliferation in HEK293 cells, as observed in other cells including VSMCs (Cidad *et al.*, 2010, 2012; Cheong *et al.*, 2011; Jimenez-Perez *et al.*, 2016). Although PAP-1 did not affect proliferation of WT HEK293 cells, the inhibitor in the low nanomolar range reduced proliferation of HEK293/Kv1.3 cells. Interestingly, the effect of PAP-1 on HEK293/Kv1.3 cell proliferation decreased as the concentrations of the inhibitor increased from 3nM. However, micromolar concentrations of PAP-1 were required to inhibit the membrane K^+ currents of HEK293/Kv1.3 cells in electrophysiology experiments. These findings may suggest that K^+ flux through the Kv1.3 channel in the plasma membrane is not the primary inducer of cell proliferation. This is in agreement with recent work by Cidad et al., in which they identify ion flux independent mechanisms of proliferation stimulated by Kv1.3 channels in HEK293 cells (Cidad *et al.*, 2012; Jimenez-Perez *et al.*, 2016). Another possibility is that at low concentrations, PAP-1 (0.3nM and 1nM) may pass through the plasma membrane and inhibit Kv1.3 channels at intracellular locations without complete inhibition of plasma membrane Kv1.3 channels. Previous work has shown that Kv1.3 channels at the nucleus could also be key moderators of cellular proliferation, by regulating the gene expression of transcription factors including CREB and c-Fos (Jang *et al.*, 2015). Nuclear Kv1.3 channels may also regulate ribosome biogenesis, essential for protein synthesis that is essential for cellular proliferation (Jang *et al.*, 2015). In addition, Kv1.3 in the cis-Golgi membrane may control it's function of organising and distributing cell proteins in rat astrocytes, thus potentially playing a role in cell proliferation (Zhu, Yan and Thornhill, 2014). However, this thesis identifies a role for mitochondrial Kv1.3 channels in the regulation of cellular proliferation.

Strangely, the effect of PAP-1 on cellular proliferation reduced at concentrations above low nanomolar in HEK293/Kv1.3 and HSVSMCs. Higher concentrations of PAP-1 may induce counter-regulatory mechanisms which reduce the anti-proliferative effects of the inhibitor. Cell volume is a known regulator of the cell cycle and can be modulated by K^+ ions (Deutsch and Lee, 1988). Interestingly, there exists a bell shaped relationship between cell volume and proliferation/progression of cell cycle (Perez-Garcia, Cidad

and Lopez-Lopez, 2018). When K^+ efflux is inhibited i.e. by Kv1.3 channel inhibition, cell volume may increase as a higher intracellular concentration of K^+ ions generates a chemiosmotic gradient driving water influx (Dubois and Rouzaire-Dubois, 2004). Therefore, at concentrations of PAP-1 above 3nM, the blockade of Kv1.3 channels may alter the water balance of the cell. A high cell volume may either reduce the PAP-1 inhibitory effect on proliferation or may stimulate the cell to proliferate. Interestingly, much higher concentrations of PAP-1 (100-300nM) was needed to reduce respiration in both WT HEK293 and HEK293/Kv1.3 cells. As found in Chapter Three, WT HEK293 cells do express Kv1.3 channels, and evidence suggested mitochondrial co-localisation in these cells as well as HEK293/Kv1.3 cells. PAP-1 inhibition of respiration in HEK293 cells suggests that the Kv1.3 channel regulates physiological respiration in these cells. The fact that PAP-1 had no effect on WT HEK293 cell proliferation, but can inhibit respiration, suggests that proliferation and respiration may be independently regulated by Kv1.3 channels. In addition, the fact that low nanomolar concentrations of PAP-1 inhibited HEK293/Kv1.3 proliferation, but high nanomolar concentrations were needed to supress HEK293/Kv1.3 respiration, may also indicate independent effects of Kv1.3 on these processes. However, inhibition of Kv1.3 by PAP-1 in HEK293/Kv1.3 and WT HEK293 cells reduced routine respiration, maximal uncoupled ETS respiration, ATP turnover and spare respiratory capacity, which would almost definitely reduce the energy available for proliferation in these cells. The severity of the inhibition of respiration by PAP-1 in WT HEK293 and HEK293/Kv1.3 cells may suggest that PAP-1 is having off target effects on respiration, not due to inhibition of Kv1.3 or mitochondrial Kv1.3 channels. These results are concerning and must be further investigated due to the large body of research that uses PAP-1 for treatment of various conditions (Wulff *et el*., 2009). Whether these effects on proliferation and respiration were specifically a result of mitochondrial Kv1.3 inhibition was then investigated. Initially, plasma membrane Kv1.3 channels were inhibited using ShK-Dap22, an analogue of ShK isolated from the sea anemone Stichodactyla helianthus. In 1995, Pennington and colleagues first isolated and synthesised a biologically active form of ShK toxin, that was capable of blocking K^+ channels in vitro (Pennington *et al.*, 1995). However, at sub-nanomolar concentrations this toxin also blocked Kv1.1, 1.4 and 1.6. Three years later they published their work on enhancing the specificity of the drug (Kalman *et al.*, 1998). They used mutant cycle analysis and site directed

mutagenesis to gain more information on how the ShK toxin bound to its K^+ channel target. In doing so, they identified a critical Lys 22 that was important for binding, and replaced it with a positively charged, non-natural amino acid, diamino propionic acid (ShK-Dap22) which increased the toxins specificity for Kv1.3 channels.

Although ShK-Dap22 displayed extremely potent effects on the whole cell K^+ currents of HEK293/Kv1.3 cells, it did not reduce proliferation of the cells, suggesting that intracellular but not extracellular Kv1.3 channels contribute to the proliferative phenotype. ShK analogues have previously been observed to reduce cellular proliferation in lymphocytes and other immune cells (Hu *et al.*, 2013; Chang *et al.*, 2015). However, in immune cells the membrane potential (regulated by Kv channels) is the main determinant of proliferation stimulation via modulation of Ca^{2+} influx, which is crucial to activation of immune cells (Perez-Garcia, Cidad and Lopez-Lopez, 2018). Interestingly, Margatoxin (MgTx), another membrane impermeable Kv1.3 channel inhibitor, was found to inhibit smooth muscle migration and proliferation in human and mouse smooth muscle cells (Cheong *et al.*, 2011). MgTx reduced the migration of HSVSMCs by 40%, therefore targeting both intracellular and plasma membrane Kv1.3 channels may further inhibit proliferation in VSMCs. Cheong and colleagues suggested the reduction in proliferation and migration by Kv1.3 channel inhibition was primarily driven by a reduction in Ca^{2+} entry. However this work may be confounded by the reported inhibitory action of MgTx on other Kv channels (Bartok *et al.*, 2014), such as Kv1.2, whose inhibition has been found to reduce proliferation of rat mesenchymal stem cells (Deng *et al.*, 2007). ShK-Dap22 also did not affect cellular respiration in either WT HEK293 or HEK293/Kv1.3 cells, suggesting that plasma membrane Kv1.3 channels are unlikely to be involved in the altered metabolic phenotype in HEK293/Kv1.3 cells. Therefore, depolarisation of the plasma membrane by PAP-1 is unlikely to have altered cation entry, specifically Ca^{2+} entry into the cell, causing or contributing to the reduction in respiration by the inhibitor. More specifically, these results suggest that intracellular Kv1.3 channels are likely to have a role in the regulation of respiration, particularly OXPHOS. It is of note that upregulation of Kv1.3 expression would lead to increased plasma membrane, mitochondrial, cis-Golgi and nuclear levels of the channel and therefore may alter multiple signalling pathways that could contribute to the increased proliferation. Elucidating the Kv1.3-mediated

signalling pathways with the greatest effect on proliferation would have significant benefit for the development of targeted, highly specific and safe future treatments for Kv1.3-induced proliferative disorders of vascular smooth muscle cells.

A mitochondrially-targeted Kv1.3 inhibitor, PAPTP, was then used to investigate the role of mitochondrial Kv1.3 in cellular proliferation and respiration. PAPTP had differential effects on WT HEK293 cells and HEK293/Kv1.3 cell proliferation. In WT HEK293 cells, PAPTP had no effect on proliferation whereas in HEK293/Kv1.3 cells there was a trend for PAPTP to decrease proliferation. PAPTP at 100nM did not reduce cell viability or exhibit cytotoxic effects in HEK293/Kv1.3 or WT HEK293 cells, but this concentration did significantly reduce proliferation when normalised to the final Day 3 control count in HEK293/Kv1.3 cells. This suggests that mitochondrial Kv1.3 plays a role in the proliferation in HEK293 cells. However, this is in contrast to other prominent work in the field. For example, Cidad et al., found that the shuttling of Kv1.3 channels to the plasma membrane was necessary to induce proliferation in HEK293 cells (Cidad *et al.*, 2012). In addition, Leanza and colleagues propose that mitochondrial Kv1.3 regulates apoptosis in cancer cells (Leanza *et al.*, 2012, 2017; Luigi Leanza *et al.*, 2013; Venturini *et al.*, 2017; Mattarei *et al.*, 2018). However, in these studies, concentrations of Kv1.3 and mitochondrial Kv1.3 inhibitors were far higher (between 1-20µM) than the concentrations used in this study (3-100nM), which may have accounted for the difference in cytotoxicity. In HEK293/Kv1.3 cells PAPTP significantly reduced Routine Respiration and Maximal Uncoupled Respiration in response to FCCP, and significantly increased Leak Respiration. In WT HEK293 cells, 100nM PAPTP significantly increased Leak Respiration. An ability to increase IMM leak would suggest that 100nM PAPTP increases the proton motive force across the IMM. This could *either* be due to an increase in the electrical gradient across the inner mitochondrial membrane i.e. the mitochondrial membrane potential *or* due to an increase in the chemical gradient for proton entry, mitochondrial pH (Brand and Nicholls, 2011). In terms of the mitochondrial membrane potential, a hyperpolarisation of the IMM would increase the proton motive which would attract more H^+ into the matrix, increasing the leak. This suggests that under normal circumstances, without pharmacological inhibition, mitochondrial Kv1.3 channels cause a depolarisation of the MMP. This would make sense in terms of ion flow dynamics, as an influx of K^+, through Kv1.3 channels, and

into the matrix would make the matrix less negative (depolarisation) and therefore reduce the MMP. This situation would dispel the current thinking that mitochondrial Kv1.3 channels are not open under normal circumstances and at physiological mitochondrial membrane potentials. This is because any ion flow across the IMM would dissipate the energy generated by oxidative phosphorylation and the ETS. Disruption of the electrochemical gradient across the IMM should uncouple OXPHOS from ATP synthesis. However, this is not the case, as we saw in Chapter Three, as HEK293/Kv1.3 cells have significantly increased respiration across all stages, apart from Leak Respiration. If PAPTP increases Leak Respiration, then overexpression of Kv1.3 channels should reduce leak, but interestingly this was not the case. The effect of Kv1.3 on the MMP will be explored in the following chapter.

The changes in respiration led to a reduction in ATP turnover in both WT HEK293 and HEK293/Kv1.3 cells, which would mean less ATP is available for cell proliferation. PAPTP had a larger effect on respiration of HEK293/Kv1.3 cells than WT HE2K93 cells, reducing the ATP turnover by 45% vs 22% (respectively) and the SRC by 8% vs 0% (respectively). Both ATP turnover and SRC are commonly used measures to assess mitochondrial dysfunction in cells (Brand and Nicholls, 2011). These measures require the inhibition of the ATP synthase using oligomycin, but it is important to note that using the inhibition of the ATP synthase to calculate ATP turnover is only an estimation, and is likely to underestimate actual ATP synthesis rate by up to 10% (Affourtit and Brand, 2009). In Chapter Three, HEK293/Kv1.3 cells were shown to have a larger SRC than WT HEK293 cells. In this chapter inhibiting the mitochondrial Kv1.3 channels reduced the SRC. SRC by definition is the ability of electron transport to increase in response to a demand for energy. Thus, if the HEK293/Kv1.3 cells are more rapidly proliferating, they would have a greater demand for ATP, and so a larger SRC would be of benefit. This data suggests that increased Kv1.3 expression gives HEK293/Kv1.3 cells a greater SRC than WT HEK293 cells, which operate closer to their bioenergetic capacity, which may limit their ability to respond to increases in energy demand, as seen in proliferation. The larger reduction in ATP turnover and SRC in HEK293/Kv1.3 cells treated with PAPTP may account for why 100nM PAPTP was able to significantly reduce proliferation in HEK293/Kv1.3 cells, but not in WT HEK293 cells. However, these results still suggest that mitochondrial Kv1.3 channels are involved in

maintaining respiration in these HEK293 cells. This is a novel finding that indicates respiration in non-cancerous cells may be regulated by Kv1.3 under physiological conditions. However, the effect of PAPTP on cellular respiration was blunted in comparison with PAP-1. This could suggest that PAP-1 has off target effects within the cell, inhibiting OXPHOS. Regardless, it is clear that mitochondrial Kv1.3 channels regulate more than just apoptosis in cells (Mattarei *et al.*, 2018).

It would appear counterintuitive that K^+ flow into the matrix could lead to increased respiration, as the integrity of the ETS depends on the IMM being impermeable to ions. Any cation flow into the matrix could potentially dissipate the proton motive force and uncouple respiration. However, there are numerous instances where K^+ flow into the matrix does not cause uncoupling of respiration (Bajgar *et al.*, 2001; Kowaltowski *et al.*, 2001; Garlid *et al.*, 2003). In these studies, K^+ influx through the channels correlated to a 1-2mV change in the MMP and a very small stimulation of around 5ng atom O/min-1 mg-1 on respiration, clearly abrogating the notion that K^+ influx through mitochondrial K^+ channels can uncouple the functioning of the ETS. However, these results may have been due to the fact that there could have been a relatively low amount of the K^+ channels in the IMM. In scenarios where there would exist an upregulation of certain K^+ channels i.e. an increase in Kv1.3 channels in proliferating HSVSMCs or artificially enhanced levels in our HEK293/Kv1.3 cells, mitochondrial K^+ influx may have greater effects. Obviously, this might result in more of a depolarisation of the IMM and a lowering of the MMP, but it has been found that mitochondria may be able to compensate for situations like this and increase respiratory activity. For example, stimulation of OXPHOS occurs in response to K^+ influx in yeast mitochondria, and ATP synthesis increases (Manon *et al.*, 1995). Although the work in this study was focusing on the mitoK_{ATP} channel, it is a good indication that such K^+ ion flow into the matrix can work efficiently in a physiological situation and not just in a pathological one.

If Kv1.3 channels are affecting mitochondrial respiration, there is a possibility that they are also affecting ROS levels in HEK293 cells. Leanza and colleagues found that PAPTP treatment raised levels of ROS in cancer cells which led to apoptosis (Leanza *et al.*, 2012, 2017; L Leanza *et al.*, 2013; Peruzzo *et al.*, 2017; Mattarei *et al.*, 2018). As mentioned previously, ROS can be both a benefit or burden to cells; depending on the

level and length of exposure. One explanation for the differing results in the Leanza studies (above) and this work may be the levels of ROS generated. In the cancer cells treated with mitochondrial Kv1.3 inhibitors, the ROS levels exceed threshold levels and induce apoptosis. As a high level of ROS generation is a hallmark of rapidly proliferating cells (Trachootham *et al.*, 2008), due to their high rate of respiration, it is possible that HE293/Kv1.3 cells also have increased levels of ROS to WT HEK293 cells, but reduced levels compared to cancer cells. Therefore, PAPTP treatment of HEK293/Kv1.3 cells may push ROS levels up to a point where they become detrimental to cells and reduce proliferation levels. This would explain the variation in results with 100nM PAPTP treatment in HEK293/Kv1.3 cells and WT HEK293 cells. At this stage, this is just hypothetical and would need to be tested further to make any conclusions. However, there is likely a key window of ROS levels, specific for each cell type, in which the ROS has beneficial cell signalling effects (Linley *et al.*, 2012; Peers *et al.*, 2015). Any ROS level lying outside of this window may be detrimental and/or have different signalling effect i.e. increased proliferation rather than decreased proliferation. ROS are able to regulate ion channels to control proliferation and ROS can both increase or decrease cell proliferation (Scragg *et al.*, 2008; Elies, Scragg, *et al.*, 2014; Duckles *et al.*, 2015). An increase in ROS with increasing levels of PAP-1 in HEK293/Kv1.3 and HSVSM cells may be one explanation for the increasing proliferation with higher concentrations of the Kv1.3 inhibitor, as displayed by the bell-shaped proliferation curve. The discrepancy between the low concentrations of PAP-1 needed to reduced proliferation in HEK293/Kv1.3 cells, and the higher nanomolar concentrations needed to reduce respiration may also be explained by ROS. The high doses of PAP-1 used in the respiratory experiments may promote ROS generation in the cell (Luigi Leanza *et al.*, 2013), which may surpass a threshold level and act as cell signalling molecules to regulate respiration (Holzerova and Prokisch, 2015). For example, increased ROS by PAP-1 treatment could have inhibited proteins and enzyme complexes of the electron transport chain (Murphy, 2009). In the following chapter, ROS levels in HEK293/Kv1.3 and WT HEK293 cells have been explored.

It is important to note that there are some caveats to using a mitochondrially targeted ion channel inhibitor, such as PAPTP, in this work. The first is that it is difficult to prove whether or not the compound actually targets the mitochondrial channel of interest, in

this case mitochondrial Kv1.3. Electrophysiology of isolated mitoplasts would be required (Leanza et al., 2017) and fluorescent tagging of the TPP moiety may help to visualise the location of this compound in the mitochondrial networks. Electrophysiology experiments would also need to test whether 100nM PAPTP blocks any plasma membrane Kv channels. There is also evidence to suggest that TPP is toxic to cells when it accumulates in the mitochondria (Murphy et al., 2009) (Trnka, Elkalaf and Anděl, 2015). This toxicity presents as disruption of the inner mitochondrial integrity, respiration and ATP synthesis. This makes it hard to ascertain if the effect on respiration and proliferation seen in this study is due to the inhibition of mitochondrial Kv1.3 channels, or down to the TPP molecule the inhibitor is attached to. However, evidence exists which supports the former scenario. Murphy et al., state that concentrations of TPP compounds which lie in the range of 0.1-1µM, which was the case for our experiments, avoid toxicity. Many published studies are using PAPTP at the same concentrations as in this study and do not report negative consequences of the compound (Checchetto *et al.*, 2018; Mattarei *et al.*, 2018). In addition, when 100nM PAPTP was tested on the respiration of both WT HEK293 and HEK293/Kv1.3 cells, there was a differential response between the cell types, with HEK293/Kv1.3 cell respiration being significantly affected by the compound. If the effects we saw were solely due to the TPP moiety, then the effects on both WT HEK293 and HEK293/Kv1.3 cells would be expected to be the same. However, to improve this study, our results would need to be repeated using control cells treated with 100nM decylTPP only. Finally, optimal targeting of PAP-1 to the mitochondria would involve conjugating PAP-1 to TPP using the smallest possible linker molecule to minimise any chance of disruption to the mitochondrial membrane (Trnka, Elkalaf and Anděl, 2015).

To summarise, these findings suggest that mitochondrial Kv1.3 channels contribute to normal respiratory function in HEK293 cells. In situations where there are high numbers of these channels, as in the HEK293/Kv1.3 cell line, mitochondrial Kv1.3 channels contribute to increased respiration and proliferation. What remains uncertain is how K^+ influx into the matrix, through Kv1.3 channels, alters the levels of oxidative phosphorylation and proliferation.

Chapter Five

Probing the mechanisms through which mitochondrial Kv1.3 regulates respiration and proliferation.

5.1 Introduction

In Chapter Four of this thesis, it was suggested that mitochondrial Kv1.3 channels regulate proliferation and respiration of HEK293/Kv1.3 cells. By targeting Kv1.3 inhibitors to the mitochondria, it may be possible to specifically control cellular energy metabolism and limit proliferation, whilst minimising unwanted effects relating to channel inhibition at other cellular sites. However, the mechanism through which Kv1.3 links mitochondrial function to proliferation is unknown.

Research conducted in cancer cell lines, suggests that mitochondrial Kv1.3 has a role in apoptosis (Leanza *et al.*, 2017; Mattarei *et al.*, 2018). It has been proposed that on inhibition of mitochondrial Kv1.3, the inner mitochondrial membrane (IMM) is hyperpolarised as K^+ cations are prevented from entering the matrix. This leads to an increase in cellular reactive oxygen species (ROS), which surpasses a threshold level and triggers the apoptotic cascade by activating the mitochondrial permeability transition pore (MPTP). The mitochondria experience an influx of solutes into the matrix, which causes water to follow. The mitochondria swell, and their transmembrane potential is lost. This leads to a loss of cytochrome c and production of further ROS, triggering apoptosis. In contrast, the work described in Chapters Three and Four of this thesis demonstrate that the inhibition of Kv1.3 in HEK293/Kv1.3 cells did not cause cell death but rather reduced the rate of cellular proliferation. Cancer cells display an altered metabolic phenotype, characterised by high rates of ROS (Liou and Storz, 2010). This difference may account for the discrepancies in observed phenotypes. In addition, the higher concentrations of mitochondrial Kv1.3 inhibitors used by Leanza and colleagues (10-20μM), compared to the concentrations used in this study (100nM), may have accounted for the abnormally high levels of ROS in these

studies that led to apoptosis of cancer cells (Leanza *et al.*, 2017; Mattarei *et al.*, 2018). Nevertheless, this does not preclude a role for ROS in the anti-proliferative effect of Kv1.3 inhibition in HEK293/Kv1.3 cells.

As mentioned previously, the level of ROS is critical in determining the effect seen in the cells. Hypothetically, there could be alternative mechanisms, involving ROS, for why mitochondrial Kv1.3 inhibitors reduce proliferation. As in the work by Leanza and colleagues (referenced above), PAPTP may raise ROS to a level where proliferation is inhibited (Yang *et al.*, 2012; Moloney and Cotter, 2017), but to a level not high enough to induce apoptosis (as seen in (Leanza *et al.*, 2017)). However, cell ROS have also been found to be pro-proliferative in various cell types, such as microglia, colon cancer cells and B cells (Wheeler and DeFranco, 2012; Bordt and Polster, 2014; Juhasz *et al.*, 2017). Therefore, PAPTP may reduce ROS via a reduction in OXPHOS (Koopman *et al.*, 2010; Shadel and Horvath, 2015), and therefore a pro-proliferative ROS stimulus on proliferation may be switched off. Since expression of Kv1.3 in HEK293 cells increased the cellular respiration rate, this thesis will ask whether enhanced respiration in these cells leads to greater ROS production and whether this ROS production contributes to the enhanced proliferative phenotype of HEK293/Kv1.3 cells.

Another potential mechanism of action underlying the effect of Kv1.3 on mitochondrial respiration is the influx of K^+ ions into the mitochondrial matrix through the mitochondrial Kv1.3 channels, which may affect the MMP. Changes to the ionic balance of the mitochondrial matrix may then have reciprocal effects for OXPHOS (Garlid and Paucek, 2003; Garlid *et al.*, 2003). In addition, any changes to the concentration of one ion in the matrix may have subsequent effects on the concentration of other ions. Mitochondrial Ca^{2+} has been observed to stimulate OXPHOS (Griffiths and Rutter, 2009; Vinnakota, Dash and Beard, 2011; Doonan *et al.*, 2014). Therefore, the effect of Kv1.3 expression in HEK293 cells on both the MMP and mitochondrial Ca^{2+} levels are explored in this chapter.

Kv1.3 can regulate peripheral glucose homeostasis in mouse adipose and skeletal muscle cells, by modulating the expression of GLUT transporters in response to insulin (Xu *et al.*, 2004). Therefore, an increased Kv1.3 expression in HEK293/Kv1.3 cells may alter glucose metabolism. Altered glycolysis would impact the amount of Acetyl-CoA entering the TCA cycle, which could either stimulate or inhibit the ETS via alterations to

NADH and $FADH_2$. Altered glucose metabolism occurs in cancer, whereby many tumour cells increase glycolysis despite adequate O_2 for OXPHOS, in a phenomenon known as the Warburg effect (Kroemer and Pouyssegur, 2008). This is thought to be a beneficial adaptation to support the biosynthesis of macromolecules for proliferation (Kroemer and Pouyssegur, 2008). In other cells, an increase/decrease in one bioenergetic pathway leads to a compensatory decrease/increase in another pathway, highlighting the flexibility of bioenergetic regulation (Jose, Bellance and Rossignol, 2011; Goetzman and Prochownik, 2018). However, in some proliferating cells, such as retinoblastoma cells, both glycolysis and OXPHOS are increased (Takebayashi *et al.*, 2015). With this in mind, we decided to investigate glycolysis in HEK293/Kv1.3 cells to see if it was increased or decreased to WT HEK293 cells.

This chapter will focus on probing these potential mechanisms to elucidate how mitochondrial Kv1.3 channels drive the oxidative and proliferative phenotype in HEK293 cells previously defined in Chapters Three and Four of this thesis.

5.2 Aims and Objectives

The aim of this chapter was to explore the mechanism/s through which mitochondrial Kv1.3 regulate and link cellular oxidative metabolism and proliferation. To achieve this aim a key set of objectives were designed:

1) To assess the cellular energy status and glycolytic function of HEK293/Kv1.3 cells.

2) To investigate the effect of Kv1.3 expression on the MMP in HEK293/Kv1.3 cells.

3) To examine mitochondrial Ca^{2+} status of HEK293/Kv1.3 cells.

4) To define the production of ROS in HEK293/Kv1.3 cells, and using the mitochondrial-targeted antioxidant MitoQ, establish the effect of decreased ROS availability on cellular proliferation (Kelso *et al.*, 2001; Smith, Hartley and Murphy, 2011).

5.3 Results

5.3.1 Kv1.3 increases cellular NADH in HEK293 cells.

Chapters Three and Four identified that HEK293/Kv1.3 cells have an increased rate of OXPHOS. NADH is the principal electron carrier during OXPHOS and is generated during glycolysis, pyruvate conversion into Acetyl-CoA and in the TCA Cycle. NADH displays auto-fluorescence with a wavelength of 470nm following excitation, and an emission wavelength of 350-360nm. This auto-fluorescence is an indicator of mitochondrial redox status, OXPHOS activity and ATP production (Bonuccelli *et al.*, 2017). A large proportion of NADH autofluorescence is due to mitochondrial NADH because NAD is non-fluorescent and the level of cytosolic NADH is normally low (Buckler and Turner, 2013). NADH autofluorescence was measured in WT HEK293 and HEK293/Kv1.3 cells. NADH concentrations were greater in HEK293/Kv1.3 compared with HEK293 cells (black bars, Figure 5.1A). NADH auto-fluorescence was also measured with the addition of 20µM CCCP to maximally oxidise the NAD^+/NADH pool, and measured with the addition of both 0.5µM rotenone plus 2.5µM antimycin A to maximally reduce the NAD^+/NADH pool (Figure 5.1A). NADH concentrations were significantly higher in HEK293/Kv1.3 cells compared with HEK293 cells following treatment with CCCP or rotenone and antimycin A. The difference in fluorescence between the maximally oxidised and maximally reduced NAD^+/NADH pools (NADH range) estimates the total mitochondrial NADH and NAD^+ (Buckler and Turner, 2013). HEK293/Kv1.3 cells also had an increased mitochondrial NADH autofluorescence range compared to WT HEK293 cells (Figure 5.1B). HEK293/Kv1.3 cells were then treated with 100nM PAPTP to see if mitochondrial Kv1.3 inhibition could reduce the NADH autofluorescence. 100nM PAPTP had no effect on NADH autofluorescence in HEK293/Kv1.3 cells (Figure 5.1C).

.

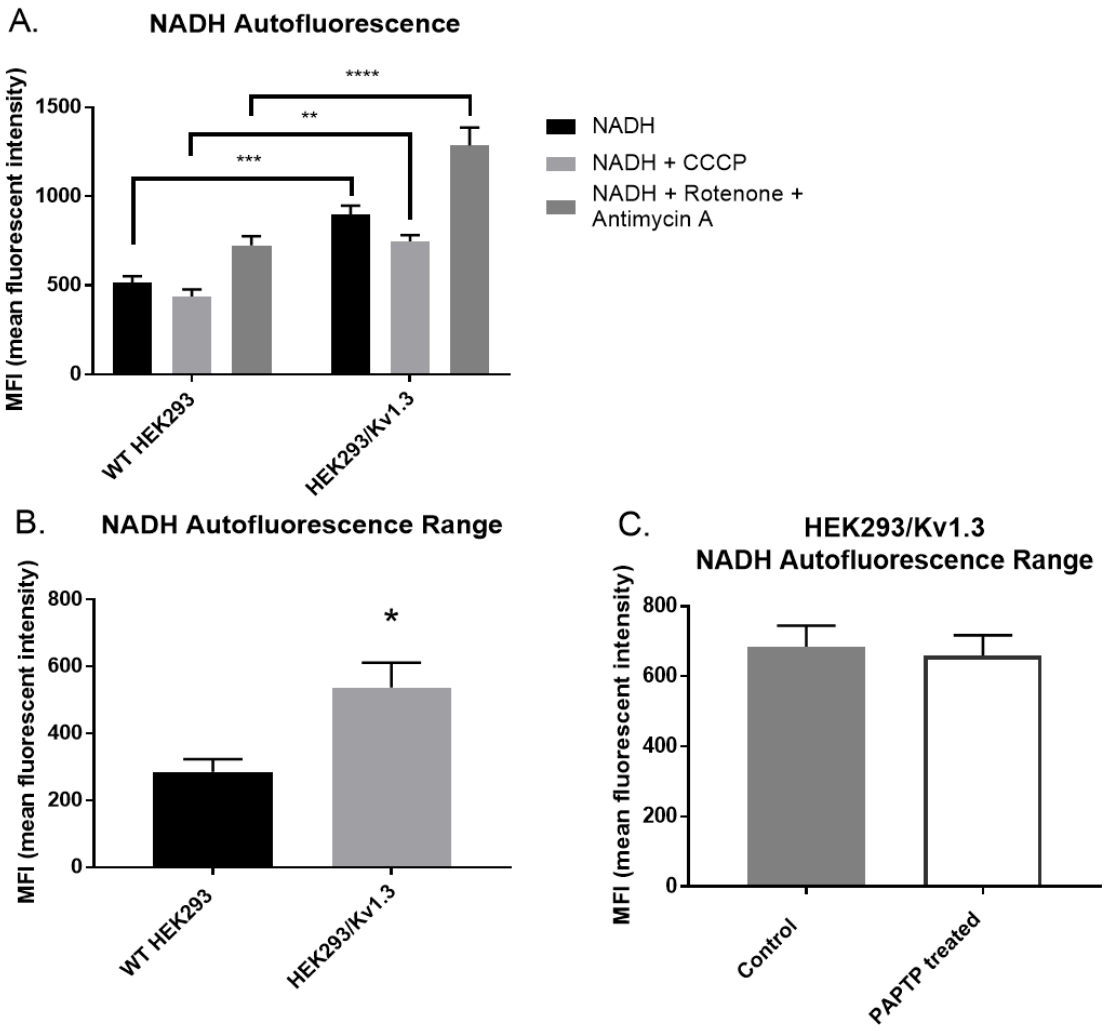

Figure 5.1 HEK293/Kv1.3 cells have increased NADH autofluorescence to WT HEK293 cells. A. NADH autofluorescence baseline (black bars), NADH autofluorescence with 20µM CCCP (light grey bars) and NADH autofluorescence with 0.5µM rotenone and 2.5µM antimycin A (dark grey bars) in WT HEK293 cells (left columns) and HEK293/Kv1.3 cells (right columns). Data is expressed as the mean fluorescent intensity (MFI) ± SEM (WT HEK293 cells, n=5, HEK293/Kv1.3 cells, n=6). Data analysed by Student's t-tests, * $p<0.05$, ** $p<0.01$, *** $p<0.001$. B. NADH range in WT HEK293 cells (black bar) and HEK293/Kv1.3 cells (grey bar). NADH range is the difference between NADH autofluorescence with CCCP and NADH autofluorescence with rotenone and antimycin a (as in A). Data expressed as the MFI ± SEM (WT HEK293 cells, n=5, HEK293/Kv1.3 cells, n=6). Data analysed using Student's t-tests, * $p<0.05$. C. NADH autofluorescence in control HEK293/Kv1.3 cells (grey bar) and 100nM PAPTP treated HEK293/Kv1.3 cells (white bar). Data is the NADH range, as in (B), expressed as the MFI ± SEM (n=3). Data was analysed using Student's t-tests, $p>0.05$.

5.3.2 Manipulation of the malate/aspartate shuttle with Dimethyl-2-Oxoglutarate and Phenylsuccinate did not affect respiration in HEK293 cells.

In Figure 5.2, WT HEK293 cells were treated with Dimethyl-2-Oxoglutarate (DM-2OG) to stimulate the malate/aspartate shuttle. In Figure 5.2, 2mM DM-2OG had no effect on the O_2 consumption of WT HEK293 cells at Routine, Leak and Maximum Uncoupled Respiration. DM-2OG also did not affect residual O_2 consumption (ROX). In Figure 5.3, HEK293/Kv1.3 cells were treated with 5mM Phenylsuccinate (PhS) to inhibit the malate/aspartate shuttle. 5mM PhS had no effect on the O_2 consumption of HEK293/Kv1.3 cells at Routine, Leak and Maximum Uncoupled Respiration. DM-2OG also did not affect ROX. This suggests that the increase in HEK293 cell respiration is not due to the mitochondrial Kv1.3 channel having an effect on the malate/aspartate shuttle.

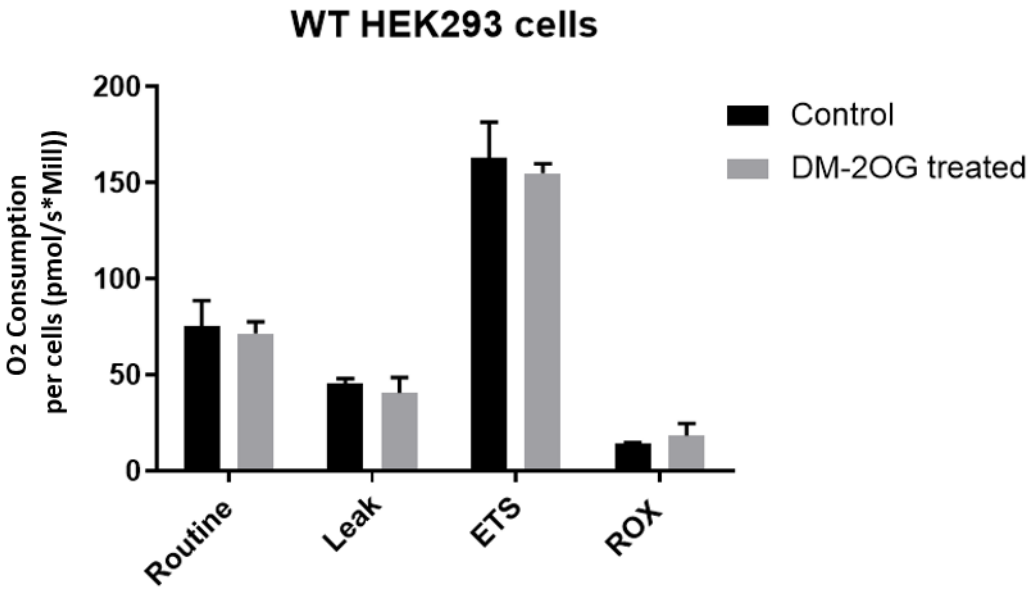

Figure 5.2 Dimethyl-2-Oxoglutarate has no effect on WT HEK293 cell respiration. A. Respiration of WT HEK293 control cells (black bars) and WT HEK293 cells treated with 2mM Dimethyl-2-Oxoglutarate (DM-2OG) (grey bars). Data expressed as mean O_2 consumption (pmol) per million cells per second (pmol/(s*Mill)) ± SEM (n=3). Data was analysed using Student's t-tests between control and drug treated cells, $p>0.05$.

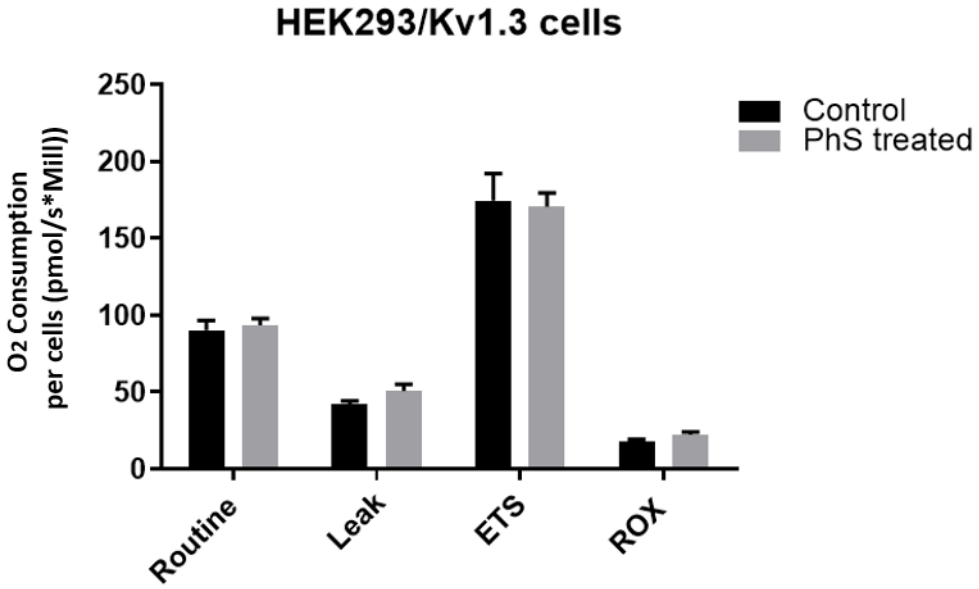

Figure 5.3 Phenylsuccinate has no effect on HEK293/Kv1.3 cell respiration. A. Respiration of HEK293/Kv1.3 control cells (black bars) and HEK293/Kv1.3 cells treated with 5mM Phenylsuccinate (PhS) (grey bars). Data expressed as mean O_2 consumption (pmol) per million cells per second (pmol/(s*Mill)) ± SEM (n=7). Data was analysed using Student's t-tests between control and drug treated cells, $p>0.05$.

5.3.3 HEK293/Kv1.3 cells have an increased O_2 consumption compared to WT HEK293 cells when glycolysis is knocked down by 2-Deoxy-D-Glucose.

HEK293/Kv1.3 cells had increased concentrations of NADH. NADH can be generated through several cellular metabolic processes including glycolysis and the TCA cycle. To investigate the source of increased intracellular NADH in HEK293/Kv1.3 cells and its contribution to the increased OXPHOS rate and energy production In HEK293/Kv1.3 cells, these cells were treated for 24 hours with the glucose analogue and competitive inhibitor of glycolysis 2-Deoxy-D-Glucose (2DDG) (5mM) before being analysed by respirometry.

24-hour pre-treatment of cells with 5mM 2DDG demonstrated that competitive inhibition of glycolysis significantly decreased both Leak Respiration and ROX in HEK293/Kv1.3 cells but not WT HEK293 cells (Figure 5.4A). There was no significant effect on Routine (baseline) or ETS Respiration (Figure 5.4A). To examine mitochondrial-specific effects the data was corrected for ROX (Figure 5.4B). HEK293/Kv1.3 cells treated with 2DDG still had a significantly reduced Leak Respiration, but interestingly their Routine Respiration was significantly increased (Figure 5.4B). This would suggest that competitive inhibition of glycolysis in HEK293/Kv1.3 cells reduces non-mitochondrial O_2 consumption (ROX), which is compensated for by a reciprocal increase in routine OXPHOS. This phenomenon was not observed in WT HEK293 cells (Figure 5.4B), and although not statistically significant, there was a trend for 2DDG to reduce the O_2 consumption at each stage of respiration in WT HEK293 cells (Routine, Leak and ETS).

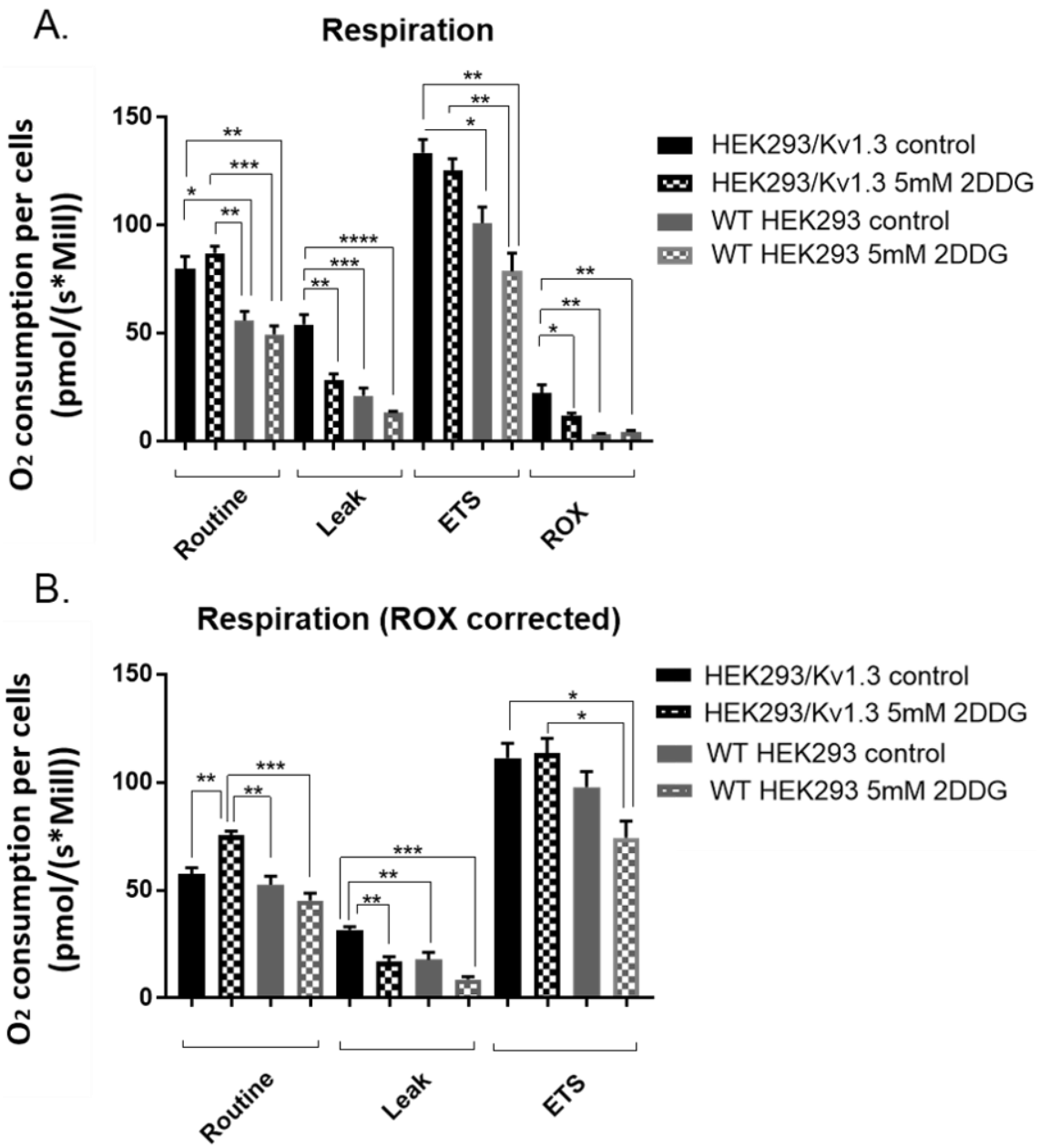

Figure 5.4 5mM 2-Deoxy-D-Glucose reduced the residual oxygen consumption and leak oxygen consumption in HEK293/Kv1.3 cells. A. Effect of 5mM 2-Deoxy-D-Glucose (2DDG) on HEK293/Kv1.3 and WT HEK293 cell respiration. Black solid bars = control HEK293/Kv1.3 cells (n=4), black dotted bars = 2DDG treated HEK293/Kv1.3 cells (n=4). Grey solid bars = control WT HEK293 cell respiration (n=3), grey dotted bars = 2DDG treated WT HEK293 cells (n=3). Respiration was measured at four stages; Routine, Leak, ETS and ROX. Data expressed as the mean oxygen (O_2) consumption per million cells per second (pmol/(s*Mill)) ± SEM. Data analysed using one-way ANOVA and Tukey's multiple comparison post hoc test within each stage of respiration, * p<0.05, ** p<0.01, *** p<0.001, **** p<0.0001. B. Data in (A) corrected for residual O_2 consumption (ROX). Data expressed as the mean O_2 consumption per million cells per second (pmol/(s*Mill)) ± SEM. Data analysed using one-way ANOVA and Tukey's multiple comparison post hoc test within each stage of respiration, * p<0.05, ** p<0.01, *** p<0.001.

5.3.4 HEK293/Kv1.3 cells have a hyperpolarised mitochondrial membrane potential compared with WT HEK293 cells.

Next, the MMP of HEK293/Kv1.3 and WT HEK293 cells was investigated using the Cairn Photometry system (Figures 5.5A and 5.5B). Tetramethylrhodamine, methyl ester (TMRM) is a cell-permeant dye that accumulates in active mitochondria with intact membrane potentials. TMRM is attracted to the negative charge of the mitochondrial membrane, accumulating more readily when the hyperpolarisation of mitochondria is greater. Figure 5.5A shows that TMRM accumulation is greater in HEK293/Kv1.3 cells. This suggests a more hyperpolarised membrane potential in HEK293/Kv1.3 cells. To confirm this, the uncoupler FCCP was applied to the cells to dissipate the MMP. The difference in the TMRM signal after FCCP addition gives an accurate indication of mitochondrial TMRM accumulation, since mitochondrial TMRM is released as the MMP is dissipated. In HEK293/Kv1.3 cells, there was a trend towards a greater decrease in mean fluorescent intensity (MFI) with FCCP, indicating a potentially greater hyperpolarised MMP than in WT HEK293 cells, however this failed to reach significance (Figure 5.5B).

Flow cytometry was then utilised as an independent means of verifying the effect of Kv1.3 on HEK293 MMP (Figure 5.5C and 5.5D). Cells were stained with TMRM only, and then some were treated with FCCP (Figure 5.5C). The results in Figure 5.5D display the difference in the MFI between the two conditions. The difference in TMRM fluorescence with and without FCCP treatment was significantly larger in HEK293/Kv1.3 cells (Figure 5.5D), confirming that these cells had a higher MMP.

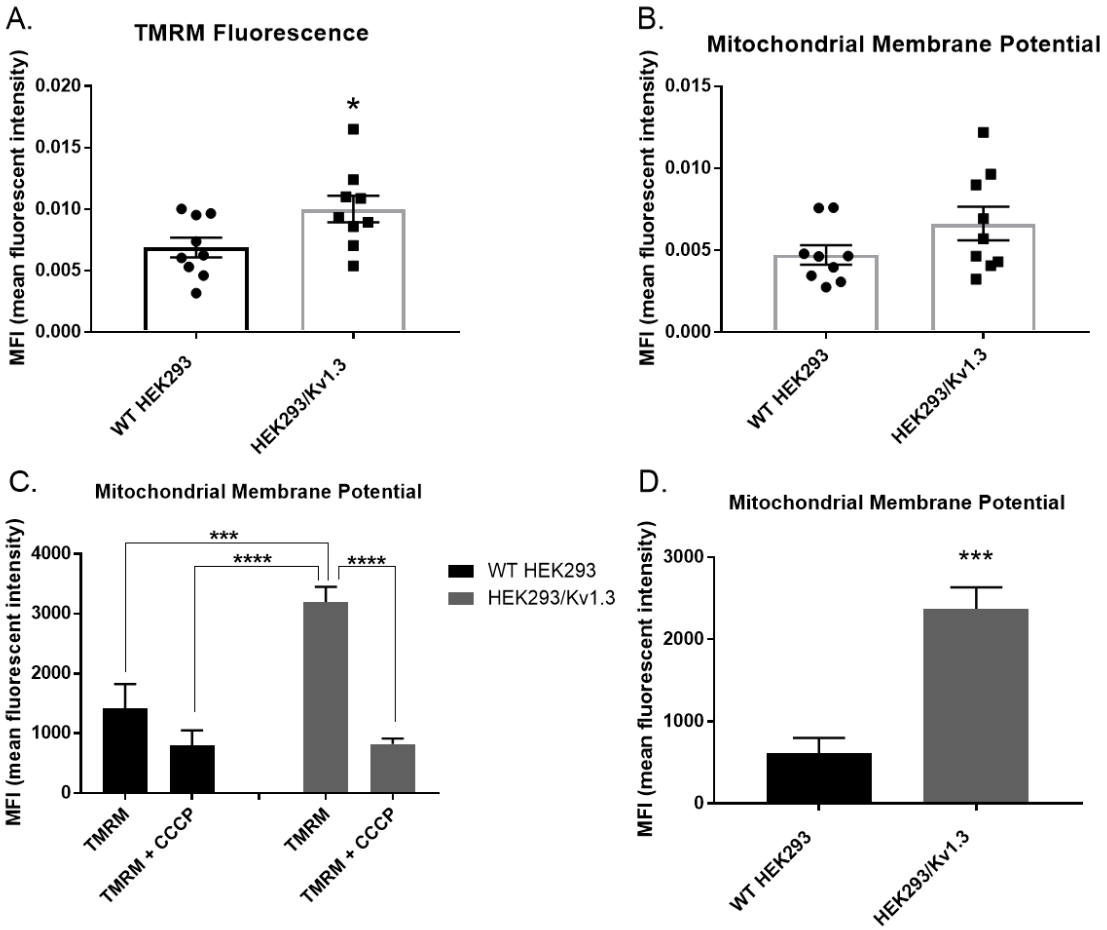

Figure 5.5 HEK293/Kv1.3 cells have greater hyperpolarisation of the mitochondrial membrane potential than WT HEK293. (A-B) Data from Cairn Photometry experiments. A. Mean fluorescence intensity (MFI) of cells treated with 20nM TMRM (WT HEK293 cells shown in left column, HEK293/Kv1.3 cells in right column). Data expressed as the voltage-corrected raw MFI ± SEM (n=9 for both WT HEK293 and HEK293/Kv1.3 cells). Student's t-tests confirmed HEK293/Kv1.3 cells had a significantly higher initial TMRM fluorescence than WT HEK293 cells (* $p<0.05$). B. Mitochondrial membrane potential (MMP) of WT HEK293 (left column) and HEK293/Kv1.3 (right column) cells. MMP is the difference between initial TMRM fluorescence and the TMRM fluorescence when cells were treated with 20µM FCCP, and 2µg/ml Oligomycin (n=9 for both WT HEK293 and HEK293/Kv1.3 cells). Data displayed as MFI ± SEM. Student's t-test was used to analyse the data ($p>0.05$). (C-D) Data from Flow Cytometry experiments. C. TMRM initial fluorescence (20nM) and CCCP effect (20µM) on TMRM fluorescence in WT HEK293 cells (n=7) and HEK293/Kv1.3 cells (n=9). Left two data columns represent WT HEK293 cell data, and right two columns represent HEK293/Kv1.3 cell data. Data expressed as MFI of TMRM fluorescence ± SEM. Data analysed by one-way ANOVA with Tukey's multiple comparisons post hoc test *** $p<0.001$, **** $p<0.0001$. D. Mitochondrial membrane potential (MMP) of WT HEK293 cells (Black bar, n=7) and HEK293/Kv1.3 cells (Grey bar, n=9). Data expressed as the difference in TMRM (20nM) MFI and the TMRM MFI when cells were treated with FCCP (20µM) ± SEM. Student's t-test confirmed the difference was significant (*** $p<0.001$).

To investigate the role of mitochondrial Kv1.3 channels in the MMP phenotype, the mitochondrially targeted Kv1.3 channel inhibitor PAPTP was applied to cells WT HEK293 and HEK293/Kv1.3 cells. Flow cytometry was again used to assess MFI of TMRM and TMRM + FCCP treated cells, but with the addition of additional treatments; TMRM + PAPTP and TMRM + FCCP + PAPTP (Figures 5.6A and 5.6B). PAPTP was added during TMRM incubation in both HEK293/Kv1.3 and WT HEK293 cells. PAPTP did not affect the MMP (Figures 5.6C and 5.6D), suggesting that the increased MMP observed in HEK293/Kv1.3 cells is not directly dependent on mitochondrial Kv1.3 channels.

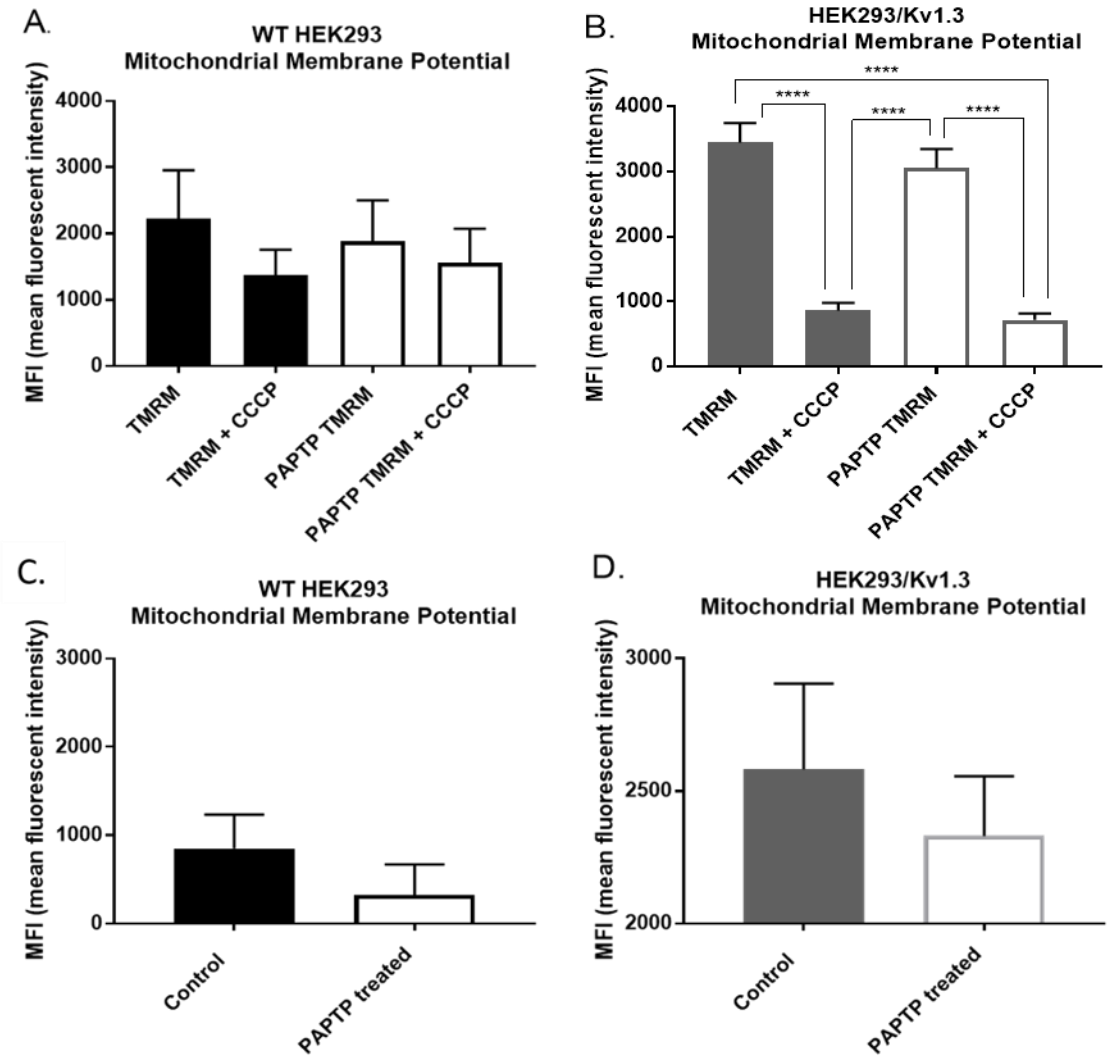

Figure 5.6 100nM PAPTP has no significant effect on the mitochondrial membrane potential of HEK293 cells. A-D) All data gathered by flow cytometry. A. TMRM (20nM) fluorescence and TMRM fluorescence with CCCP (20µM) in WT HEK293 control cells (black bars) and PAPTP treated (100nM) WT HEK293 cells (white bars). Data expressed as mean fluorescent intensity (MFI) of TMRM fluorescence ± SEM (n=3). Data was analysed using one-way ANOVA and Tukey's pot hoc test, $p>0.05$. B. TMRM (20nM) fluorescence and TMRM fluorescence with CCCP (20µM) in HEK293/Kv1.3 control cells (grey bars) and PAPTP treated (100nM) HEK293/Kv1.3 cells (white bars). Data expressed as MFI of TMRM fluorescence ± SEM (n=4). Data was analysed using one-way ANOVA and Tukey's post hoc test, **** $p<0.0001$. C. MMP in WT HEK293 control cells (black bar) and PAPTP (100nM) treated WT HEK293 cells (white bar). MMP is the difference between TMRM (20nM) MFI and TMRM MFI with CCCP (20µM). Data expressed as MFI of TMRM fluorescence ± SEM (n=3). Data was analysed using Student's t-tests, $p>0.05$. D. MMP in HEK293/Kv1.3 control cells (grey bar) and PAPTP (100nM) treated WT HEK293 cells (white bars). Data expressed as MFI of TMRM fluorescence ± SEM (n=3). Data was analysed using Student's t-tests, $p>0.05$.

5.3.5 Mitochondrial Ca^{2+} is not increased by Kv1.3 expression HEK293 cells.

WT HEK293 and HEK293/Kv1.3 cells were screened for differences in their cellular and mitochondrial Ca^{2+} levels using flow cytometry. Cells were stained with the fluorescent Ca^{2+} indicator Rhod-2 AM. Cellular and mitochondrial Ca^{2+} levels were tested across two conditions; baseline Rhod-2 AM fluorescence and Rhod-2 AM fluorescence with 20µM CCCP. There was no significant difference in cellular Ca^{2+} concentrations between HEK293/Kv1.3 and WT HEK293 cells in either condition (Figure 5.7A).The mitochondrial Ca^{2+} range can be estimated by examining the difference in Rhod-2 AM fluorescence between baseline and CCCP treatment (Figure 5.7B). The mean mitochondrial range in HEK293/Kv1.3 cells was larger than in WT HEK293 cells, however this result was not significant (Figure 5.7B).

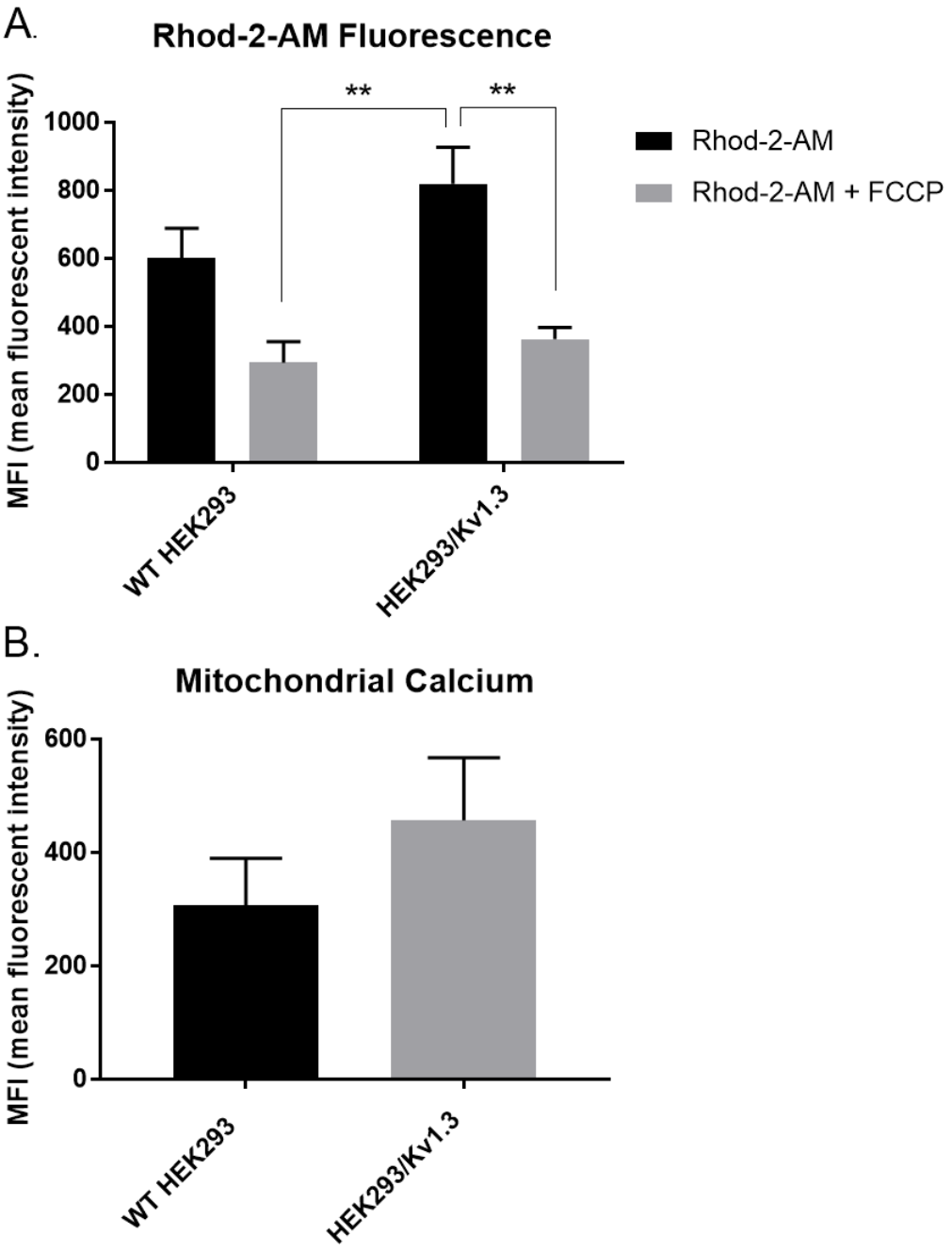

Figure 5.7 Mitochondrial calcium is not significantly different in HEK293/Kv1.3 cells compared to WT HEK293 cells. A. Data expressed as mean fluorescence intensity (MFI ± SEM) of Rhod-2 AM fluorescence. The two left data columns represent WT HEK293 cell data (n=5), while the right two columns represent HEK293/Kv1.3 cell data (n=5). In both WT HEK293 and HEK293/Kv1.3 cells, the black bars represent baseline Rhod-2 AM fluorescence, and the grey bars represent Rhod-2 AM fluorescence with the addition of 20µM FCCP. Data analysed using one-way ANOVA and Tukey's multiple comparison post hoc test, ** $p<0.01$. B. Mitochondrial calcium in WT HEK293 cells (n=5) and HEK293/Kv1.3 cells (n=5). Data was calculated by finding the difference between the baseline and the FCCP results (in A) for each repeat of the experiment. Results are displayed as the MFI ± SEM. Student's t-test confirmed there was no difference in mitochondrial calcium range in HEK293/Kv1.3 cells and WT HEK293 cells, $p>0.05$.

5.3.6 HEK293/Kv1.3 cells have a greater concentration of cellular reactive oxygen species than WT HEK293 cells.

Mitochondria are one of the main sites of cellular reactive oxygen species (ROS) production through the action of ETS leak. As HEK293/Kv1.3 cells have increased basal respiration and increased Maximum ETS Respiration (Chapter Three) compared to WT HEK293 cells, it was hypothesised that this may result in an increased level of ROS in these cells. WT HEK293 and HEK293/Kv1.3 cells from equal passages were stained using the cell permanent dye CellROX Deep Red reagent which exhibits fluorescence upon oxidation by ROS. HEK293/Kv1.3 cells had significantly greater levels of ROS than WT HEK293 cells (Figure 5.8). Representative images of cell ROS in HEK293/Kv1.3 and WT HEK293 cells are shown in Figure 5.9.

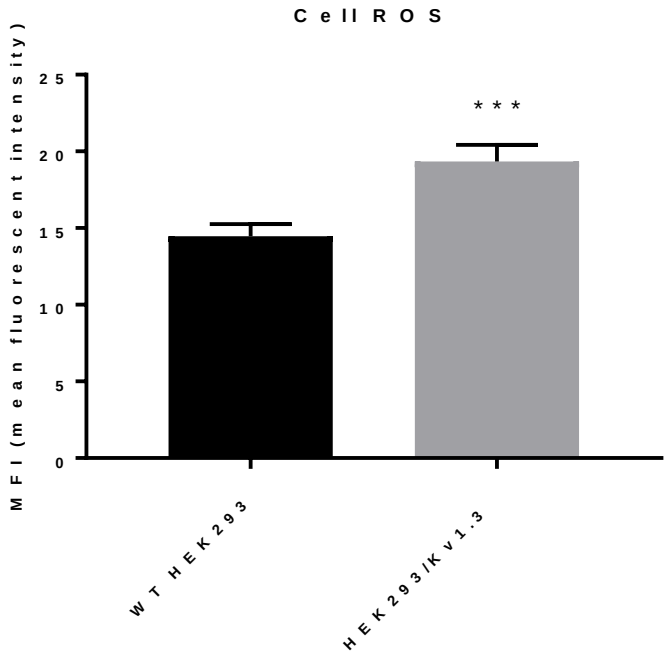

Figure 5.8 HEK293/Kv1.3 cells have a higher level of reactive oxygen species than WT HEK293 cells. A. Reactive oxygen species (ROS) in WT HEK293 cells (black bar) and HEK293/Kv1.3 cells (grey bar). Cells were stained with 5µM CellROX deep red reagent. Data expressed as the mean fluorescent intensity (MFI) of CellROX ± SEM (n=3). Data was analysed using Student's t-test, *** $p<0.001$.

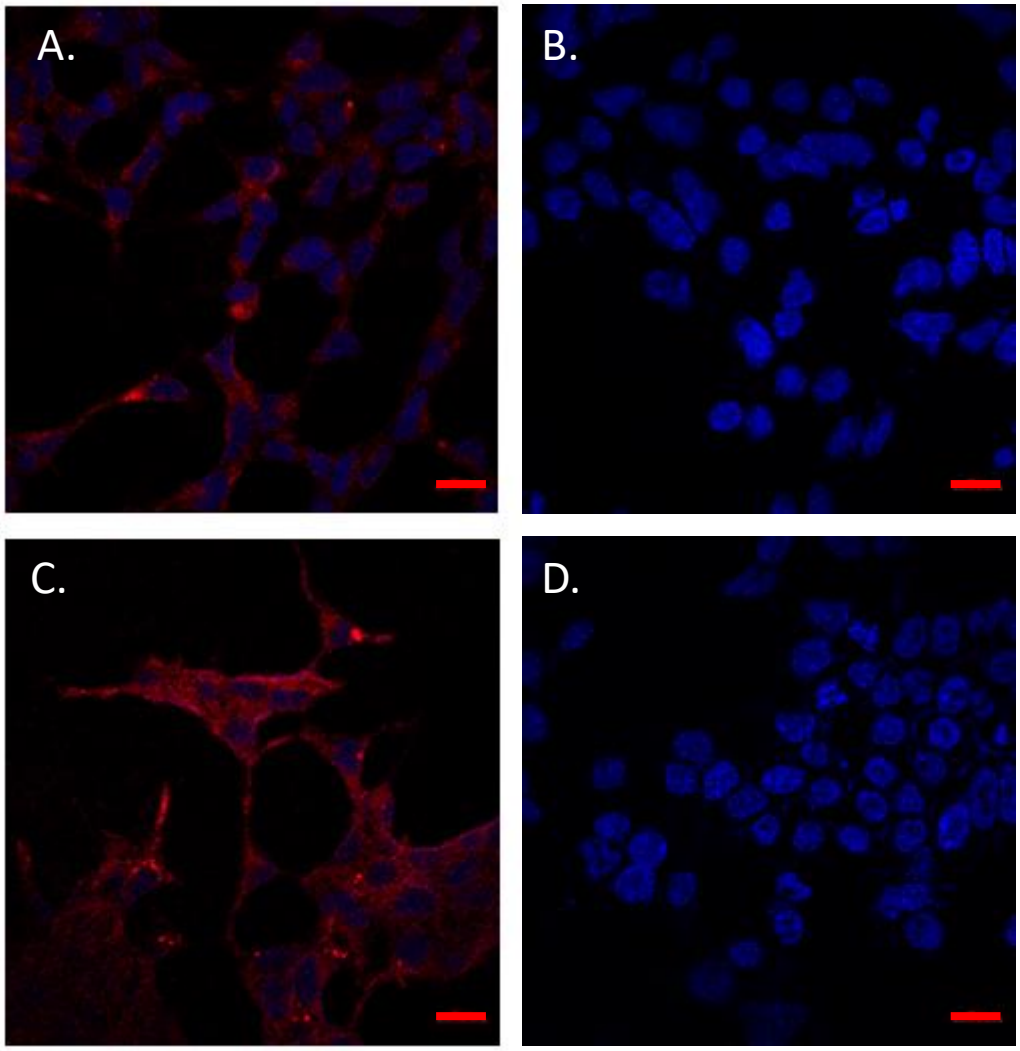

Figure 5.9 Representative images showing HEK293/Kv1.3 cells have a higher level of reactive oxygen species (ROS) than WT HEK293 cells. A. Reactive oxygen species (ROS) (red) in WT HEK293 cells stained with 5µM CellROX deep red reagent and diamidino-2-phenylindole (DAPI) to highlight cell nuclei (blue). B. Control for non-specific binding by the CellROX reagent. Staining was performed as in (A) but without CellROX. C. ROS (red) in HEK293/Kv1.3 cells stained with 5µM CellROX deep red reagent and DAPI to highlight cell nuclei (blue). D. Control for non-specific binding by the CellROX reagent in HEK293/Kv1.3 cells. Staining was performed as in (C) but without CellROX. All scale bars represent 20µm.

The compound menadione generates cellular ROS through redox cycling. WT HEK293 and HEK293/Kv1.3 cells were treated with 100µM menadione. ROS production in response to menadione was greater in HEK293/Kv1.3 cells than WT HEK293 cells (Figure 5.10). Together, with the respirometry data this data suggests that the increased mitochondrial respiration in HEK293/Kv1.3 cells leads to greater concentration of cellular ROS. Although commonly associated with negative cellular consequences, ROS are important chemical messengers which have been found to enhance cellular proliferation. Therefore, the increased ROS in HEK293/Kv1.3 cells may contribute to the proliferative phenotype induced by Kv1.3 expression.

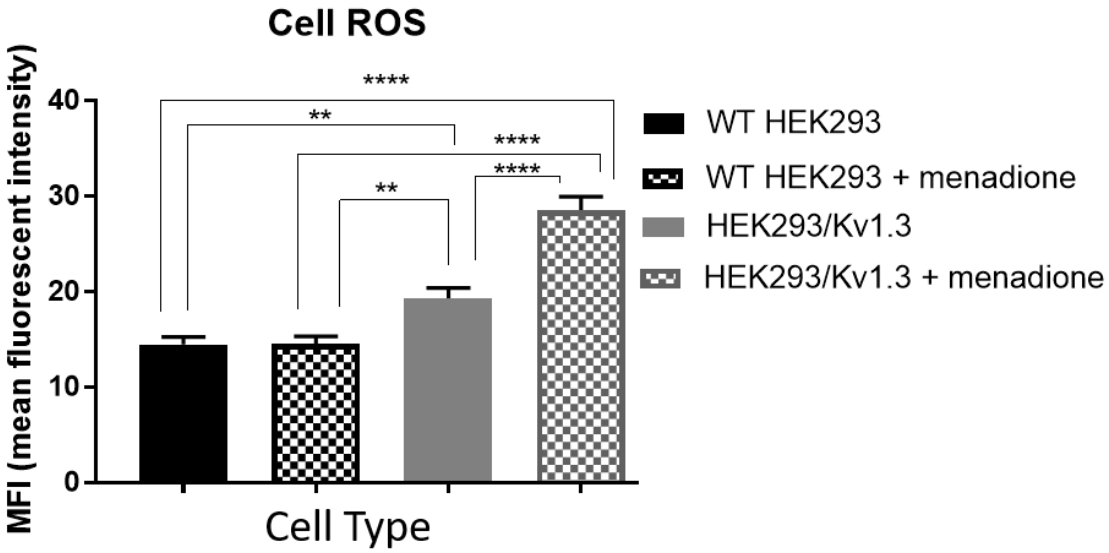

Figure 5.10 HEK293/Kv1.3 cells have a greater increase in cell reactive oxygen species (ROS) in response to 100µM menadione than WT HEK293 cells. From left to right, first two columns represent WT HEK293 cell data, last two columns represent HEK293/Kv1.3 cell data. Data expressed as mean fluorescence intensity (± SEM) of 5µM CellROX deep red reagent (patterned bars) and without (solid bars) pre-treatment of 100µM menadione (n=3). Data was analysed using one-way ANOVA and Tukey's post hoc multiple comparison test, ** $p<0.01$, **** $p<0.001$.

5.3.7 The ROS scavenger MitoQ, may reduce proliferation of HEK293 cells.

To determine whether ROS in HEK293/Kv1.3 cells was contributing to the proliferative phenotype of these cells, a ROS scavenger, MitoQ, was applied to the cells in a proliferation assay (Figures 5.11 and 5.12). In both HEK293/Kv1.3 cells and WT HEK9293 cells, in individual experiments there was occasions when, MitoQ was able to reduce cellular proliferation (Figure 5.11A and 5.11B). In WT HEK293 cells, there was a less consistent and distinct effect of MitoQ on the proliferation of these cells (Figure 5.12A and 5.12B). Although not significant, perhaps due to the variation in the cell counts, the reduction in proliferation by MitoQ in HEK293/Kv1.3 cells translated to a mean Day 3 count over 30% lower than untreated control counts (Figure 5.11B). In WT HEK293 cells, the mean Day 3 count was around 20% lower than untreated control counts (Figure 5.12B). The effect of MitoQ on cell viability was not significant in either cell type, but more repeats, would be needed to confirm that this ROS scavenger was not effecting cell viability at all, as the MitoQ treated cells had slightly lower viability in both HEK293/Kv1.3 and WT HEK293 cells.

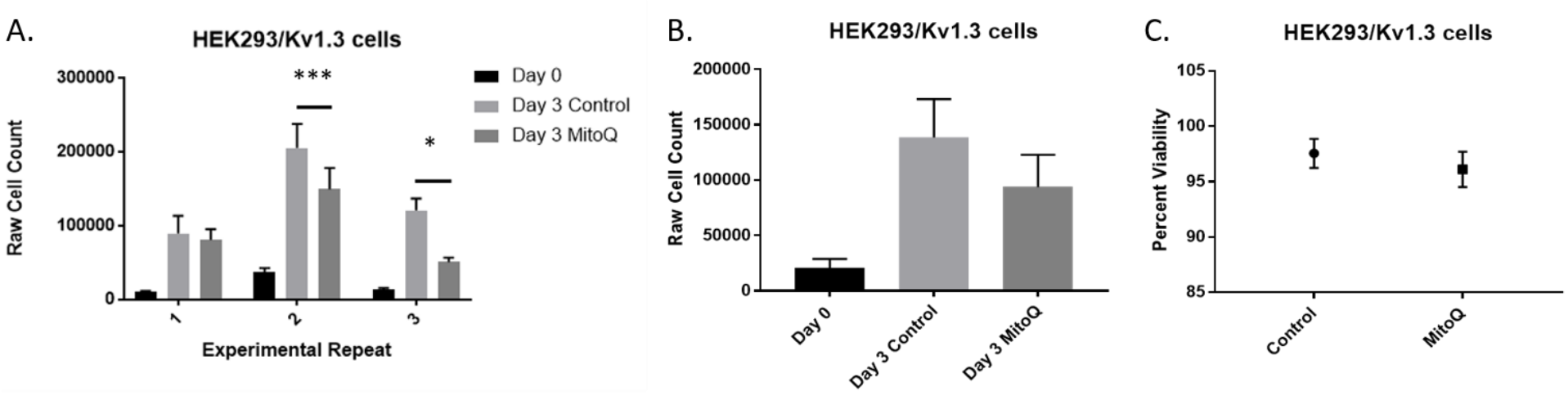

Figure 5.11 MitoQ had no effect on proliferation of HEK293/Kv1.3 cells. A. Proliferation of HEK293 cells treated with 5µM MitoQ (n=3). Cell counts on Day 0 (black bars), Day 3 (light grey bars) and on Day 3 when treated with MitoQ (dark grey bars). Wells were counted in triplicate and expressed as the raw cell count mean ± SEM. Student's t-tests were used to analyse Day 3 control counts with Day 3 MitoQ counts, * $p<0.05$, *** $p<0.001$. B. Mean day 3 data from the experiments in (A) ± SEM (n=3). Data was analysed using Student's t-tests, $p>0.05$. C. Viability counts for HEK293/Kv1.3 control (left data point) and 5µM MitoQ treated HEK293/Kv1.3 cells (right data point). Data expressed as percent viability of cells counted on Day 3, using trypan blue. Data analysed using Student's t-tests and MitoQ had no significant effect on cell viability, $p>0.05$.

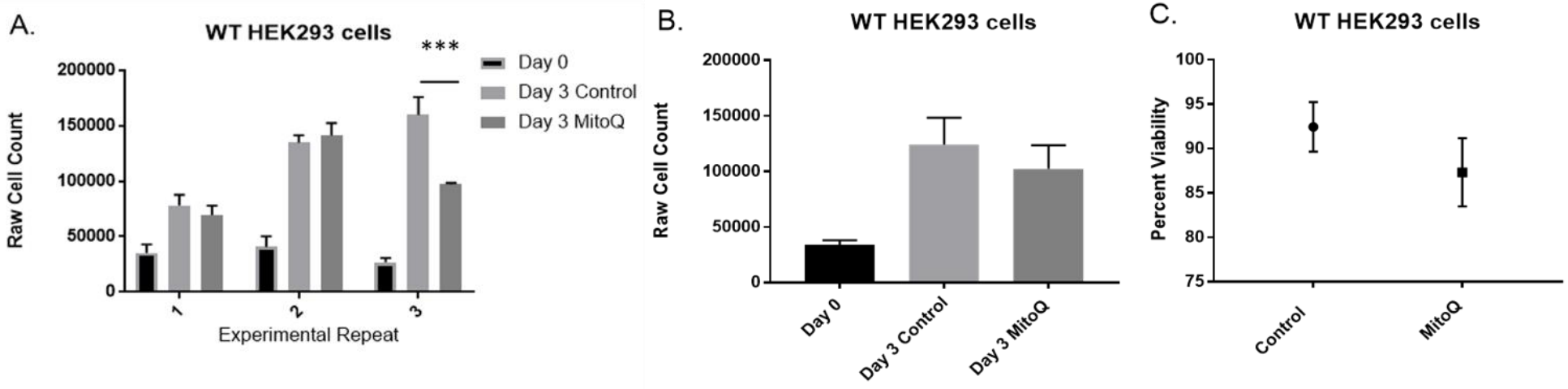

Figure 5.12 MitoQ had no effect on WT HEK293 proliferation. A. Proliferation of WT HEK293 cells treated with 5µM MitoQ (n=3). Cell counts on Day 0 (black bars), Day 3 (light grey bars) and on Day 3 when treated with MitoQ (dark grey bars). Wells were counted in triplicate and expressed as the raw cell count mean ± SEM. Student's t-tests were used to analyse Day 3 control counts with Day 3 MitoQ counts, *** $p<0.001$. B. Mean data from the experiments in (A) ± SEM (n=3). Data was analysed using Student's t-tests, $p>0.05$. C. Viability counts for WT HEK293 control (left data point) and 5µM MitoQ treated WT HEK293 cells (right data point). Data expressed as the percent viability of cells counted on Day 3, using trypan blue. Data analysed using Student's t-tests and MitoQ had no significant effect on cell viability, $p>0.05$.

5.4 Discussion

This chapter aimed to examine the potential mechanisms through which Kv1.3 channels induce an increased oxidative and proliferative phenotype, with a focus on several processes including cellular NADH production and glycolysis, MMP, mitochondrial Ca^{2+} and ROS production and signalling.

HEK293/Kv1.3 cells were shown to have increased concentrations of cellular NAD(P)H compared to WT HEK293 cells, consistent with data from Chapter Three which showed a greater ATP turnover rate in HEK293/Kv1.3 cells. This may indicate a link between the energy generated in HEK293/Kv1.3 cells and their rate of proliferation. The mechanisms through which Kv1.3 may be altering cellular NADH were therefore explored. Whether shuttling of NADH into the mitochondria was influenced by Kv1.3 was investigated through inhibition and stimulation of the malate/aspartate shuttle using phenylsuccinate (PhS) and dimethyl-2-oxoglutarate (DM-2OG), respectively. In HEK293/Kv1.3 cells, if OXPHOS were being fuelled by greater transportation of NADH into the matrix via the malate/aspartate shuttle, then inhibition by PhS should reduce OXPHOS. Conversely, stimulating the malate/aspartate shuttle with DM-2OG in WT HEK293 cells should increase the levels of OXPHOS. Treatment of WT HEK293 cells with DM-2OG, and inhibition of the activity of the malate/aspartate shuttle using PhS in HEK293/Kv1.3 cells, did not affect respiration. Alternatively, increased cellular NADH concentrations may be generated by increased TCA cycle activity in the mitochondrial matrix. Citrate synthase activity is a measure of matrix volume and its activity regulates the rate of the TCA cycle (Halestrap, 1989; Garlid, 1996). However, in Chapter Three, there was no difference in citrate synthase activity between HEK293/Kv1.3 and WT HEK293 cells, suggesting the increased NADH is not due to increased activity of the TCA cycle via citrate synthase.

Therefore, the increased NADH in HEK293/Kv1.3 cells may result from upstream of the TCA cycle, perhaps by enhanced glycolysis. Increased glucose uptake, glycolysis and lactate production in the presence of adequate cellular O_2 levels, is well described in cancer biology and is known as aerobic glycolysis, or the Warburg Effect (Warburg, 1925). Both aerobic glycolysis and OXPHOS can be upregulated in cells (Liberti and Locasale, 2016) and highly proliferating cells retain their capacity for OXPHOS (Jose,

Bellance and Rossignol, 2011; Ho *et al.*, 2012; Robinson *et al.*, 2012; Gentric, Mieulet and Mechta-Grigoriou, 2017). When glycolysis in HEK293/Kv1.3 cells and WT HEK293 cells was inhibited using 2-Deoxy-D-Glucose (2DDG) only the respiration of HEK293/Kv1.3 cells was affected. This would suggest that glycolysis is of greater importance for cellular energy balance in the HEK293/Kv1.3 cells. Interestingly, 2DDG was observed to increase routine respiration in HEK293/Kv1.3 cells. This could suggest that HEK293/Kv1.3 cells can upregulate O_2 consumption via OXPHOS in times of 'stress' i.e. knockdown of glycolysis. This plasticity in energy metabolism has been described as a key hallmark of rapidly proliferating cancer cells (Robinson *et al.*, 2012). In addition, inhibition of glycolysis in H460 tumour cells led to activation of pro-survival oncoproteins like Akt (Zhong *et al.*, 2009), which regulate energy metabolism and may be responsible for the rise in routine respiration (Robey and Hay, 2009).

To directly interrogate the effect of the mitochondrial Kv1.3 channels on the cellular NADH concentrations, the effect of mitochondrial-specific Kv1.3 channel inhibitor, PAPTP, was tested on NADH concentration in HEK293/Kv1.3 cells. PAPTP did not affect cellular NADH concentrations (Figure 5.1C). Intriguingly, this may suggest that non-mitochondrial Kv1.3 channels influence cellular NADH, especially as glycolysis is a cytosolic process. However, PAPTP inhibits ion conductance through the mitochondrial Kv1.3 channel, and Kv1.3 channels have been found to have cell signalling functions independent to their ion conducting properties (Cidad *et al.*, 2012; Jimenez-Perez *et al.*, 2016). Therefore, these results cannot preclude non-conducting roles of the channel that may affect cellular NADH concentrations.

An important caveat to this work is that the NAD(P)H autofluorescence protocol, does not separate the proportion of NAD(P)H autofluorescence attributable to NADH and NADPH. To quantify the levels of NADH and NADPH in these cells, NADPH fluorescent lifetime imaging microscopy (FLIM) may be an applicable method for future work (Blacker and Duchen, 2016). Nevertheless, an increase in NAD(P)H autofluorescence would still require an initial increase in NADH.

This thesis may highlight a link between glycolysis and the MMP in HEK293/Kv1.3 cells. 2DDG treatment significantly reduced leak respiration in HEK293/Kv1.3 cells (Figure 5.4). Therefore, MMP may be becoming more depolarised in a setting of impaired glycolysis. This suggests that glycolysis could regulate the MMP in HEK293/Kv1.3 cells.

NADH molecules are negatively charged, and a greater concentration of NADH, originating from glycolysis, may lead to MMP hyperpolarisation. In support of this, glycolysis has been found to regulate MMP oscillations (Olsen *et al.*, 2009). Olsen et al., suggested that glycolysis is coupled to MMP through ATP. ATP generated by glycolysis can be hydrolysed by the ATP-synthase, which hyperpolarises the MMP. They previously concluded that the ADP/ATP antiporter is an essential part of this process, as it determines the level of ATP reaching the ATP-synthase (Poulsen *et al.*, 2008). Beltran et al., found that in response to inhibition of respiration, Jurkat cells displayed MMP hyperpolarisation due to the hydrolysis of glycolytic ATP (Beltrán *et al.*, 2000). Aerobic glycolysis also caused IMM hyperpolarisation in cancer cells, due to reverse proton pumping of the ATP synthase (Forrest, 2015). In this chapter HEK293/Kv1.3 cells were found to have a larger MMP compared to WT HEK293 cells. However, inhibition of mitochondrial Kv1.3 channels with PAPTP did not decrease the MMP, suggesting the mechanism for this effect is independent of ion conductance through the mitochondrial Kv1.3 channels, and may be via a glycolysis-mediated mechanism.

Indeed, a hyperpolarised MMP upon opening of the mitochondrial Kv1.3 channel is the opposite of what would be expected. Opening of the Kv1.3 channels would likely result in an influx of K^+ ions into the matrix, depolarising the MMP. Nevertheless, the identification of a greater hyperpolarisation in HEK293/Kv1.3 cells is consistent with other findings of this study. HEK293/Kv1.3 cells have an oxidative and highly proliferative phenotype. Greater hyperpolarisation of the MMP is advantageous for, and in evidence in highly proliferating cells (Heerdt, Houston and Augenlicht, 2005; Houston, Augenlicht and Heerdt, 2011; Forrest, 2015; Martinez-Reyes *et al.*, 2016). A more negative MMP increases the proton motive force that drives protons through the ATP-synthase during OXPHOS, which would ultimately increase the amount of ATP generated. In addition to providing the energy for proliferation, a more hyperpolarised MMP may protect the cell from apoptosis. A depolarisation of MMP, via influx of Ca^{2+} though the MCU, triggers the opening of the MPTP (Luigi Leanza *et al.*, 2013). Therefore, a more hyperpolarised MMP inhibits the activation of the apoptotic cascade.

HEK293/Kv1.3 cells were observed to have increased levels of cellular ROS compared to WT HEK293, using the MMP independent dye CellROX. Mitochondria are considered

the primary source of ROS in the cell, so any enhancement of the mitochondrial ETS could potentially alter the level of these molecules (Murphy, 2009). These findings are consistent with the enhanced respiratory phenotype of HEK293/Kv1.3 cells. Increased ROS may result from the increased OXPHOS (Holzerova and Prokisch, 2015), specifically at Complexes 1 (Koopman *et al.*, 2010) and Complexes 3 (Raha *et al.*, 2000). The increased oxidation of NADH at complex 1, combined with the overall increase in ETS activity, would lead to electrons combining with ambient O_2 to produce superoxide. Moreover, ROS levels in HEK293/Kv1.3 cells increased significantly more than in WT HEK293 cells in response to treatment with the oxidant menadione (Figure 5.10). Menadione is metabolised in the mitochondria by Complex 1 (Criddle *et al.*, 2006). The ability of Complex 1 to reduce menadione depends on the ability of NADH to donate electrons. The resulting semiquinone can combine with O_2 and enter a redox pathway where it is regenerated as menadione, whilst concomitantly releasing ROS. As ROS is generated, levels of NADH decline. Therefore, increased levels of NADH in HEK293/Kv1.3 cells would increase the capacity for ROS production by menadione metabolism. Although, it is also possible that WT HEK293 cells could more readily adapt to oxidative insult by menadione treatment. HEK293/Kv1.3 cells have higher basal levels of ROS and so may have a lower pool of available ROS scavenger molecules.

Interestingly ROS may underlie the observed decrease in ROX specific to HEK293/Kv1.3 cells treated with 2DDG, since ROX is related to ROS (Hutter *et al.*, 2002). Glycolysis can stimulate ROS in cells, and these ROS can in turn further stimulate glycolysis (Liemburg-Apers *et al.*, 2015), the latter being a process that can occur in highly proliferating cells (Brand, 1997). Glycolysis not only contributes to energy and redox balance of the cell, but recent developments link this pathway to cellular proliferation. Glycolysis synthesises the macromolecular building blocks necessary for cells to grow i.e. NADH and carbon from Acetyl-CoA (Vander Heiden, Cantley and Thompson, 2009), and NADPH via the pentose phosphate pathway (PPP) (Riganti *et al.*, 2012; Du *et al.*, 2013).

In addition, the decreased ROX in response to 2DDG (Figure 5.4a) may also suggest that non-mitochondrial O_2 consumption is fuelled by glycolysis in HEK293/Kv1.3 cells. This would suggest that in HEK293/Kv1.3 cells, a higher level of glycolysis may

contribute to the greater ROX, despite not being an O_2 consuming process. An increase in OXPHOS supported glycolysis is described by the Warburg effect and is a phenomenon that is seen in many cancer cells (Vander Heiden, Cantley and Thompson, 2009; Liberti and Locasale, 2016; Gentric, Mieulet and Mechta-Grigoriou, 2017). In order for glycolysis to continue at a high rate, NADH must be continuously re-oxidised (Herst *et al.*, 2004). The main method of NADH regeneration is by lactate dehydrogenase, which catalyses the reduction of pyruvate by NADH to form lactate and NAD^+ (Augoff, Hryniewicz-Jankowska and Tabola, 2015). However, lactate dehydrogenase can also be a source of NADH, facilitating the oxidation of lactate to pyruvate and the subsequent reduction of NAD^+ to NADH (Kim *et al.*, 2017). Lactate dehydrogenase could therefore be involved in the increased NADH in HEK293/Kv1.3 cells. The activity of lactate dehydrogenase has been linked to metabolism (Brooks, 2018) and its activity has been found to be necessary for vascular smooth muscle cell proliferation and migration (Kim *et al.*, 2017). Thus, investigation of lactate dehydrogenase activity in HEK293/Kv1.3 cells would be necessary to identify any links to the high NADH in these cells and their proliferative phenotype.

Another redox reaction which regenerates NAD^+ occurs in the plasma membrane, where, in a similar way to that in the IMM, electrons are transported across the membrane to bind with O_2 (Goldenberg, Crane and Morre, 1979). Both plasma membrane and mitochondrial electron transport compete for NADH, as it is their source of electrons (Herst *et al.*, 2004). This plasma membrane O_2 consumption may be responsible for O_2 dependent cell growth when mitochondrial ETS activity is reduced (Shen *et al.*, 2003). In 2004, inhibitors of glycolysis and glucose inhibited cell surface O_2 consumption in HL60 tumour cells (Herst *et al.*, 2004). Non-mitochondrial O_2 consumption is essential to recycle NADH to maintain glycolysis and may explain why 2DDG treatment reduced ROX in HEK293/Kv1.3 cells. These results suggest that Kv1.3 may be involved in the regulation of plasma membrane O_2 consumption.

Under inhibitory glycolytic conditions (2DDG), OXPHOS was still greater in HEK293/Kv1.3 cells compared with WT HEK293 cells (Figure 5.4). The increased ATP that likely results from this greater OXPHOS may also fuel cell proliferation (Ho *et al.*, 2012). In addition, increased ATP might also increase proliferation via a reduction in AMP activated protein kinase (AMPK) (Motoshima *et al.*, 2006), since high levels of ATP

decrease the AMP/ATP ratio, deactivating AMPK signalling, leading to a stimulation of the cell cycle.

Plasma membrane O_2 consumption, and the associated activity of plasma membrane NADPH oxidases, are sources of ROS (Shen *et al.*, 2003). However, there are numerous other sites of extra-mitochondrial ROS production in cells, such as the endoplasmic reticulum, peroxisomes and the cytosol, that may have contributed to the higher basal ROS detected in HEK293/Kv1.3 cells (Brown and Borutaite, 2012). Oxidase enzymes, such as diamine oxidase, D-amino acid oxidase, nitric oxide synthases and lipoxygenase are enzymes involved in nutrient metabolism and may be sites of ROS generation(Brown and Borutaite, 2012) (Holzerova and Prokisch, 2015). Their links to substrate metabolism are interesting and would require further investigation to determine if they are involved in the altered metabolic and proliferative phenotype of HEK293/Kv1.3 cells.

There was a trend for MitoQ to decrease HEK293/Kv1.3 cell proliferation (Figure 5.11), and so ROS may directly stimulate proliferation in these cells. ROS have been found to stimulate proliferation in various cell types; microglia (Bordt and Polster, 2014), immune cells (Wheeler and DeFranco, 2012), colon (Juhasz *et al.*, 2017) and other cancers (Sullivan *et al.*, 2015; Moloney and Cotter, 2017). ROS have also been known to regulate ion channel function (Scragg *et al.*, 2008; Elies, Dallas, *et al.*, 2014; Elies, Scragg, *et al.*, 2014; Al-Owais *et al.*, 2015; Duckles *et al.*, 2015; Peers *et al.*, 2015). In Figure 5.11 the results suggest that the increased ROS production may contribute to the proliferative phenotype of these HEK293/Kv1.3 cells, as the mean proliferation for MitoQ treated cells was 68% that of untreated controls.

Further work needs to be done to establish whether K^+ influx through mitochondrial Kv1.3 is large enough to significantly alter the MMP without any non-mitochondrial factors such as glycolysis. Alterations in the ionic balance of the matrix may affect the MMP, so it would need to be established whether the mitochondrial ultrastructure is altered in HEK293/Kv1.3 cells. Mitochondrial volume has been implicated in cellular bioenergetics (Halestrap, 1989), and alterations to the ionic balance are likely to have some effect on the water content of the matrix. A more advanced investigation into the ultrastructure and volume of the matrix is necessary compared to the basic investigation into mitochondrial structure in Chapter Three. Pharmacological inhibition

of the different exchangers involved in the mitochondrial K^+ cycle, for example the LETM1, H^+/K^+ and H^+/Pi exchangers would need to be tested on the MMP and on the respiration and proliferation of HEK293/Kv1.3 cells. To improve these investigations, they could also be tested in isolated mitochondria. Finally, regarding glycolysis it would also be interesting to explore the effect of glycolysis inhibition on the MMP of HEK293/Kv1.3 cells, and also an investigation into the reasons for the increased glycolysis is needed. Two key avenues could be explored:

1) Do the Kv1.3 channels cause more glucose to enter the cell? There could be a physical interaction between the Kv1.3 channel and GLUT transporters whereby activation of the channel could also activate GLUT proteins. GLUT channels have PDZ domains (Bunn, Jensen and Reed, 1999), which may interact with Kv1.3 and lead to altered function. Or perhaps there exists a cell signalling pathway/s whereby the metabolic milieu is sensed by the Kv1.3 channels and this information is relayed to the nucleus which upregulates glucose influx (Tucker *et al.*, 2013). Identification of GLUT transporters and/or their activity in HEK293/Kv1.3 compared to WT HEK293 cells would be necessary.

2) Do the Kv1.3 channels cause there to be an increase in the expression of enzymes in glycolysis which may lead to an increased rate of glycolysis (Lee *et al.*, 2018). Again, perhaps a cell signalling pathway exists between mitochondrial Kv1.3 channels and the nucleus which increases these enzymes. Measurement of enzymes such as hexokinase, phosphofructokinase and pyruvate kinase would be needed to determine if any are significantly upregulated compared to WT HEK293 cells

This chapter explored the mechanisms in which mitochondrial Kv1.3 may contribute to enhanced respiration and proliferation. HEK293/Kv1.3 cells have increased NADH levels, likely due to increased rates of glycolysis. Interestingly, the increased cellular NADH may be independent of the ion-conducting role of mitochondrial Kv1.3 channels. Moreover HEK293/Kv1.3 cells in which glycolysis is inhibited have higher levels of OXPHOS than WT HEK293 cells. HEK293/Kv1.3 cells have a more hyperpolarised MMP which may arise from the increased glycolysis or due to an imbalance in cation and anion composition of the mitochondrial matrix. Compellingly, HEK293/Kv1.3 cells have increased cellular ROS compared to WT HEK293 cells and this may directly contribute to the high proliferation rate of these cells.

How the overexpression of the Kv1.3 ion channel, specifically the mitochondrial Kv1.3 channel, leads to the upregulation of metabolic pathways warrants further exploration. Mitochondrial Kv1.3 may act as a metabolic sensor to upregulate glycolysis and OXPHOS. Kv1.3 function as a K^+ channel may not be essential for its role in stimulating proliferation. In the final results chapter, non-conducting Kv1.3 channel mutants will be tested to determine whether the channel has ion-conducting independent effects on respiration.

Chapter Six

Kv1.3 channels have non-conducting properties which increase respiration and proliferation in HEK293 cells.

6.1 Introduction

In Chapter Five of this thesis, inhibition of mitochondrial Kv1.3 channels with PAPTP had no significant effect on redox metabolism (NADH autofluorescence) or MMP. Therefore Kv1.3-mediated K^+ flow into the mitochondrial matrix may not be responsible for the increased NADH autofluorescence and hyperpolarised MMP in HEK293/Kv1.3 cells. This suggests that the Kv1.3 ion channel may have non-conducting properties which function to increase respiration and proliferation.

In recent years, ion-conducting independent roles of ion channels have been established, in which channel proteins can act as cell signalling mediators. K^+ channels can have permeation independent mechanisms involving voltage dependent conformational changes or protein-protein interactions which modulate proliferation (Urrego *et al.*, 2014). EAG and K_{Ca} channels can increase proliferation via ion independent signalling (Hegle, Marble and Wilson, 2006; Millership *et al.*, 2011, respectively). Kv1.3 inhibition with MgTx and PAP-1 prevents proliferation and depolarises VSMCs, but depolarisation, with either inhibitors of other Kv channels or by increasing extracellular K^+ concentration, does not prevent proliferation in HEK293 cells (Cidad *et al.*, 2010). In addition, activation of Kv1.3 channels and Kv1.5 channels both hyperpolarise the plasma membrane, but Kv1.3 channels increase proliferation whilst Kv1.5 channels reduce it (Cidad *et al.*, 2012). These studies suggest the proliferation stimulating effect of Kv1.3 channels may not be caused by K^+ flow through the channel. Eight phosphorylation residues, either threonine, serine or tyrosine, on the C-terminus of the Kv1.3 channel have been identified (Jimenez-Perez *et al*., 2016), and three of these residues are essential for the proliferation stimulating

effect of Kv1.3 channels, as their mutation to alanine abolished Kv1.3 induced proliferation (Jimenez-Perez *et al*., 2016).

To investigate whether these residues also have an effect on mitochondrial respiration, we were kindly gifted three plasmids encoding the mutant Kv1.3 channels from López López *et al*. The first two mutants are described in their 2012 paper (Cidad *et al*., 2012), where they were called Kv1.3WF and Kv1.3WF3X. From here on in, Kv1.3WF will be referred to as Kv1.3-P89, and Kv1.3WF3X as Kv1.3-P93. Kv1.3-P89 is a voltage sensitive but non-conducting Kv1.3 channel with intact gating properties. It is unable to conduct due to a single point mutation in the channel pore region (S5-S6). Kv1.3-P93 is a voltage insensitive and non-conducting Kv1.3 channel. As well as having the same point mutation as Kv1.3-P89 channel in the pore region, it has three additional point mutations in the voltage sensor (S4). The final mutant that was used in this work was described in the 2016 López López *et al*. paper (Jimenez-Perez *et al.*, 2016), where it was designated Kv1.3-Y447A. From here on in, this channel will be referred to as HEK293/Kv1.3-P121. Kv1.3-P121 is a phosphorylation defective Kv1.3 mutant, which is voltage sensitive and able to conduct K^+ ions. It is phosphorylation defective due to an alanine substitution of a tyrosine residue at position 447 on its C-terminus which prevents ERK1/2 dependent phosphorylation (Jimenez-Perez *et al.*, 2016).

Kv1.3-P89, Kv1.3-P93 and Kv1.3-P121 mutants were expressed in HEK293 cells and used to show that Kv1.3 channels require an intact voltage sensor to increase proliferation (Cidad *et al.*, 2012). It is thought that upon voltage sensing, the Kv1.3 channel exhibits a conformational change which exposes key phosphorylation sites, and enables them to be phosphorylated as part of a signalling cascade that drives proliferation (Jimenez-Perez *et al.*, 2016). This signalling cascade requires ERK, but the exact mechanism through which this signalling cascade increases proliferation is unknown. Interestingly, ERK is located in mitochondria (Wainstein and Seger, 2016) and may have roles in cell survival (Lee *et al.*, 2004), proliferation and tumour cell phenotype (Galli *et al.*, 2008; Lan *et al.*, 2018), phosphorylation of transcription factors (Gough, Koetz and Levy, 2013) and mitochondrial gene expression (Fehrenbacher, Bar-Sagi and Philips, 2009). There are also suggestions that ERK acts as a signalling molecule between the mitochondria and the nucleus (Galli *et al.*, 2009) and as a kinase which directly phosphorylates respiratory complex proteins (Horbinski and Chu, 2005).

Thus, there may be signalling cascades in the mitochondria which function downstream of Kv1.3 activation which affect cell respiration and proliferation. The effect of mutant Kv1.3 channels on respiration is unknown, and in this chapter the link between the non-conducting properties of Kv1.3 channels, proliferation and respiration in HEK293 cells was investigated.

6.2 Aims and Objectives

The aim of this chapter was to explore whether the Kv1.3 channel-stimulated respiration in HEK293 cells is regulated by non-conducting mechanisms. To achieve this aim a key set of objectives were designed:

1) To stably transfect HEK293 cells with the mutant Kv1.3 channels. The channels either had a functioning voltage sensor but a mutated pore (Kv1.3-P89), neither a functioning pore nor a functioning voltage sensor (Kv1.3-P93) or a functioning pore and voltage sensor, but non-functional phosphorylation sites (Kv1.3-P121).

2) To confirm that non-conducting Kv1.3-P89 mutant channels, possessing a functioning voltage sensor and disrupted pore, could increase proliferation of HEK293 cells.

3) To investigate mitochondrial respiration in HEK293 cells transfected with the Kv1.3-P89, Kv1.3-P121 and Kv1.3-P93 mutant Kv1.3 channels to elucidate whether the channel voltage sensor, pore or phosphorylation sites are key to Kv1.3-stimulated respiration.

6.3 Results

6.3.1 The Kv1.3-P89, Kv1.3-P93 and Kv1.3-P121 mutant channels co-localise with mitochondria in HEK293 cells.

In Chapter Three, Kv1.3 channels were found in the mitochondria of WT HEK293 (Figure 3.9), HEK293/Kv1.3 (Figure 3.9 and 3.11) and HSVSM cells (Figure 3.12). Therefore, whether the mutant Kv1.3 channels also co-localized with mitochondria in HEK293/Kv1.3-P89, HEK293/Kv1.3-P93 and HEK293/Kv1.3-P121 cells was investigated. In Figure 6.1 staining for Kv1.3-P89 and Kv1.3-P93 is shown, where nuclei are stained blue, mitochondria red and mutant Kv1.3 in green. The yellow/orange fluorescence in panels D and L (Figure 6.1) highlights mitochondrial mutant Kv1.3 channels in HEK293/Kv1.3-P89 and HEK293/Kv1.3-P93 cells (respectively). In Figure 6.2 HEK293/Kv1.3-P121 cells were stained for mitochondrial Kv1.3 localisation, where nuclei are stained blue, mitochondria green and mutant Kv1.3 in red. Co-localisation was shown as yellow/orange fluorescence in panel D (Figure 6.2). The mCherry red fluorescence of mutant Kv1.3 channels in panels C and G (Figure 6.2), is lower than the GFP staining of mutant Kv1.3 channels in panels C,G,K and O (Figure 6.1) which suggests a lower expression of mutant Kv1.3 channels in HEK293/Kv1.3-P121 cells than in HEK293/Kv1.3-P89 or HEK293/Kv1.3-P93 cells. To ensure the yellow/orange fluorescence was not an optical illusion/artefact of just closely situated (but not co-localised) Kv1.3 channels and mitochondria, co-localisation analysis was carried out to determine exact pixel intensity correlation (Johannes Schindelin, no date). The results are shown in Figure 6.3, where the white dots reflect areas of the cell where there is perfect correlation between mitochondria and Kv1.3 channels. All cells exhibited some degree of mitochondrial Kv1.3 co-localisation (Figure 6.3.

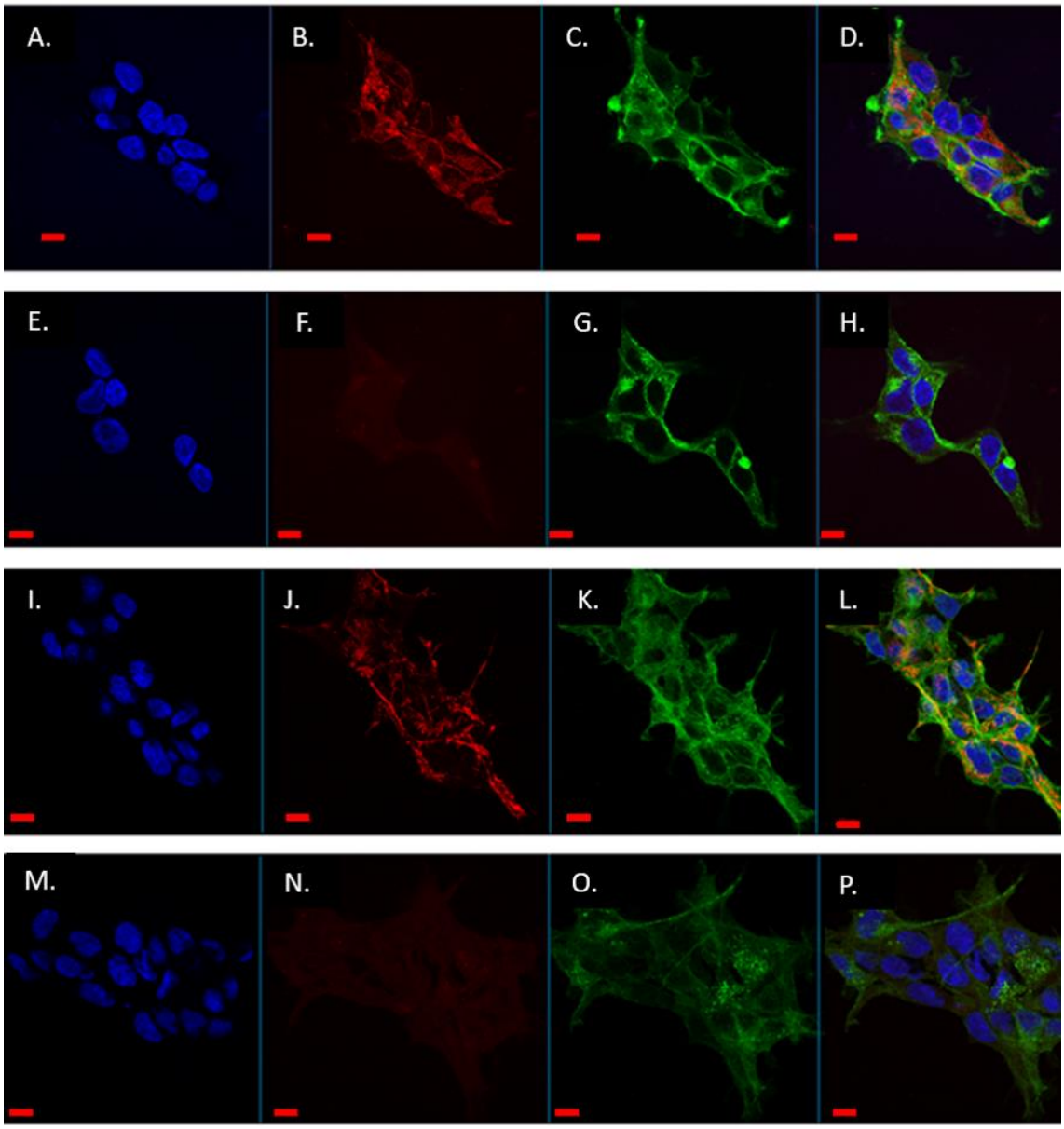

Figure 6.1 Mitochondrial and Kv1.3 co-localisation in HEK293/Kv1.3-P89 and HEK293/Kv1.3-P93 cells. A – H) Mutant Kv1.3 channel and mitochondrial co-localisation in HEK293/Kv1.3-P89 cells. A. DAPI staining of HEK293/Kv1.3-P89 cell nuclei (blue). B. Immunostaining of cytochrome C oxidase in HEK293/Kv1.3-P89 cells to visualise the mitochondria (red). C. GFP tagged mutant Kv1.3 channels in HEK293/Kv1.3-P89 cells (green). D. Composite image of DAPI nuclear stain (blue), cytochrome C oxidase immunostain (red) and GFP-tagged mutant Kv1.3 cells (green). E. DAPI staining of HEK293/Kv1.3-P89 cell nuclei (blue). F, Control for non-specific binding by the Alexa Fluor secondary antibody. Staining was performed as in (B) but without anti-COX IV antibody. G. GFP tagged mutant Kv1.3 channels in HEK293/Kv1.3-P89 cells (green). H. Composite image of E, F and G. **I - P)** Mutant Kv1.3 channel and mitochondrial co-localisation in HEK293/Kv1.3-P93 cells. I. DAPI staining of HEK293/Kv1.3-P93 cell nuclei (blue). J. Immunostaining of cytochrome C oxidase in HEK293/Kv1.3-P93 cells to visualise the mitochondria (red). K. GFP tagged mutant Kv1.3 channels in HEK293/Kv1.3-P93 cells (green). L. Composite image of DAPI nuclear stain (blue), cytochrome C oxidase immunostain (red) and GFP-tagged mutant Kv1.3 cells (green). M. DAPI staining of HEK293/Kv1.3-P93 cell nuclei (blue). N. Control for non-specific binding by the Alexa Fluor secondary antibody. Staining was performed as in (J) but without anti-COXIV antibody. O. GFP tagged mutant Kv1.3 channels in HEK293/Kv1.3-P93 cells (green). P. Composite image of E, F and G. All scale bars are 10µm.

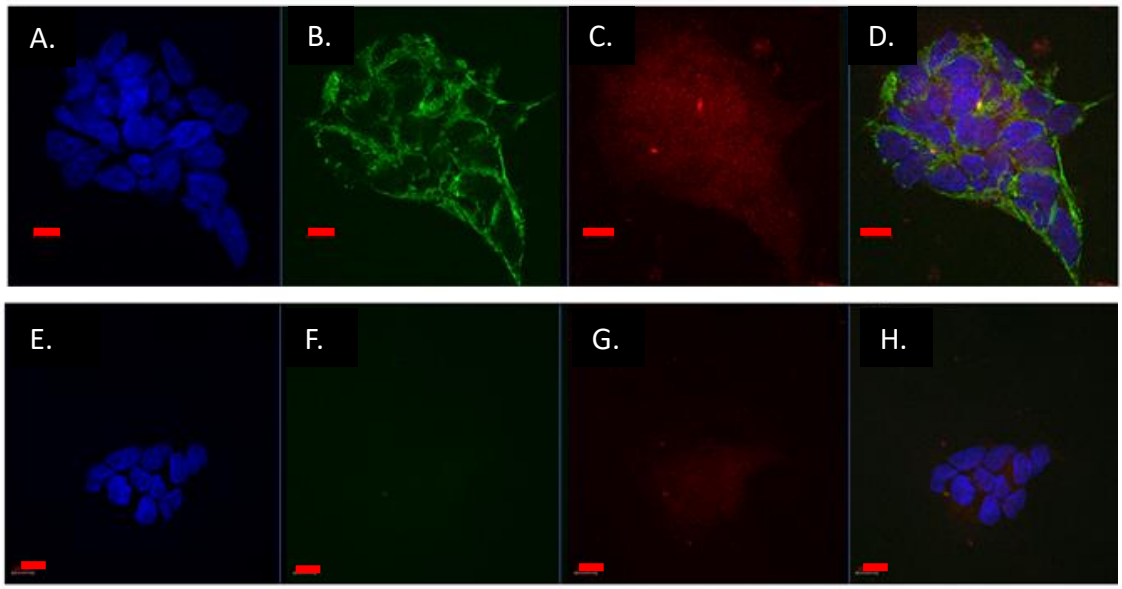

Figure 6.2 Mitochondrial and Kv1.3 co-localisation in HEK293/Kv1.3-P121 cells. A – D) Mutant Kv1.3 channel and mitochondrial co-localisation in HEK293/Kv1.3-P121 cells. A. DAPI staining of HEK293/Kv1.3-P121 cell nuclei (blue). B. Immunostaining of cytochrome C oxidase in HEK293/Kv1.3-P121 cells to visualise the mitochondria (green). C. mCherry tagged mutant Kv1.3 channels in HEK293/Kv1.3-P121 cells (red). D. Composite image of DAPI nuclear stain (blue), cytochrome C oxidase immunostain (green) and mCherry-tagged mutant Kv1.3 cells (red). E. DAPI staining of HEK293/Kv1.3-P121 cell nuclei (blue). F. Control for non-specific binding by the Alexa Fluor secondary antibody. Staining was performed as in (B) but without anti-COXIV antibody. G. mCherry tagged mutant Kv1.3 channels in HEK293/Kv1.3-P121 cells (red). H. Composite image of E, F and G. All scale bars are 10µm.

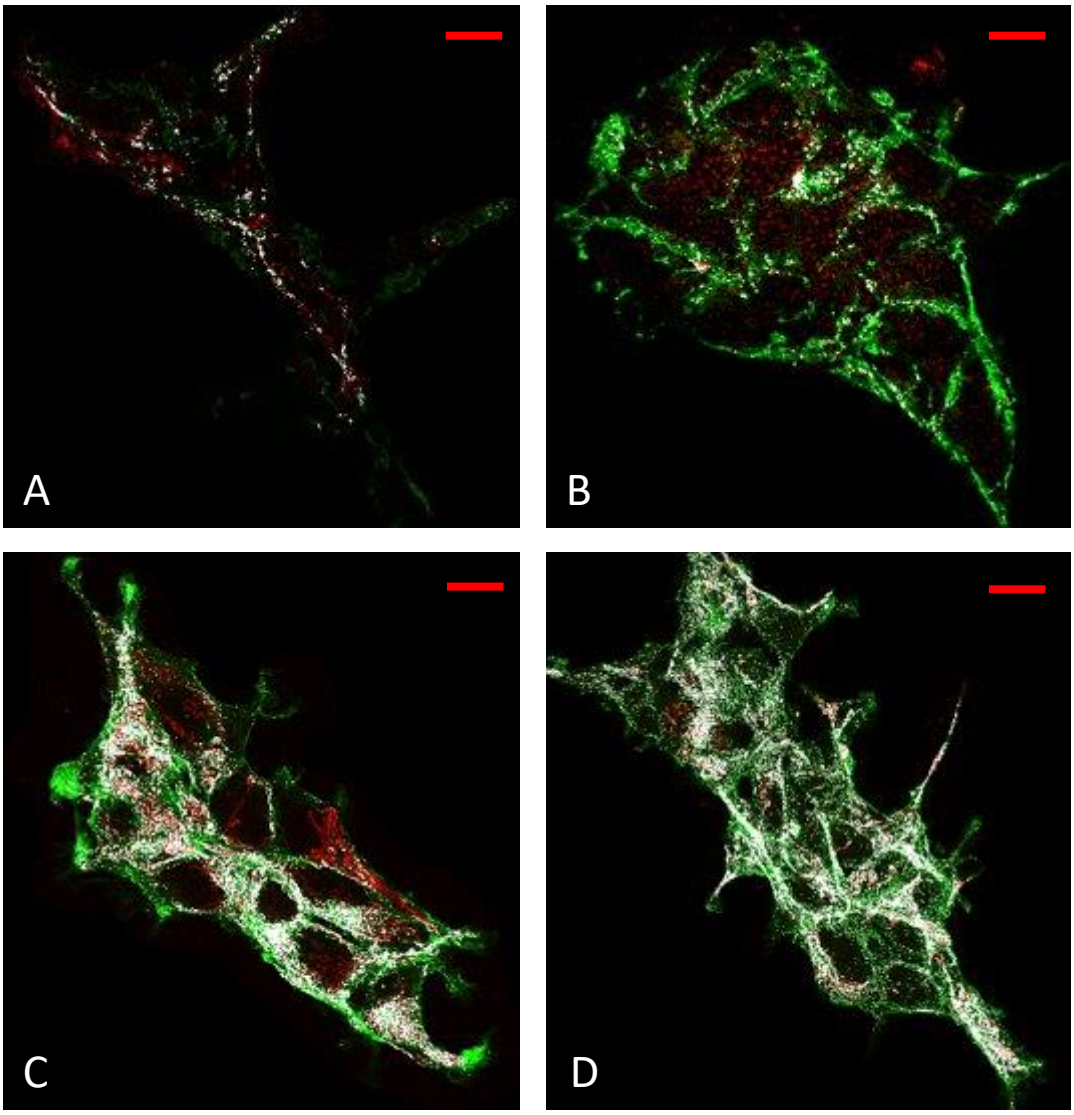

Figure 6.3 Mitochondrial Kv1.3 co-localisation analysis of HEK293/Kv1.3 and HEK293/Kv1.3 mutant cells. A. HEK293/Kv1.3-P118 cells. B. HEK293/Kv1.3-P121 cells. C. HEK293/Kv1.3-P89 cells. D. HEK293/Kv1.3-P93 cells. A - B. Immunostaining of cytochrome C oxidase in cells to visualise the mitochondria (green). Kv1.3 channels in these cells were tagged with mCherry (red). White dots indicate areas of co-localisation between mitochondria and Kv1.3 channels. C - D. Immunostaining of cytochrome C oxidase in cells to visualise the mitochondria (red). Kv1.3 channels in these cells were tagged with GFP (green). White dots indicate areas of co-localisation between mitochondria and Kv1.3 channels. Co-localisation analysis was carried out using the Coloc 2 plugin within Image J analysis software. Scale bars are 10µm.

6.3.2 HEK293/Kv1.3-P89, HEK293/Kv1.3-P93 and HEK293/Kv1.3-P121 had reduced K^+ currents compared to HEK293/Kv1.3 cells.

To determine if the mutations in the Kv1.3 channel functionally impair K^+ currents in the transfected cells, whole cell patch clamp electrophysiology was carried out (Figure 6.4). HEK293/Kv1.3 cells have larger K^+ currents than WT HEK293 cells (Chapter Three, Figure 3.3). Figure 6.4 shows the IV curve of HEK293/Kv1.3 cells, when depolarised from -60mV to +60mV, compared to the Kv1.3-P121, Kv1.3-P89 and Kv1.3-P93 mutant HEK293 cells. HEK293/Kv1.3 cells had significantly greater K^+ currents compared to HEK293/Kv1.3-P121, HEK293/Kv1.3-P89 and HEK293/Kv1.3-P93 cells (Figure 6.4). HEK293/Kv1.3-P121 cells displayed larger K^+ currents compared to HEK293/Kv1.3-P89 and HEK293/Kv1.3-P93 at +60mV. HEK293/Kv1.3-P121 cells have an intact voltage sensor and a functional pore region, and only have a mutation at a tyrosine residue at position 447. Therefore, these cells should illicit K^+ currents which are no different to those in HEK293/Kv1.3 cells (Jimenez Perez et al., 2016), unless phosphorylation of the Y447 residue increases K^+ conductance of these channels. The lower K^+ currents in HEK293/Kv1.3-P121 cells compared to HEK293/Kv1.3 cells could also be due to lower Kv1.3-P121 channel expression in these cells, as suggested by their low mCherry red fluorescence (Figure 6.2), compared to the GFP green fluorescence of mutant channels in HEK293/Kv1.3-P89 and HEK293/Kv1.3-P93 cells (Figure 6.1). HEK293/Kv1.3-P89 cells have Kv1.3 channels with a non-functioning K^+ conducting pore and HEK293/Kv1.3-P93 cells have Kv1.3 channels with neither a functioning voltage sensor nor a K^+ conducting pore. As expected, HEK293/Kv1.3-P89 and HEK293/Kv1.3-P93 cells displayed greatly reduced K^+ currents upon depolarisation from -60mV to +60mV.

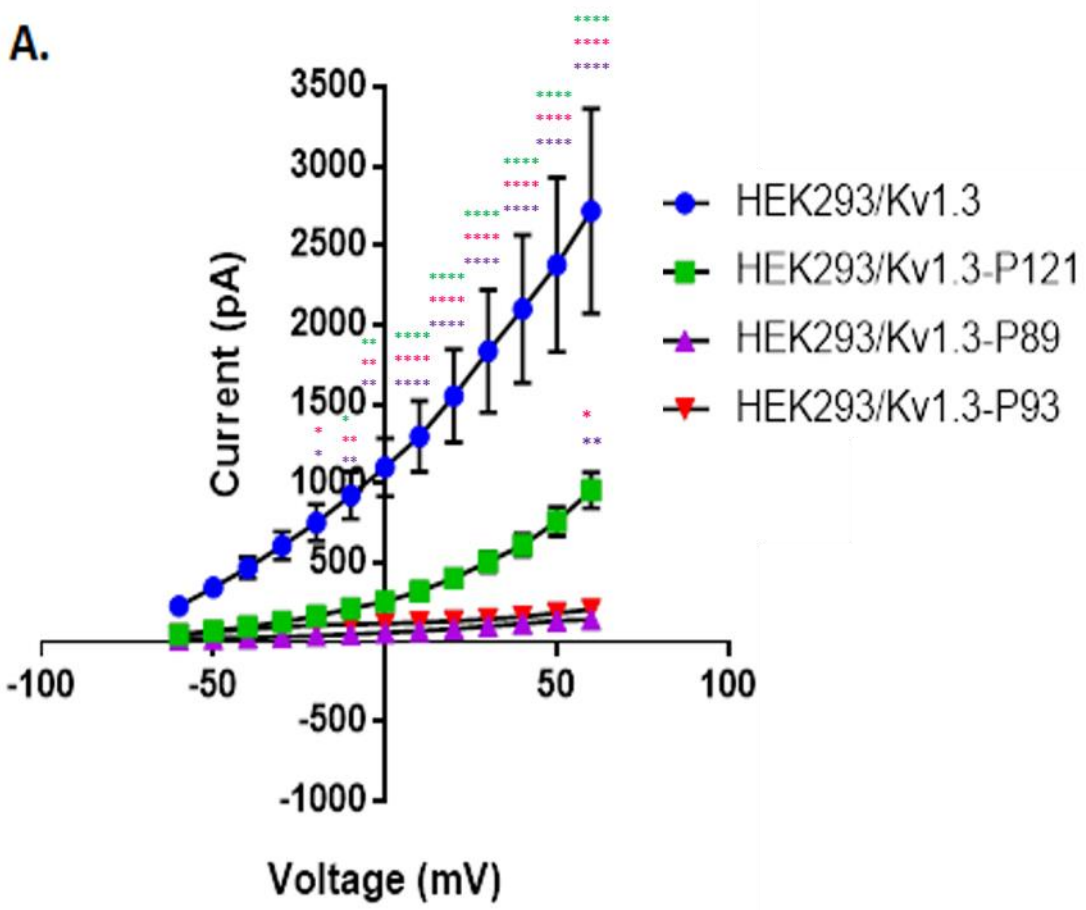

Figure 6.4 Potassium ion currents in Kv1.3 mutant cells. A. Current/voltage (IV) relationship for potassium ion currents between -60mV and +60mV in HEK293/Kv1.3 cells (n=7, blue circles), HEK293/Kv1.3-P121 cells (n=7, green squares), HEK293/Kv1.3-P89 cells (n=6, purple triangles) and HEK293/Kv1.3-P93 cells (n=6, red triangles). Data expressed as the mean current (pA) ± SEM at each voltage. At each voltage, one-way ANOVA with post hoc Tukey's multiple comparison test was used to define significant differences between the potassium currents in each cell type. Green stars = mean current is significantly different to that in HEK293/Kv1.3-P121 cells. Purple stars = mean current is significantly different to that in HEK293/Kv1.3-P89 cells. Red stars = mean current is significantly different to that in HEK293/Kv1.3-P93 cells. * $p<0.05$, ** $p<0.01$, *** $p<0.001$. **** $p<0.0001$.

6.3.3 HEK293/Kv1.3-P89 cells have increased proliferation compared to WT HEK293 cells.

HEK293/Kv1.3-P89 cells displayed increased proliferation compared to WT HEK293 cells (Figure 6.5). This suggests that Kv1.3 channels which have an intact voltage sensor, without an ion conducting pore, can increase the proliferation of HEK293 cells. However, the proliferation of HEK293/Kv1.3-P89 cells was still significantly decreased compared with HEK293/Kv1.3 cells, perhaps indicating that ion flow through the Kv1.3 channel can further increase proliferation. HEK293/Kv1.3-P121 cells did not have increased proliferation compared to WT HEK293 cells, despite having a functional Kv1.3 voltage sensor and ion pore (Figure 6.5). The point mutation of tyrosine 447 to alanine on the C-terminal of the Kv1.3-P121 channel prevents the increase in proliferation. This tyrosine is a phosphorylation site and so the Kv1.3-P121 channel is phosphorylation defective. In HEK293/Kv1.3-P93 cells, the lack of an ion conducting pore and a mutated voltage sensor on the Kv1.3 channel prevented Kv1.3-dependent proliferation of HEK293 cells (Figure 6.5).

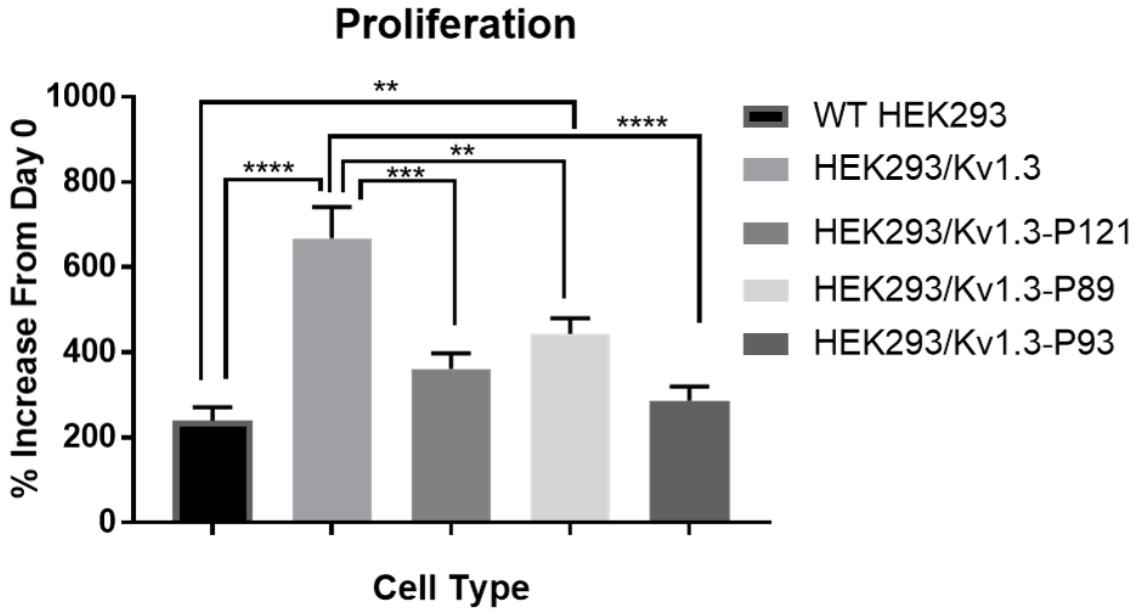

Figure 6.5 HEK293/Kv1.3-P89 cells have increased proliferation compared to WT HEK293 cells. Proliferation of WTHEK293, HEK293/Kv1.3, HEK293/Kv1.3-P121, HEK293/Kv1.3-P89 and HEK293/Kv1.3-P93 cells (from left to right, respectively). Data expressed as percent increase from Day 0 to Day 3. Wells counted in triplicate and data expressed as the mean ± SEM (WT HEK293 cells, n=9, HEK293/Kv1.3 cells, n=4, HEK293/Kv1.3-P121 cells, n=7, HEK293/Kv1.3-P89 cells, n=9 and HEK293/Kv1.3-P93 cells, n=6). Data was analysed using one-way ANOVA with Tukeys post hoc test., ** $p<0.01$, *** $p<0.001$, **** $p<0.0001$.

6.3.4 Disruption of the Kv1.3 channel pore in the Kv1.3-P89 mutation did not abrogate Kv1.3-stimulated respiration in HEK293 cells.

Using the standard respirometry assay employed in previous chapters, the Routine, Leak, ETS and ROX Respiration of the mutant Kv1.3 cells was measured. In Chapter Three, we showed that HEK293/Kv1.3 cells have increased respiration compared to WT HEK293 cells (Figures 3.5 and 3.6). The Routine, Leak, ETS and ROX Respiration of HEK293/Kv1.3-P89 cells was not significantly different from that of HEK293/Kv1.3 cells (Figure 6.6A). It is worth noting however that the ETS Respiration (Maximum Uncoupled Respiration) in HEK293/Kv1.3-P89 cells trended towards being lower than that in HEK293/Kv1.3 cells. In addition, HEK293/Kv1.3-P89 cells displayed significantly increased Routine Respiration, as well as an increased level of residual O_2 consumption (ROX) compared to WT HEK293 cells (Figure 6.6A). Although both the mean Leak Respiration and the mean Maximum Uncoupled Respiration trended higher in HEK293/Kv1.3-P89 cells compared to WT HEK293 cells, these were not statistically significant increases. When respiration was corrected for ROX, only Routine Respiration was significantly increased compared to WT HEK293 cells (6.6B) However, Routine, Leak and ETS Respiration were no different from that of HEK293/Kv1.3 cells. There were no differences in Leak Respiration between any of the cell types (6.5B). Since the Kv1.3-P89 mutation disrupts the channel pore, an increase in Routine Respiration in HEK293/Kv1.3-P89 cells indicates that K^+ flow into the mitochondria is not necessary to increase the respiration of HEK293 cells. The presence of an intact voltage sensor may be needed to increase the respiration of HEK293 cells. The increased respiration rate is consistent with the increased proliferation rate in the HEK293/Kv1.3-P89 cells (Figure 6.5).

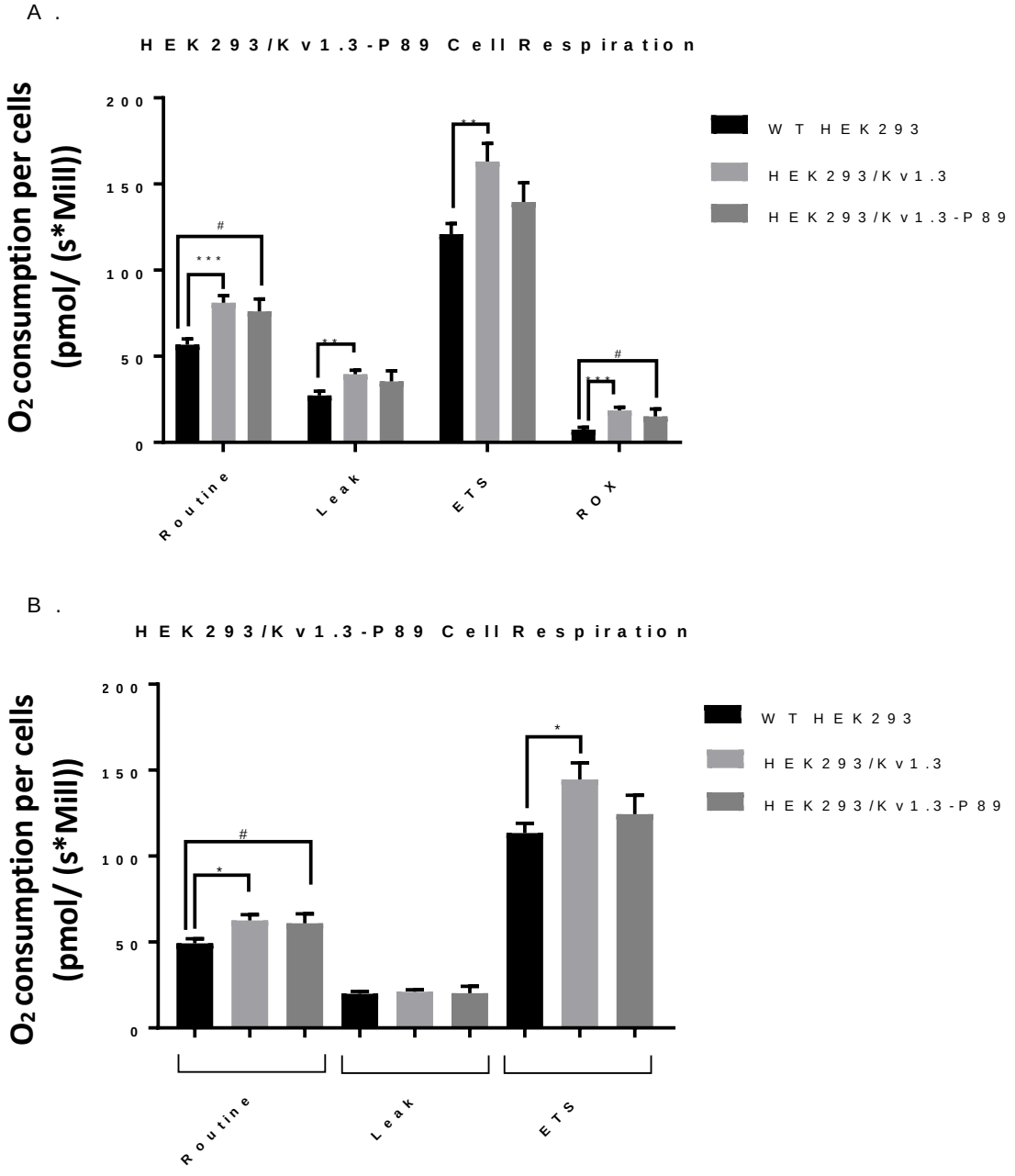

Figure 6.6 HEK293/Kv1.3-P89 cells have increased routine respiration compared to WT HEK293 cells. A. Respiration of WT HEK293 (black bars), HEK293/ Kv1.3 (light grey bars) and HEK293/Kv1.3-P89 (dark grey bars) cells. HEK293/Kv1.3 and WT HEK293 data is from total experiments (n=38 and n=27, respectively), HEK293/Kv1.3-P89 (n=9). Data is the mean O_2 consumption (O_2 per cells per second, pmol/(s*Mill)) uncorrected for residual O_2 consumption (ROX). One-way ANOVA and Tukey's post hoc test was used to analyse the data, * $p<0.05$, ** $p<0.01$ and *** $p<0.001$. Student's t-test found HEK293/Kv1.3-P89 routine and ROX respiration significantly higher than in WT HEK293 cells, # = $p<0.05$. B. Data in (A) corrected for ROX. One-way ANOVA and Tukey's post hoc test was used to analyse the data, * $p<0.05$. Student's t-test found HEK293/Kv1.3-P89 routine respiration significantly higher than in WT HEK293 cells, # = $p<0.05$.

6.3.5 Disruption of both the Kv1.3 voltage sensor and ion pore in HEK293/Kv1.3-P93 cells reduces respiration compared to HEK293/Kv1.3 cells.

HEK293/Kv1.3-P93 cells have both a non-functioning voltage sensor and non-functioning ion conducting pore. The Routine, Leak, ETS and ROX Respiration was reduced in HEK293/Kv1.3-P93 cells compared to HEK293/Kv1.3 cells (Figure 6.7A). There was no difference between the respiration of HEK293/Kv1.3-P93 cells and WT HEK293 cells (Figure 6.7A). When respiration data was corrected for ROX (Figure 6.7B), there was once again no difference in Leak Respiration between any of the cell types. Despite not being statistically significant, the mean Routine and ETS respiration of HEK293/Kv1.3-93 trended towards being lower than that of HEK293/Kv1.3 cells (Figure 6.7B). This suggests that the reduced respiration of HEK293/Kv1.3-P93 cells compared to HEK293/Kv1.3 cells is consistent with their reduced proliferation (Figure 6.5). In addition, the results in Figure 6.7 suggest that mitochondrial Kv1.3 channels also increase non-mitochondrial cellular respiration.

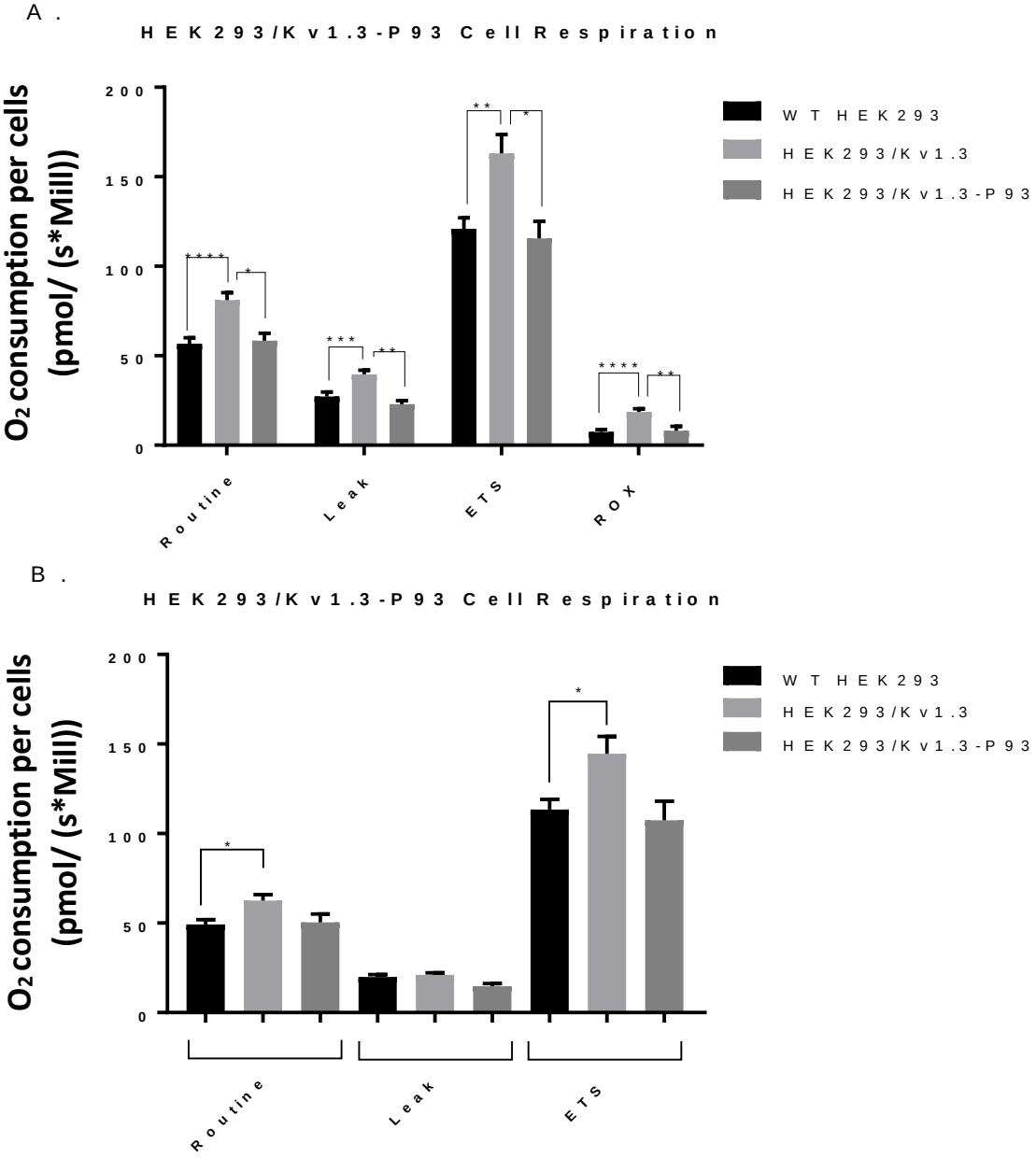

Figure 6.7 Loss of the functioning ion channel pore and voltage sensor in Kv1.3 channels abrogates Kv1.3 induced respiration in HEK293 cells. A. Respiration of WT HEK293 (black bars), HEK293/Kv1.3 (light grey bars) and HEK293/Kv1.3-P93 (dark grey bars) cells. HEK293/Kv1.3 and WT HEK293 data is from total experiments (n=38 and n=27, respectively), HEK293/Kv1.3-P93 (n=9). Data is the mean O_2 consumption (O_2 per cells per second, pmol/(s*Mill)) uncorrected for residual O_2 consumption (ROX). One-way ANOVA and Tukey's post hoc test was used to analyse the data, * $p<0.05$, ** $p<0.01$, *** $p<0.001$ and *** $p<0.0001$. B. Data in (A) corrected for ROX. One-way ANOVA and Tukey's post hoc test was used to analyse the data, * $p<0.05$.

6.3.6 Mutation of tyrosine 447 to alanine in the Kv1.3-P121 mutant prevents Kv1.3 induced respiration in HEK293 cells.

HEK293/Kv1.3-P121 cells have a single point mutation of tyrosine to alanine at position 447 on the C-terminal of the Kv1.3 channel. This tyrosine is a putative phosphorylation site, which is thought to involve the MAP kinase ERK (Jimenez-Perez *et al.*, 2016), and so the Kv1.3-P121 channel is phosphorylation defective. The Routine, Leak, ETS and ROX Respiration in HEK293/Kv1.3-P121 cells was reduced compared to HEK293/Kv1.3 cells (Figure 6.8A). Maximum Uncoupled Respiration (ETS) of HEK293/Kv1.3-P121 cells was decreased below that of WT HEK293 cells (Figure 6.8A). When data was corrected for ROX (Figure 6.8B), Leak Respiration was not significantly different between the three cell types. Both Routine and ETS Respiration were reduced in HEK293/Kv1.3-P121 cells compared to HEK293/Kv1.3 cells (Figure 6.8B). These data suggest that the loss of the putative phosphorylation site on tyrosine 447 in Kv1.3-P121 channels reduces the Maximum Uncoupled Respiration in HEK293/Kv1.3-P121 cells. The reduced respiration of HEK293/Kv1.3-P121 cells is consistent with their reduced proliferation compared to HEK293/Kv1.3 cells (Figure 6.5).

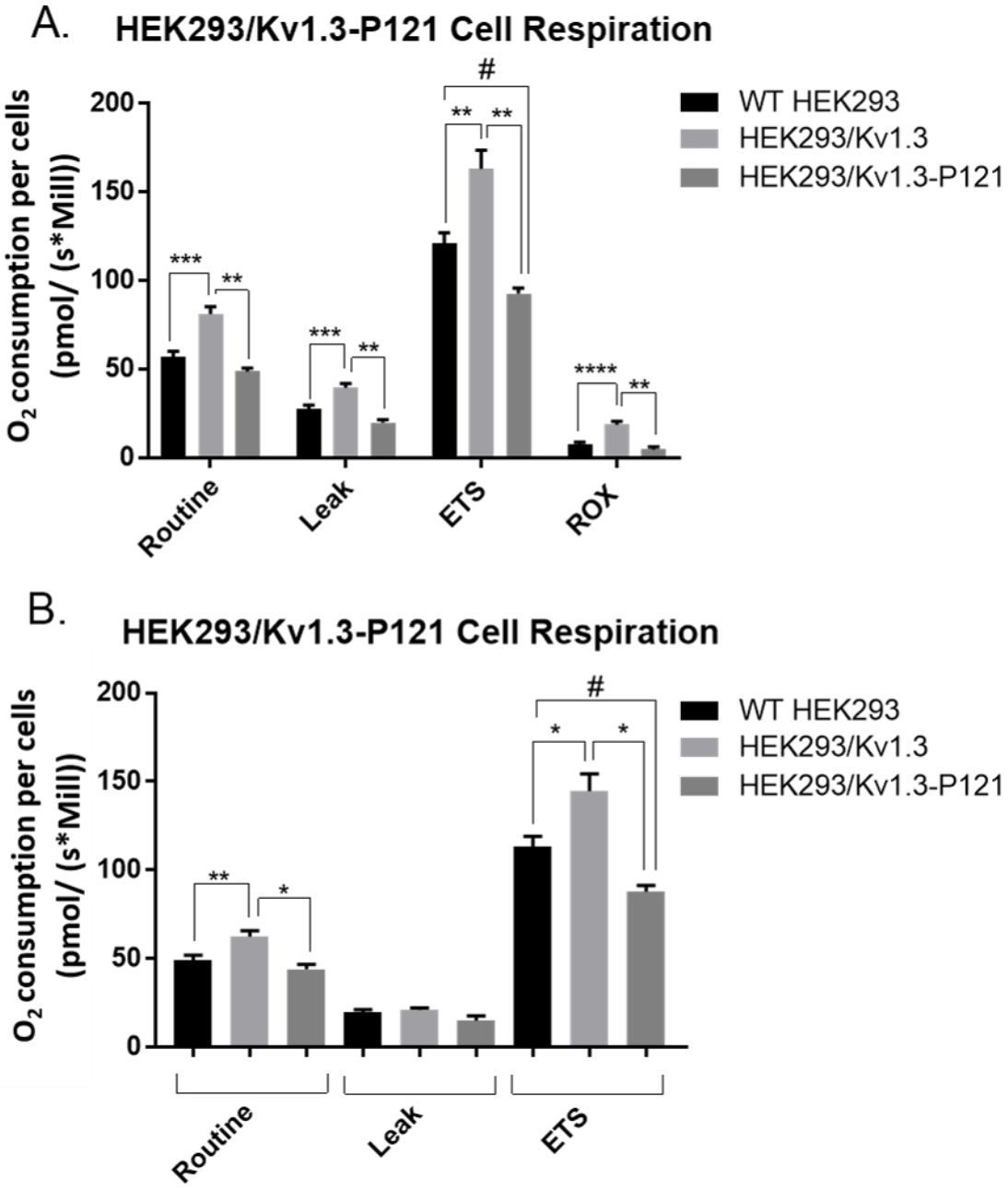

Figure 6.8 Mutation of tyrosine 447 to alanine on the C terminus of the Kv1.3-P121 channel abolishes Kv1.3 stimulated respiration in HEK293 cells. A. Respiration of WT HEK293 (black bars), HEK293/ Kv1.3 (light grey bars) and HEK293/Kv1.3-P121 (dark grey bars) cells. HEK293/Kv1.3 and WT HEK293 data is from total experiments (n=38 and n=27, respectively), HEK293/Kv1.3-P121 (n=6). Data is the mean O_2 consumption (O_2 per cells per second, pmol/(s*Mill)) uncorrected for residual O_2 consumption (ROX). One-way ANOVA and Tukey's post hoc test was used to analyse the data, ** $p<0.01$, *** $p<0.001$ and **** $p<0.0001$. Student's t-test found HEK293/Kv1.3-P121 ETS respiration significantly lower than in WT HEK293 cells, # = $p<0.05$. B. Data in (A) corrected for ROX. One-way ANOVA and Tukey's post hoc test was used to analyse the data, * $p<0.05$. Student's t-test found HEK293/Kv1.3-P121 ETS respiration significantly lower than in WT HEK293 cells, # = $p<0.05$.

6.3.7 Disruption of the Kv1.3 channel pore in the Kv1.3-P89 mutation did not abrogate Kv1.3-stimulated residual oxygen consumption in HEK293 cells.

On collection of the data from the standard respirometry assays, ROX Respiration in the mutant Kv1.3 HEK293 cells was analysed (Figure 6.9). In Chapter Three we showed that HEK293/Kv1.3 cells have increased ROX compared to WT HEK293 cells. As stated in Figure 6.6, HEK293/Kv1.3-P89 ROX Respiration was no different to HEK293/Kv1.3 cells, while HEK293/Kv1.3-P93 (Figure 6.7) and HEK293/Kv1.3-P121 (Figure 6.8) was significantly lower. In Figure 6.9, HEK293/Kv1.3-P89 ROX Respiration trended towards being around twice that of HEK293/Kv1.3-P93 cells, and around three times that of HEK293/Kv1.3-P121 cells. This may indicate that a voltage dependent conformational change in the Kv1.3 channel exposes key phosphorylation residues on the C-terminus of the channel, which are essential for stimulating the non-mitochondrial respiration in HEK293 cells. Phosphorylation of tyrosine 447 is especially important in this signalling pathway as mutation to alanine in HEK293/Kv1.3-P121 cells abolished Kv1.3 stimulated ROX Respiration (Figure 6.9), despite having a functional voltage sensing and K^+ conducting Kv1.3 channel.

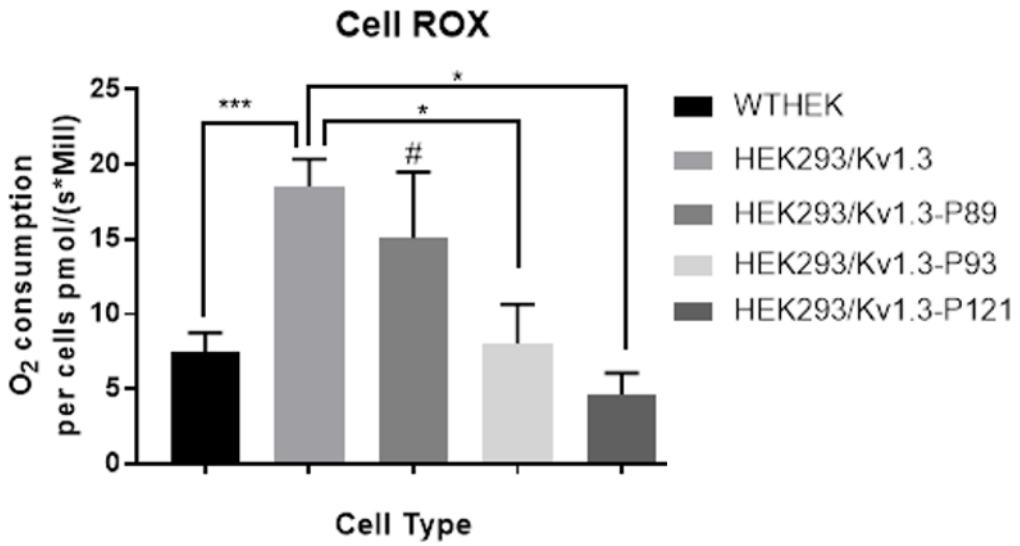

Figure 6.9 Comparison of Residual Oxygen Consumption in WT HEK293, HEK293/Kv1.3 and HEK293/Kv1.3 mutant cells. Data obtained and collated from previous figures (Figures 6.5, 6.6 and 6.7). Data expressed as the mean O_2 consumption per million cells per second (pmol/(s*Mill)) ± SEM. One-way ANOVA and Tukey's post hoc test was used to analyse the data, * $p<0.05$ and *** $p<0.001$. Student's t-test found HEK293/Kv1.3-P89 ROX was significantly higher than in WT HEK293 cells, # = $p<0.05$.

6.3.8 Mutation of the Kv1.3 pore independent of the voltage sensor did not affect Kv1.3 channel-stimulated ATP turnover in HEK293/Kv1.3-P89

From the respirometry data ATP turnover rate was calculated for WT, Kv1.3, Kv1.3-P121, Kv1.3-P89 and Kv1.3-P93 HEK 293 cells (Figure 6.10). HEK293/Kv1.3-P89 cells had a significantly higher ATP turnover rate than WT HEK293 cells, with no significant difference between the ATP turnover rate of HEK293/Kv1.3 and HEK293/Kv1.3-P89 cells (Figure 6.10). There was no difference between the ATP turnover in WT HEK293 cells, HEK293/Kv1.3-P93 and HEK293/Kv1.3-P121 cells (Figure 6.10). These data suggest that the Kv1.3 channel voltage sensor, but not the ion pore, contribute to Kv1.3 channel-mediated ATP turnover. The data also suggests that in HEK293/Kv1.3-P121 cells, the phosphorylation defective Kv1.3-P121 channel abolishes the Kv1.3 induced increase in ATP turnover, indicating the tyrosine 447 residue as being essential for the increased ATP turnover in HEK293/Kv1.3 cells.

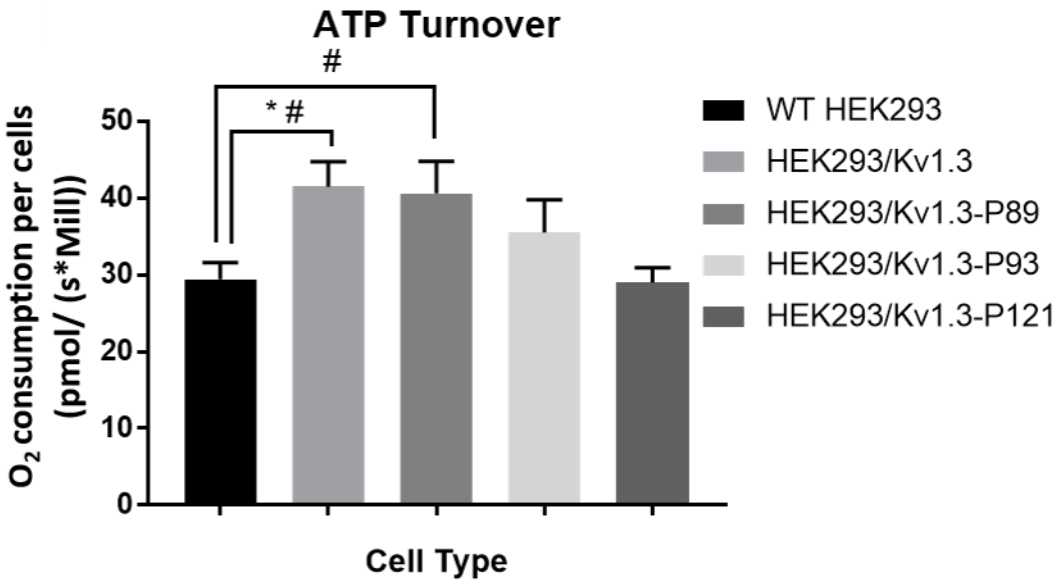

Figure 6.10 HEK293/Kv1.3-P89 cells have ATP turnover increased to WT HEK293 cells and no different to HEK293/Kv1.3 cells. ATP turnover rate in WT HEK293, HEK293/Kv1.3, HEK293/Kv1.3-P89, HEK293/Kv1.3-P93 and HEK293/Kv1.3-P121 cells (left to right columns). ATP turnover is the difference between routine respiration and leak respiration. Data expressed as the mean O_2 consumption per cells (pmol/(s*mill)) ± SEM (WT HEK293, n=27, HEK293/Kv1.3, n=38, HEK293/Kv1.3-P89, n=9, HEK293/Kv1.3-P93, n=9, HEK293/Kv1.3-P121, n=6). Data analysed using One-way ANOVA with Tukey's post hoc test, * $p<0.05$. Student's t-tests were used to analyse results, # $p<0.05$.

6.3.9 HEK293/Kv1.3-P121 cells had reduced spare respiratory capacity compared to WT HEK293 cells.

The spare respiratory capacity (SRC) was calculated for WT, Kv1.3, Kv1.3-P121, Kv1.3-P89 and Kv1.3-P93 HEK293 cells (Figure 6.11). Compared to WT HEK293 cells, none of the Kv1.3 mutant cell lines displayed an increased SRC (Figure 6.11), seen in HEK293/Kv1.3 cells. HEK293/Kv1.3-P121 cells had a significantly reduced SRC compared to WT HEK293 and HEK293/Kv1.3 cells (Figure 6.11), due to their significantly reduced ETS respiration (Figure 6.8). In contrast to previous data in this chapter, which showed both HEK293/Kv1.3 and HEK293/Kv1.3-P89 cells share a similar respiratory phenotype, with increased respiration compared to WT HEK293 cells, this was not the case for the SRC in these cells (Figure 6.11). The difference in SRC between HEK293/Kv1.3 and HEK293/Kv1.3-P89 cells could be due to the K^+ flow through the channel in HEK293/Kv1.3 cells, whereby the inability of K^+ flow through the Kv1.3 channel in HEK293/Kv1.3-P89 cells, due to the pore mutation, may prevent the increase in SRC. However, Kv1.3-P121 channels have similar biophysics to Kv1.3 channels, yet HEK293/Kv1.3-P121 cells had a reduced SRC compared to HEK293/Kv1.3 cells, suggesting it is not the flow of K^+ through the channel that contributes to the SRC. The data suggests that the presence of both the channel pore and the tyrosine 447 phosphorylation site are needed in unison for the increased SRC seen in HEK293/Kv1.3 cells.

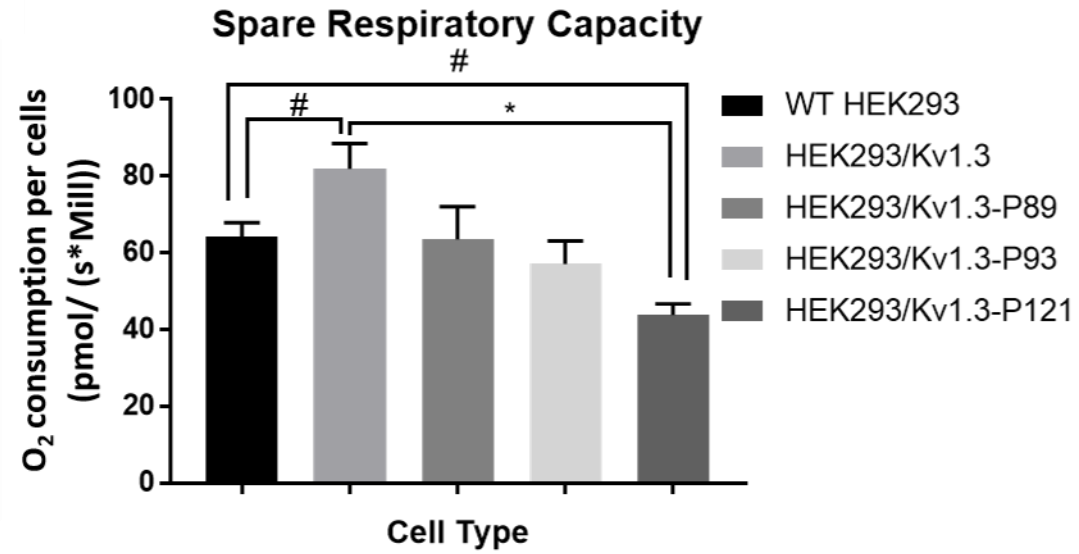

Figure 6.11 HEK293/Kv1.3-P121 cells have a reduced spare respiratory capacity compared to WT HEK293 and HEK293/Kv1.3 cells. Spare respiratory capacity in WT HEK293, HEK293/Kv1.3, HEK293/Kv1.3-P89, HEK293/Kv1.3-P93 and HEK293/Kv1.3-P121 cells (left to right columns). Spare respiratory capacity is the difference between routine respiration and maximum uncoupled respiration. Data expressed as the mean O_2 consumption per million cells per second (pmol/(s*mill)) ± SEM (WT HEK293, n=27, HEK293/Kv1.3, n=38, HEK293/Kv1.3-P89, n=9, HEK293/Kv1.3-P93, n=9, HEK293/Kv1.3-P121, n=6). Data analysed using one way ANOVA with Tukeys post hoc test, * $p<0.05$. Student's t-tests used to analyse results, # $p<0.05$.

6.4 Discussion

In this chapter we show that mutant Kv1.3 channels co-localise to the mitochondria in HEK293/Kv1.3-P89, HEK293/Kv1.3-P93 and HEK293/Kv1.3-P121 cells. Mitochondrial Kv1.3 channels have not previously been described in HEK293 cells. We confirmed that HEK293/Kv1.3-P89 cells have increased proliferation compared to WT HEK293 cells, and, since the Kv1.3-P89 mutant has a defective channel pore, that this was independent of K^+ flow through the channel. As the proliferation of HEK293/Kv1.3-P121 cells was no different to WT HEK293 cells, despite having voltage sensitive Kv1.3 channels with functional K^+ conduction, we confirmed that the presence of tyrosine at position 447 on the C-terminus of the channel is necessary for the Kv1.3 induced increase in proliferation (in HEK293/Kv1.3-P121 cells the tyrosine at 447 is mutated to alanine). These findings are in support of those described by Cidad et al., (2012) and Jimenez-Perez et al., (2016).

A link between Kv1.3 non-canonical functions and metabolism has not previously been explored. These results present a novel finding which shows that disruption of the Kv1.3 channel pore in HEK293/Kv1.3-P89 cells did not abrogate Kv1.3 stimulated respiration in HEK293 cells; however disruption of both the voltage sensor and the pore did impair Kv1.3 stimulated respiration (HEK293/Kv1.3-P93 cells). Therefore, the Kv1.3 voltage sensor must be key to increasing respiration in HEK293/Kv1.3 cells. In addition, it seems that the presence of tyrosine 447 on the C-terminal is also necessary to increase the respiration of HEK293 cells. Mutation of tyrosine 447 to alanine abolished the Kv1.3 stimulated respiration in HEK293/Kv1.3-P121 cells, despite the Kv1.3 channels in these cells having a functional voltage sensor and an intact pore. HEK293/Kv1.3-P121 cells also had significantly lower SRC than WT HEK293 cells, suggesting that under physiological conditions, tyrosine at position 447 in Kv1.3 channels is essential for maintaining respiration in HEK293 cells. However, presence of tyrosine 447 must not be the only factor which contributes to SRC, as HEK293/Kv1.3-P89 cells have a SRC no different to WT HEK293 cells, despite having intact tyrosine 447 at the C-terminus. This suggests that in addition to tyrosine 447, K^+ flow through the Kv1.3 channel may also contribute to the increased SRC seen in HEK293/Kv1.3 cells. Also, our results indicate that increased non-mitochondrial respiration (ROX) in

HEK293/Kv1.3 cells may depend on the presence of a functional voltage sensor and tyrosine 447. HEK293/Kv1.3-P89 cells had ROX Respiration no different to HEK293/Kv1.3 cells, but this was abolished in cells with a mutated Kv1.3 channel voltage sensor (HEK293/Kv1.3-P93 cells) or had tyrosine 447 on their C-terminus substituted to alanine (HEK293/Kv1.3-P121 cells). This suggests that the Kv1.3 channel effects respiration at other locations in the cell, in addition to in the mitochondria, and this depends on the channel having a functional voltage sensor and tyrosine 447 at the C-terminus. Non-mitochondrial O_2 consumption has been described at the cell surface (Herst *et al*., 2004, 2008; Herst and Berridge, 2006) due to trans-plasma membrane electron transport (t-PMET). T-PMET is ubiquitous to all cells (Principe *et al.*, 2011) and is involved in NADH redox regulation (Herst *et al*., 2004). It functions to recycle NADH to NAD^+, which is necessary to maintain glycolysis and proliferation in some highly proliferating cells, like leukemic cancer cells (Herst and Berridge, 2007). As in the mitochondrial ETS, O_2 is the terminal electron acceptor in t-PMET, and so an increase in t-PMET would lead to increased O_2 consumption at the membrane. NADPH oxidases are a class of enzymes which contribute to t-PMET, and are another source of O_2 consumption at the plasma membrane as they reduce O_2 to superoxide (Principe *et al.*, 2011). In Chapter Five, HEK293/Kv1.3 cells were found to have higher NADH autofluorescence, and so t-PMET may be higher in these cells, possibly contributing to the higher level of ROX compared to WT HEK293 cells. It is possible that Kv1.3 channels may contribute to O_2 consumption at the plasma membrane, by a yet unknown mechanism. This may involve a cell signalling cascade involving ERK, as mutation of tyrosine to alanine in HEK293/Kv1.3-P121 cells renders the channels phosphorylation defective at tyrosine 447 (Jimenez-Perez *et al.*, 2016) and is sufficient to abolish the increased ROX. T-PMET has been found to have roles in cell signalling involving the phosphorylation and activation of other protein kinases, such as $p70^{S6K}$. Interestingly, T-PMET dependent phosphorylation of $p70^{S6K}$ is needed for ribosomal protein synthesis which supports proliferation in skeletal muscle (Kelly et al., 2018), which suggests t-PMET may also support proliferation in other cells and by other cell signalling cascades. T-PMET cell signalling depends on generation of ROS from NADPH oxidases in the plasma membrane (Kelly et al., 2018). Therefore, a link between plasma membrane Kv1.3 channels, phosphorylation of tyrosine 447 on the C-terminus, ROS generation and proliferation may exist and warrants further exploration.

The lack of a channel pore in HEK293/Kv1.3-P89 cells did not affect the ATP turnover rate, but mutation of the voltage sensor (HEK293/Kv1.3-P93) and tyrosine 447 on the C-terminus (HEK293/Kv1.3-P121) did reduce it. This suggests that the voltage sensor and tyrosine 447 in Kv1.3 channels are key to the maintenance of ATP turnover in HEK293 cells. For the first time we have shown that the non-conducting properties of Kv1.3 channels can affect cellular respiration. Not only do these non-canonical properties of the Kv1.3 channel increase OXPHOS of HEK293 cells, but they appear to also increase non-mitochondrial respiration. These Kv1.3 mediated changes to respiration result in an increase in ATP turnover which may then support cellular proliferation. In the quest for new therapeutics for proliferative disorders with a Kv1.3 channel component, such as atherosclerosis, restenosis and hypertension, this research suggests potential new drug targets, including the channel voltage sensor and putative phosphorylation site, tyrosine 447. Specific targeting of signalling pathways which prominently increase proliferation means that selective treatments with minimal side effects can be developed. What remains to be confirmed is the signalling cascades and mechanisms which underly how the non-conducting properties of Kv1.3 channels can mediate respiration and proliferation.

Several of the observed effects of Kv1.3 on HEK293 respiration are dependent on both a functioning voltage sensor and presence of an intact tyrosine residue at position 447 on the C-terminus of the Kv1.3 channel. Therefore, a signalling pathway may link the putative phosphorylation of tyrosine 447 to the respiration of HEK293 cells. Upon voltage sensing, it is thought the Kv1.3 channel undergoes a conformational change which exposes key residues on the C-terminal to various kinases (Jimenez-Perez *et al.*, 2016; Lopez-Lopez, Cidad and Perez-Garcia, 2018; Perez-Garcia, Cidad and Lopez-Lopez, 2018). There are three key residues on the C-terminus of Kv1.3 channels which can abolish Kv1.3 stimulated proliferation when they are mutated (Jimenez Perez *et al*., 2016). Tyrosine 447, serine 459 and tyrosine 477 all abolish Kv1.3 induced proliferation when they are mutated to alanine, with tyrosine 447 having the most potent effects (Jimenez Perez *et al*., 2016). The mechanism by which these residues increase proliferation is not clear, however, at least for the case of tyrosine 447, it is thought to involve phosphorylation of the residue by ERK1/2 (extracellular signal related kinase). ERK1/2 is involved in Kv1.3 induced proliferation of VSMCS because

treatment of these cells with either blockers of the channel, or of the ERK1/2 signalling pathway inhibited VSMC proliferation in a non-additive fashion (Cidad *et al.*, 2015). In VSMCs the exact ERK signalling cascades have not been confirmed. The results from this work and Jimenez Perez et al.'s work (2016) present the possibility that phosphorylation of tyrosine 447 on the mitochondrial Kv1.3 channel may increase respiration and proliferation of HEK293 cells via an ERK1/2 dependent pathway. Therefore, the possibility of mitochondria as key signalling organelles in Kv1.3 induced cell proliferation must be considered. Interestingly, many kinases like PKC, PKA, Akt and MAPKs have already been found to participate in mitochondrial signalling pathways (Antico Arciuch *et al.*, 2009). ERK has also been observed to localise to the mitochondria (Wainstein and Seger, 2016), where it is found near the IMM, IMS and OMM.

Our results would suggest that availability of tyrosine 447 on the Kv1.3 channel increases respiration. Kinases, such as ERK1/2 have been found to have a role in energy homeostasis. For example, ERK1/2 can increase lipolysis in adipocytes (Jeong *et al.*, 2015), which would increase the substrates available for the TCA cycle and therefore increase the activity of the ETS. ERK1/2 has also been found to regulate the transition by which adipocytes change from energy-storing white cells to energy-consuming brown cells, by increasing O_2 consumption and uncoupling protein in the mitochondria (Zhang *et al.*, 2016). HEK293/Kv1.3-P89 cells (poreless mutants with accessible tyrosine 447 on the C-terminus) had increased mitochondrial O_2 consumption and ROX compared to WT HEK293 cells. As mentioned previously, a source of non-mitochondrial O_2 consumption is t-PMET at the cell surface. T-PMET is dependent on glycolysis (and the TCA cycle) to generate NADH, because for O_2 to be reduced at the plasma membrane, electrons from NADH must be donated to a ubiquinone in the plasma membrane. In highly proliferating cancer cells, an increase in glucose entering the cell via GLUT1, and an increase in hexokinase activity (the enzyme that catalyses the first step of glycolysis, generating glucose-6-phosphate), increases the amount of t-PMET and O_2 consumption. Therefore, the level of non-mitochondrial O_2 consumption is very much dependent on the level of glycolysis. In HEK293/Kv1.3 cells, results in Chapter Five indicated that they had increased glycolysis compared to WT HEK293 cells. If glycolysis increases non-mitochondrial O_2 consumption at the

plasma membrane, then an increase in ROX in HEK293/Kv1.3-P89 cells suggests they too have an increase in glycolysis. Interestingly, ERK has been found to regulate glucose entry into proliferating cells via its activation of the transcription factor, c-myc, which increases GLUT1 at the plasma membrane (Papa, Choy and Bubici, 2019). An increase in glucose entering HEK293/Kv1.3 cells may lead to an increase in glycolysis, and thus generation of NADH. An increase in T-PMET would need to occur in order to minimise reductive stress (an increase in NADH), which would inhibit respiratory pathways if NAD^+ was unavailable for reduction. An increase in t-PMET in HEK293/Kv1.3 cells may also contribute to the increased ROS seen in these cells (Chapter Five), as activity of NADPH oxidases in the plasma membrane generate superoxide. The levels of ROS in the mutant Kv1.3 cells would need to be determined in future work.

Regardless of the extent to which non-mitochondrial respiration is mediated by Kv1.3 channels, HEK293/Kv1.3-P89 cells still displayed increased mitochondrial respiration compared to WT HEK293 cells. Ion-conduction independent roles for the channels must exist and are likely to involve phosphorylation of tyrosine 447 on the C-terminus. Interestingly, there exists ROS dependent, ERK mediated mitochondrial-nuclear communication in Leydig cells (Galli *et al.,* 2008). Galli *et al*., (2008) demonstrate that low levels of ROS can initiate oxidation and translocation of ERK to the nucleus, whilst high levels of ROS can inhibit activation of ERK. If ERK is ROS dependent, then the levels of ROS exhibited in HEK293/Kv1.3 and HEK293/Kv1.3-P89 cells may be optimum for ERK activation, leading to translocation of ERK to the nucleus and stimulation of proliferation. The level of ROS in a cell is also linked to its SRC. The SRC provides the mitochondria with extra capacity during times of oxidative stress and is therefore important for cell survival (Nicholls and Ferguson, 2013). The higher the basal ROS level in cells, the higher the SRC would be expected to be. A low SRC in phosphorylation defective HEK293/Kv1.3-P121 cells indicates these cells are less able to cope with oxidative stress than their WT Kv1.3 counterpart (Brand and Nicholls, 2011). The high SRC in HEK293/Kv1.3 cells may be an adaptation to a higher level of ROS, generated in part by the increased mitochondrial (and perhaps non-mitochondrial) respiration in these cells. The reduction in SRC in HEK293/Kv1.3-P121 cells, compared to both WT HEK293 and HEK293/Kv1.3 cells, suggests that

phosphorylation of tyrosine 447 initiates a signalling cascade which is important for normal cellular respiration and the ability of the respiratory system to adapt to changes in the oxidative environment.

It is important to note that non-conducting roles of the channel are not the only mechanism by which Kv1.3 channels increase proliferation. Proliferation is significantly different between the HEK293/Kv1.3 and HEK293/Kv1.3-P89 cells, but their respiration is the same. This confirms that there must be non-metabolic and/or K^+ conduction dependent Kv1.3 mechanisms contributing to the proliferative phenotype of HEK293/Kv1.3 cells. For example, hyperpolarisation from K^+ flow through plasma membrane K channels has previously been found to be necessary for proliferation of VSMCs (Neylon *et al.*, 1999; Ivanov *et al.*, 2006). As previously mentioned, multiple mechanisms have been proposed for Kv1.3 induced proliferation and they may not be mutually exclusive (Lopez-Lopez, Cidad and Perez-Garcia, 2018). These mechanisms involving K^+ conductance, such as regulation of membrane potential, cell volume and intracellular Ca^{2+} concentration could also be contributing to the increased proliferation rate of HEK293/Kv1.3 cells (Lopez-Lopez, Cidad and Perez-Garcia, 2018).

Currently we are only able to speculate, based on the literature, that ERK is involved in the proliferation and respiration of mutant Kv1.3 cells. Furthermore, we do not explore the contributions to proliferation and respiration of the other phosphorylation residues on the Kv1.3 C-terminus and potential associated signalling mechanisms. We are unable to confirm whether the increase in respiration driven by Kv1.3 is directly linked to the proliferative phenotype of the channel.

To build on the data found in Chapter Five, it would be interesting to measure MMP, cell ROS, glycolysis and NADH levels in HEK293/Kv1.3-P89, H3K293/Kv1.3-P93 and HEK293/Kv1.3-P121 cells. This would enable us to identify whether key sites on the Kv1.3 channel were responsible for changing the unique phenotypes observed in these parameters via a cell signalling mechanism. Moreover, inhibition of respiration, whilst measuring proliferation would confirm if the increased respiration in HEK293/Kv1.3-P89 cells does generate the energy required to drive the proliferative phenotype. Treatment of cells with the antioxidant MitoQ would allow us to determine if ROS contributed to the increased proliferation in HEK293/Kv1.3 cells. Treating the HEK293/Kv1.3 and Kv1.3-P121 cells with an inhibitor of the ERK signalling pathway and

monitoring proliferation and respiration would be important to investigate the potential Kv1.3/mitochondrial/nuclear signalling cascades. Finally, it will be important to identify other putative phosphorylation residues on the Kv1.3 channel which may affect respiration.

In summary, Kv1.3 channels increase cellular respiration in a K^+ conduction-independent manner which requires an intact voltage sensor and the putative phosphorylation site at tyrosine 447 of the C-terminal region. The proliferation rate of HEK293/Kv1.3 mutant clones mirrors the respiration rate. This may suggest that cell signalling via the Kv1.3 channel stimulates respiration in the mitochondria, which provides the energy for proliferation. Non-conducting mutant channels also have increased ROX. Future identification of the non-conducting Kv1.3 mechanisms which drive changes in metabolism will be needed.

Chapter Seven

General Discussion and Future Directions

7.1 Summary

Pathological proliferation of VSMCs occurs in vascular diseases like atherosclerosis, hypertension and restenosis (Owens, 1988; Lusis, 2000; Rzucidlo, Martin and Powell, 2007). Atherosclerosis and hypertension lead to vascular remodelling which can result in myocardial infarction and stroke, two of the most common causes of death in the western world (World Health Organisation, 2018). The number of deaths from these conditions are expected to rise in coming years (Khavjou, Phelps and Leib, 2016; Wilkins *et al.*, 2017). An additional concern is that the incidence of these morbidities in developing countries is rising (Gaziano *et al.*, 2010). A better understanding of the mechanisms which drive pathological proliferation of VSMCs is of upmost importance to reduce the numbers of deaths from CVD. The phenotypic switch in VSMCs sees them change from contractile cells, to proliferative and secretory cells (Owens, Kumar and Wamhoff, 2004). The Kv1.3 channel has been implicated in this phenotypic switch, but the mechanism underlying how it contributes to proliferation is a subject of debate (Perez-Garcia, Cidad and Lopez-Lopez, 2018). Elucidating the mechanisms driving this proliferation will be key to the development of new therapies. Previously thought to only exist in the plasma membrane, the Kv1.3 channel has now been found at multiple intracellular positions, notably on membranes of the nucleus, the cis-Golgi and the mitochondria (Szabo *et al.*, 2005; Zhu, Yan and Thornhill, 2014; Jang *et al.*, 2015). The contribution of these intracellular Kv1.3 channels to VSMC proliferation has not been explored. However, a role for mitochondrial Kv1.3 channels in the apoptosis of cancer cells has been described (Szabó *et al.*, 2008; Leanza *et al.*, 2017; Venturini *et al.*, 2017; Mattarei *et al.*, 2018). Whether these channels regulate *physiological* mitochondrial functions was not known. This work aimed to explore the role of mitochondrial Kv1.3 channels in HEK293 cell proliferation and respiration. The work was carried out in

stable ion channel overexpression HEK293 cell system (Scragg *et al.*, 2008; Cidad *et al.*, 2010, 2012; Duckles *et al.*, 2015; Jimenez-Perez *et al.*, 2016).

7.2 Principle Findings

In Chapters Three and Four, the relationship between mitochondrial Kv1.3 channels, proliferation and respiration were assessed in HEK293/Kv1.3 cells. In line with previous reports (Cidad *et al.*, 2012), overexpression of Kv1.3 channels in HEK293 cells increased their proliferation. For the first time, we reported that overexpression of Kv1.3 in HEK293 cells increased respiration, correlating to increased ATP turnover and SRC. Increased respiration in HEK293/Kv1.3 cells could not be attributed to differences in mitochondrial number or mitochondrial network structure, despite some suggestions that Kv1.3 may alter these parameters (DeCoursey *et al.*, 1984; Kovach *et al.*, 2016). Kv1.3 channels were detected in the mitochondria of HEK293 cells and HSVSM cells. While mitochondrial channels have been found in various cells types (Szabo *et al.*, 2005; Bednarczyk *et al.*, 2010; Cheng, Debska-Vielhaber and Siemen, 2010; Leanza *et al.*, 2017; Mattarei *et al.*, 2018), this is the first report of their location in HSVSMCs. Targeted inhibition of these channels reduces proliferation and respiration in HEK293 cells, which opens up the possibility that the channels may have a physiological role in increasing these processes in proliferating VSMCS, where Kv1.3 is upregulated (Cidad *et al.*, 2010; Cheong *et al.*, 2011).

The mechanisms behind mitochondrial Kv1.3 induced respiration and proliferation in HEK293 cells were further elucidated. Chapter Five presented data suggesting increased cellular glycolysis and NADH, a more hyperpolarised MMP and an increase in ROS level in HEK293/Kv1.3 cells. Inhibition of mitochondrial Kv1.3 with 100nM PAPTP had no effect on overall MMP but was able to increase leak respiration in HEK293 cells, suggesting that it could hyperpolarise the MMP. This indicates that while K^+ flow through mitochondrial Kv1.3 depolarises the MMP, it is not large enough to affect the overall MMP in HEK293 cells. This is in line with previous reports suggesting K^+ flow into the mitochondria through IMM channels has little effect on the MMP (Kowaltowski *et al.*, 2001; Heinen *et al.*, 2007). We speculated that the increased glycolysis in HEK293/Kv1.3 cells could be the reason behind the hyperpolarisation of the MMP (Beltrán *et al.*, 2000; Poulsen *et al.*, 2008; Olsen *et al.*, 2009; Forrest, 2015),

but further work is required to confirm this. A hyperpolarised MMP would increase the protonmotive force between the IMS and the matrix, and thus would increase ATP production at the ATP synthase (Nicholls and Ferguson, 2013). In addition, glycolysis may have additional functions in supporting the biosynthesis of molecules necessary for growth (Vander Heiden, Cantley and Thompson, 2009). Increased mitochondrial NADH may also result from the increased glycolysis (Herst and Berridge, 2006; Vander Heiden, Cantley and Thompson, 2009). As mitochondrial Kv1.3 had no effect on the NADH level in HEK293/Kv1.3 cells, the increase in NADH may have originated from non-mitochondrial metabolism (Herst and Berridge, 2006, 2007). Increased NADH delivery to complex one would result in more electrons being donated to the ETS, leading to increased proton pumping and ATP synthesis via the ATP-synthase (Nicholls and Ferguson, 2013). In addition, increased NADH would result in increased ROS formation caused by electron slip at the complexes (Nicholls and Ferguson, 2013). These ROS were found to have direct stimulatory effects on proliferation of HEK293/Kv1.3 cells. Thus, in the case of HEK293 cells, glycolysis and OXPHOS are both upregulated and may complement each other to maximise ATP production and support growth.

The influence of non-conducting roles of Kv1.3 (Cidad *et al.*, 2012; Jimenez-Perez *et al.*, 2016) on cellular respiration were further investigated in Chapter Six. It had previously been established that a functional voltage sensor and intact phosphorylation residues on the C-terminus of Kv1.3 channels were necessary to increase proliferation in HEK293 cells (Cidad *et al.*, 2012; Jimenez-Perez *et al.*, 2016). It is suggested that upon sensing of voltage, there is a conformational change in the Kv1.3 channel, which along with opening the channel pore can expose key residues to phosphorylation, which activates a signalling cascade regulating proliferation. Three residues, tyrosine 447, serine 459 and threonine 477 were involved in Kv1.3 induced proliferation(Jimenez-Perez *et al.*, 2016). Tyrosine 447 was identified as being part of a signalling pathway, involving phosphotyrosine activation and ERK1/2 activity (Jimenez Perez *et al*., 2016). ERK1/2 is involved in cell proliferation, most commonly by increasing the transcription of cell cycle machinery (Mebratu and Tesfaigzi, 2009). In Chapter Six, we used Kv1.3 channel mutants to investigate their effects on respiration in HEK293 cells. It was found that to increase respiration, K^+ conduction through Kv1.3 was unnecessary, as

non-conducting pore mutants which had a functioning voltage sensor and intact tyrosine 447 increased respiration in HEK293 cells to a similar extent as was observed in HEK293/Kv1.3 cells. These results correlated with an increased rate of proliferation in these cells (Cidad *et al.*, 2012; Jimenez-Perez *et al.*, 2016). The increase in respiration in these pore mutants correlated to an increased ATP turnover rate and ROX. As glycolysis contributed significantly to both these parameters in HEK293/Kv1.3 cells (Chapter Five), it suggests that glycolysis may also be increased in the pore mutants and future experiments will be required to confirm this. Glycolysis would increase NADH levels and t-PMET activity, leading to O_2 consumption at the cell surface (Herst *et al.*, 2004) which would contribute to ROX. In addition t-PMET is regulated by oxidases in the plasma membrane, such as NOX1, which would produce ROS, further increasing ROX (Kelly *et al.*, 2018). An increase in glycolysis (and the associated NADH) and an increase in OXPHOS, would likely increase ROS in HEK293/Kv1.3-P89 cells (Nicholls and Ferguson, 2013) as was the case in HEK293/Kv1.3 cells with a similar respiratory profile. In support of this, the increased ROX in HEK293/Kv1.3-P89 cells suggests that ROS is higher in these cells, which may then contribute to their higher level of proliferation (as in HEK293/Kv1.3 cells). In addition, other sources of non-mitochondrial O_2 consumption may contribute to HEK293/Kv1.3 ROX, for example desaturase enzymes involved in lipid metabolism (Shanklin *et al.*, 2009) or P450 types enzymes involved in the metabolism of various substances (Lynch and Price, 2007; Guengerich, Waterman and Egli, 2016).The conclusions from Chapter Six identified that the Kv1.3 channel can increase respiration via non-canonical cell signalling pathways, which rely on the presence of a functional voltage sensor and presence of tyrosine 447 on the C-terminus. Although the exact cell signalling pathways are unknown, availability of tyrosine 447 suggests that phosphotyrosine and ERK1/2 could be involved (Jimenez Perez *et al*., 2016). We have shown that the Kv1.3 channel has profound effects on cellular bioenergetics which may regulate Kv1.3 induced proliferation. Importantly, there are some key areas for future work which have arisen from this study.

7.3 Future Work

Identification of non-conducting roles of *mitochondrial* Kv1.3 channels

We show that mitochondrial Kv1.3 has a direct role in respiration and proliferation in HEK293 cells. In Chapter Six, we can only deduce that the mutated Kv1.3 channel, which retains its ability to sense voltage and expose tyrosine 447, increases respiration. Treatment of all three mutant Kv1.3 cell types used in Chapter Six with PAPTP, PAP-1 and SHK-Dap22 would be essential to dissect the contributions of the signalling by Kv1.3 channels at different cellular locations. Using these inhibitors, with the mutants, it would also be necessary to measure other parameters such as glycolysis and ROS to identify their origin.

Identification of the Kv1.3 signalling pathways involved

Based on previous work (Cidad *et al.*, 2012; Jimenez-Perez *et al.*, 2016) we can only hypothesise that ERK1/2 is involved in the signalling cascade from Kv1.3 tyrosine 447. Its mitochondrial localisation (Antico Arciuch *et al.*, 2009), roles in mitochondrial-nuclear signalling (Poderoso *et al.*, 2008; Galli *et al.*, 2009), potential to phosphorylate ETS complexes (Kowalczyk and Zablocka, 2008), role as an ATP sensor in the mitochondria (Monick *et al.*, 2008) and ability to regulate glycolysis (Papa, Choy and Bubici, 2019) make it an attractive candidate as a signalling molecule involved in Kv1.3 induced respiration and proliferation. Investigations could focus on knock-down of ERK1/2 and subsequent measurement of respiration (glycolysis and OXPHOS) and proliferation. As there are additional phosphorylation residues on the Kv1.3 C-terminal which have been found to contribute to the non-canonical regulation of proliferation (Jimenez Perez *et al*., 2016), it would also be necessary to investigate if any additional phosphorylation residues on the Kv1.3 channel that stimulate respiration and proliferation.

Characterising increased glycolysis in HEK293/Kv1.3 cells

Investigation into the ERK 1/2 signalling pathway may shed light onto how Kv1.3 causes a coordinated increase in glycolysis, as many signalling pathways and kinases have been found to be involved in regulating glycolysis (Ward and Thompson, 2012). It would also be interesting to measure the enzymes which regulate glycolysis in WT

HEK293 vs HEK293/Kv1.3 vs HEK293/Kv1.3 mutants to assess if the Kv1.3 channel is involved in upregulating them. Increased glycolysis may provide energy for the enhanced OXPHOS by providing the TCA cycle with increased pyruvate. In terms of measuring the effects of glycolysis upregulation on HEK293 cells, it would be interesting to inhibit/stimulate glycolysis in HEK293 cells and measure MMP and NADH and ROS to determine if these parameters were affected by glycolysis. And finally, treating cells with PAPTP, PAP-1 and SHK-Dap22 before measuring glycolysis could help identify any effects of specific cellular populations of Kv1.3 channels on glycolysis.

Measurement of t-PMET

Increased ROX and glycolysis in HEK293/Kv1.3 cells suggests that t-PMET may also be increased in these cells to limit reduction stress and maintain glycolysis, which may contribute to the proliferation of these cells (Herst and Berridge, 2006, 2007; Kelly *et al.*, 2018). Measurement of t-PMET would need to be carried out to confirm this as an alternative mechanism of ROS generation (Kelly *et al.*, 2018). Methods could include measuring the disappearance of the electron donor NADPH, measuring ubiquinone reduction or measuring hydroquinone oxidation (Principe *et al.*, 2011). In addition, monitoring the reduction of artificial electron acceptors like ferricyanide using ^{13}C nuclear magnetic resonance spectroscopy would allow real-time measurement of t-PMET using a non-invasive technique (Himmelreich and Kuchel, 1997).

Determination of the physiological relevance of Kv1.3 in human primary models

This work would first need to be extended into HSVSMCs. Initial results, showing PAP-1 reduces HSVMC proliferation and Kv1.3 channels exist in the mitochondria of HSVSMCs (Chapter Three) suggests this work in HEK293 cells may be translatable to HSVSMCs. Identification of the effect of PAPTP on HSVSMC respiration and proliferation is essential, as is determining the contribution of ROS to proliferation in these cells. Inhibiting signalling molecules like phosphotyrosine and ERK1/2 would also be necessary to examine if the non-conducting roles of Kv1.3 channels translate in HSVSMCs. Finally, this work would need to move into in vivo knockout mouse models to further explore the mechanisms. Mouse models of hyperplasia could be used to elucidate clinical relevance and determine if mitochondrial Kv1.3 channel blockers are viable drug targets in whole organisms to reduce Kv1.3 induced proliferation.

Optimisation of mitochondrial Kv1.3 inhibitors

The initial findings in this thesis support a role for mitochondrial Kv1.3 inhibitors such as PAPTP in reducing Kv1.3 induced proliferation and respiration. Further work is needed to optimise the dosage and specificity which allows for the optimum inhibition of respiration and proliferation without off target effects. There is likely a key window where the therapeutic potential of mitochondrial Kv1.3 inhibitors exceeds potential detrimental effects on respiration. In addition, the mitochondrial content of cells varies among individuals and tissue type and depends on a variety of factors, such as age and activity levels (Chistiakov *et al.*, 2014; Marquez and Han, 2017). To minimise off target effects on mitochondrial function, mitochondrially targeted pro-drugs such as PAPOH could be a better alternative to TPP containing molecules which may lead to TPP build up in the mitochondria over time (Nicholls and Ferguson, 2013; Leanza *et al.*, 2017). PAPTP and other mitochondrial Kv1.3 inhibitors have received attention as putative therapeutics in the cancer field (Leanza *et al.*, 2017; Venturini *et al.*, 2017; Checchetto *et al.*, 2018; Mattarei *et al.*, 2018) for their specificity to target pathological cells. This relies on drugs like PAPTP and PAPOH being attracted to the negatively charged mitochondrial matrix. This characteristic of these molecules is exploited since cancer cells, like HEK293/Kv1.3 cells, exhibit greater hyperpolarisation of the MMP than WT cells. Therefore, these molecules selectively accumulate in diseased cells (Leanza et al., 2017).

7.4 Conclusions

Kv1.3 channels contribute to normal mitochondrial function in HEK293 cells. The Kv1.3 channel may also increase glycolysis to fuel enhanced OXPHOS. Thus, there are two fundamental differences in the metabolism of WT HEK293 cells and HEK293/Kv1.3 cells; HEK293/Kv1.3 cells have both increased glycolysis and increased OXPHOS. In addition, HEK293/Kv1.3 cells have increased levels of ROS which may drive proliferation. Enhanced cellular respiration driven by Kv1.3 is independent of K^+ flow through the Kv1.3 channel. However, a functioning voltage sensor and putative phosphorylation site, tyrosine 447, are essential for Kv1.3 driven respiration. Further investigation into the non-canonical mechanisms which lead to Kv1.3 induced respiration and proliferation are needed. However, targeting potential therapies to

subcellular organelles may be a novel way to increase the specificity and thus reduce side effects in treatment of Kv1.3 induced proliferative disorders.

References

Abcam (no date) *Beta Oxidation of Fatty Acids*. Available at: https://www.abcam.com/pathways/fatty-acid-oxidation (Accessed: 19 November 2019).

Affourtit, C. and Brand, M. D. (2009) 'Measuring mitochondrial bioenergetics in INS-1E insulinoma cells.', *Methods in enzymology*. United States, 457, pp. 405–424. doi: 10.1016/S0076-6879(09)05023-X.

Al-Owais, M. M. *et al.* (2015) 'Heme Oxygenase-1 Influences Apoptosis via CO-mediated Inhibition of K+ Channels.', *Advances in experimental medicine and biology*. United States, 860, pp. 343–351. doi: 10.1007/978-3-319-18440-1_39.

Al-Owais, M. M. *et al.* (2017) 'Multiple mechanisms mediating carbon monoxide inhibition of the voltage-gated K+ channel Kv1.5', *Cell Death &Amp; Disease*. The Author(s), 8, p. e3163.

Alexander, M. R. and Owens, G. K. (2012) 'Epigenetic control of smooth muscle cell differentiation and phenotypic switching in vascular development and disease.', *Annual review of physiology*. United States, 74, pp. 13–40. doi: 10.1146/annurev-physiol-012110-142315.

Alonso-Carbajo, L. *et al.* (2017) 'Muscling in on TRP channels in vascular smooth muscle cells and cardiomyocytes', *Cell Calcium*, 66, pp. 48–61. doi: https://doi.org/10.1016/j.ceca.2017.06.004.

Antico Arciuch, V. G. *et al.* (2009) 'Mitochondrial kinases in cell signaling: Facts and perspectives.', *Advanced drug delivery reviews*. Netherlands, 61(14), pp. 1234–1249. doi: 10.1016/j.addr.2009.04.025.

Aon, M. A. *et al.* (2010) 'Energetic performance is improved by specific activation of K+ fluxes through KCa channels in heart mitochondria', *Biochimica et Biophysica Acta (BBA) - Bioenergetics*, 1797(1), pp. 71–80. doi: https://doi.org/10.1016/j.bbabio.2009.08.002.

Attali, B. *et al.* (1997) 'Characterization of delayed rectifier Kv channels in oligodendrocytes and progenitor cells.', *The Journal of neuroscience : the official*

journal of the Society for Neuroscience. United States, 17(21), pp. 8234–8245.

Augoff, K., Hryniewicz-Jankowska, A. and Tabola, R. (2015) 'Lactate dehydrogenase 5: an old friend and a new hope in the war on cancer.', *Cancer letters*. Ireland, 358(1), pp. 1–7. doi: 10.1016/j.canlet.2014.12.035.

Bajgar, R. *et al.* (2001) 'Identification and properties of a novel intracellular (mitochondrial) ATP-sensitive potassium channel in brain.', *The Journal of biological chemistry*. United States, 276(36), pp. 33369–33374. doi: 10.1074/jbc.M103320200.

Ballinger, S. W. (2005) 'Mitochondrial dysfunction in cardiovascular disease', *Free Radical Biology and Medicine*. Elsevier, 38(10), pp. 1278–1295.

Bartok, A. *et al.* (2014) 'Margatoxin is a non-selective inhibitor of human Kv1.3 K+ channels.', *Toxicon : official journal of the International Society on Toxinology*. England, 87, pp. 6–16. doi: 10.1016/j.toxicon.2014.05.002.

Bednarczyk, P. *et al.* (2010) 'Identification of a voltage-gated potassium channel in gerbil hippocampal mitochondria.', *Biochemical and biophysical research communications*. United States, 397(3), pp. 614–620. doi: 10.1016/j.bbrc.2010.06.011.

Bednarczyk, P. *et al.* (2013) 'Putative Structural and Functional Coupling of the Mitochondrial BKCa Channel to the Respiratory Chain.', *PloS one*. United States, 8(6), p. e68125. doi: 10.1371/journal.pone.0068125.

Beltrán, B. *et al.* (2000) 'The effect of nitric oxide on cell respiration: A key to understanding its role in cell survival or death', *Proceedings of the National Academy of Sciences of the United States of America*. The National Academy of Sciences, 97(26), pp. 14602–14607.

Benani, A. *et al.* (2009) 'Method for functional study of mitochondria in rat hypothalamus.', *Journal of neuroscience methods*. Netherlands, 178(2), pp. 301–307. doi: 10.1016/j.jneumeth.2008.12.023.

Bennett, M. R., Sinha, S. and Owens, G. K. (2016) 'Vascular Smooth Muscle Cells in Atherosclerosis', *Circulation Research*, 118(4), p. 692 LP-702.

Bernardi, P. (1999) 'Mitochondrial Transport of Cations: Channels, Exchangers, and Permeability Transition', *Physiological Reviews*. American Physiological Society, 79(4),

pp. 1127–1155. doi: 10.1152/physrev.1999.79.4.1127.

Bielanska, J. *et al.* (2010) 'Voltage-dependent potassium channels Kv1.3 and Kv1.5 in human fetus.', *Cellular physiology and biochemistry : international journal of experimental cellular physiology, biochemistry, and pharmacology*. Germany, 26(2), pp. 219–226. doi: 10.1159/000320528.

Bielanska, J. *et al.* (2012) 'Increased voltage-dependent K(+) channel Kv1.3 and Kv1.5 expression correlates with leiomyosarcoma aggressiveness', *Oncology letters*. Molecular Physiology Laboratory, Department of Biochemistry and Molecular Biology, Institute of Biomedicine, University of Barcelona, E-08028 Barcelona., 4(2), pp. 227–230. doi: 10.3892/ol.2012.718.

Blacker, T. S. and Duchen, M. R. (2016) 'Investigating mitochondrial redox state using NADH and NADPH autofluorescence', *Free Radical Biology & Medicine*. Elsevier Science, 100, pp. 53–65. doi: 10.1016/j.freeradbiomed.2016.08.010.

Blackiston, D. J., McLaughlin, K. A. and Levin, M. (2009) 'Bioelectric controls of cell proliferation: ion channels, membrane voltage and the cell cycle.', *Cell cycle (Georgetown, Tex.)*. United States, 8(21), pp. 3527–3536. doi: 10.4161/cc.8.21.9888.

Boerth, N. J. *et al.* (1997) 'Cyclic GMP-Dependent Protein Kinase Regulates Vascular Smooth Muscle Cell Phenotype', *Journal of Vascular Research*, 34(4), pp. 245–259. doi: 10.1159/000159231.

Bonnet, S. *et al.* (2006) 'An abnormal mitochondrial-hypoxia inducible factor-1alpha-Kv channel pathway disrupts oxygen sensing and triggers pulmonary arterial hypertension in fawn hooded rats: similarities to human pulmonary arterial hypertension.', *Circulation*. United States, 113(22), pp. 2630–2641. doi: 10.1161/CIRCULATIONAHA.105.609008.

Bonnet, S. *et al.* (2007) 'A mitochondria-K+ channel axis is suppressed in cancer and its normalization promotes apoptosis and inhibits cancer growth.', *Cancer cell*. United States, 11(1), pp. 37–51. doi: 10.1016/j.ccr.2006.10.020.

Bonuccelli, G. *et al.* (2017) 'NADH autofluorescence, a new metabolic biomarker for cancer stem cells: Identification of Vitamin C and CAPE as natural products targeting "stemness".', *Oncotarget*. United States, 8(13), pp. 20667–20678. doi:

10.18632/oncotarget.15400.

Bordt, E. A. and Polster, B. M. (2014) 'NADPH Oxidase- and Mitochondria-derived Reactive Oxygen Species in Proinflammatory Microglial Activation: A Bipartisan Affair?', *Free radical biology & medicine*, 0, pp. 34–46. doi: 10.1016/j.freeradbiomed.2014.07.033.

Brancati, M. F. *et al.* (2017) 'Coronary stents and vascular response to implantation: literature review', *Pragmatic and Observational Research*. Dove Medical Press, 8, pp. 137–148. doi: 10.2147/POR.S132439.

Brand, K. (1997) 'Aerobic glycolysis by proliferating cells: protection against oxidative stress at the expense of energy yield.', *Journal of bioenergetics and biomembranes*. United States, 29(4), pp. 355–364.

Brand, M. D. and Nicholls, D. G. (2011) 'Assessing mitochondrial dysfunction in cells.', *The Biochemical journal*. England, 435(2), pp. 297–312. doi: 10.1042/BJ20110162.

British Heart Foundation (2018) *Cardiovascular Disease Statistics BHF UK Factsheet*. Available at: https://www.bhf.org.uk/informationsupport/conditions/cardiovascular-disease (Accessed: 25 November 2018).

Brooks, G. A. (2018) 'The Science and Translation of Lactate Shuttle Theory', *Cell Metabolism*, 27(4), pp. 757–785. doi: https://doi.org/10.1016/j.cmet.2018.03.008.

Brophy, C. M. *et al.* (2002) 'cGMP-Dependent Protein Kinase Expression Restores Contractile Function in Cultured Vascular Smooth Muscle Cells', *Journal of Vascular Research*, 39(2), pp. 95–103. doi: 10.1159/000057758.

Brown, G. C. and Borutaite, V. (2012) 'There is no evidence that mitochondria are the main source of reactive oxygen species in mammalian cells', *Mitochondrion*, 12(1), pp. 1–4. doi: https://doi.org/10.1016/j.mito.2011.02.001.

Buckler, K. J. and Turner, P. J. (2013) 'Oxygen sensitivity of mitochondrial function in rat arterial chemoreceptor cells.', *The Journal of physiology*. England, 591(14), pp. 3549–3563. doi: 10.1113/jphysiol.2013.257741.

Bunn, R. C., Jensen, M. A. and Reed, B. C. (1999) 'Protein interactions with the glucose transporter binding protein GLUT1CBP that provide a link between GLUT1 and the

cytoskeleton', *Molecular biology of the cell*. The American Society for Cell Biology, 10(4), pp. 819–832. doi: 10.1091/mbc.10.4.819.

Butler, T. M. and Siegman, M. J. (1985) 'High-energy phosphate metabolism in vascular smooth muscle.', *Annual review of physiology*. United States, 47, pp. 629–643. doi: 10.1146/annurev.ph.47.030185.003213.

Cahalan, M. D. *et al.* (1985) 'A voltage-gated potassium channel in human T lymphocytes.', *The Journal of physiology*. England, 358, pp. 197–237. doi: 10.1113/jphysiol.1985.sp015548.

Canto, C., Menzies, K. J. and Auwerx, J. (2015) 'NAD(+) Metabolism and the Control of Energy Homeostasis: A Balancing Act between Mitochondria and the Nucleus.', *Cell metabolism*. United States, 22(1), pp. 31–53. doi: 10.1016/j.cmet.2015.05.023.

Cayabyab, F. S. *et al.* (2000) 'Suppression of the rat microglia Kv1.3 current by src-family tyrosine kinases and oxygen/glucose deprivation.', *The European journal of neuroscience*. France, 12(6), pp. 1949–1960.

Chamley-Campbell, J., Campbell, G. R. and Ross, R. (1979) 'The smooth muscle cell in culture.', *Physiological reviews*. United States, 59(1), pp. 1–61. doi: 10.1152/physrev.1979.59.1.1.

Chandel, N. S. (2015) 'Evolution of Mitochondria as Signaling Organelles', *Cell Metabolism*. Elsevier, 22(2), pp. 204–206. doi: 10.1016/j.cmet.2015.05.013.

Chandy, K. G. (1991) 'Simplified gene nomenclature.', *Nature*. England, p. 26. doi: 10.1038/352026b0.

Chandy, K. G. *et al.* (2004) 'K+ channels as targets for specific immunomodulation.', *Trends in pharmacological sciences*. England, 25(5), pp. 280–289. doi: 10.1016/j.tips.2004.03.010.

Chang, S. C. *et al.* (2015) 'N-Terminally extended analogues of the K(+) channel toxin from Stichodactyla helianthus as potent and selective blockers of the voltage-gated potassium channel Kv1.3.', *The FEBS journal*. England, pp. 2247–2259. doi: 10.1111/febs.13294.

Checchetto, V. *et al.* (2018) 'Mitochondrial potassium channels in cell death.',

Biochemical and biophysical research communications. United States, 500(1), pp. 51–58. doi: 10.1016/j.bbrc.2017.06.095.

Chen, H. *et al.* (2003) 'Mitofusins Mfn1 and Mfn2 coordinately regulate mitochondrial fusion and are essential for embryonic development.', *The Journal of cell biology*. United States, 160(2), pp. 189–200. doi: 10.1083/jcb.200211046.

Chen, M. S. *et al.* (2006) 'Bare metal stent restenosis is not a benign clinical entity.', *American heart journal*. United States, 151(6), pp. 1260–1264. doi: 10.1016/j.ahj.2005.08.011.

Chen, X. *et al.* (2010) 'Structure of the full-length Shaker potassium channel Kv1.2 by normal-mode-based X-ray crystallographic refinement', *Proceedings of the National Academy of Sciences*, 107(25), p. 11352 LP-11357. doi: 10.1073/pnas.1000142107.

Chen, Y.-J. *et al.* (2018) 'Inhibition of the potassium channel Kv1.3 reduces infarction and inflammation in ischemic stroke.', *Annals of clinical and translational neurology*. United States, 5(2), pp. 147–161. doi: 10.1002/acn3.513.

Cheng, Y., Debska-Vielhaber, G. and Siemen, D. (2010) 'Interaction of mitochondrial potassium channels with the permeability transition pore.', *FEBS letters*. England, 584(10), pp. 2005–2012. doi: 10.1016/j.febslet.2009.12.038.

Cheong, A. *et al.* (2011) 'Potent suppression of vascular smooth muscle cell migration and human neointimal hyperplasia by KV1.3 channel blockers.', *Cardiovascular research*. England, 89(2), pp. 282–289. doi: 10.1093/cvr/cvq305.

Chiong, M. *et al.* (2014) 'Mitochondrial metabolism and the control of vascular smooth muscle cell proliferation', *Frontiers in cell and developmental biology*. Frontiers Media S.A., 2, p. 72. doi: 10.3389/fcell.2014.00072.

Chistiakov, D. A. *et al.* (2014) 'Mitochondrial aging and age-related dysfunction of mitochondria.', *BioMed research international*. United States, 2014, p. 238463. doi: 10.1155/2014/238463.

Chittajallu, R. *et al.* (2002) 'Regulation of Kv1 subunit expression in oligodendrocyte progenitor cells and their role in G1/S phase progression of the cell cycle.', *Proceedings of the National Academy of Sciences of the United States of America*. United States,

99(4), pp. 2350–2355. doi: 10.1073/pnas.042698399.

Chung, I. and Schlichter, L. C. (1997a) ‘Native Kv1.3 channels are upregulated by protein kinase C.’, *The Journal of membrane biology*. United States, 156(1), pp. 73–85.

Chung, I. and Schlichter, L. C. (1997b) ‘Regulation of native Kv1.3 channels by cAMP-dependent protein phosphorylation.’, *The American journal of physiology*. United States, 273(2 Pt 1), pp. C622-33. doi: 10.1152/ajpcell.1997.273.2.C622.

Cidad, P. *et al.* (2010) ‘Characterization of ion channels involved in the proliferative response of femoral artery smooth muscle cells.’, *Arteriosclerosis, thrombosis, and vascular biology*. United States, 30(6), pp. 1203–1211. doi: 10.1161/ATVBAHA.110.205187.

Cidad, P. *et al.* (2012) ‘Kv1.3 channels can modulate cell proliferation during phenotypic switch by an ion-flux independent mechanism.’, *Arteriosclerosis, thrombosis, and vascular biology*. United States, 32(5), pp. 1299–1307. doi: 10.1161/ATVBAHA.111.242727.

Cidad, P. *et al.* (2015) ‘Kv1.3 channels modulate human vascular smooth muscle cells proliferation independently of mTOR signaling pathway.’, *Pflugers Archiv : European journal of physiology*. Germany, 467(8), pp. 1711–1722. doi: 10.1007/s00424-014-1607-y.

Comes, N. *et al.* (2013) ‘The voltage-dependent K(+) channels Kv1.3 and Kv1.5 in human cancer.’, *Frontiers in physiology*. Switzerland, 4, p. 283. doi: 10.3389/fphys.2013.00283.

Costa, A. D. T. *et al.* (2006) ‘The direct physiological effects of mitoK(ATP) opening on heart mitochondria.’, *American journal of physiology. Heart and circulatory physiology*. United States, 290(1), pp. H406-15. doi: 10.1152/ajpheart.00794.2005.

Criddle, D. N. *et al.* (2006) ‘Menadione-induced reactive oxygen species generation via redox cycling promotes apoptosis of murine pancreatic acinar cells.’, *The Journal of biological chemistry*. United States, 281(52), pp. 40485–40492. doi: 10.1074/jbc.M607704200.

Cutini, P. H. and Massheimer, V. L. (2010) ‘Role of progesterone on the regulation of

vascular muscle cells proliferation, migration and apoptosis', *Steroids*, 75(4), pp. 355–361. doi: https://doi.org/10.1016/j.steroids.2010.01.017.

DeCoursey, T. E. *et al.* (1984) 'Voltage-gated K+ channels in human T lymphocytes: a role in mitogenesis?', *Nature*. England, 307(5950), pp. 465–468.

Deng, X. L. *et al.* (2007) 'Cell cycle-dependent expression of potassium channels and cell proliferation in rat mesenchymal stem cells from bone marrow', *Cell Proliferation*. John Wiley & Sons, Ltd (10.1111), 40(5), pp. 656–670. doi: 10.1111/j.1365-2184.2007.00458.x.

Deutsch, C. and Lee, S. C. (1988) 'Cell volume regulation in lymphocytes.', *Renal physiology and biochemistry*. Switzerland, 11(3–5), pp. 260–276.

Dolga, A. M. *et al.* (2013) 'Mitochondrial small conductance SK2 channels prevent glutamate-induced oxytosis and mitochondrial dysfunction.', *The Journal of biological chemistry*. United States, 288(15), pp. 10792–10804. doi: 10.1074/jbc.M113.453522.

Doonan, P. J. *et al.* (2014) 'LETM1-dependent mitochondrial Ca2+ flux modulates cellular bioenergetics and proliferation.', *FASEB journal : official publication of the Federation of American Societies for Experimental Biology*. United States, 28(11), pp. 4936–4949. doi: 10.1096/fj.14-256453.

Doyle, D. A. *et al.* (1998) 'The structure of the potassium channel: molecular basis of K+ conduction and selectivity.', *Science (New York, N.Y.)*. United States, 280(5360), pp. 69–77.

Dromparis, P. and Michelakis, E. D. (2013) 'Mitochondria in Vascular Health and Disease', *Annual Review of Physiology*. Annual Reviews, 75(1), pp. 95–126. doi: 10.1146/annurev-physiol-030212-183804.

Du, W. *et al.* (2013) 'TAp73 enhances the pentose phosphate pathway and supports cell proliferation.', *Nature cell biology*. England, 15(8), pp. 991–1000. doi: 10.1038/ncb2789.

Dubois, J.-M. and Rouzaire-Dubois, B. (2004) 'The influence of cell volume changes on tumour cell proliferation.', *European biophysics journal : EBJ*. Germany, 33(3), pp. 227–232. doi: 10.1007/s00249-003-0364-1.

Duckles, H. *et al.* (2015) 'T-Type Ca2+ Channel Regulation by CO: A Mechanism for Control of Cell Proliferation.', *Advances in experimental medicine and biology*. United States, 860, pp. 291–300. doi: 10.1007/978-3-319-18440-1_33.

Eigentler, A. *et al.* (2015) 'Laboratory Protocol: Citrate synthase a mitochondrial marker enzyme.', *Mitochondr Physiol Network*, 17(04), pp. 1–11.

Elies, J., Scragg, J. L., *et al.* (2014) 'Hydrogen sulfide inhibits Cav3.2 T-type Ca2+ channels.', *FASEB journal : official publication of the Federation of American Societies for Experimental Biology*. United States, 28(12), pp. 5376–5387. doi: 10.1096/fj.14-257113.

Elies, J., Dallas, M. L., *et al.* (2014) 'Inhibition of the cardiac Na(+) channel Nav1.5 by carbon monoxide.', *The Journal of biological chemistry*. United States, 289(23), pp. 16421–16429. doi: 10.1074/jbc.M114.569996.

Fadool, D. A. *et al.* (1997) 'Tyrosine phosphorylation modulates current amplitude and kinetics of a neuronal voltage-gated potassium channel.', *Journal of neurophysiology*. United States, 78(3), pp. 1563–1573. doi: 10.1152/jn.1997.78.3.1563.

Fadool, D. A. *et al.* (2000) 'Brain insulin receptor causes activity-dependent current suppression in the olfactory bulb through multiple phosphorylation of Kv1.3.', *Journal of neurophysiology*. United States, 83(4), pp. 2332–2348. doi: 10.1152/jn.2000.83.4.2332.

Fadool, D. A. and Levitan, I. B. (1998) 'Modulation of olfactory bulb neuron potassium current by tyrosine phosphorylation.', *The Journal of neuroscience : the official journal of the Society for Neuroscience*. United States, 18(16), pp. 6126–6137.

Fantin, V. R. *et al.* (2002) 'A novel mitochondriotoxic small molecule that selectively inhibits tumor cell growth.', *Cancer cell*. United States, 2(1), pp. 29–42.

Fehrenbacher, N., Bar-Sagi, D. and Philips, M. (2009) 'Ras/MAPK signaling from endomembranes.', *Molecular oncology*. United States, 3(4), pp. 297–307. doi: 10.1016/j.molonc.2009.06.004.

Forrest, M. D. (2015) 'Why cancer cells have a more hyperpolarised mitochondrial membrane potential and emergent prospects for therapy', *bioRxiv*.

Galis, Z. S. *et al.* (1994) 'Cytokine-stimulated human vascular smooth muscle cells synthesize a complement of enzymes required for extracellular matrix digestion.', *Circulation Research*. American Heart Association, 75(1), pp. 181–189. doi: 10.1161/01.RES.75.1.181.

Galli, S. *et al.* (2008) 'Tumor cell phenotype is sustained by selective MAPK oxidation in mitochondria', *PloS one*. Public Library of Science, 3(6), pp. e2379–e2379. doi: 10.1371/journal.pone.0002379.

Galli, S. *et al.* (2009) 'A new paradigm for MAPK: structural interactions of hERK1 with mitochondria in HeLa cells.', *PloS one*. United States, 4(10), p. e7541. doi: 10.1371/journal.pone.0007541.

Garedew, A., Henderson, S. O. and Moncada, S. (2010) 'Activated macrophages utilize glycolytic ATP to maintain mitochondrial membrane potential and prevent apoptotic cell death.', *Cell death and differentiation*. England, 17(10), pp. 1540–1550. doi: 10.1038/cdd.2010.27.

Garlid, K. D. (1996) 'Cation transport in mitochondria--the potassium cycle.', *Biochimica et biophysica acta*. Netherlands, 1275(1–2), pp. 123–126.

Garlid, K. D. *et al.* (2003) 'Mitochondrial potassium transport: the role of the mitochondrial ATP-sensitive K(+) channel in cardiac function and cardioprotection.', *Biochimica et biophysica acta*. Netherlands, 1606(1–3), pp. 1–21.

Garlid, K. D. and Paucek, P. (2003) 'Mitochondrial potassium transport: the K(+) cycle.', *Biochimica et biophysica acta*. Netherlands, 1606(1–3), pp. 23–41.

Gaziano, T. A. *et al.* (2010) 'Growing epidemic of coronary heart disease in low- and middle-income countries', *Current problems in cardiology*, 35(2), pp. 72–115. doi: 10.1016/j.cpcardiol.2009.10.002.

Gentric, G., Mieulet, V. and Mechta-Grigoriou, F. (2017) 'Heterogeneity in Cancer Metabolism: New Concepts in an Old Field', *Antioxidants & Redox Signaling*. 140 Huguenot Street, 3rd FloorNew Rochelle, NY 10801USA: Mary Ann Liebert, Inc., 26(9), pp. 462–485. doi: 10.1089/ars.2016.6750.

Gnaiger, E. (2014) *Mitochondrial Pathways and Respiratory Control. An introduction to*

OXPHOS analysis.

Gnaiger, E. (2016) 'O2k-calibration by DatLab', *Mitochondrial Physiology Network*, Version D0.

Goetzman, E. S. and Prochownik, E. V (2018) 'The Role for Myc in Coordinating Glycolysis, Oxidative Phosphorylation, Glutaminolysis, and Fatty Acid Metabolism in Normal and Neoplastic Tissues ', *Frontiers in Endocrinology* , p. 129.

Goldenberg, H., Crane, F. L. and Morre, D. J. (1979) 'NADH oxidoreductase of mouse liver plasma membranes.', *The Journal of biological chemistry*. United States, 254(7), pp. 2491–2498.

Gomez, D. and Owens, G. K. (2012) 'Smooth muscle cell phenotypic switching in atherosclerosis.', *Cardiovascular research*. England, 95(2), pp. 156–164. doi: 10.1093/cvr/cvs115.

Gough, D. J., Koetz, L. and Levy, D. E. (2013) 'The MEK-ERK pathway is necessary for serine phosphorylation of mitochondrial STAT3 and Ras-mediated transformation.', *PloS one*. United States, 8(11), p. e83395. doi: 10.1371/journal.pone.0083395.

Griffiths, E. J. and Rutter, G. A. (2009) 'Mitochondrial calcium as a key regulator of mitochondrial ATP production in mammalian cells', *Biochimica et Biophysica Acta (BBA) - Bioenergetics*, 1787(11), pp. 1324–1333. doi: https://doi.org/10.1016/j.bbabio.2009.01.019.

Grunnet, M. *et al.* (2003) 'KCNE4 is an inhibitory subunit to Kv1.1 and Kv1.3 potassium channels', *Biophysical journal*. Biophysical Society, 85(3), pp. 1525–1537. doi: 10.1016/S0006-3495(03)74585-8.

Gubitosi-Klug, R. A., Mancuso, D. J. and Gross, R. W. (2005) 'The human Kv1.1 channel is palmitoylated, modulating voltage sensing: Identification of a palmitoylation consensus sequence', *Proceedings of the National Academy of Sciences*, 102(17), p. 5964 LP-5968.

Guengerich, F. P., Waterman, M. R. and Egli, M. (2016) 'Recent Structural Insights into Cytochrome P450 Function.', *Trends in pharmacological sciences*. England, 37(8), pp. 625–640. doi: 10.1016/j.tips.2016.05.006.

Gulbins, E. *et al.* (2010) 'Role of Kv1.3 mitochondrial potassium channel in apoptotic signalling in lymphocytes', *Biochimica et Biophysica Acta (BBA) - Bioenergetics*, 1797(6), pp. 1251–1259. doi: https://doi.org/10.1016/j.bbabio.2010.01.018.

Gutman, G. A. *et al.* (2005) 'International Union of Pharmacology. LIII. Nomenclature and molecular relationships of voltage-gated potassium channels.', *Pharmacological reviews*. United States, 57(4), pp. 473–508. doi: 10.1124/pr.57.4.10.

Hadrava, V. *et al.* (1991) 'Vascular smooth muscle cell proliferation and its therapeutic modulation in hypertension', *American Heart Journal*, 122(4, Part 2), pp. 1198–1203. doi: https://doi.org/10.1016/0002-8703(91)90939-F.

Hajdu, P. *et al.* (2015) 'The C-terminus SH3-binding domain of Kv1.3 is required for the actin-mediated immobilization of the channel via cortactin.', *Molecular biology of the cell*. United States, 26(9), pp. 1640–1651. doi: 10.1091/mbc.E14-07-1195.

Halestrap, A. P. (1989) 'The regulation of the matrix volume of mammalian mitochondria in vivo and in vitro and its role in the control of mitochondrial metabolism', *Biochimica et Biophysica Acta (BBA) - Bioenergetics*, 973(3), pp. 355–382. doi: https://doi.org/10.1016/S0005-2728(89)80378-0.

Hamilton, D. L. *et al.* (2014) 'Kv1.3 inhibitors have differential effects on glucose uptake and AMPK activity in skeletal muscle cell lines and mouse ex vivo skeletal muscle.', *The journal of physiological sciences : JPS*. Japan, 64(1), pp. 13–20. doi: 10.1007/s12576-013-0285-4.

Hardie, R.-A. *et al.* (2017) 'Mitochondrial mutations and metabolic adaptation in pancreatic cancer', *Cancer & Metabolism*, 5(1), p. 2. doi: 10.1186/s40170-017-0164-1.

Heerdt, B. G., Houston, M. A. and Augenlicht, L. H. (2005) 'The intrinsic mitochondrial membrane potential of colonic carcinoma cells is linked to the probability of tumor progression.', *Cancer research*. United States, 65(21), pp. 9861–9867. doi: 10.1158/0008-5472.CAN-05-2444.

Hegle, A. P., Marble, D. D. and Wilson, G. F. (2006) 'A voltage-driven switch for ion-independent signaling by ether-à-go-go K+ channels', *Proceedings of the National Academy of Sciences of the United States of America*. 2006/02/13. National Academy of Sciences, 103(8), pp. 2886–2891. doi: 10.1073/pnas.0505909103.

Vander Heiden, M. G., Cantley, L. C. and Thompson, C. B. (2009) 'Understanding the Warburg Effect: The Metabolic Requirements of Cell Proliferation', *Science (New York, N.Y.)*, 324(5930), pp. 1029–1033. doi: 10.1126/science.1160809.

Heidenreich, P. *et al.* (2011) 'Forecasting the Future of Cardiovascular Disease in the United States', *Circulation*. American Heart Association, 123(8), pp. 933–944. doi: 10.1161/CIR.0b013e31820a55f5.

Heinen, A. *et al.* (2007) 'Mitochondrial Ca2+-induced K+ influx increases respiration and enhances ROS production while maintaining membrane potential.', *American journal of physiology. Cell physiology*. United States, 292(1), pp. C148-56. doi: 10.1152/ajpcell.00215.2006.

Henke, G. *et al.* (2004) 'Regulation of the voltage gated K+ channel Kv1.3 by the ubiquitin ligase Nedd4-2 and the serum and glucocorticoid inducible kinase SGK1.', *Journal of cellular physiology*. United States, 199(2), pp. 194–199. doi: 10.1002/jcp.10430.

Herrmann, S. *et al.* (2012) 'Cortactin Controls Surface Expression of the Voltage-gated Potassium Channel K(V)10.1', *The Journal of Biological Chemistry*. 9650 Rockville Pike, Bethesda, MD 20814, U.S.A.: American Society for Biochemistry and Molecular Biology, 287(53), pp. 44151–44163. doi: 10.1074/jbc.M112.372540.

Herst, P. M. *et al.* (2004) 'Cell surface oxygen consumption by mitochondrial gene knockout cells', *Biochimica et Biophysica Acta (BBA) - Bioenergetics*, 1656(2), pp. 79–87. doi: https://doi.org/10.1016/j.bbabio.2004.01.008.

Herst, P. M. *et al.* (2008) 'Plasma membrane electron transport in Saccharomyces cerevisiae depends on the presence of mitochondrial respiratory subunits.', *FEMS yeast research*. England, 8(6), pp. 897–905. doi: 10.1111/j.1567-1364.2008.00418.x.

Herst, P. M. *et al.* (2017) 'Functional Mitochondria in Health and Disease', *Frontiers in endocrinology*. Frontiers Media S.A., 8, p. 296. doi: 10.3389/fendo.2017.00296.

Herst, P. M. and Berridge, M. V (2006) 'Plasma membrane electron transport: a new target for cancer drug development.', *Current molecular medicine*. Netherlands, 6(8), pp. 895–904.

Herst, P. M. and Berridge, M. V (2007) ‘Cell surface oxygen consumption: a major contributor to cellular oxygen consumption in glycolytic cancer cell lines.’, *Biochimica et biophysica acta*. Netherlands, 1767(2), pp. 170–177. doi: 10.1016/j.bbabio.2006.11.018.

Hill-Eubanks, D. C. *et al.* (2003) ‘NFAT regulation in smooth muscle.’, *Trends in cardiovascular medicine*. United States, 13(2), pp. 56–62.

Hille, B. (2001) *Ion Channels of Excitable Membranes*. 3rd Editio. Sinauer Associates, Sunderland, MA.

Himmelreich, U. and Kuchel, P. W. (1997) ‘13C-NMR Studies of Transmembrane Electron Transfer to Extracellular Ferricyanide in Human Erythrocytes’, *European Journal of Biochemistry*. John Wiley & Sons, Ltd (10.1111), 246(3), pp. 638–645. doi: 10.1111/j.1432-1033.1997.t01-1-00638.x.

Hirschi, K. K., Rohovsky, S. A. and D'Amore, P. A. (1998) ‘PDGF, TGF-β, and Heterotypic Cell–Cell Interactions Mediate Endothelial Cell–induced Recruitment of 10T1/2 Cells and Their Differentiation to a Smooth Muscle Fate’, *The Journal of Cell Biology*, 141(3), p. 805 LP-814. doi: 10.1083/jcb.141.3.805.

Ho, J. *et al.* (2012) ‘Importance of glycolysis and oxidative phosphorylation in advanced melanoma.’, *Molecular cancer*. England, 11, p. 76. doi: 10.1186/1476-4598-11-76.

Hodgkin, A. L. and Huxley, A. F. (1952) ‘A quantitative description of membrane current and its application to conduction and excitation in nerve.’, *The Journal of physiology*. England, 117(4), pp. 500–544.

Holzerova, E. and Prokisch, H. (2015) ‘Mitochondria: Much ado about nothing? How dangerous is reactive oxygen species production?’, *The international journal of biochemistry & cell biology*. Netherlands, 63, pp. 16–20. doi: 10.1016/j.biocel.2015.01.021.

Horbinski, C. and Chu, C. T. (2005) ‘Kinase signaling cascades in the mitochondrion: a matter of life or death’, *Free Radical Biology and Medicine*, 38(1), pp. 2–11. doi: https://doi.org/10.1016/j.freeradbiomed.2004.09.030.

Hoshi, T. and Armstrong, C. M. (2013) ‘C-type inactivation of voltage-gated K+

channels: pore constriction or dilation?', *The Journal of general physiology*. United States, 141(2), pp. 151–160. doi: 10.1085/jgp.201210888.

Houston, M. A., Augenlicht, L. H. and Heerdt, B. G. (2011) 'Stable differences in intrinsic mitochondrial membrane potential of tumor cell subpopulations reflect phenotypic heterogeneity.', *International journal of cell biology*. United States, 2011, p. 978583. doi: 10.1155/2011/978583.

Hu, L. *et al.* (2013) 'Blockade of Kv1.3 potassium channels inhibits differentiation and granzyme B secretion of human CD8+ T effector memory lymphocytes.', *PloS one*. United States, 8(1), p. e54267. doi: 10.1371/journal.pone.0054267.

Hutter, E. *et al.* (2002) 'Biphasic oxygen kinetics of cellular respiration and linear oxygen dependence of antimycin A inhibited oxygen consumption.', *Molecular biology reports*. Netherlands, 29(1–2), pp. 83–87.

Ivanov, A. *et al.* (2006) 'Adenylate cyclase 5 and KCa1.1 channel are required for EGFR up-regulation of PCNA in native contractile rat basilar artery smooth muscle', *The Journal of Physiology*. John Wiley & Sons, Ltd (10.1111), 570(1), pp. 73–84. doi: 10.1113/jphysiol.2005.100883.

Jaimes-Hoy, L. *et al.* (2017) 'The Kv1.3 channel blocker Vm24 enhances muscle glucose transporter 4 mobilization but does not reduce body-weight gain in diet-induced obese male rats', *Life Sciences*, 181, pp. 23–30. doi: https://doi.org/10.1016/j.lfs.2017.05.027.

Jang, S. H. *et al.* (2015) 'Nuclear localization and functional characteristics of voltage-gated potassium channel Kv1.3.', *The Journal of biological chemistry*. United States, 290(20), pp. 12547–12557. doi: 10.1074/jbc.M114.561324.

Jeong, H. Y. *et al.* (2015) 'Widdrol-induced lipolysis is mediated by PKC and MEK/ERK in 3T3-L1 adipocytes.', *Molecular and cellular biochemistry*. Netherlands, 410(1–2), pp. 247–254. doi: 10.1007/s11010-015-2558-0.

Jeremy, J. Y. *et al.* (1999) 'Nitric oxide and the proliferation of vascular smooth muscle cells', *Cardiovascular Research*, 43(3), pp. 580–594. doi: 10.1016/S0008-6363(99)00171-6.

Jerng, H. H., Pfaffinger, P. J. and Covarrubias, M. (2004) 'Molecular physiology and

modulation of somatodendritic A-type potassium channels.', *Molecular and cellular neurosciences*. United States, 27(4), pp. 343–369. doi: 10.1016/j.mcn.2004.06.011.

Jiang, B. *et al.* (2002) 'Endogenous Kv channels in human embryonic kidney (HEK-293) cells.', *Molecular and cellular biochemistry*. Netherlands, 238(1–2), pp. 69–79.

Jiang, D., Zhao, L. and Clapham, D. E. (2009) 'Genome-wide RNAi screen identifies Letm1 as a mitochondrial Ca2+/H+ antiporter.', *Science (New York, N.Y.)*. United States, 326(5949), pp. 144–147. doi: 10.1126/science.1175145.

Jimenez-Perez, L. *et al.* (2016) 'Molecular Determinants of Kv1.3 Potassium Channels-induced Proliferation.', *The Journal of biological chemistry*. United States, 291(7), pp. 3569–3580. doi: 10.1074/jbc.M115.678995.

Johannes Schindelin (no date) *Coloc 2*. Available at: https://imagej.net/Coloc_2 (Accessed: 20 November 2019).

Jose, C., Bellance, N. and Rossignol, R. (2011) 'Choosing between glycolysis and oxidative phosphorylation: a tumor's dilemma?', *Biochimica et biophysica acta*. Netherlands, 1807(6), pp. 552–561. doi: 10.1016/j.bbabio.2010.10.012.

Juhasz, A. *et al.* (2017) 'NADPH oxidase 1 supports proliferation of colon cancer cells by modulating reactive oxygen species-dependent signal transduction', *The Journal of Biological Chemistry*. 11200 Rockville Pike, Suite 302, Rockville, MD 20852-3110, U.S.A.: American Society for Biochemistry and Molecular Biology, 292(19), pp. 7866–7887. doi: 10.1074/jbc.M116.768283.

Kalman, K. *et al.* (1998) 'ShK-Dap22, a potent Kv1.3-specific immunosuppressive polypeptide.', *The Journal of biological chemistry*. United States, 273(49), pp. 32697–32707.

Kalyanaraman, B. *et al.* (2017) 'A review of the basics of mitochondrial bioenergetics, metabolism, and related signaling pathways in cancer cells: Therapeutic targeting of tumor mitochondria with lipophilic cationic compounds', *Redox biology*. Elsevier, 14, pp. 316–327. doi: 10.1016/j.redox.2017.09.020.

Kamb, A., Tseng-Crank, J. and Tanouye, M. A. (1988) 'Multiple products of the Drosophila Shaker gene may contribute to potassium channel diversity.', *Neuron*.

United States, 1(5), pp. 421–430.

Kan, X.-H. *et al.* (2016) 'Kv1.3 potassium channel mediates macrophage migration in atherosclerosis by regulating ERK activity.', *Archives of biochemistry and biophysics*. United States, 591, pp. 150–156. doi: 10.1016/j.abb.2015.12.013.

Kang, S. H. *et al.* (2007) 'Mitochondrial Ca2+-activated K+ channels more efficiently reduce mitochondrial Ca2+ overload in rat ventricular myocytes.', *American journal of physiology. Heart and circulatory physiology*. United States, 293(1), pp. H307-13. doi: 10.1152/ajpheart.00789.2006.

Kazama, I. *et al.* (2012) 'Overexpression of Delayed Rectifier K(+) Channels Promotes In situ Proliferation of Leukocytes in Rat Kidneys with Advanced Chronic Renal Failure.', *International journal of nephrology*. United States, 2012, p. 581581. doi: 10.1155/2012/581581.

Kazama, I. (2015) 'Roles of lymphocyte Kv1.3-channels in gut mucosal immune system: Novel therapeutic implications for inflammatory bowel disease.', *Medical hypotheses*. United States, 85(1), pp. 61–63. doi: 10.1016/j.mehy.2015.03.023.

Kazama, I. and Tamada, T. (2016) 'Lymphocyte Kv1.3-channels in the pathogenesis of chronic obstructive pulmonary disease: novel therapeutic implications of targeting the channels by commonly used drugs', *Allergy, Asthma & Clinical Immunology*, 12(1), p. 60. doi: 10.1186/s13223-016-0168-3.

Kelly, S. C. *et al.* (2018) 'Glucose-dependent trans-plasma membrane electron transport and p70S6k phosphorylation in skeletal muscle cells', *Redox Biology*, p. 101075. doi: https://doi.org/10.1016/j.redox.2018.101075.

Kelso, G. F. *et al.* (2001) 'Selective targeting of a redox-active ubiquinone to mitochondria within cells: antioxidant and antiapoptotic properties.', *The Journal of biological chemistry*. United States, 276(7), pp. 4588–4596. doi: 10.1074/jbc.M009093200.

Khanna, R. *et al.* (2001) 'K+ channels and the microglial respiratory burst.', *American journal of physiology. Cell physiology*. United States, 280(4), pp. C796-806. doi: 10.1152/ajpcell.2001.280.4.C796.

Khavjou, O., Phelps, D. and Leib, A. (2016) *Projections of Cardiovascular Disease Prevalence and Cost 2015-2035*.

Kim, J.-H. *et al.* (2017) 'Lactate dehydrogenase-A is indispensable for vascular smooth muscle cell proliferation and migration', *Biochemical and Biophysical Research Communications*, 492(1), pp. 41–47. doi: https://doi.org/10.1016/j.bbrc.2017.08.041.

Koch Hansen, L. *et al.* (2014) 'Expression of T-cell KV1.3 potassium channel correlates with pro-inflammatory cytokines and disease activity in ulcerative colitis.', *Journal of Crohn's & colitis*. England, 8(11), pp. 1378–1391. doi: 10.1016/j.crohns.2014.04.003.

Kolisek, M. *et al.* (2003) 'Mrs2p is an essential component of the major electrophoretic Mg2+ influx system in mitochondria.', *The EMBO journal*. England, 22(6), pp. 1235–1244. doi: 10.1093/emboj/cdg122.

Koopman, W. J. H. *et al.* (2010) 'Mammalian mitochondrial complex I: biogenesis, regulation, and reactive oxygen species generation.', *Antioxidants & redox signaling*. United States, 12(12), pp. 1431–1470. doi: 10.1089/ars.2009.2743.

Kopustinskiene, D. M. *et al.* (2010) 'Direct effects of K(ATP) channel openers pinacidil and diazoxide on oxidative phosphorylation of mitochondria in situ.', *Cellular physiology and biochemistry : international journal of experimental cellular physiology, biochemistry, and pharmacology*. Switzerland, 25(2–3), pp. 181–186. doi: 10.1159/000276552.

Kopustinskiene, D. M., Pollesello, P. and Saris, N.-E. L. (2004) 'Potassium-specific effects of levosimendan on heart mitochondria.', *Biochemical pharmacology*. England, 68(5), pp. 807–812. doi: 10.1016/j.bcp.2004.05.018.

Koshy, S. *et al.* (2013) 'Blocking KCa3.1 channels increases tumor cell killing by a subpopulation of human natural killer lymphocytes.', *PloS one*. United States, 8(10), p. e76740. doi: 10.1371/journal.pone.0076740.

Koshy, S. *et al.* (2014) 'Blocking KV1.3 channels inhibits Th2 lymphocyte function and treats a rat model of asthma.', *The Journal of biological chemistry*. United States, 289(18), pp. 12623–12632. doi: 10.1074/jbc.M113.517037.

Kotecha, S. A. and Schlichter, L. C. (1999) 'A Kv1.5 to Kv1.3 Switch in Endogenous

Hippocampal Microglia and a Role in Proliferation', *The Journal of Neuroscience*, 19(24), p. 10680 LP-10693. doi: 10.1523/JNEUROSCI.19-24-10680.1999.

Kovach, C. P. *et al.* (2016) 'Mitochondrial Ultrastructure and Glucose Signaling Pathways Attributed to the Kv1.3 Ion Channel', *Frontiers in Physiology*. Frontiers Media S.A., 7, p. 178. doi: 10.3389/fphys.2016.00178.

Kowalczyk, J. E. and Zablocka, B. (2008) '[Protein kinases in mitochondria].', *Postepy biochemii*. Poland, 54(2), pp. 209–216.

Kowaltowski, A. J. *et al.* (2001) 'Bioenergetic consequences of opening the ATP-sensitive K(+) channel of heart mitochondria.', *American journal of physiology. Heart and circulatory physiology*. United States, 280(2), pp. H649-57. doi: 10.1152/ajpheart.2001.280.2.H649.

Krabbendam, I. E. *et al.* (2018) 'Mitochondrial Ca(2+)-activated K(+) channels and their role in cell life and death pathways.', *Cell calcium*. Netherlands, 69, pp. 101–111. doi: 10.1016/j.ceca.2017.07.005.

Kroemer, G. and Pouyssegur, J. (2008) 'Tumor cell metabolism: cancer's Achilles' heel.', *Cancer cell*. United States, 13(6), pp. 472–482. doi: 10.1016/j.ccr.2008.05.005.

Kuang, Q., Purhonen, P. and Hebert, H. (2015) 'Structure of potassium channels', *Cellular and molecular life sciences : CMLS*. 2015/06/13. Springer Basel, 72(19), pp. 3677–3693. doi: 10.1007/s00018-015-1948-5.

Kundu-Raychaudhuri, S. *et al.* (2014) 'Kv1.3 in psoriatic disease: PAP-1, a small molecule inhibitor of Kv1.3 is effective in the SCID mouse psoriasis--xenograft model.', *Journal of autoimmunity*. England, 55, pp. 63–72. doi: 10.1016/j.jaut.2014.07.003.

Kuzmicic, J. *et al.* (2011) '[Mitochondrial dynamics: a potential new therapeutic target for heart failure].', *Revista espanola de cardiologia*. Spain, 64(10), pp. 916–923. doi: 10.1016/j.recesp.2011.05.018.

Kuznetsov, A. and Gnaiger, E. (2018) *Oxygraph Assay of Cytochrome c Oxidase Activity: Chemical Background Correction*.

Kuznetsov, A. V *et al.* (2009) 'The cell-type specificity of mitochondrial dynamics.', *The international journal of biochemistry & cell biology*. Netherlands, 41(10), pp. 1928–

1939. doi: 10.1016/j.biocel.2009.03.007.

Lacolley, P. *et al.* (2012) 'The vascular smooth muscle cell in arterial pathology: a cell that can take on multiple roles.', *Cardiovascular research*. England, 95(2), pp. 194–204. doi: 10.1093/cvr/cvs135.

Lan, L. *et al.* (2018) 'Deferoxamine suppresses esophageal squamous cell carcinoma cell growth via ERK1/2 mediated mitochondrial dysfunction.', *Cancer letters*. Ireland, 432, pp. 132–143. doi: 10.1016/j.canlet.2018.06.012.

Lang, F. *et al.* (2007) 'Chapter Eleven - Cell Volume Regulatory Ion Channels in Cell Proliferation and Cell Death', in Häussinger, D. and Sies, H. B. T.-M. in E. (eds) *Osmosensing and Osmosignaling*. Academic Press, pp. 209–225. doi: https://doi.org/10.1016/S0076-6879(07)28011-5.

Larsen, S. *et al.* (2012) 'Biomarkers of mitochondrial content in skeletal muscle of healthy young human subjects', *The Journal of physiology*. 2012/05/14. Blackwell Science Inc, 590(14), pp. 3349–3360. doi: 10.1113/jphysiol.2012.230185.

Laskowski, M. *et al.* (2016) 'What do we not know about mitochondrial potassium channels?', *Biochimica et Biophysica Acta (BBA) - Bioenergetics*, 1857(8), pp. 1247–1257. doi: https://doi.org/10.1016/j.bbabio.2016.03.007.

Leanza, L. *et al.* (2012) 'Inhibitors of mitochondrial Kv1.3 channels induce Bax/Bak-independent death of cancer cells', *EMBO Molecular Medicine*. Weinheim: WILEY-VCH Verlag, 4(7), pp. 577–593. doi: 10.1002/emmm.201200235.

Leanza, L. *et al.* (2013) 'Clofazimine, Psora-4 and PAP-1, inhibitors of the potassium channel Kv1.3, as a new and selective therapeutic strategy in chronic lymphocytic leukemia.', *Leukemia*. England, pp. 1782–1785. doi: 10.1038/leu.2013.56.

Leanza, L. *et al.* (2013) 'Intracellular ion channels and cancer ', *Frontiers in Physiology* , p. 227.

Leanza, L. *et al.* (2014) 'Correlation between potassium channel expression and sensitivity to drug-induced cell death in tumor cell lines.', *Current pharmaceutical design*. United Arab Emirates, 20(2), pp. 189–200.

Leanza, L. *et al.* (2017) 'Direct Pharmacological Targeting of a Mitochondrial Ion

Channel Selectively Kills Tumor Cells In Vivo.', *Cancer cell*. United States, 31(4), p. 516–531.e10. doi: 10.1016/j.ccell.2017.03.003.

Lee, A. *et al.* (2014) 'More Than a Pore: Ion Channel Signaling Complexes', *The Journal of Neuroscience*. Society for Neuroscience, 34(46), pp. 15159–15169. doi: 10.1523/JNEUROSCI.3275-14.2014.

Lee, H. J. *et al.* (2004) 'Mitogen-activated protein kinase/extracellular signal-regulated kinase attenuates 3-hydroxykynurenine-induced neuronal cell death.', *Journal of neurochemistry*. England, 88(3), pp. 647–656.

Lee, N. C. W. *et al.* (2018) 'High Expression of Glycolytic Genes in Cirrhosis Correlates With the Risk of Developing Liver Cancer ', *Frontiers in Cell and Developmental Biology* , p. 138.

Legany, N. *et al.* (2016) 'Calcium influx kinetics, and the features of potassium channels of peripheral lymphocytes in primary Sjogren's syndrome.', *Immunobiology*. Netherlands, 221(11), pp. 1266–1272. doi: 10.1016/j.imbio.2016.06.004.

Lehninger, A. L. (1982) 'Proton and electric charge translocation in mitochondrial energy transduction.', *Advances in experimental medicine and biology*. United States, 148, pp. 171–186.

Levite, M. *et al.* (2000) 'Extracellular K(+) and opening of voltage-gated potassium channels activate T cell integrin function: physical and functional association between Kv1.3 channels and beta1 integrins.', *The Journal of experimental medicine*. United States, 191(7), pp. 1167–1176.

Liberti, M. V and Locasale, J. W. (2016) 'The Warburg Effect: How Does it Benefit Cancer Cells?', *Trends in biochemical sciences*, 41(3), pp. 211–218. doi: 10.1016/j.tibs.2015.12.001.

Liemburg-Apers, D. C. *et al.* (2015) 'Interactions between mitochondrial reactive oxygen species and cellular glucose metabolism', *Archives of Toxicology*. Berlin/Heidelberg: Springer Berlin Heidelberg, 89(8), pp. 1209–1226. doi: 10.1007/s00204-015-1520-y.

Liistro, F. *et al.* (2002) 'First clinical experience with a paclitaxel derivate-eluting

polymer stent system implantation for in-stent restenosis: immediate and long-term clinical and angiographic outcome.', *Circulation*. United States, 105(16), pp. 1883–1886.

Lin, C.-Y. *et al.* (2013) 'Enhanced expression of glucose transporter-1 in vascular smooth muscle cells via the Akt/tuberous sclerosis complex subunit 2 (TSC2)/mammalian target of rapamycin (mTOR)/ribosomal S6 protein kinase (S6K) pathway in experimental renal failure.', *Journal of vascular surgery*. United States, 57(2), pp. 475–485. doi: 10.1016/j.jvs.2012.07.037.

Lindner, V. and Reidy, M. A. (1991) 'Proliferation of smooth muscle cells after vascular injury is inhibited by an antibody against basic fibroblast growth factor', *Proceedings of the National Academy of Sciences of the United States of America*, 88(9), pp. 3739–3743. doi: 10.1073/pnas.88.9.3739.

Linley, J. E. *et al.* (2012) 'Reactive oxygen species are second messengers of neurokinin signaling in peripheral sensory neurons', *Proceedings of the National Academy of Sciences of the United States of America*. National Academy of Sciences, 109(24), pp. E1578–E1586. doi: 10.1073/pnas.1201544109.

Liou, G.-Y. and Storz, P. (2010) 'Reactive oxygen species in cancer', *Free radical research*, 44(5), p. 10.3109/10715761003667554. doi: 10.3109/10715761003667554.

Liu, B. *et al.* (2007) 'Protein kinase C-delta regulates migration and proliferation of vascular smooth muscle cells through the extracellular signal-regulated kinase 1/2', *Journal of vascular surgery*, 45(1), pp. 160–168. doi: 10.1016/j.jvs.2006.09.053.

Liu, C. *et al.* (2010) 'PI3K/Akt signaling transduction pathway is involved in rat vascular smooth muscle cell proliferation induced by apelin-13', *Acta Biochimica et Biophysica Sinica*, 42(6), pp. 396–402. doi: 10.1093/abbs/gmq035.

Lodish H, Berk A, Zipursky SL, Matsudaira P, Baltimore D, D. J. (2000) *Molecular Cell Biology*. 4th Editio. Edited by F. WH.

Long, S. B., Campbell, E. B. and MacKinnon, R. (2005) 'Crystal Structure of a Mammalian Voltage-Dependent Shaker Family K⁺ Channel', *Science*, 309(5736), p. 897 LP-903.

Lopez-Lopez, J. R., Cidad, P. and Perez-Garcia, M. T. (2018) 'Kv channels and vascular smooth muscle cell proliferation.', *Microcirculation (New York, N.Y. : 1994)*. United States, 25(1). doi: 10.1111/micc.12427.

Lowinus, T. *et al.* (2016) 'Immunomodulation by memantine in therapy of Alzheimer's disease is mediated through inhibition of K(v)1.3 channels and T cell responsiveness', *Oncotarget*. Impact Journals LLC, 7(33), pp. 53797–53807. doi: 10.18632/oncotarget.10777.

Lu, C.-L. *et al.* (2015) 'Tumor cells switch to mitochondrial oxidative phosphorylation under radiation via mTOR-mediated hexokinase II inhibition--a Warburg-reversing effect.', *PloS one*. United States, 10(3), p. e0121046. doi: 10.1371/journal.pone.0121046.

Lusis, A. J. (2000) 'Atherosclerosis', *Nature*, 407(6801), pp. 233–241. doi: 10.1038/35025203.

Lynch, T. and Price, A. (2007) 'The effect of cytochrome P450 metabolism on drug response, interactions, and adverse effects.', *American family physician*. United States, 76(3), pp. 391–396.

MacFarlane, S. N. and Sontheimer, H. (1997) 'Electrophysiological changes that accompany reactive gliosis in vitro.', *The Journal of neuroscience : the official journal of the Society for Neuroscience*. United States, 17(19), pp. 7316–7329.

Mahnke, Y. D. *et al.* (2013) 'The who's who of T-cell differentiation: human memory T-cell subsets.', *European journal of immunology*. Germany, 43(11), pp. 2797–2809. doi: 10.1002/eji.201343751.

Mahoney., E. *et al.* (2008) 'One-Year Costs in Patients With a History of or at Risk for Atherothrombosis in the United States', *Circulation: Cardiovascular Quality and Outcomes*. American Heart Association, 1(1), pp. 38–45. doi: 10.1161/CIRCOUTCOMES.108.775247.

Malik, A. N. and Czajka, A. (2013) 'Is mitochondrial DNA content a potential biomarker of mitochondrial dysfunction?', *Mitochondrion*, 13(5), pp. 481–492. doi: https://doi.org/10.1016/j.mito.2012.10.011.

Malinska, D., Mirandola, S. R. and Kunz, W. S. (2010) 'Mitochondrial potassium channels and reactive oxygen species', *FEBS Letters*. No longer published by Elsevier, 584(10), pp. 2043–2048. doi: 10.1016/J.FEBSLET.2010.01.013.

Maljevic, S. and Lerche, H. (2013) 'Potassium channels: a review of broadening therapeutic possibilities for neurological diseases.', *Journal of neurology*. Germany, 260(9), pp. 2201–2211. doi: 10.1007/s00415-012-6727-8.

Manon, S. *et al.* (1995) 'Stimulation of oxidative phosphorylation by electrophoretic K+ entry associated to electroneutral K+/H+ exchange in yeast mitochondria.', *Biochimica et biophysica acta*. Netherlands, 1231(3), pp. 282–288.

Marks, D. R. and Fadool, D. A. (2007) 'Post-synaptic density perturbs insulin-induced Kv1.3 channel modulation via a clustering mechanism involving the SH3 domain.', *Journal of neurochemistry*. England, 103(4), pp. 1608–1627. doi: 10.1111/j.1471-4159.2007.04870.x.

Marquez, J. and Han, J. (2017) 'Exercise-Induced Mitochondrial Adaptations in Addressing Heart Failure.', *Advances in experimental medicine and biology*. United States, 1000, pp. 323–332. doi: 10.1007/978-981-10-4304-8_17.

Marsboom, G. *et al.* (2012) 'Dynamin-related protein 1-mediated mitochondrial mitotic fission permits hyperproliferation of vascular smooth muscle cells and offers a novel therapeutic target in pulmonary hypertension.', *Circulation research*. United States, 110(11), pp. 1484–1497. doi: 10.1161/CIRCRESAHA.111.263848.

Martinez-Reyes, I. *et al.* (2016) 'TCA Cycle and Mitochondrial Membrane Potential Are Necessary for Diverse Biological Functions.', *Molecular cell*. United States, 61(2), pp. 199–209. doi: 10.1016/j.molcel.2015.12.002.

Marx, S. O., Totary-Jain, H. and Marks, A. R. (2011) 'Vascular smooth muscle cell proliferation in restenosis', *Circulation. Cardiovascular interventions*, 4(1), pp. 104–111. doi: 10.1161/CIRCINTERVENTIONS.110.957332.

Matsumoto, T. and Nagayama, K. (2012) 'Tensile properties of vascular smooth muscle cells: bridging vascular and cellular biomechanics.', *Journal of biomechanics*. United States, 45(5), pp. 745–755. doi: 10.1016/j.jbiomech.2011.11.014.

Mattarei, A. *et al.* (2018) 'Novel Mitochondria-Targeted Furocoumarin Derivatives as Possible Anti-Cancer Agents.', *Frontiers in oncology*. Switzerland, 8, p. 122. doi: 10.3389/fonc.2018.00122.

Maziar, R. *et al.* (2006) 'Allograft Vasculopathy Versus Atherosclerosis', *Circulation Research*. American Heart Association, 99(8), pp. 801–815. doi: 10.1161/01.RES.0000246086.93555.f3.

McCommis, K. S. and Finck, B. N. (2015) 'Mitochondrial pyruvate transport: a historical perspective and future research directions.', *The Biochemical journal*. England, 466(3), pp. 443–454. doi: 10.1042/BJ20141171.

McCormack, T. *et al.* (1999) 'The effects of Shaker beta-subunits on the human lymphocyte K+ channel Kv1.3.', *The Journal of biological chemistry*. United States, 274(29), pp. 20123–20126.

Mebratu, Y. and Tesfaigzi, Y. (2009) 'How ERK1/2 activation controls cell proliferation and cell death: Is subcellular localization the answer?', *Cell cycle (Georgetown, Tex.)*. 2009/04/11, 8(8), pp. 1168–1175. doi: 10.4161/cc.8.8.8147.

Mercer, J. R. *et al.* (2012) 'The mitochondria-targeted antioxidant MitoQ decreases features of the metabolic syndrome in ATM+/-/ApoE-/- mice.', *Free radical biology & medicine*. United States, 52(5), pp. 841–849. doi: 10.1016/j.freeradbiomed.2011.11.026.

Miano, J. M. (2003) 'Serum response factor: toggling between disparate programs of gene expression', *Journal of Molecular and Cellular Cardiology*, 35(6), pp. 577–593. doi: https://doi.org/10.1016/S0022-2828(03)00110-X.

Millership, J. E. *et al.* (2011) 'Calcium-activated K+ channels increase cell proliferation independent of K+ conductance', *American journal of physiology. Cell physiology*. 2010/12/01. American Physiological Society, 300(4), pp. C792–C802. doi: 10.1152/ajpcell.00274.2010.

Mitchell, P. (1961) 'Coupling of phosphorylation to electron and hydrogen transfer by a chemi-osmotic type of mechanism.', *Nature*. England, 191, pp. 144–148.

Mitra, K. (2013) 'Mitochondrial fission-fusion as an emerging key regulator of cell

proliferation and differentiation.', *BioEssays : news and reviews in molecular, cellular and developmental biology*. United States, 35(11), pp. 955–964. doi: 10.1002/bies.201300011.

Moloney, J. N. and Cotter, T. G. (2017) 'ROS signalling in the biology of cancer.', *Seminars in cell & developmental biology*. England. doi: 10.1016/j.semcdb.2017.05.023.

Moncada, S., Higgs, E. A. and Colombo, S. L. (2012) 'Fulfilling the metabolic requirements for cell proliferation.', *The Biochemical journal*. England, 446(1), pp. 1–7. doi: 10.1042/BJ20120427.

Monick, M. M. *et al.* (2008) 'Constitutive ERK MAPK activity regulates macrophage ATP production and mitochondrial integrity', *Journal of immunology (Baltimore, Md. : 1950)*, 180(11), pp. 7485–7496. doi: 10.4049/jimmunol.180.11.7485.

Motoshima, H. *et al.* (2006) 'AMPK and cell proliferation – AMPK as a therapeutic target for atherosclerosis and cancer', *The Journal of Physiology*. Blackwell Science Inc, 574(Pt 1), pp. 63–71. doi: 10.1113/jphysiol.2006.108324.

Mulvany, M. J. (1993) *Resistance Vessel Structure in Hypertension*, *Journal of cardiovascular pharmacology*. doi: 10.1097/00005344-199322005-00008.

Murphy, M. P. (2009) 'How mitochondria produce reactive oxygen species.', *The Biochemical journal*. England, 417(1), pp. 1–13. doi: 10.1042/BJ20081386.

Nabel, E. G. (2003) 'Cardiovascular Disease', *New England Journal of Medicine*. Massachusetts Medical Society, 349(1), pp. 60–72. doi: 10.1056/NEJMra035098.

Naish, J., Syndercombe Court, D. and Revest, P. (2009) *Medical Science*. Elsevier Health Science.

National Health Service (2018) *Cardiovascular Disease*. Available at: https://www.nhs.uk/conditions/Cardiovascular-disease/ (Accessed: 21 May 2019).

Navale, A. M. and Paranjape, A. N. (2016) 'Glucose transporters: physiological and pathological roles.', *Biophysical reviews*. Germany, 8(1), pp. 5–9. doi: 10.1007/s12551-015-0186-2.

Nekouzadeh, A. and Rudy, Y. (2016) 'Conformational changes of an ion-channel during

gating and emerging electrophysiologic properties: Application of a computational approach to cardiac Kv7.1', *Progress in Biophysics and Molecular Biology*, 120(1), pp. 18–27. doi: https://doi.org/10.1016/j.pbiomolbio.2015.12.014.

Nemenoff, A. R. *et al.* (2011) 'SDF-1α Induction in Mature Smooth Muscle Cells by Inactivation of PTEN Is a Critical Mediator of Exacerbated Injury-Induced Neointima Formation', *Arteriosclerosis, Thrombosis, and Vascular Biology*. American Heart Association, 31(6), pp. 1300–1308. doi: 10.1161/ATVBAHA.111.223701.

Neylon, C. *et al.* (1999) 'Molecular Cloning and Characterization of the Intermediate-Conductance Ca2+-Activated K+ Channel in Vascular Smooth Muscle', *Circulation Research*. American Heart Association, 85(9), pp. e33–e43. doi: 10.1161/01.RES.85.9.e33.

Neylon, C. B. (2002) 'Potassium channels and vascular proliferation', *Vascular Pharmacology*, 38(1), pp. 35–41. doi: https://doi.org/10.1016/S1537-1891(02)00124-6.

Nicholls, D. G. and Ferguson, S. J. (2013) *Bioenergetics 4*. Fourth, *Bioenergetics 4*. Fourth. Elsevier Science.

Nissanka, N. and Moraes, C. T. (2018) 'Mitochondrial DNA damage and reactive oxygen species in neurodegenerative disease', *FEBS Letters*. John Wiley & Sons, Ltd, 592(5), pp. 728–742. doi: 10.1002/1873-3468.12956.

Norton, R. S., Pennington, M. W. and Wulff, H. (2004) 'Potassium channel blockade by the sea anemone toxin ShK for the treatment of multiple sclerosis and other autoimmune diseases.', *Current medicinal chemistry*. Netherlands, 11(23), pp. 3041–3052.

Obermeyer, G. *et al.* (2013) 'Dynamic adaption of metabolic pathways during germination and growth of lily pollen tubes after inhibition of the electron transport chain', *Plant physiology*. 2013/05/09. American Society of Plant Biologists, 162(4), pp. 1822–1833. doi: 10.1104/pp.113.219857.

Olsen, L. F. *et al.* (2009) 'Regulation of Glycolytic Oscillations by Mitochondrial and Plasma Membrane H(+)-ATPases', *Biophysical Journal*. The Biophysical Society, 96(9), pp. 3850–3861. doi: 10.1016/j.bpj.2009.02.026.

Oronsky, B. T. *et al.* (2014) 'Follow the ATP: tumor energy production: a perspective.', *Anti-cancer agents in medicinal chemistry*. Netherlands, 14(9), pp. 1187–1198.

Ouadid-Ahidouch, H. and Ahidouch, A. (2013) 'K(+) channels and cell cycle progression in tumor cells.', *Frontiers in physiology*. Switzerland, 4, p. 220. doi: 10.3389/fphys.2013.00220.

Owens, G. (1988) *Transforming growth factor-beta-induced growth inhibition and cellular hypertrophy in cultured vascular smooth muscle cells*, *The Journal of Cell Biology*. doi: 10.1083/jcb.107.2.771.

Owens, G. K., Kumar, M. S. and Wamhoff, B. R. (2004) 'Molecular regulation of vascular smooth muscle cell differentiation in development and disease.', *Physiological reviews*. United States, 84(3), pp. 767–801. doi: 10.1152/physrev.00041.2003.

Panyi, G. (2005) 'Biophysical and pharmacological aspects of K+ channels in T lymphocytes.', *European biophysics journal : EBJ*. Germany, 34(6), pp. 515–529. doi: 10.1007/s00249-005-0499-3.

Papa, S., Choy, P. M. and Bubici, C. (2019) 'The ERK and JNK pathways in the regulation of metabolic reprogramming', *Oncogene*, 38(13), pp. 2223–2240. doi: 10.1038/s41388-018-0582-8.

Park, J. L. *et al.* (2005) 'GLUT4 facilitative glucose transporter specifically and differentially contributes to agonist-induced vascular reactivity in mouse aorta.', *Arteriosclerosis, thrombosis, and vascular biology*. United States, 25(8), pp. 1596–1602. doi: 10.1161/01.ATV.0000170137.41079.ab.

Parra, V. *et al.* (2008) 'Changes in mitochondrial dynamics during ceramide-induced cardiomyocyte early apoptosis.', *Cardiovascular research*. England, 77(2), pp. 387–397. doi: 10.1093/cvr/cvm029.

Parra, V. *et al.* (2011) 'The complex interplay between mitochondrial dynamics and cardiac metabolism.', *Journal of bioenergetics and biomembranes*. United States, 43(1), pp. 47–51. doi: 10.1007/s10863-011-9332-0.

Paul, R. J. (1983) 'Functional compartmentalization of oxidative and glycolytic metabolism in vascular smooth muscle.', *The American journal of physiology*. United

States, 244(5), pp. C399-409. doi: 10.1152/ajpcell.1983.244.5.C399.

Peers, C. *et al.* (2005) 'A central role for ROS in the functional remodelling of L-type Ca(2+) channels by hypoxia', *Philosophical Transactions of the Royal Society B: Biological Sciences*. London: The Royal Society, 360(1464), pp. 2247–2254. doi: 10.1098/rstb.2005.1761.

Peers, C. *et al.* (2015) 'Diverse mechanisms underlying the regulation of ion channels by carbon monoxide', *British Journal of Pharmacology*. Oxford, UK: BlackWell Publishing Ltd, 172(6), pp. 1546–1556. doi: 10.1111/bph.12760.

Pegg, A. E. (2016) 'Functions of Polyamines in Mammals.', *The Journal of biological chemistry*. United States, 291(29), pp. 14904–14912. doi: 10.1074/jbc.R116.731661.

Pennington, M. W. *et al.* (1995) 'Chemical synthesis and characterization of ShK toxin: a potent potassium channel inhibitor from a sea anemone.', *International journal of peptide and protein research*. Denmark, 46(5), pp. 354–358.

Perez-Garcia, M. T., Cidad, P. and Lopez-Lopez, J. R. (2018) 'The secret life of ion channels: Kv1.3 potassium channels and proliferation.', *American journal of physiology. Cell physiology*. United States, 314(1), pp. C27–C42. doi: 10.1152/ajpcell.00136.2017.

Perez-Verdaguer, M. *et al.* (2016) 'Caveolin interaction governs Kv1.3 lipid raft targeting.', *Scientific reports*. England, 6, p. 22453. doi: 10.1038/srep22453.

Perez, J. *et al.* (2010) 'Role of cellular bioenergetics in smooth muscle cell proliferation induced by platelet-derived growth factor', *The Biochemical journal*, 428(2), pp. 255–267. doi: 10.1042/BJ20100090.

Peruzzo, R. *et al.* (2017) 'Regulation of Proliferation by a Mitochondrial Potassium Channel in Pancreatic Ductal Adenocarcinoma Cells ', *Frontiers in Oncology* , p. 239.

Peter, R. *et al.* (1996) 'Mechanical Strain Increases Smooth Muscle and Decreases Nonmuscle Myosin Expression in Rat Vascular Smooth Muscle Cells', *Circulation Research*. American Heart Association, 79(5), pp. 1046–1053. doi: 10.1161/01.RES.79.5.1046.

Piepoli, M. F. *et al.* (2016) '2016 European Guidelines on cardiovascular disease

prevention in clinical practice: The Sixth Joint Task Force of the European Society of Cardiology and Other Societies on Cardiovascular Disease Prevention in Clinical Practice (constituted by representati', *Atherosclerosis*. Ireland, 252, pp. 207–274. doi: 10.1016/j.atherosclerosis.2016.05.037.

Poderoso, C. *et al.* (2008) 'A mitochondrial kinase complex is essential to mediate an ERK1/2-dependent phosphorylation of a key regulatory protein in steroid biosynthesis.', *PloS one*. United States, 3(1), p. e1443. doi: 10.1371/journal.pone.0001443.

Pontes, M. H., Sevostyanova, A. and Groisman, E. A. (2015) 'When Too Much ATP Is Bad for Protein Synthesis', *Journal of molecular biology*. 2015/07/04, 427(16), pp. 2586–2594. doi: 10.1016/j.jmb.2015.06.021.

Porter, K. E. *et al.* (1999) 'Production and Inhibition of the Gelatinolytic Matrix Metalloproteinases in a Human Model of Vein Graft Stenosis', *European Journal of Vascular and Endovascular Surgery*, 17(5), pp. 404–412. doi: https://doi.org/10.1053/ejvs.1998.0761.

Porter, K. E. *et al.* (2002) 'Simvastatin inhibits human saphenous vein neointima formation via inhibition of smooth muscle cell proliferation and migration.', *Journal of vascular surgery*. United States, 36(1), pp. 150–157.

Poulsen, A. K. *et al.* (2008) 'Probing glycolytic and membrane potential oscillations in Saccharomyces cerevisiae.', *Biochemistry*. United States, 47(28), pp. 7477–7484. doi: 10.1021/bi800396e.

Powell, R. J. *et al.* (1998) 'Coculture conditions alter endothelial modulation of TGF-β1 activation and smooth muscle growth morphology', *American Journal of Physiology-Heart and Circulatory Physiology*. American Physiological Society, 274(2), pp. H642–H649. doi: 10.1152/ajpheart.1998.274.2.H642.

Principe, D. Del *et al.* (2011) 'Trans-plasma membrane electron transport in mammals: functional significance in health and disease', *Antioxidants & redox signaling*. Mary Ann Liebert, Inc. 140 Huguenot Street, 3rd Floor New Rochelle, NY 10801 USA, 14(11), pp. 2289–2318.

Public Health England (2014) *New figures show high blood pressure costs NHS billions*

each year. Available at: https://www.gov.uk/government/news/new-figures-show-high-blood-pressure-costs-nhs-billions-each-year.

Qiu, J. *et al.* (2014) 'Biomechanical regulation of vascular smooth muscle cell functions: from in vitro to in vivo understanding', *Journal of the Royal Society, Interface*. The Royal Society, 11(90), p. 20130852. doi: 10.1098/rsif.2013.0852.

Raha, S. *et al.* (2000) 'Superoxides from mitochondrial complex III: the role of manganese superoxide dismutase.', *Free radical biology & medicine*. United States, 29(2), pp. 170–180.

Rangaraju, S. *et al.* (2015) 'Potassium channel Kv1.3 is highly expressed by microglia in human Alzheimer's disease.', *Journal of Alzheimer's disease : JAD*. Netherlands, 44(3), pp. 797–808. doi: 10.3233/JAD-141704.

Rashid, M. H. *et al.* (2013) 'A potent and selective peptide blocker of the Kv1.3 channel: prediction from free-energy simulations and experimental confirmation.', *PloS one*. United States, 8(11), p. e78712. doi: 10.1371/journal.pone.0078712.

Rashid, M. H. *et al.* (2014) 'A potent and Kv1.3-selective analogue of the scorpion toxin HsTX1 as a potential therapeutic for autoimmune diseases.', *Scientific reports*. England, 4, p. 4509. doi: 10.1038/srep04509.

Rasmusson, R. L. *et al.* (1998) 'Inactivation of voltage-gated cardiac K+ channels.', *Circulation research*. United States, 82(7), pp. 739–750.

Riganti, C. *et al.* (2012) 'The pentose phosphate pathway: an antioxidant defense and a crossroad in tumor cell fate.', *Free radical biology & medicine*. United States, 53(3), pp. 421–436. doi: 10.1016/j.freeradbiomed.2012.05.006.

Rizzuto, R. *et al.* (2012) 'Mitochondria as sensors and regulators of calcium signalling.', *Nature reviews. Molecular cell biology*. England, 13(9), pp. 566–578. doi: 10.1038/nrm3412.

Robey, R. B. and Hay, N. (2009) 'Is Akt the "Warburg kinase"?-Akt-energy metabolism interactions and oncogenesis', *Seminars in cancer biology*. 2008/12/14, 19(1), pp. 25–31. doi: 10.1016/j.semcancer.2008.11.010.

Robinson, G. L. *et al.* (2012) 'Switching from aerobic glycolysis to oxidative

phosphorylation modulates the sensitivity of mantle cell lymphoma cells to TRAIL.', *Oncogene*. England, 31(48), pp. 4996–5006. doi: 10.1038/onc.2012.13.

Robinson, J. G. *et al.* (2015) 'Efficacy and safety of alirocumab in reducing lipids and cardiovascular events.', *The New England journal of medicine*. United States, 372(16), pp. 1489–1499. doi: 10.1056/NEJMoa1501031.

Ronchi, J. A. *et al.* (2013) 'A spontaneous mutation in the nicotinamide nucleotide transhydrogenase gene of C57BL/6J mice results in mitochondrial redox abnormalities.', *Free radical biology & medicine*. United States, 63, pp. 446–456. doi: 10.1016/j.freeradbiomed.2013.05.049.

Ross, R. (1981) 'George Lyman Duff Memorial Lecture. Atherosclerosis: a problem of the biology of arterial wall cells and their interactions with blood components.', *Arteriosclerosis (Dallas, Tex.)*. United States, 1(5), pp. 293–311.

Rzucidlo, E. M., Martin, K. A. and Powell, R. J. (2007) 'Regulation of vascular smooth muscle cell differentiation', *Journal of Vascular Surgery*, 45(6, Supplement), pp. A25–A32. doi: https://doi.org/10.1016/j.jvs.2007.03.001.

Sakamoto, K. *et al.* (2008) 'A novel opener of large-conductance Ca2+ -activated K+ (BK) channel reduces ischemic injury in rat cardiac myocytes by activating mitochondrial K(Ca) channel.', *Journal of pharmacological sciences*. Japan, 108(1), pp. 135–139.

Salabei, J. K. and Hill, B. G. (2013) 'Mitochondrial fission induced by platelet-derived growth factor regulates vascular smooth muscle cell bioenergetics and cell proliferation.', *Redox biology*. Netherlands, 1, pp. 542–551. doi: 10.1016/j.redox.2013.10.011.

Sassi, N. *et al.* (2010) 'An investigation of the occurrence and properties of the mitochondrial intermediate-conductance Ca2+-activated K+ channel mtKCa3.1', *Biochimica et Biophysica Acta (BBA) - Bioenergetics*, 1797(6), pp. 1260–1267. doi: https://doi.org/10.1016/j.bbabio.2009.12.015.

Scaduto, R. C. J. (1994) 'Calcium and 2-oxoglutarate-mediated control of aspartate formation by rat heart mitochondria.', *European journal of biochemistry*. England, 223(3), pp. 751–758.

Schmitz, A. *et al.* (2005) 'Design of PAP-1, a selective small molecule Kv1.3 blocker, for the suppression of effector memory T cells in autoimmune diseases.', *Molecular pharmacology*. United States, 68(5), pp. 1254–1270. doi: 10.1124/mol.105.015669.

Schulick, A. H. *et al.* (1998) 'Overexpression of transforming growth factor beta1 in arterial endothelium causes hyperplasia, apoptosis, and cartilaginous metaplasia', *Proceedings of the National Academy of Sciences of the United States of America*. The National Academy of Sciences, 95(12), pp. 6983–6988. doi: 10.1073/pnas.95.12.6983.

Scragg, J. L. *et al.* (2008) 'Carbon Monoxide Inhibits L-type Ca(2+) Channels via Redox Modulation of Key Cysteine Residues by Mitochondrial Reactive Oxygen Species', *The Journal of Biological Chemistry*. American Society for Biochemistry and Molecular Biology, 283(36), pp. 24412–24419. doi: 10.1074/jbc.M803037200.

Selzman, C. H. *et al.* (1998) 'Interleukin-10 Inhibits Human Vascular Smooth Muscle Proliferation', *Journal of Molecular and Cellular Cardiology*, 30(4), pp. 889–896. doi: https://doi.org/10.1006/jmcc.1998.0642.

Serruys, P. W. and Rutherford, J. D. (2016) 'The Birth, and Evolution, of Percutaneous Coronary Interventions: A Conversation With Patrick Serruys, MD, PhD.', *Circulation*. United States, pp. 97–100. doi: 10.1161/CIRCULATIONAHA.116.023681.

Servier Medical Art (no date). Available at: https://smart.servier.com (Accessed: 21 November 2019).

Shadel, G. S. and Horvath, T. L. (2015) 'Mitochondrial ROS signaling in organismal homeostasis.', *Cell*. United States, 163(3), pp. 560–569. doi: 10.1016/j.cell.2015.10.001.

Shah, N. H. and Aizenman, E. (2014) 'Voltage-gated potassium channels at the crossroads of neuronal function, ischemic tolerance, and neurodegeneration.', *Translational stroke research*. United States, 5(1), pp. 38–58. doi: 10.1007/s12975-013-0297-7.

Shanklin, J. *et al.* (2009) 'Desaturases: emerging models for understanding functional diversification of diiron-containing enzymes.', *The Journal of biological chemistry*. United States, 284(28), pp. 18559–18563. doi: 10.1074/jbc.R900009200.

Sharma, N. *et al.* (2005) 'Regulation of pyruvate dehydrogenase activity and citric acid cycle intermediates during high cardiac power generation.', *The Journal of physiology*. England, 562(Pt 2), pp. 593–603. doi: 10.1113/jphysiol.2004.075713.

Shen, J. *et al.* (2003) 'Oxygen Consumption Rates and Oxygen Concentration in Molt-4 Cells and Their mtDNA Depleted (ρ0) Mutants', *Biophysical Journal*, 84(2), pp. 1291–1298. doi: https://doi.org/10.1016/S0006-3495(03)74944-3.

Smith, C. O., Nehrke, K. and Brookes, P. S. (2017) 'The Slo(w) path to identifying the mitochondrial channels responsible for ischemic protection.', *The Biochemical journal*. England, 474(12), pp. 2067–2094. doi: 10.1042/BCJ20160623.

Smith, R. A. J., Hartley, R. C. and Murphy, M. P. (2011) 'Mitochondria-targeted small molecule therapeutics and probes.', *Antioxidants & redox signaling*. United States, 15(12), pp. 3021–3038. doi: 10.1089/ars.2011.3969.

Sole, L. *et al.* (2009) 'KCNE4 suppresses Kv1.3 currents by modulating trafficking, surface expression and channel gating.', *Journal of cell science*. England, 122(Pt 20), pp. 3738–3748. doi: 10.1242/jcs.056689.

Sonoyama, K. *et al.* (2007) 'Review: Vascular remodeling: implications for small artery function and target organ damage', *Therapeutic Advances in Cardiovascular Disease*. SAGE Publications, 1(2), pp. 129–137. doi: 10.1177/1753944707086358.

Spinelli, A. M. and Trebak, M. (2016) 'Orai channel-mediated Ca2+ signals in vascular and airway smooth muscle.', *American journal of physiology. Cell physiology*. United States, 310(6), pp. C402-13. doi: 10.1152/ajpcell.00355.2015.

Stamenkovic, J. A. *et al.* (2015) 'Inhibition of the malate-aspartate shuttle in mouse pancreatic islets abolishes glucagon secretion without affecting insulin secretion.', *The Biochemical journal*. England, 468(1), pp. 49–63. doi: 10.1042/BJ20140697.

Stebbing, M. J., Cottee, J. M. and Rana, I. (2015) 'The Role of Ion Channels in Microglial Activation and Proliferation - A Complex Interplay between Ligand-Gated Ion Channels, K(+) Channels, and Intracellular Ca(2.).', *Frontiers in immunology*. Switzerland, 6, p. 497. doi: 10.3389/fimmu.2015.00497.

Stepanenko, A. A. and Dmitrenko, V. V (2015) 'HEK293 in cell biology and cancer

research: phenotype, karyotype, tumorigenicity, and stress-induced genome-phenotype evolution.', *Gene*. Netherlands, 569(2), pp. 182–190. doi: 10.1016/j.gene.2015.05.065.

Stewart, J., Manmathan, G. and Wilkinson, P. (2017) 'Primary prevention of cardiovascular disease: A review of contemporary guidance and literature.', *JRSM cardiovascular disease*. England, 6, p. 2048004016687211. doi: 10.1177/2048004016687211.

Straub, S. V *et al.* (2011) 'Pharmacological inhibition of Kv1.3 fails to modulate insulin sensitivity in diabetic mice or human insulin-sensitive tissues.', *American journal of physiology. Endocrinology and metabolism*. United States, 301(2), pp. E380-90. doi: 10.1152/ajpendo.00076.2011.

Stuhmer, W. *et al.* (1989) 'Molecular basis of functional diversity of voltage-gated potassium channels in mammalian brain.', *The EMBO journal*. England, 8(11), pp. 3235–3244.

Su, B. *et al.* (2001) 'Redox Regulation of Vascular Smooth Muscle Cell Differentiation', *Circulation Research*. American Heart Association, 89(1), pp. 39–46. doi: 10.1161/hh1301.093615.

Sullivan, L. B. *et al.* (2015) 'Supporting Aspartate Biosynthesis Is an Essential Function of Respiration in Proliferating Cells.', *Cell*. United States, 162(3), pp. 552–563. doi: 10.1016/j.cell.2015.07.017.

Summerhayes, I. C. *et al.* (1982) 'Unusual retention of rhodamine 123 by mitochondria in muscle and carcinoma cells.', *Proceedings of the National Academy of Sciences of the United States of America*. United States, 79(17), pp. 5292–5296.

Susan, C. *et al.* (2012) 'Mitochondrial Motility and Vascular Smooth Muscle Proliferation', *Arteriosclerosis, Thrombosis, and Vascular Biology*. American Heart Association, 32(12), pp. 3000–3011. doi: 10.1161/ATVBAHA.112.255174.

Suwanabol, P. A. *et al.* (2012) 'Transforming growth factor-β increases vascular smooth muscle cell proliferation through the Smad3 and extracellular signal-regulated kinase mitogen-activated protein kinases pathways', *Journal of vascular surgery*. 2012/04/21, 56(2), pp. 446–454. doi: 10.1016/j.jvs.2011.12.038.

Swanson, R. *et al.* (1990) 'Cloning and expression of cDNA and genomic clones encoding three delayed rectifier potassium channels in rat brain.', *Neuron*. United States, 4(6), pp. 929–939.

Sylvester, A. M. *et al.* (1998) *Role of c-fos and E2F in the induction of cyclin A transcription and vascular smooth muscle cell proliferation*, *The Journal of clinical investigation*. doi: 10.1172/JCI1630.

Szabo, I. *et al.* (2005) 'A novel potassium channel in lymphocyte mitochondria.', *The Journal of biological chemistry*. United States, 280(13), pp. 12790–12798. doi: 10.1074/jbc.M413548200.

Szabó, I. *et al.* (2008) 'Mitochondrial potassium channel Kv1.3 mediates Bax-induced apoptosis in lymphocytes', *Proceedings of the National Academy of Sciences of the United States of America*. 2008/09/25. National Academy of Sciences, 105(39), pp. 14861–14866. doi: 10.1073/pnas.0804236105.

Szabo, I. and Zoratti, M. (2014) 'Mitochondrial channels: ion fluxes and more.', *Physiological reviews*. United States, 94(2), pp. 519–608. doi: 10.1152/physrev.00021.2013.

Szilagyi, O. *et al.* (2013) 'The role of PSD-95 in the rearrangement of Kv1.3 channels to the immunological synapse.', *Pflugers Archiv : European journal of physiology*. Germany, 465(9), pp. 1341–1353. doi: 10.1007/s00424-013-1256-6.

Takebayashi, S.-I. *et al.* (2015) 'Retinoblastoma protein promotes oxidative phosphorylation through upregulation of glycolytic genes in oncogene-induced senescent cells', *Aging cell*. 2015/05/25. John Wiley & Sons, Ltd, 14(4), pp. 689–697. doi: 10.1111/acel.12351.

Tanner, M. R. *et al.* (2017) 'Prolonged immunomodulation in inflammatory arthritis using the selective Kv1.3 channel blocker HsTX1[R14A] and its PEGylated analog.', *Clinical immunology (Orlando, Fla.)*. United States, 180, pp. 45–57. doi: 10.1016/j.clim.2017.03.014.

Tarcha, E. J. *et al.* (2017) 'Safety and pharmacodynamics of dalazatide, a Kv1.3 channel inhibitor, in the treatment of plaque psoriasis: A randomized phase 1b trial.', *PloS one*. United States, 12(7), p. e0180762. doi: 10.1371/journal.pone.0180762.

Teisseyre, A., Gasiorowska, J. and Michalak, K. (2015) 'Voltage-Gated Potassium Channels Kv1.3--Potentially New Molecular Target in Cancer Diagnostics and Therapy.', *Advances in clinical and experimental medicine : official organ Wroclaw Medical University*. Poland, 24(3), pp. 517–524.

Testai, L. *et al.* (2015) 'Expression and function of Kv7.4 channels in rat cardiac mitochondria: possible targets for cardioprotection', *Cardiovascular Research*, 110(1), pp. 40–50. doi: 10.1093/cvr/cvv281.

Thomas, P. and Smart, T. G. (2005) 'HEK293 cell line: a vehicle for the expression of recombinant proteins.', *Journal of pharmacological and toxicological methods*. United States, 51(3), pp. 187–200. doi: 10.1016/j.vascn.2004.08.014.

Tongul, B. and Tarhan, L. (2014) 'The effect of menadione-induced oxidative stress on the in vivo reactive oxygen species and antioxidant response system of Phanerochaete chrysosporium', *Process Biochemistry*, 49(2), pp. 195–202. doi: https://doi.org/10.1016/j.procbio.2013.11.004.

Touyz, R. *et al.* (2018) *Vascular Smooth Muscle Contraction in Hypertension*, *Cardiovascular research*. doi: 10.1093/cvr/cvy023.

Trachootham, D. *et al.* (2008) 'Redox regulation of cell survival.', *Antioxidants & redox signaling*. United States, 10(8), pp. 1343–1374. doi: 10.1089/ars.2007.1957.

Trnka, J., Elkalaf, M. and Anděl, M. (2015) 'Lipophilic triphenylphosphonium cations inhibit mitochondrial electron transport chain and induce mitochondrial proton leak', *PloS one*. Public Library of Science, 10(4), pp. e0121837–e0121837. doi: 10.1371/journal.pone.0121837.

Tschritter, O. *et al.* (2006) 'A New Variant in the Human Kv1.3 Gene Is Associated with Low Insulin Sensitivity and Impaired Glucose Tolerance', *The Journal of Clinical Endocrinology & Metabolism*, 91(2), pp. 654–658.

Tucker, K. *et al.* (2013) 'Glucose sensitivity of mouse olfactory bulb neurons is conveyed by a voltage-gated potassium channel.', *The Journal of physiology*. England, 591(10), pp. 2541–2561. doi: 10.1113/jphysiol.2013.254086.

Tucker, K., Overton, J. M. and Fadool, D. A. (2008) 'Kv1.3 gene-targeted deletion alters

longevity and reduces adiposity by increasing locomotion and metabolism in melanocortin-4 receptor-null mice.', *International journal of obesity (2005)*. England, 32(8), pp. 1222–1232. doi: 10.1038/ijo.2008.77.

Ueda, K. *et al.* (2013) 'Rapid estrogen receptor signaling mediates estrogen-induced inhibition of vascular smooth muscle cell proliferation', *Arteriosclerosis, thrombosis, and vascular biology*. 2013/06/06, 33(8), pp. 1837–1843. doi: 10.1161/ATVBAHA.112.300752.

Upadhyay, S. K. *et al.* (2013) 'Selective Kv1.3 channel blocker as therapeutic for obesity and insulin resistance', *Proceedings of the National Academy of Sciences*, 110(24), p. E2239 LP-E2248.

Urrego, D. *et al.* (2014) 'Potassium channels in cell cycle and cell proliferation.', *Philosophical transactions of the Royal Society of London. Series B, Biological sciences*. England, 369(1638), p. 20130094. doi: 10.1098/rstb.2013.0094.

Varghese, A. *et al.* (2006) 'Endogenous channels in HEK cells and potential roles in HCN ionic current measurements.', *Progress in biophysics and molecular biology*. England, 90(1–3), pp. 26–37. doi: 10.1016/j.pbiomolbio.2005.05.002.

Vautier, F. *et al.* (2004) 'Shaker-type potassium channel subunits differentially control oligodendrocyte progenitor proliferation.', *Glia*. United States, 48(4), pp. 337–345. doi: 10.1002/glia.20088.

Veh, R. W. *et al.* (1995) 'Immunohistochemical localization of five members of the Kv1 channel subunits: contrasting subcellular locations and neuron-specific co-localizations in rat brain.', *The European journal of neuroscience*. France, 7(11), pp. 2189–2205.

Velez, P. *et al.* (2016) 'Ubiquitin ligase Nedd4-2 modulates Kv1.3 current amplitude and ion channel protein targeting.', *Journal of neurophysiology*. United States, 116(2), pp. 671–685. doi: 10.1152/jn.00874.2015.

Venturini, E. *et al.* (2017) 'Targeting the Potassium Channel Kv1.3 Kills Glioblastoma Cells.', *Neuro-Signals*. Switzerland, 25(1), pp. 26–38. doi: 10.1159/000480643.

Verdin, E. (2015) 'NAD(+) in aging, metabolism, and neurodegeneration.', *Science (New York, N.Y.)*. United States, 350(6265), pp. 1208–1213. doi: 10.1126/science.aac4854.

Vicente, R. *et al.* (2003) 'Differential voltage-dependent K+ channel responses during proliferation and activation in macrophages.', *The Journal of biological chemistry*. United States, 278(47), pp. 46307–46320. doi: 10.1074/jbc.M304388200.

Villalonga, N. *et al.* (2007) 'Kv1.3/Kv1.5 heteromeric channels compromise pharmacological responses in macrophages', *Biochemical and Biophysical Research Communications*, 352(4), pp. 913–918. doi: https://doi.org/10.1016/j.bbrc.2006.11.120.

Vinnakota, K. C., Dash, R. K. and Beard, D. A. (2011) 'Stimulatory effects of calcium on respiration and NAD(P)H synthesis in intact rat heart mitochondria utilizing physiological substrates cannot explain respiratory control in vivo.', *The Journal of biological chemistry*. United States, 286(35), pp. 30816–30822. doi: 10.1074/jbc.M111.242529.

Wainstein, E. and Seger, R. (2016) 'The dynamic subcellular localization of ERK: mechanisms of translocation and role in various organelles.', *Current opinion in cell biology*. England, 39, pp. 15–20. doi: 10.1016/j.ceb.2016.01.007.

Walewska, A., Szewczyk, A. and Koprowski, P. (2018) 'Gas Signaling Molecules and Mitochondrial Potassium Channels', *International journal of molecular sciences*. MDPI, 19(10), p. 3227. doi: 10.3390/ijms19103227.

Wang, X. and Sun, Z. (2010) 'Thyroid hormone induces artery smooth muscle cell proliferation: discovery of a new TRalpha1-Nox1 pathway', *Journal of cellular and molecular medicine*. 2008/09/04. Blackwell Publishing Ltd, 14(1–2), pp. 368–380. doi: 10.1111/j.1582-4934.2008.00489.x.

Warburg, O. (1925) 'The Metabolism of Carcinoma Cells', *The Journal of Cancer Research*, 9(1), p. 148 LP-163.

Warburg, O., Posener, K. and Negelein, E. (1924) 'The metabolism of cancer cells', *Biochem Z*, 152, pp. 319–344.

Ward, P. S. and Thompson, C. B. (2012) 'Signaling in control of cell growth and metabolism', *Cold Spring Harbor perspectives in biology*. Cold Spring Harbor Laboratory Press, 4(7), pp. a006783–a006783. doi: 10.1101/cshperspect.a006783.

Wheeler, M. L. and DeFranco, A. L. (2012) 'Prolonged production of reactive oxygen species in response to BCR stimulation promotes B cell activation and proliferation', *Journal of immunology (Baltimore, Md. : 1950)*, 189(9), pp. 4405–4416. doi: 10.4049/jimmunol.1201433.

Wilkins, E. *et al.* (2017) *European Cardiovascular Disease Statistics 2017*. Brussels.

Wojtovich, A. P. *et al.* (2011) 'SLO-2 is cytoprotective and contributes to mitochondrial potassium transport', *PloS one*. Public Library of Science, 6(12), pp. e28287–e28287. doi: 10.1371/journal.pone.0028287.

World Health Organisation (2013) *A Global Brief on Hypertension: Silent Killer, Global Public Health Crisis*. Geneva.

World Health Organisation (2018) *World Health Organisation*, *Cardiovascular Disease*. Available at: http://www.who.int/cardiovascular_diseases/en/ (Accessed: 25 November 2018).

Wulff, H. *et al.* (2003) 'The voltage-gated Kv1.3 K(+) channel in effector memory T cells as new target for MS', *The Journal of clinical investigation*. American Society for Clinical Investigation, 111(11), pp. 1703–1713. doi: 10.1172/JCI16921.

Wulff, H. *et al.* (2004) 'K+ channel expression during B cell differentiation: implications for immunomodulation and autoimmunity.', *Journal of immunology (Baltimore, Md. : 1950)*. United States, 173(2), pp. 776–786.

Xie, N. *et al.* (2017) 'SRSF1 promotes vascular smooth muscle cell proliferation through a Delta133p53/EGR1/KLF5 pathway.', *Nature communications*. England, 8, p. 16016. doi: 10.1038/ncomms16016.

Xie, Y. *et al.* (2015) 'Phosphorylation of GATA-6 is required for vascular smooth muscle cell differentiation after mTORC1 inhibition', *Science Signaling*, 8(376), p. ra44 LP-ra44. doi: 10.1126/scisignal.2005482.

Xu, J. *et al.* (2003) 'The voltage-gated potassium channel Kv1.3 regulates energy homeostasis and body weight.', *Human molecular genetics*. England, 12(5), pp. 551–559.

Xu, J. *et al.* (2004) 'The voltage-gated potassium channel Kv1.3 regulates peripheral

insulin sensitivity.', *Proceedings of the National Academy of Sciences of the United States of America*. United States, 101(9), pp. 3112–3117. doi: 10.1073/pnas.0308450100.

Yang, L.-H. *et al.* (2012) 'Butein inhibits the proliferation of breast cancer cells through generation of reactive oxygen species and modulation of ERK and p38 activities.', *Molecular medicine reports*. Greece, 6(5), pp. 1126–1132. doi: 10.3892/mmr.2012.1023.

Yang, W. *et al.* (2014) 'BF9, the first functionally characterized snake toxin peptide with Kunitz-type protease and potassium channel inhibiting properties.', *Journal of biochemical and molecular toxicology*. United States, 28(2), pp. 76–83. doi: 10.1002/jbt.21538.

Yu, E. P. K. and Bennett, M. R. (2014) 'Mitochondrial DNA damage and atherosclerosis.', *Trends in endocrinology and metabolism: TEM*. United States, 25(9), pp. 481–487. doi: 10.1016/j.tem.2014.06.008.

Yuan, X.-L. *et al.* (2018) 'A Kv1.3 channel-specific blocker alleviates neurological impairment through inhibiting T-cell activation in experimental autoimmune encephalomyelitis.', *CNS neuroscience & therapeutics*. England. doi: 10.1111/cns.12848.

Zamzami, N. *et al.* (1996) 'Inhibitors of permeability transition interfere with the disruption of the mitochondrial transmembrane potential during apoptosis', *FEBS Letters*. John Wiley & Sons, Ltd, 384(1), pp. 53–57. doi: 10.1016/0014-5793(96)00280-3.

Zhang, Y. *et al.* (2016) 'Irisin exerts dual effects on browning and adipogenesis of human white adipocytes.', *American journal of physiology. Endocrinology and metabolism*. United States, 311(2), pp. E530-41. doi: 10.1152/ajpendo.00094.2016.

Zhang, Y. *et al.* (2018) 'TREM2 modulates microglia phenotypes in the neuroinflammation of Parkinson's disease.', *Biochemical and biophysical research communications*. United States. doi: 10.1016/j.bbrc.2018.03.226.

Zhao, M. *et al.* (2002) 'Vascular smooth muscle cell proliferation requires both p38 and BMK1 MAP kinases', *Archives of Biochemistry and Biophysics*, 400(2), pp. 199–207. doi:

https://doi.org/10.1016/S0003-9861(02)00028-0.

Zhong, D. *et al.* (2009) 'The glycolytic inhibitor 2-deoxyglucose activates multiple prosurvival pathways through IGF1R.', *The Journal of biological chemistry*. United States, 284(35), pp. 23225–23233. doi: 10.1074/jbc.M109.005280.

Zhu, J., Yan, J. and Thornhill, W. B. (2012) 'N-glycosylation promotes the cell surface expression of Kv1.3 potassium channels.', *The FEBS journal*. England, 279(15), pp. 2632–2644. doi: 10.1111/j.1742-4658.2012.08642.x.

Zhu, J., Yan, J. and Thornhill, W. B. (2014) 'The Kv1.3 potassium channel is localized to the cis-Golgi and Kv1.6 is localized to the endoplasmic reticulum in rat astrocytes', *The FEBS Journal*. John Wiley & Sons, Ltd (10.1111), 281(15), pp. 3433–3445. doi: 10.1111/febs.12871.